Fall 2015

An investigation of shear-friction of lightweight aggregate concretes

Kristian Krc

Recommended Citation

AN INVESTIGATION OF SHEAR-FRICTION OF LIGHTWEIGHT AGGREGATE

CONCRETES

by

KRISTIAN KRC

A THESIS

Presented to the Faculty of the Graduate School of the

MISSOURI UNIVERSITY OF SCIENCE AND TECHNOLOGY

In Partial Fulfillment of the Requirements for the Degree

MASTER OF SCIENCE

in

CIVIL ENGINEERING

2015

Approved by

Dr. Lesley Sneed, Advisor
Dr. John Myers
Dr. Mohamed ElGawady
Dr. Donald Meinheit

ABSTRACT

This thesis reports the results of research initiated to evaluate the influence of lightweight aggregate type and casting procedure on shear transfer across an interface of concretes cast at different times. The topic of shear transfer has been evaluated and revisited in recent PCI Design Handbooks. In this test program, a series of cold joint as well as monolithic specimens are evaluated. The peak shear strength and post peak behavior are examined. The experimental matrix included 28 push-off specimens that were either cast monolithically or cast at different times creating the condition referred to as a cold joint. The variables included lightweight aggregate type (expanded shale, expanded slate, expanded clay); unit weight (88 – 148 pcf); and shear interface condition (monolithic uncracked, monolithic pre-cracked, cold joint roughened, cold joint smooth). A load cell, six DC-LVDTs, and three strain gages were used to monitor the behavior of each specimen.

Results suggest that the shear strength of monolithic specimens increased with increasing concrete unit weight. The shear strength of cold joint specimens with an intentionally roughened interface increased as the concrete unit weight increased. The shear strength of cold joint specimens with smooth interface was independent of concrete unit weight. The shear strength was predicted conservatively by the PCI Design Handbook 7th Edition and the ACI 318-14 code for all cold joint interface specimens. The effective coefficient of friction μ_e used by the PCI Design Handbook was found to be conservative for both sand-lightweight and all-lightweight cold joint specimens regardless of the type of lightweight aggregate used. This research was sponsored by Precast/Prestressed Concrete Institute (PCI) and the American Concrete Institute (ACI) Concrete Research Council (CRC).

ACKNOWLEDGMENTS

First I would like to thank my advisor Dr. Lesley Sneed. She took me under her wings regardless of my undergraduate degree being in Physics. She was very encouraging and helpful in times when I needed help with research, classes, or securing employment. Next I would like to thank my committee members, Dr. John J. Myers, Dr. Mohamed ElGawady, and Dr. Don Meinheit for providing feedback throughout my study as well as for being excellent professors.

I would like to thank the Precast/Prestressed Concrete Institute and the American Concrete Institute Concrete Research Council for providing the funds for this research.

I would like to thank my colleague and friend Samantha Wermager who was also working on this research. Laboratory work would not have been possible without the help from excellent staff members including John Bullock, Gary Abbott, Brian Swift, and Greg Lackrone.

I would like to thank my parents for the ultimate sacrifice they made for me as well as for teaching me to work hard and always being there for me. Lastly, I would like to thank the families that have adopted me here and took me in as one of their own.

TABLE OF CONTENTS

LIST OF ILLUSTRATIONS

LIST OF TABLES

NOMENCLATURE

Symbol	Description
A_{cr}	area of concrete shear interface, in^2
A_{vf}	area of shear reinforcement across shear plane, in^2
f'_c	28-day concrete compressive strength, lb/in^2
f_{ct}	tensile strength of concrete, measured by splitting tension test, lb/in^2
f_y	yield stress of reinforcement, lb/in^2
V_n	nominal shear strength, lb
v_n	nominal shear stress, lb/in^2
V_u	ultimate shear strength, lb
v_u	ultimate shear stress, lb/in^2
v_{ur}	residual shear stress, lb/in^2
λ	modification factor reflecting the reduced mechanical properties of lightweight concrete, relative to normalweight concrete of the same compressive strength
μ	coefficient of friction
μ_e	effective coefficient of friction
ρ	shear-friction reinforcement ratio, A_{vf}/A_{cr}
ϕ	strength reduction factor
ACI	American Concrete Institute
ASCE	American Society of Civil Engineers
ASTM	American Society for Testing and Materials
DC-LVDT	direct current - linear voltage displacement transducer
PCI	Precast/Prestressed Concrete Institute

1. INTRODUCTION

1.1. PROBLEM STATEMENT

Lightweight aggregate concretes are being used more widely in the concrete industry and especially in the precast concrete industry to reduce the cost of shipping by reducing the weight of concrete elements. Many precast concrete elements, including connections, are designed based on the shear-friction design provisions. One such connection is a column corbel, shown in Figure 1.1. Reinforced concrete bearings, connection of shear walls to foundations, and composite sections implement the shear-friction design concepts as well. Previous research studies, discussed in Section 2, have shown that unit weight of concrete, reinforcement ratio, concrete strength, and surface preparation influence the shear transfer strength. However, little research has actually been conducted on lightweight aggregate concretes and the influence of the different lightweight aggregates on the shear transfer strength, especially for concretes cast at different times (cold joint interface). This topic was identified by the Precast/Prestressed Concrete Institute (PCI) as an important research topic for the precast concrete industry, especially since the shear-friction design provisions in the PCI Design Handbook 7th Edition (2010) and the ACI 318-14 (2014) code were developed based on test data primarily from experiments with normalweight concrete specimens.

Figure 1.1 Typical Corbel Design (ACI 318-14)

The lightweight aggregate modification factor, λ, is used to account for the effects of lightweight aggregate concrete in shear design provisions in the PCI Design Handbook 7th Edition and the ACI 318-14 code, and their previous editions. This factor is used to account for the weaker mechanical properties of lightweight aggregate compared to those of normalweight aggregates. For shear-friction design, the lightweight aggregate modification factor is used to calculate the shear-friction design capacity, which is a function of the coefficient of friction μ in ACI 318-14 (Table 22.9.4.2) and the PCI Design Handbook 7th Edition (PCI Handbook) and the effective coefficient of friction $μ_e$ in the PCI Handbook (Eq. 5-33). The coefficient of friction varies for different crack interface conditions and concrete type. Both the PCI Handbook and ACI 318-14 code recognize four crack interface conditions (cases) for defining the shear-friction coefficient values. These are summarized in Table 1.1. Cases 1, 2, and 3, which refer to concrete cast monolithically and concretes cast against hardened concrete (also referred to as a "cold joint"), are of interest in this research study. Cold joint conditions are common in the precast industry particularly in elements such as corbels or ledges. For example, it is the practice of many precast facilities to independently cast corbels and then, at a later time, place them into the plastic concrete of another element, such as a column.

The PCI Handbook allows using the effective coefficient of friction, $μ_e$, in conditions where load reversal does not occur. However, there are limitations on the effective coefficient of friction. It is only applicable for the monolithic case (Case 1) and intentionally roughened, cold joint interface (Case 2) in the PCI Handbook. The effective coefficient of friction does not take into account unit weight of concrete. PCI Handbook also states that care should be exercised when using self-consolidating concrete (SCC) due to its fluidity.

As mentioned above, very few test results exist on the shear friction behavior of lightweight aggregate concretes, and furthermore, the potential influence of the different lightweight aggregate types has not been investigated. Different types of aggregate can be used in the production of lightweight concretes. Types commonly used in the U.S. include expanded shale, expanded slate, and expanded clay aggregates. These aggregates can have different densities and mechanical properties, which may play a role in the

direct shear transfer. Recent results by Shaw (2013) highlighted the need to study this variable.

This thesis work investigates the direct shear transfer of lightweight aggregate concretes with different interface conditions (Cases 1, 2, and 3 in Table 1.1) constructed with different lightweight aggregate types. Test results obtained from lightweight aggregate concrete tests are compared to normalweight concrete results with the same compressive strength and surface preparation. These test results are added to previous research results to broaden the database of results from lightweight aggregate concretes.

Table 1.1 Recommended Shear-friction Coefficients

Case	Crack interface condition	Coefficient of friction - μ
1	Concrete to concrete, monolithic	1.4λ
2	Concrete to concrete, cold joint – roughened	1.0λ
3	Concrete to concrete, cold joint – not intentionally roughened	0.6λ
4	Concrete to steel	0.7λ

1.2. OBJECTIVES AND SCOPE

The work included in this thesis is part of a larger project sponsored by the Precast/Prestressed Concrete Institute (PCI) and the American Concrete Institute (ACI) Concrete Research Council (CRC). The objective of the project was to determine the effect of using different types of lightweight concrete aggregates on the direct shear transfer across a shear plane with different interface conditions. A total of 52 specimens were included, of which 28 pertain to this thesis work. Specimens included in this thesis had a constant reinforcement ratio. Specimens with varying reinforcement ratios were also included in the project, but those results are presented in the thesis work by Samantha Wermager.

Specific objectives of this thesis work were to:

- Compare the shear strength of various lightweight aggregate concretes constructed with different lightweight aggregates.
- Evaluate the current shear-friction provisions set forth by the PCI Design Handbook 7th Edition and the ACI 318-14 code to determine their applicability to lightweight aggregate concretes.
- Bridge the gap in the literature regarding direct shear transfer strength of lightweight aggregate concrete cast at different times creating a cold joint interface.
- Examine the current coefficients of friction used in the PCI Design Handbook 7th Edition and the ACI 318-14 code and their effectiveness for design using lightweight aggregate concrete.

The scope of this study contained the following tasks to accomplish the objectives set forth above:

- Design, construct, and test a matrix of test specimens where the variables included unit weight (88 pcf – 148 pcf); lightweight aggregate type (expanded shale, expanded slate, expanded clay); interface condition (monolithic, cold joint – roughened, cold joint – smooth).
- Analyze the above mentioned variables and their influence on shear transfer strength.
- Analyze the effective coefficient of friction μ_e and its applicability for use in the PCI Design Handbook shear-friction design provisions.
- Study the need for the lightweight aggregate modification factor λ and recommend any necessary changes to the shear-friction design provisions in the PCI Design Handbook 7th Edition and ACI 318-14 code.

1.3. SUMMARY OF THESIS CONTENT

The problem statement, objectives, and scope of this study are described in the introductory Section 1. Section 2 follows with a literature review, which is comprised of a summary of previous research results, as well as current and previous shear-friction

design provisions included in the PCI Design Handbook and the ACI 318 code. Section 2 also provides detailed background information needed to understand the results of this study. Section 3 is a summary of the experimental work performed, including test specimen design, size, materials used, and their properties. Results of the experimental work are also presented in this section. Section 4 provides an analysis and discussion of the test results. Results from this study are also compared to previous relevant studies discussed in Section 2. Finally, Section 5 contains the summary of key findings, conclusions, and recommendations for future work. Included are Appendix A that contains databases of shear-friction specimens and Appendix B that provides a summary of residual shear strength of shear-friction specimens.

2. LITERATURE REVIEW

2.1. INTRODUCTION

Shear-friction is an important model in the design of concrete elements where the typical shear flexure theory does not apply, such as corbels and ledger beams. These elements generally provide very little redundancy, and therefore their design is critical to the structural soundness of the entire system. This chapter provides a background on shear-friction and summarizes design provisions and the conclusions of previous research. The transfer of shear across an interface is considered in Section 2.2. Design provisions that were reviewed in this study are presented in Section 2.3. Lastly, previous studies and a summary of their key findings are discussed in Section 2.4.

2.2. INTERFACE SHEAR-FRICTION

Shear-friction has been studied since the mid-20th century. Shear-friction, sometimes referred to as aggregate interlock across sliding surfaces, is now a well-established research area. The shear-friction model was first proposed by Birkeland and Birkeland (Birkeland and Birkeland, 1966). In cases where shear has to be transferred across an interface between two structural elements that can slip relative to each other, shear-friction prevents these elements from sliding relative to each other. Resistance is achieved by providing reinforcement across the potential crack. Tension develops in the reinforcement providing a clamping force through which the shear-friction is facilitated.

The original and simplest design model for shear-friction is the model that neglects the effect of cohesion. This model assumes shear transfer is due entirely to friction as shown in Figure 2.1. Because the cohesion is neglected, artificially high values of the coefficient of friction must be used to fit the experimental data (Wight and MacGregor 2012).

The coefficient of friction is a measure of how difficult it is to slide a material of one kind over another. The coefficient of friction, μ, is defined as the ratio of shear stress to normal stress. By manipulating this equation and assuming no external clamping force is provided, Equation 2.1 can be derived:

$$\mu = \frac{V_n}{A_{vf}f_y} \hspace{3cm} (2.1)$$

where V_n is the shear force, A_{vf} is the area of reinforcement crossing the shear plane, and f_y is the yield strength of the reinforcement crossing the shear plane. The product $A_{vf}f_y$ is the clamping force.

One of the fundamental components of the shear-friction model is a surface roughness. Surface roughness can vary widely due to construction practices, especially in precast construction. The use of self-consolidating concrete (SCC), for example, can result in an extremely smooth surface. As noted by Shaw (2013), "the use of self-consolidating concrete (SCC) can lead to conditions in which projecting elements are cast against supports elements after the concrete has partially hardened. The result may be a cold-joint condition with a relatively smooth interface on the SCC concrete face on which fresh concrete is placed."

In general, factors influencing the shear strength along the interface are surface preparation, amount of reinforcement provided, cohesion, shearing strength of aggregate, dowel action, and compressive strength of concrete. Cohesion is caused by aggregates bearing onto surfaces of aggregates on the opposite side of the shear plane. Dowel action involves interaction of the reinforcing bars crossing the shear plane and concrete near the shear plane. Some models take these factors into account in determining the shear strength (e.g. AASHTO LRFD Bridge Design Specification 7th Edition).

Because lightweight aggregate concretes generally have reduced mechanical properties relative to normalweight concrete of the same compressive strength, several code design provisions account for the use of lightweight aggregates by reducing the shear strength of the concrete. For shear-friction design, some provisions do so by reducing the coefficient of friction while others reduce the cohesion.
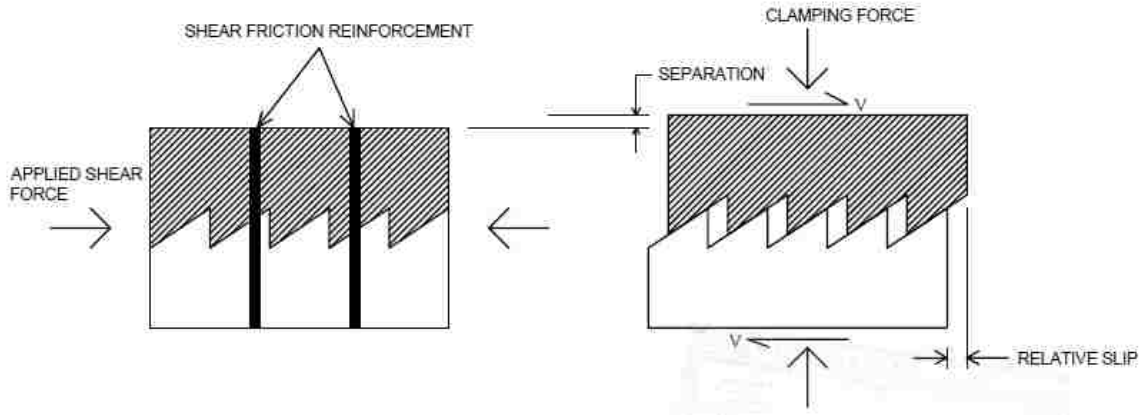
Figure 2.1 Shear-friction Model Proposed by Birkeland & Birkeland (1966)

2.3. SHEAR-FRICTION DESIGN PROVISIONS

2.3.1. ACI 318 Code. The design method used by the ACI 318-14 code is based on the simplest shear-friction model using the coefficient of friction μ. Equation 2.2 (ACI Eq. 22.9.4.2) is used to compute the nominal shear strength for all crack interface conditions and where the reinforcement is perpendicular to the shear plane. For the case of inclined reinforcement, Equation 2.3 (ACI Eq. 22.9.4.3) is used, where α is the angle between shear-friction reinforcement and the shear plane as shown in Figure 2.2. This equation only applies when the reinforcement crossing the shear plane is in tension (as shown).

$$V_n = A_{vf} f_y \mu \qquad (2.2)$$

$$V_n = A_{vf} f_y (\mu \sin\alpha + \cos\alpha) \qquad (2.3)$$

In Equations 2.2 and 2.3, the nominal shear strength is a function of the shear reinforcement area A_{vf}, the coefficient of friction μ, and the yield strength f_y of bars crossing the shear plane. The value of f_y shall not exceed 60,000 psi. The coefficient of friction used in Equations 2.2 and 2.3 is a function of crack interface condition described in Table 1.1. Upper limits are placed on the nominal shear strength. For the monolithic and roughened interface cases, V_n shall not exceed the smaller of $0.2f'_c A_c$,

(480+0.08f'$_c$)A$_c$, and 1600A$_c$, where A$_c$ is the area of the concrete section. For all other cases, V$_n$ shall not exceed 0.2f'$_c$A$_c$ or 800A$_c$. If two different concretes are used, the smaller of the two concrete compressive strengths f'$_c$ is to be used.
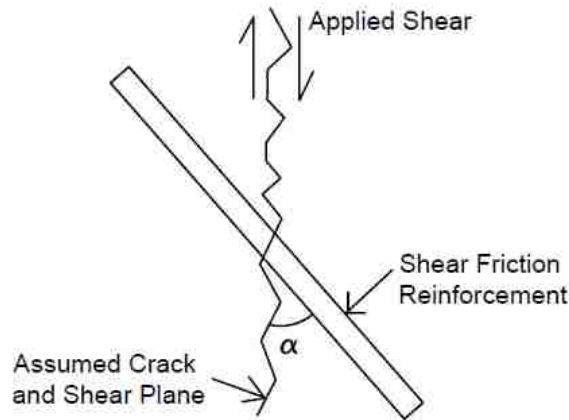
Figure 2.2 Inclined Shear Reinforcement

2.3.2. PCI Design Handbook 6th Edition. For shear-friction design, the area of reinforcement required by the PCI Design Handbook 6th Edition is shown in Equation 2.4 (PCI Eq. 4.3.6.1). V$_u$ is the applied (factored) shear force, $\emptyset$ is the strength reduction factor equal to 0.75 for shear, f$_y$ is the yield stress of reinforcement limited to 60 ksi, and μ_e is the so-called effective coefficient of friction evaluated according to Equation 2.5 (PCI Eq. 4.3.6.2) where λ is the lightweight concrete reduction factor and μ is the coefficient of friction in accordance with Table 2.1. It should be noticed that μ_e in Equation 2.5 is a function of λ^2 because μ is also a function of λ as shown in Table 2.1. Maximum values of V$_u$ and μ_e in Equations 2.4 and 2.5 are limited by the values shown in Table 2.1.

$$A_{vf} = \frac{V_u}{\emptyset f_y \mu_e} \tag{2.4}$$

$$\mu_e = \frac{1000\lambda A_{cr}\mu}{V_u} \tag{2.5}$$

The effective coefficient of friction μ_e is different than the coefficient of friction μ; it was introduced to be more realistic and to achieve more economical designs.

Table 2.1 Shear-friction Coefficients in the PCI Design Handbook 6th Edition (2004)

Case	Crack interface condition	μ	Maximum μ_e	Maximum $V_u = \emptyset V_n$
1	Concrete to concrete, monolithic	1.4λ	3.4	$0.30\lambda^2 f'_c A_{cr} \leq 1000\ \lambda^2 A_{cr}$
2	Concrete to concrete, cold joint - roughened	1.0λ	2.9	$0.25\lambda^2 f'_c A_{cr} \leq 1000\ \lambda^2 A_{cr}$
3	Concrete to concrete, cold joint – not intentionally roughened	0.6λ	2.2	$0.20\lambda^2 f'_c A_{cr} \leq 800\ \lambda^2 A_{cr}$
4	Concrete to steel	0.7λ	2.4	$0.20\lambda^2 f'_c A_{cr} \leq 800\ \lambda^2 A_{cr}$

2.3.3. PCI Design Handbook 7th Edition. Major changes were made to the shear-friction design provisions from the 6th Edition to the 7th Edition of the PCI Design Handbook. Tanner (Tanner, 2008) pointed out several mathematical anomalies associated with the calculation of μ_e (discussed further in Section 2.4). This prompted the changes made to the 7th Edition of the PCI Design Handbook. In addition to Equation 2.4 using the effective coefficient of friction, μ_e, given in Section 2.3.2, a new equation was introduced to determine the area of shear reinforcement using the coefficient of friction μ (similar to the ACI 318 approach discussed in Section 2.3.1). These equations are labeled as Equations 2.6 and 2.8, respectively (PCI Eq. 5-32b and 5-32a, respectively in the PCI Design Handbook 7th Edition). The calculation of μ_e was adjusted by the strength reduction factor ϕ as shown in Equation 2.7 (PCI Eq. 5-33).

$$A_{vf} = \frac{V_u}{\emptyset f_y \mu_e} \tag{2.6}$$

$$\mu_e = \frac{\emptyset 1000 \lambda A_{cr} \mu}{V_u} \tag{2.7}$$

$$A_{vf} = \frac{V_u}{\emptyset f_y \mu} \tag{2.8}$$

Another change made to this edition was limiting the use of Equation 2.6 to Cases 1 and 2, that is, the monolithic and roughened interface cases, respectively. Equation 2.6 shall not be used for Cases 3 and 4, that is, smooth interface and concrete to steel conditions. The values for μ_e in Table 2.2 have been removed. Lastly, it should be noted that the maximum value of V_u/ϕ is a function of λ instead of λ^2, as it was the case for the 6th edition. Table 2.2 summaries the shear-friction coefficients and maximum values for the PCI Design handbook 7th Edition.

Table 2.2 Shear-friction Coefficients in the PCI Design Handbook 7th Edition (2010)

Case	Crack interface condition	μ	Maximum μ_e	Maximum $V_n = V_u \emptyset$
1	Concrete to concrete, monolithic	1.4λ	3.4	$0.30\lambda f'_c A_{cr} \leq 1000\ \lambda A_{cr}$
2	Concrete to concrete, cold joint - roughened	1.0λ	2.9	$0.25\lambda f'_c A_{cr} \leq 1000\ \lambda A_{cr}$
3	Concrete to concrete, cold joint – not intentionally roughened	0.6λ	NA	$0.20\lambda f'_c A_{cr} \leq 800\ \lambda A_{cr}$
4	Concrete to steel	0.7λ	NA	$0.20\lambda f'_c A_{cr} \leq 800\ \lambda A_{cr}$

2.3.4. AASHTO LRFD Bridge Design Specifications 7ᵗʰ Edition. The main difference between the shear-friction design provisions in the AASHTO LRFD (2014) and the ACI and PCI provisions is the incorporation of a cohesion component into the design equations. This can be seen in calculating the nominal shear resistance of the interface plane V_{ni} given by Equation 2.9 (AASHTO Eq. 5.8.4.1-3), where c is the cohesion factor; A_{cv} is the area of concrete subjected to shear transfer; A_{vf} is the cross-sectional area of the interface reinforcement; μ is the friction factor, f_y is the yield stress of reinforcement limited to 60 ksi; and P_c is the permanent net compressive force normal to the shear plane.

$$V_{ni} = cA_{cv} + \mu(A_{vf}f_y + P_c) \tag{2.9}$$

The nominal shear resistance, V_{ni}, should not be larger than the lesser of $K_1f'_cA_{cv}$ or K_2A_{cv}, where K_1 is a fraction of concrete strength available to resist interface shear, K_2 is the limiting interface shear resistance, and A_{cv} is the area of concrete engaged in interface shear transfer. The values for K_1 and K_2 are specified in Table 2.3.

The AASHTO provisions also require a minimum cross-sectional area of interface reinforcement. This area A_{vf} is a function of the interface area A_{cv} and yield strength of reinforcement f_y used as shown in Equation 2.10 (AASHTO Eq. 5.8.4.4-1).

$$A_{vf} \geq \frac{0.05 * A_{cv}}{f_y} \tag{2.10}$$

While the AASHTO provisions account for the use of lightweight concrete, they do not differentiate between all-lightweight and sand-lightweight concrete when determining the coefficient of friction μ. This is also true for the cohesion factor. These factors are summarized in Table 2.3.

Table 2.3 Summary of AASHTO Cohesion and Friction Factors (2014)

Interface Condition	Cohesion Factor c (ksi)	Friction Factor μ	K_1, K_2 Factors
Normalweight concrete - monolithic	0.40	1.4	K_1=0.25 K_2=1.5 ksi
Lightweight concrete – monolithic or roughened	0.24	1.0	K_1=0.25 K_2=1.0 ksi
Normalweight concrete - roughened	0.24	1.0	K_1=0.25 K_2=1.5 ksi
Concrete placed against not intentionally roughened concrete	0.075	0.6	K_1=0.2 K_2=0.8 ksi

2.4. PREVIOUS STUDIES

This section summarizes previous studies on shear-friction in concrete related to this thesis work. These studies influenced the current shear-friction design provisions discussed in Section 2.3. These studies also helped to serve as the basis for designing the experiments discussed in Section 3.

2.4.1. Hanson. Research conducted by Hanson (Hanson, 1960) included push-off specimens as well as precast concrete T-girders to investigate the composite action in concrete members. Hanson tested 62 push-off specimens and 10 girders. The shear plane interface condition of the push-off specimens was varied from smooth to rough. The measured concrete strength varied but was not specifically considered in this study.

Both types of tests reported a maximum shear strength of 500 psi for a rough bonded surface and 300 psi for a smooth surface. In addition, Hanson proposed that roughly 175 psi of shear capacity can be added for each percent of shear reinforcement crossing the shear plane. The push-off specimens showed that the existence of keys used in combination with a rough interface did not change the strength of the connection. Results also indicated that the peak shear occurs at a slip of 0.005 in.

2.4.2. Birkeland and Birkeland. Birkeland and Birkeland (Birkeland and Birkeland, 1966) studied the application of shear-friction theory in precast concrete connections. Connections included elements such as corbels, ledger beams, and bearing shoes. In these types of connections the traditional provisions for shear-flexure and principal tension analysis are not applicable. The authors defined shear failure as slip along a crack, not as a tension crack in the usual sense. If shear reinforcement is provided, it experiences a tensile force providing an external clamping force across the interface. They described interface roughness as a frictionless series of fine saw tooth ramps. The authors explained the role of the interface condition based on the principles of the shear-friction hypothesis.

The authors described the ultimate shear capacity across the interface when reinforcement reaches its yield point as shown in Eq. 2.11:

$$Vu = Asfy\,tan(\theta) \tag{2.11}$$

where:

A_s = total cross-sectional area of reinforcing across the interface

f_y = yield strength of reinforcing ($\leq$ 60 ksi)

$tan\,\theta$ = 1.7 for monolithic concrete

         = 1.4 for artificially roughened construction joints

         = 0.8 to 1.0 for ordinary construction joints and for concrete to steel interfaces

Equation 2.11 is limited to a maximum reinforcing bar size of No. 6 or 1/2 in. diameter headed studs, a yield stress f_y of less than or equal to 60 ksi, and a concrete compressive strength f'_c greater than 4000 psi. The authors required that the reinforcement be anchored on both sides of the failure plane, in order to develop yield in steel. The concrete must well confined, providing sufficient amount of hoops. The authors also suggest subtracting any amount of external tension force from the clamping force. Lastly, the authors required the interface to be sound and free from any laitance, sawdust, paint or loose rust.

2.4.3. Mast. In 1968 Mast (Mast, 1968) studied the shear-friction theory. The author pointed out that because of fabrication and erection tolerances; there are no two identical connections. He also pointed out that addition stresses due to creep and shrinkage must be accounted for. A simple method based on a physical model was presented for the design of auxiliary reinforcement in concrete connections. Mast assumed that cracking had occurred in an unfavorable manner rather than trying to predict its nature. In Mast's model the shearing force was resisted by virtue of friction along the crack. The coefficient of friction may be quite high due to roughness of the surface. This roughness will result in a slight separation (dilation) of the two cracked pieces of concrete as shown in Figure 2.3. This slight separation can be resisted by reinforcement normal to the shear plane. The reinforcement experiences tensile stress which, in turn, provides compressive stress along the crack. The equation presented by Birkeland and Birkeland (1969) (Eq. 2.11) was capped with an upper limit of $0.15f'_c$ tan (θ) where the friction coefficient tan (θ) was expanded as follows:

$\tan(\theta)$ = 1.4 to 1.7 for a crack in monolithic concrete

= 1.4 for a rough interface between precast and cast-in-place concrete

= 1.0 for concrete cast against steel

= 0.7 for concrete against smooth concrete

This model did not include the strength of concrete or the effect of adhesion.
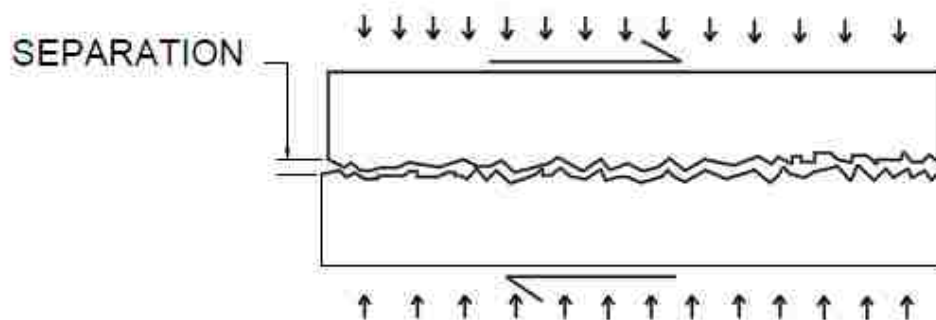
Figure 2.3 Separation Due to Slip According to Mast (1968)

2.4.4. Hofbeck, Ibrahim, Mattock. Hofbeck, Ibrahim, and Mattock (Hofbeck et al., 1969) tested 38 push-off specimens (shown in Figure 2.4) to study shear transfer in reinforced concrete elements such as in a precast beam and a cast-in-place slab. Some of the specimens were pre-cracked and some were not. This test set up provided the basis for push-off specimens of other researchers including Hoff (1993), Mattock (2001), Kahn and Mitchell (2002), and Shaw (2013).

This study concluded that the shear-friction theory provides conservative values for shear strength across initially cracked concrete, such as concrete cracked due to service loads or shrinkage. Their results indicate that if initial cracking is present, the slip will be greater at all stages of loading then for uncracked specimens. The initial crack also reduces the ultimate strength by a value of roughly 250 psi. There was no effect of changing the reinforcement ratio on shear strength. Dowel action did not contribute significantly to the shear transfer in initially uncracked specimens. However, the data indicated that there is a considerable contribution due to dowel action in initially cracked specimens.
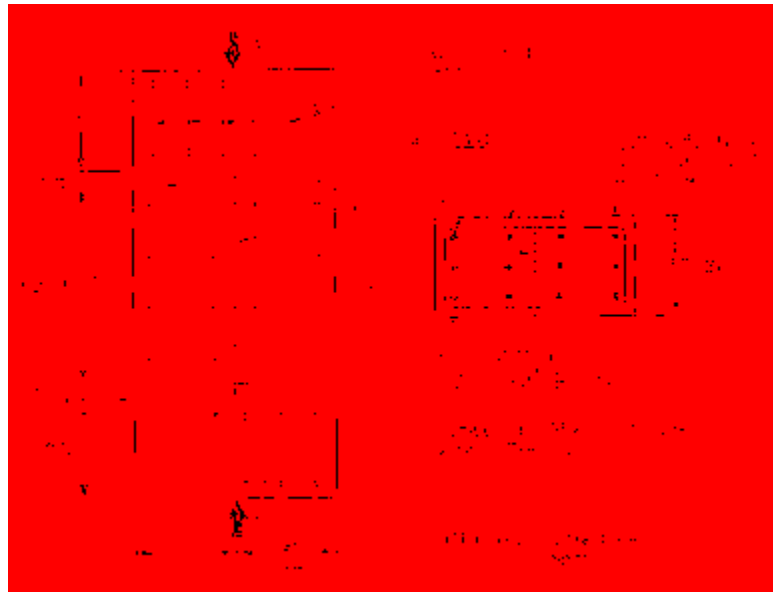
Figure 2.4 Detail of Push-off Specimen Used by Hofbeck, Ibrahim, Mattock (1969)

2.4.5. Mattock and Hawkins. Among the factors studied by Mattock and Hawkins (Mattock and Hawkins, 1972) were characteristics of the shear plane, characteristics of the reinforcement, concrete strength, and direct stresses acting parallel and transverse to the shear plane. Three variations of specimens (shown in Figure 2.5) were tested: standard push-off, pull-off, and push-off specimens with angled reinforcement. Pre-cracked and uncracked conditions were studied.

The first conclusion of this study verified the previously observed trend that the shear-friction provisions used at that time were conservative for shear strength in pre-cracked and uncracked shear planes. The authors also determined that a higher shear strength than the previously observed 800 psi can be developed with properly designed reinforcement. It was concluded that direct tension stresses parallel to the shear plane reduce the shear transfer strength of initially uncracked concrete but do not reduce the shear transfer strength of initially cracked concrete. Furthermore, the shear transfer strength of initially cracked concrete with a moderately reinforced shear plane is primarily due to the frictional resistance to sliding of the two faces of the crack and to the dowel action of the reinforcement across the crack. However, when large amounts of reinforcement or a sufficient external clamping force is present, the shear plane can "lock up", and the shear transfer strength is developed similarly to that of initially uncracked concrete. The authors found that for initially cracked concrete, there is an upper limit for $\rho_v f_y$ set by the concrete strength. Below this limit, the relationship between the shear strength v_u and $\rho_v f_y$ is independent of concrete compressive strength. On the other hand, above this limit of $\rho_v f_y$, the shear strength increases at much slower rate for lower strength concrete and is equal to that of similarly reinforced, initially uncracked concrete.

Mattock and Hawkins also proposed an equation, given in Eq. 2.12, that accounts for the effect of cohesion. The value of 200 in Eq. 2.12 accounts for the cohesion across the interface, and this term is referred to as asperity shear. The term σ_{nx} refers to externally applied direct stress acting across the shear plane.

$$v_u = 200 + 0.8(\rho_v f_y + \sigma_{nx}) \tag{2.12}$$
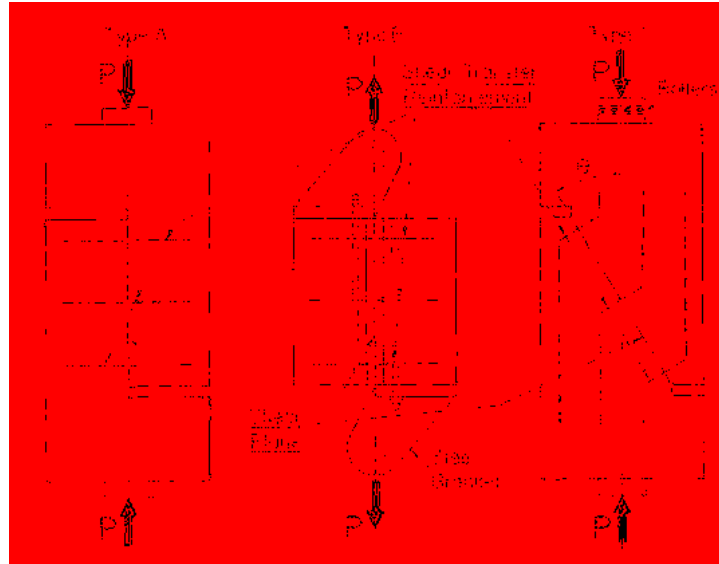
Figure 2.5 From Left: Push-off, Pull-off, and Modified Pull-off Specimens Used by
Mattock and Hawkins (1972)

2.4.6. Mattock. Mattock (Mattock, 1974) studied the shear transfer across a plane
with an inclined and orthogonal array of reinforcement. Twenty-three push-off specimens
were tested, and about 15 of those were pre-cracked. Specimens were made out of 4000
psi concrete and No. 3 reinforcing steel bars with the actual yield point of approximately
50 ksi. The experimental work focused on single direction loading only.

Mattock concluded that the shear transfer behavior hypothesis for both initially
cracked and uncracked concrete with reinforcement normal to the shear plane can be
extended to orthogonal reinforcement or the parallel reinforcement inclined at any angle
to the shear plane, if the component of the bar forces parallel to the shear plane is also
taken into account in calculating shear resistance.

It was discovered that for a given normal spacing of reinforcing bars, the
maximum ultimate shear transfer stress occurs when bars are inclined at roughly 110
degrees to the shear plane. However, Mattock's calculations yield that for constant bar
spacing and varied angle, the highest shear stress was achieved at angle of 135 degrees.

2.4.7. Mattock, Johal, Chow. The study by Mattock, Johal, and Chow (Mattock et al., 1975) examined the effect of normal force and moment in the shear plane on single direction shear transfer strength. Two types of specimens were tested: typical push-off specimens and corbel type push-off specimens shown in Figure 2.6. The target compressive strength of concrete was 4000 psi, and the yield strength of reinforcement was reported as 53 ksi.

It was concluded that simultaneous action of moment that is less than or equal to the flexural ultimate strength of the cracked section does not reduce the shear strength across the shear plane. To effectively transfer shear and moment across the plane, the reinforcement should be located in flexural tension zone. The authors suggested that it is appropriate to add the normal stress from the bending moment, σ_{nx}, to the reinforcement parameter ρf_y when calculating shear transfer strength. It was also found that tension across the shear plane reduces the shear transfer strength equal to a reduction of shear reinforcement parameter ρf_y due to tensile stress. This study also found that equations proposed by Birkeland (Eq. 2.13) and Mattock (Eq. 2.14) to be both applicable and economical.

$$v_u = 33.5\sqrt{\rho f_y} \tag{2.13}$$

$$v_u = 400 + 0.8\rho f_y \geq 0.3f'_c \tag{2.14}$$

where v_u is the nominal ultimate shear strength in psi, f_y is the yield stress of reinforcement, ρ is defined as the ratio of area of shear-friction reinforcement to the area of shear plane, and f'_c is the compressive strength of concrete.
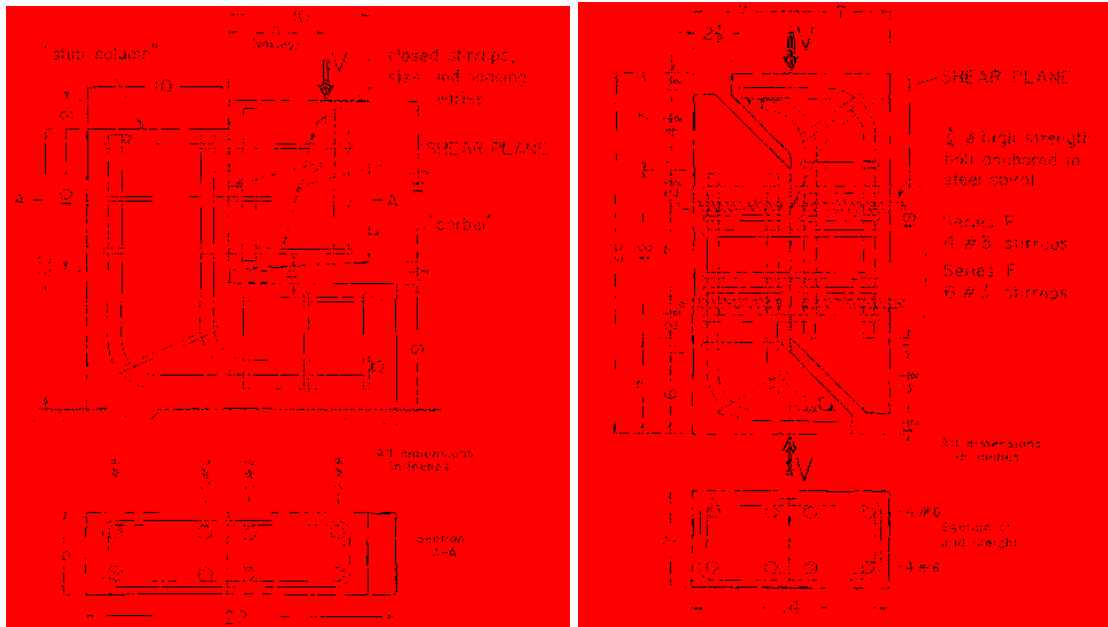
Figure 2.6 Corbel Type Push-off Specimen (left), Typical Push-off Specimen (right)

2.4.8. Mattock, Li, Wang. Mattock, Li, and Wang studied the effects of lightweight aggregate on the shear-transfer strength. Push-off specimens with a shear plane area of 50 in^2 were used for this research. The types of aggregates used were natural gravel and sand, rounded lightweight aggregate, crushed angular lightweight aggregate, and sand-lightweight aggregate. It was a common practice in 1960's and 1970's to pretreat (coat) the lightweight aggregate with a "waterproofing" chemical to prevent excessive bleeding and to reduce the amount of shrinkage, and so some of the lightweight aggregate was coated. The type of lightweight aggregate was not specified. Concrete compressive strength ranged from 2500 psi to 6000 psi.

On the basis of this study the authors concluded that the shear-transfer strength of lightweight aggregate is less than that of normalweight concrete of the same compressive strength. The coating of lightweight aggregate did not significantly affect the shear transfer strength. The authors suggested a multiplier to be used with the ACI 318-71 shear-friction provions to account for the influence of lightweight aggregate on the shear strength. This multiplier had a value of 0.75 for all-lightweight (>92 pcf) and 0.85

for sand-lightweight concrete (>105 pcf). Two equations for shear strength were

provided. The sand-lightweight equation is given in Eq. 2.15:

$$v_u = 0.8\rho\, f_y + 250\text{psi} \;<\; 0.2\text{f'}_c \text{ or } 1000\text{psi} \tag{2.15}$$

where v_u is the ultimate shear stress, ρ is the shear-friction reinforcement ratio but not to

be taken less than 200 psi, f_y is defined as the yield stress of the reinforcing bars crossing

the shear plane, and f'_c is taken to be the compressive strength of concrete.

The all-lightweight concrete equation is given in Eq. 2.16:

$$v_u = 0.8\rho\, f_y + 200\text{psi} \;\leq\; 0.2\text{f'}_c \text{ or } 800\text{psi} \tag{2.16}$$

2.4.9. Shaikh. Shaikh (Shaikh, 1978) addressed the conservatism of the shear-

friction concept relative to the research data provided before 1978. Shaikh proposed

revisions to equations for the PCI Design Manual. His research focused on both

normalweight and lightweight concretes. Another test variable was the interface

condition of the shear plane. The shear reinforcement normal to the plane can be

calculated by Eq. 2.17:

$$A_{vf} = \frac{V_u}{\phi\, f_y \mu_e} \tag{2.17}$$

where A_{vf} is the area of reinforcement crossing the shear plane, f_y is the yield stress of

reinforcement, and V_u is the ultimate shear stress.

The term μ_e is the effective coefficient of friction calculated using Equation 2.18:

$$\mu_e = \frac{1000 C_s^2 \mu}{v_u} \tag{2.18}$$

In Eq. 2.18, C_s is a constant used to account for the effect of concrete density (1.0 for

normalweight, 0.85 for sand-lightweight, 0.75 for all-lightweight concrete). Shaikh proposed

values for the coefficient of friction μ for lightweight concrete that ranged from 0.4 for cold

joint smooth interface to 1.4 for monolithic concrete. This equation was based on previous studies by Birkeland (1968), Mattock (1974), and Raths (1977). Shaikh proposed limits for shear-friction coefficient μ and maximum shear stress values, v_u, for various interface conditions. These proposed values and limits are similar to those implemented by the ACI 318 code (2011 and 2014) and the PCI Design Handbook (2004 and 2010). The proposed values are summarized in Table 2.4.

Table 2.4 Shear-friction Coefficients, μ, and Maximum Shear Stress Values, v_u, as Proposed by Shaikh

Crack Interface Condition	Recommended μ	Maximum v_u (psi)
Concrete to concrete, cast monolithically	1.4	$0.30f'_cC^2_s \le 1200C^2_s$
Concrete to hardened concrete, 1/4 in. roughness	1.0	$0.25f'_cC^2_s \le 1000C^2_s$
Concrete to concrete, smooth interface	0.4	$0.15f'_cC^2_s \le 600C^2_s$
Concrete to steel	0.6	$0.20f'_cC^2_s \le 800C^2_s$

2.4.10. Hsu, Mau, Chen. This study focuses on initially uncracked push-off specimens. Hsu, Mau, and Chen (Hsu et al., 1987) identified a critical zone in the vicinity of a shear plane where a uniform stress distribution is assumed after the formation of the crack. A truss model is used to establish their theory that incorporates a softened compression stress-strain relation along the concrete struts. A key finding of their research was the realization that not only does the reinforcement crossing the shear plane effect the strength but also the parallel reinforcement contributes to shear transfer strength. The conclusion of this research was that the ACI 318 Code shear-friction provisions may not be conservative based on this truss model due to small amounts of reinforcement parallel to the shear plane in design compared to heavily reinforced test specimens.

2.4.11. Loov and Patnaik. The study by Loov and Patnaik (Loov and Patnaik, 1994) focused on 16 composite concrete beams to develop a more consistent limit of shear strength, v_n, by replacing the five equations provided by the ACI 318 Code to prescribe the limiting horizontal shear stress for different amount of reinforcing steel with one parabolic equation. This parabolic equation was derived by modifying the equation presented in the PCI Design Handbook. This new equation combines the effect of concrete strength and clamping force. The horizontal shear strength of composite beams without stirrups was approximated as:

$$v_{no} = 0.6\sqrt{15f'_c} \ (psi) \tag{2.19}$$

where v_{no} is the ultimate shear strength of an interface without stirrups, and f'$_c$ is the compressive strength of concrete.

The authors suggested a general equation to provide a continuous curve as given in Eq. 2.20:

$$v_n = k\lambda\sqrt{(15 + \rho_v f_y)f'_c} \leq 0.25f'_c \ (psi) \tag{2.20}$$

where v_n is the nominal shear strength, f'$_c$ is the compressive strength of concrete, ρ_v is the steel ratio of shear-friction reinforcement, and f$_y$ is the specified yield strength of reinforcement.

With k=0.6, Equation 2.20 provides good lower bound for range of concrete compressive strength from 2500 psi to 7000 psi. For higher clamping forces the additive term (15 psi) becomes negligible. This general equation is applicable to both all-lightweight and sand-lightweight concrete and results in designs with less stirrup reinforcing for concrete strengths higher than 4350 psi compared to designs that used the ACI 318-92 equations. The authors concluded that elastic analysis using cracked transform section properties appears to be the easiest and most practical way of estimating the horizontal shear stress. It was discovered that an as-cast concrete surface with aggregate protruding from the surface can alone develop sufficient horizontal shear resistance. Similarly, it was

concluded that slip and stirrup stresses are insignificant until beams reached a horizontal shear stress of 220 psi to 290 psi.

2.4.12. Mattock. Shear transfer behavior of high strength normalweight concrete of cracked and uncracked interface was examined in Mattock's study (Mattock, 2001). The problem at hand was that the ACI 318-99 code used the simple shear-friction theory that did not allow to take full advantage of high-strength concrete properties. Interface condition was also considered in this study. Non-monolithic roughened and smooth specimens were examined. A lower bound shear transfer condition was achieved by pre-cracking of the interface. Simple equations were set forth for shear-friction design that allow the full potential shear transfer strength of all compressive strengths of concrete to be utilized.

2.4.13. Kahn and Mitchell. Kahn and Mitchell (Kahn and Mitchell, 2002) conducted experiments on 50 push-off specimens with a shear plane area of 60 in^2. The goal was to expand the applicability of shear-friction provisions to high-strength normalweight concrete. Concrete strengths varied from 6800 psi to 17900 psi with reinforcement ratio variation from 0.37% to 1.47%. Interface condition was also varied; uncracked, initially pre-cracked, and cold joint. The load was applied concentrically to the shear plane. The load was applied continuously until a slip of 1/4 in. was achieved. Initial cracking was observed at 50% to 75% of the ultimate load. In case of the slip governing the test, the ultimate load was defined as the load resulting in slip of 0.2 in. It was concluded that the ACI 318-99 code shear-friction provisions provide a conservative estimate for the interface-shear strength for high-strength concrete. The equation proposed in Eq. 2.20 included a frictional coefficient μ=1.4 and a cohesion component 0.05 f'$_c$. This equation predicted the results more closely compared to previous provisions.

$$v_n = 0.05 f'_c + 1.4 \rho_v f_y \leq 0.2 f'_c \, (\text{psi}) \qquad (2.20)$$

where v_n is the nominal shear stress, f'$_c$ is the concrete compressive strength, ρ_v is the shear-friction reinforcement ratio, and f$_y$ is the yield stress of reinforcement.

It was recommended that the upper limit of 800 psi be eliminated and replaced with 20 percent of the compressive strength of concrete at 28 days. It was also recommended that the value of f_y be limited to 60 ksi in order to limit the slip along smooth cracks.

2.4.14. Tanner. The work conducted by Tanner (Tanner, 2008) examined the evolution of formulas used in calculating the effective coefficient of friction μ_e in the PCI Design Handbook. The author pointed out the inconsistencies in calculating the effective coefficient of friction in the 4th, 5th, and 6th Editions of the PCI Design Handbook. Tanner showed that the 6th Edition was based on the factored shear demand (V_u) instead of nominal shear strength (V_n). This change was inconsistent with the original test data used for the development of the equation. He pointed out that the ϕ factor and the load factor further exaggerate this problem. Tanner also showed that there is misunderstanding in the lightweight modification factor λ. He showed that in the PCI Design Handbook 6th Edition, the calculation for μ_e (the effective coefficient of friction) is not clearly defined with respect to λ. The previous edition calculates μ_e using a single λ term on pages 4-55 and 4-62 of the handbook, while on page 4-36 it is calculated using the λ^2 term.

2.4.15. Scott. Scott (Scott, 2010) tested 36 push-off specimens (shown in Figure 2.7) to determine if the AASHTO LRFD Specification (4th Edition) equations accurately predict the horizontal shear strength of precast concrete girders and cast-in-place concrete decks for normalweight and lightweight concrete (expanded slate manufactured by Stalite Lightweight Aggregate). The test variables were concrete unit weight used for the girder/slab combination and the amount of shear reinforcement provided across the interface.
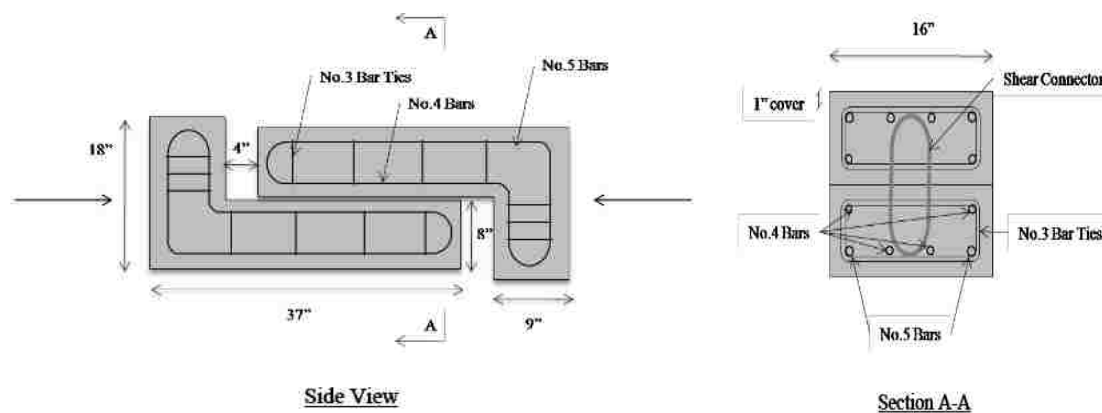
Figure 2.7 Details of Specimens used by Scott (Scott, 2010)

The results from the push-off specimens indicated that the AASHTO LRFD design equations conservatively predict interface horizontal shear strength. The lightweight concrete predictions were more conservative than the normalweight concrete predictions. The average post-cracking strength was higher for normalweight specimens than lightweight concrete specimens. Specimens without horizontal shear reinforcement had a slightly higher post-cracking interface strength when lightweight concrete was used. It was validated that the yield strength of reinforcement crossing the shear plane should be used in calculation of the shear strength. As the amount of shear reinforcement increased, the ratio of the tested horizontal shear strength to the AASHTO LRFD calculated strength decreased. This trend was more dominant in lightweight concrete specimens.

2.4.16. Shaw. Shaw (Shaw, 2013) examined the influence of concrete unit weight on the direct shear transfer across an interface of concretes cast at different times. He tested 36 push-off specimens with a cold joint interface cast using expanded shale aggregate provided by Buildex. The test variables were unit weight of concrete, compressive strength of concrete, and interface preparation (i.e., intentionally roughened or smooth). Reinforcement ratio was held constant for this study.

Shaw concluded that the unit weight of concrete did not play a significant role in the interface shear strength for cold joint specimens. He determined that the ACI 318-11 and PCI Design Handbook (2011) provisions using μ are conservative for both sand-

lightweight and all-lightweight concrete specimens. He also determined that values of μ_e in the PCI Design Handbook are conservative for both roughened and smooth cold joint interface conditions. Shaw also concluded that λ, the lightweight modification factor used in calculation for the effective coefficient of friction μ_e, was conservative for sand-lightweight and all-lightweight concrete specimens.

It was concluded that specimens with same interface condition and concrete compressive strength had similar shear strength, v_u, regardless of concrete unit weight. The shear strength of specimens with smooth interface depended on concrete compressive strength. This was not true for roughened specimens, where increasing the compressive strength increased the shear transfer strength. Residual shear strength was insensitive to the variables tested: concrete type, compressive strength, and interface condition.

3. EXPERIMENTAL PROGRAM

3.1. INTRODUCTION

This section describes the experimental program and includes materials used, specimen design, specimen assembly, test setup, and test results. Test results are presented in terms of shear strength, shear stress, slip of shear plane, dilation of shear plane, and strain in the reinforcing bars crossing the shear plane. Analysis and discussion of results are presented in Section 4 of this thesis.

3.2. SPECIMEN DESIGN

Specimens were designed similar to previous research studies to allow the direct comparison of test results. A total of 28 push-off type specimens were constructed in the portion of the experimental program presented in this thesis. This allowed the investigation of direct shear transfer of different types of concrete with different interface conditions. Specimen designation notation is explained in Figure 3.1. The test variables included lightweight aggregate type (expanded shale, expanded slate, or expanded clay), concrete type (normalweight, sand-lightweight, or all-lightweight), casting procedure (monolithic or cold joint), and interface condition (uncracked, pre-cracked, roughened, or smooth). The test matrix is summarized in Table 3.1. The normalweight concrete and shale lightweight aggregate concrete specimens were cast monolithically. The pre-cracking condition is described in Section 3.5.3. These specimens were then either pre-cracked prior to testing or left uncracked. The slate and clay lightweight aggregate specimens were constructed of sand-lightweight or all-lightweight concrete and had a cold joint interface that was either roughened or smooth. All specimens had the same target compressive strength of concrete (5000 psi) and the same reinforcement ratio (0.013).
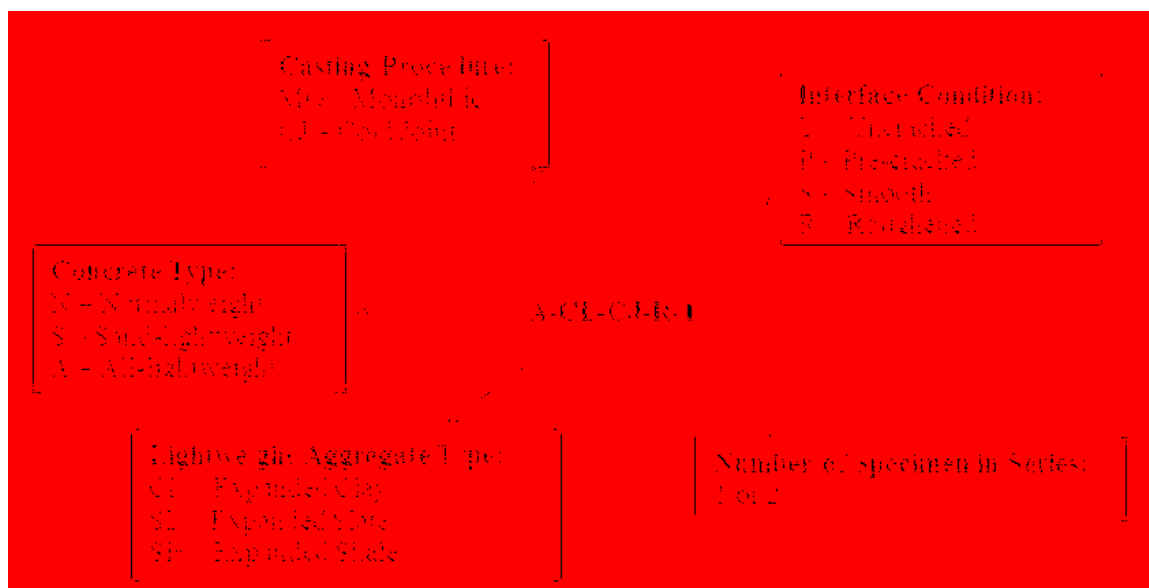
Figure 3.1 Specimen Designation Notation

Table 3.1 Test Matrix

Concrete Type	Lightweight Aggregate Type	Casting Procedure and Condition	Series Designation	Reinforcement Ratio	Number of Specimens
Normalweight	N/A	Monolithic – Uncracked	N-MO-U	0.013	2
		Monolithic – Pre-cracked	N-MO-P	0.013	2
Sand-Lightweight	Shale	Monolithic – Uncracked	S-SH-MO-U	0.013	2
		Monolithic – Pre-cracked	S-SH-MO-P	0.013	2
	Slate	Cold Joint – Roughened	S-SL-CJ-R	0.013	2
		Cold Joint – Smooth	S-SL-CJ-S	0.013	2
	Clay	Cold Joint – Roughened	S-CL-CJ-R	0.013	2
		Cold Joint – Smooth	S-CL-CJ-S	0.013	2
All-Lightweight	Shale	Monolithic – Uncracked	A-SH-MO-U	0.013	2
		Monolithic – Pre-cracked	A-SH-MO-P	0.013	2
	Slate	Cold Joint – Roughened	A-SL-CJ-R	0.013	2
		Cold Joint – Smooth	A-SL-CJ-S	0.013	2
	Clay	Cold Joint – Roughened	A-CL-CJ-R	0.013	2
		Cold Joint – Smooth	A-CL-CJ-S	0.013	2

3.3. MATERIALS

The main materials used for this research were concrete and reinforcing steel. Concrete types used were: normalweight concrete, sand-lightweight concrete, and all-lightweight concrete. Aggregates used to achieve these types of concrete are described in Section 3.3.1. Concrete mixture designs used to achieve the target compressive strength of 5000 psi are summarized in Section 3.3.2. Lastly, information about the reinforcing steel used in this study is presented in Section 3.3.3.

3.3.1. Aggregates. This section discusses the aggregates used in this research.

3.3.1.1 Normalweight aggregates. Normalweight aggregates were used to cast concrete with a unit weight in range of 145 to 150 pcf. The coarse aggregate used was crushed dolomite from the Jefferson City formation readily available in Missouri. Natural river sand was used as fines. The coarse aggregate gradation used was 100% passing the 1 in. sieve and less than 5% passing the No. 8 sieve. The fine aggregate gradation used was 100% passing No. 4 sieve and less than 1% retained on No. 200 sieve.

3.3.1.2 Lightweight aggregates. Expanded shale, expanded slate, and expanded clay were used for the lightweight concrete mixtures. Expanded shale was produced by Buildex in New Market, Missouri. Expanded slate was manufactured by STALITE in Gold Hill, North Carolina. Expanded clay was produced by Big River Industries in Livingston, Alabama. Figure 3.2 shows a photo of the expanded shale, expanded slate, and expanded clay aggregates from left to right. Aggregates used for the sand-lightweight concrete are shown in the top row of the figure. The expanded shale provided was pre-mixed (blend of coarse and fine aggregates produced by Buildex) in the case of aggregate used to achieve the all-lightweight concrete (bottom left). Expanded slate and clay provided were separated into coarse and fine aggregates. A sieve analysis was performed on the expanded slate and expanded clay aggregates, and a mixture of coarse and fine aggregates was designed such that the resulting gradation would be similar to that of the pre-mixed expanded shale aggregate. These gradations are discussed in the following sections.

Figure 3.2 From Left to Right: Expanded Shale, Expanded Slate, Expanded Clay. Coarse
Aggregates Top Row, Fine Aggregates Bottom Row

3.3.1.2.1 <u>Expanded shale aggregates.</u> The expanded shale coarse aggregate
gradation used in the production of the sand-lightweight concrete mixture was 3/8 in. x
No. 8 sieve. The all-lightweight aggregate gradation was 3/8 in. x No. 0. These
gradations are summarized in Table 3.2. The expanded shale aggregate had a density of
44 pcf for the 3/8 in. to No. 8 gradation and 54 pcf for the 3/8 in. to No. 0 gradation. Bulk
specific gravity provided by the manufacturer was 1.30 for the 3/8 in. to No. 8 gradation
and 1.45 for the 3/8 in. to No. 0 gradation.

Table 3.2 Expanded Shale Aggregate Gradations (Buildex)

	Sieve Designation	Percent Retained		Percent Passing	
		Gradation	Specification[1]	Gradation	Specification[1]
3/8 in. x No. 8 Gradation	1/2 in.	0	0	100	100
	3/8 in.	1	0-20	99	80-100
	No. 4	82	60-95	18	5-40
	No. 8	99	80-100	1	0-20
	No. 16	99	90-100	1	0-10
3/8 in. x No. 0 Gradation	1/2 in.	0	0	100	100
	3/8 in.	0	0-10	100	90-100
	No. 4	13	10-35	87	65-90
	No. 8	49	35-65	51	35-65
	No. 16	67	-	33	-
	No. 30	79	-	21	-
	No. 50	86	75-90	14	10-25
	No. 100	93	85-95	7	5-15

[1]ASTM C330

3.3.1.2.2 Expanded clay aggregates. The expanded clay coarse aggregate had a gradation shown in Table 3.3. The fine aggregate gradation is shown in Table 3.4. For the sand-lightweight concrete mixture, only the coarse aggregate was used. For the all-lightweight concrete mixture, a mixture consisting of 55% of coarse aggregate by weight and 45% of fine aggregate by weight was used so that it was similar to the expanded shale pre-mixed gradation. The expanded clay aggregate was the lightest of the aggregates used in this research. In fact, it was observed that some of the saturated clay aggregate floated in water. The loose bulk density of the expanded clay coarse aggregate was 33 lb/ft^3 and 40 lb/ft^3 for the expanded clay fine aggregate (ASTM C29-2009). These properties are summarized in Table 3.5.

Table 3.3 Expanded Clay Coarse Aggregate Gradation (Big River Industries)

Sieve Designation	Percent Passing
½ in.	100
3/8 in.	99.9
No. 4	41.8
No. 8	7.9
No. 16	2.0
No. 50	1.1
No. 100	0.9
No. 200	0.7

Table 3.4 Expanded Clay Fine Aggregate Gradation (Big River Industries)

Sieve Designation	Percent Retained Each Sieve	Percent Range Suggested[1]
3/8 in.	0	0-2
No. 4	0	0-10
No. 8	9.2	15-35
No. 16	21.5	15-35
No. 30	23.4	5-20
No. 50	15.7	5-15
No. 100	10.6	5-15
Pan	19.4	8-20

[1]ASTM C330

Table 3.5 Properties of Expanded Clay Aggregate (Big River Industries)

Expanded Clay	Bulk Density – Loose (lb/ft^3)	Specific Gravity – SSD[1]	Specific Gravity – OD[2]
Coarse Aggregate	33	1.03	1.01
Fine Aggregate	40	1.42	0.98

[1] SSD – Saturated Surface Dry

[2] OD – Oven Dry

3.3.1.2.3 <u>Expanded slate aggregates.</u> The expanded slate coarse and fine aggregates had gradations shown in Table 3.6. It was determined that a mixture of 30% coarse and 70% MS16 Fines would produce a gradation similar to that of the expanded shale gradation. The bulk loose densities of the expanded shale coarse and fine aggregate were 52 lb/ft^3 and 60 lb/ft^3, respectively (ASTM C29-2009). Values of the dry specific gravity of the expanded shale coarse and fine aggregates were 1.54 and 1.69, respectively.

Table 3.6 Expanded Slate Gradations (STALITE)

	3/8 in.	MS16 Fines (#4-0)
Sieve Designation	**Percent Passing**	**Percent Passing**
1/2 in	100	100
3/8 in	80-100	100
No. 4	5-40	97-100
No. 8	0-20	89-100
No. 16	0-10	46-66
No. 30	-	28-41
No. 50	-	17-25
No. 100	-	8-16

3.3.1.2.4 <u>**Lightweight aggregate saturation procedure.**</u> Lightweight aggregates are capable of high water absorption. This is due to the manufacturing process of being heated to high temperatures during which the aggregates expand and create a complex capillary void structure. Due to this phenomenon it is necessary to saturate lightweight aggregates prior to batching. It is usually most desirable to bring the aggregate to saturated surface dry condition (SSD). This, however, is difficult to achieve on a large scale. Instead, it is common practice for batching plants to soak lightweight aggregate with soaker hoses for a period of time prior to batching.

To achieve adequate and uniform saturation in this experimental work, a saturation tank was created by cutting off the top of a 1000 lbs liquid storage tank with a valve near the bottom. A strainer was used to catch any particles larger than 1/16 in. by gluing a piece of metal mesh over the valve opening. The tank is shown in Figure 3.3. Two days prior to batching, the tank was filled with the required amount of lightweight aggregate. Then it was filled with water until the water level was about 2 in. above the aggregate. This was to provide a water level sufficient to cover all aggregate for the duration of soaking. The tank was then allowed to sit undisturbed for 48 hours. After the 48 hour period the tank was drained using the built-in valve. The outflow of the tank was passed over a No. 100 and No. 200 sieve to retain all fines. These fines were then returned back to the tank. The saturating procedure was identical for all lightweight aggregates.

Figure 3.3 Tank Used for Lightweight Aggregate Saturation

3.3.2. Concrete Mixtures. The concrete mixtures were designed with the help from the lightweight aggregate manufacturers. The concrete mixtures were verified by numerous trial batches to achieve the target plastic and hardened properties. The target compressive strength of 5000 psi was desirable, but concretes approximately 500 psi of the target compressive strength were accepted. Low slump (~2 in.) was desired due to the nature of a "step-like" placement in the formwork. All concrete mixtures were composed of portland cement (Type I/II), water, coarse aggregates, and fine aggregates. No chemical additives were used in the concrete mixtures. The normalweight concrete mixture met the ASTM C33 (2013) specification requirements. All of the lightweight concrete mixtures met the requirements set forth by the ASTM C330 (2014) specification. All concrete mixtures were batched, mixed, and placed in the Concrete Materials Laboratory in Butler-Carlton Hall at Missouri S&T. Mixing was performed using a 6-cubic foot rotary drum mixer shown in Figure 3.4. Mixture proportions are summarized in Table 3.7 and discussed in subsequent Sections 3.3.2.1, 3.3.2.2, and 3.3.2.3.

The plastic and hardened concrete properties of the final mixture designs used for specimen casting are summarized in Table 3.8 and Table 3.9, respectively. Slump of concrete mixtures was determined following steps of ASTM C143 (2015). Density and

air content of the concrete mixtures were measured according to ASTM C138 (2014).
Unit weight of fresh concrete mixtures was measured and reported. Due to the capillary
nature of lightweight aggregate, using pressure air meter is not recommended. To
determine the air content of lightweight concrete mixtures, the ASTM C173 (2014) –
volumetric method was used. The concrete compressive strength of each batch was
measured at 3, 7, 14, 21, and 28 days. Compressive strength, splitting tensile strength,
and modulus of elasticity were determined at test day, which for this research was 28
days after casting the specimen. The compressive strength was determined according to
ASTM C39 (2015) using a minimum of three 4 in. by 8 in. cylinders. The splitting tensile
strength was determined using a minimum of one cylinder according to ASTM C496
(2011). Figure 3.5 and Figure 3.6 show the equipment used for determining the above
mentioned properties.

Table 3.7 Concrete Mixture Proportions

Concrete Type	Lightweight Aggregate Type	Mixture Design Quantities (lb/yd^3)				
		Coarse Aggregate	Fine Aggregate	Water	Cement[5]	w/c
Normalweight[1]	N/A	1728	1302	305	517	0.59
Sand-lightweight[2]	Shale	834	1498	281	535	0.53
	Slate	975	1125	265	530	0.50
	Clay	692	1251	263	612	0.43
All-lightweight[3]	Shale[4]	1885		260	610	0.43
	Slate	528	1233	378	801	0.47
	Clay	692	556	263	796	0.46

[1] Normalweight concrete coarse and fine aggregate satisfied ASTM C33 specification

[2] Sand-lightweight concrete coarse aggregate were ASTM C330, and fine aggregate were ASTM
C33

[3] All-lightweight concrete coarse and fine aggregate satisfied ASTM C330

[4] All-lightweight expanded shale aggregate was premixed by the manufacturer

[5]Type I/II cement was used

Table 3.8 Plastic Concrete Properties

Concrete Type	Lightweight Aggregate Type	Density (lb/ft^3)	Air (%)	Slump (in.)
Normalweight	N/A	148	2.5	5.5
Sand-lightweight	Shale	117	2	2.5
	Slate	117	1.5	2
	Clay	105	2.5	1.25
All-lightweight	Shale	108	3	2.5
	Slate	106	3.5	6.5
	Clay	88	4	0.5

Table 3.9 Hardened Concrete Properties

Concrete Type	28-Day Compressive Strength (psi)	Splitting Tensile Strength (psi)	Modulus of Elasticity (psi)
N-MO	4840	420	3.90 x 10^6
S-SH-MO	4770	460	3.30 x 10^6
A-SH-MO	4700	515	2.65 x 10^6
S-SL-CJ	5570	570	3.50 x 10^6
A-SL-CJ	4380	420	2.45 x 10^6
S-CL-CJ	4640	360	2.65 x 10^6
A-CL-CJ	4460	405	1.70 x 10^6
Standard Deviation	361	66	0.68 x 10^6

Figure 3.4 Six Cubic Foot Rotary Drum Mixer

Figure 3.5 Modulus of Elasticity Yoke, Brass Volumetric Meter, and Pressure Meter
(from left to right)

Figure 3.6 Cylinder Compressive Strength Test (left), Splitting Tensile Strength Test (right)

3.3.2.1 Normalweight concrete. The normalweight concrete mixture was designed with a target compressive strength of 5000 psi. Normalweight coarse aggregate used in this mixture was crushed dolomite, and fine aggregate was natural river sand. Both aggregates conformed to ASTM C33. The water cement ratio was 0.59. Mixture proportions are summarized in Table 3.7. Plastic and hardened properties achieved are summarized in Table 3.8 and Table 3.9, respectively.

3.3.2.2 Sand-lightweight concrete. The sand-lightweight concrete mixtures were designed with a target compressive strength of 5000 psi. The sand-lightweight concretes were made of lightweight coarse aggregates conforming ASTM C330 and natural river sand conforming ASTM C33. The desired density for sand-lightweight concrete was 115 lb/ft^3. Sand-lightweight concrete mixture proportions are summarized in Table 3.7. These proportions were developed with the guidance of the lightweight aggregate producers, but extensive trial batching was necessary to achieve the desired properties presented in Tables 3.8 and 3.9.

3.3.2.3 All-lightweight concrete. The all-lightweight concrete mixtures were designed with a target compressive strength of 5000 psi. To achieve the all-lightweight concretes, normalweight coarse and fine aggregates were replaced with lightweight aggregates. Unit weight of fresh all-lightweight aggregate concrete largely depends on unit weight of lightweight aggregate used. Concrete mixture proportions for the all-

lightweight concretes were developed with the guidance of the producers of each aggregate. Mixture proportions are summarized in Table 3.7, while plastic and hardened properties achieved are summarized in Table 3.8 and Table 3.9, respectively.

3.3.3. Reinforcing Steel Bars. Deformed reinforcing steel bars were provided for this research by Ambassador Steel Corporation. The bars were ASTM A615 Grade 60. All bars of the same size used in this study were supplied from the same heat. Mill certifications were provided upon shipment for quality assurance purposes. The mill certifications stated that the yield stress was 73,865 psi for the No. 3 bars and 65,818 psi for the No. 5 bars. Properties reported by the manufacturer were verified by conducting tensile tests according to ASTM A370. Strain was measured using strain gages described in Section 3.5.5.2. The strain readings were also verified using an 8 in. extensometer that was removed from the tensile coupon upon yielding.

The average yield stress of the No. 3 and No. 5 bars were 72,185 psi and 70,695 psi, respectively. The average ultimate stress of the No. 3 bars was 101,055 psi, while the average ultimate stress of the No. 5 bars was 102,390 psi. Representative stress-strain curves for the No. 3 and No. 5 bars are shown in Figure 3.7. A summary of the tensile test results is presented in Table 3.10. It should be noted that for Specimen 3-1, the extensometer slipped upon loading and damaged the strain gage as well. Therefore only the peak stress was obtained for this specimen.
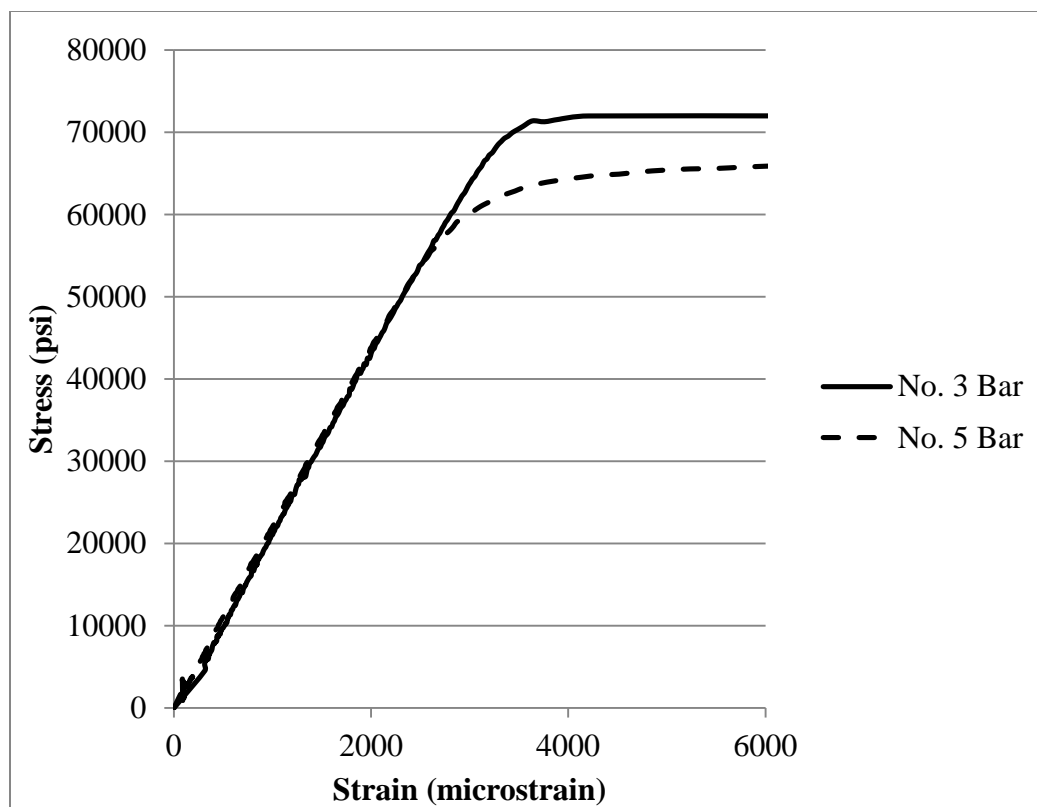
Figure 3.7 Representative Stress vs. Strain Plot for Steel Reinforcing Bars Used in This
Study

Table 3.10 Measured Reinforcing Steel Bar Properties

Tensile Specimen ID	Bar Size	Yield Stress (psi)	Peak Stress (psi)	Modulus of Elasticity (psi)
3-1	No. 3	NA	100,870	NA
3-2	No. 3	72,200	101,110	32,040,000
3-3	No. 3	72,165	100,995	28,466,000
Average		72,185	101,055	30,253,000
5-1	No. 5	70,700	102,750	27,437,000
5-2	No. 5	70,470	102,555	28,021,000
5-3	No. 5	70,915	101,870	28,871,000
Average		70,695	102,390	28,110,000

3.4. SPECIMEN FABRICATION

Specimens were fabricated during the spring of 2015. A total of 54 specimens, 28 of which are presented in this thesis, were constructed and tested including two practice specimens – one cold joint and one monolithic.

3.4.1. Reinforcing Steel Bar Cage Preparation. Reinforcing steel bars were bent and the cages were assembled in the High Bay Structural Engineering Research Laboratory at Missouri S&T. Reinforcing bars properties are discussed in Section 3.3.3. Specimens presented in this thesis had reinforcement ratio of 1.3%, which equals to three No. 3 closed stirrups orthogonal to the shear plane as shown in Figure 3.8 and Figure 3.9. Reinforcing bars located parallel to the shear plane were four No. 5 bars that were bent into an "L" shape. These No. 5 bars were confined by No. 3 closed stirrups inside the flanges. Concrete cover was 0.75 in. throughout the specimen except at the shear plane where the concrete cover was 0.25 in. (see Figure 3.8 cross section).
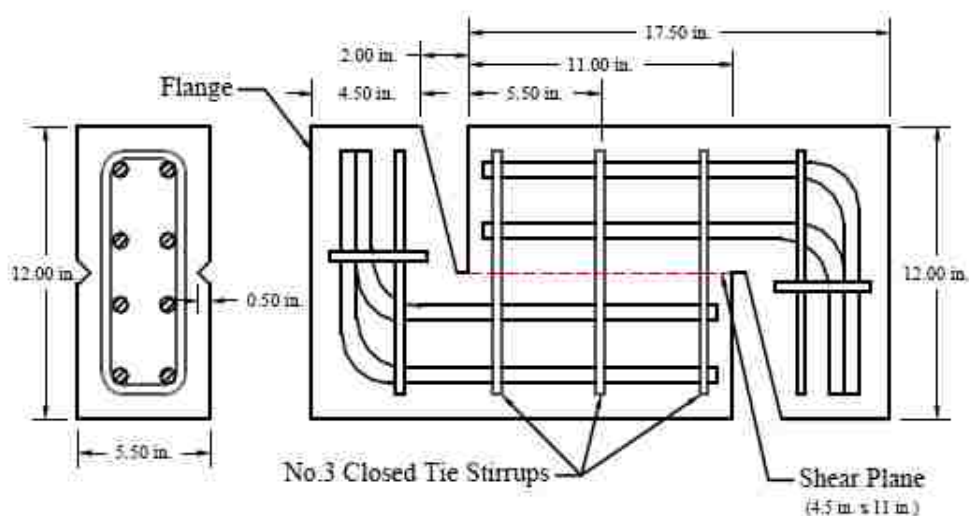
Figure 3.8 Reinforcement Detail

Figure 3.9 Reinforcement Cage with Strain Gages

3.4.2. Formwork and Assembly. All specimens were cast in the Concrete Materials Laboratory in the Butler-Carlton Building at Missouri S&T. Specimens constructed for this study required two types of formwork, one for specimens with a monolithic interface, and one for specimens with a cold joint interface. Formwork for the specimens with a monolithic interface is presented in Section 3.4.2.1, and formwork for the specimens with a cold joint interface is discussed in Section 3.4.2.2.

3.4.2.1 Formwork for the specimens with a monolithic interface. Specimens with a monolithic interface were cast on their side using formwork shown in Figure 3.10. This formwork allowed for easy placement and consolidation of concrete. The formwork was built using 0.75 in. thick untreated plywood and 2 in. by 6 in. untreated boards. Steel void formers used by Shaw (2013) were modified for this formwork. The void formers can be seen in Figure 3.10. The overall inside dimensions were 12 in. by 24 in. by 5.5 in. This size provided a shear plane of 49.5 in^2. The shape of the specimens was designed based on previous research conducted by Mattock and Hawkins (1972). Indentations along the shear plane in the cross section view of Figure 3.8 were achieved by a 0.5 in. chamfer on the bottom and by inserting an identical 11 in. long piece into the finished top surface.

Figure 3.10 Formwork for Specimens with a Monolithic Interface

3.4.2.2 Formwork for the specimens with a cold joint interface. Specimens with a cold joint interface were cast in two stages to achieve the non-monolithic condition along the shear plane. Formwork shown in Figure 3.11 was used for this type of casting. By casting specimens this way, the shear plane was fully exposed to allow for preparation of its surface. The materials and dimensions used were identical to those of the monolithic formwork in Section 3.4.2.1.

Figure 3.11 Formwork for Specimens with a Cold Joint Interface

3.4.3. Concrete Placement and Shear Interface Preparation. Concrete placement of the monolithic specimens was done in one lift without any shear interface preparation. For the cold joint specimens the concrete was placed in two lifts with a minimum of eight hours between casting each lift to achieve the cold joint condition. The cold joint specimens were cast in groups of four: two with a smooth and two with a roughened interface.

After the first lift was placed, the shear plane of the smooth interface specimens was troweled smooth. The roughened interface specimens were left alone for approximately 4 hours. After initial setting of concrete, the shear plane of the roughened interface specimens was roughened to amplitude of approximately 0.25 in. as specified by the ACI 318 (2014) and Handbook (2011). This was achieved using the tool shown in Figure 3.12. The depth of scoring was controlled by inserting one quarter of the 1 in. hook of the scoring tool. The shear plane was scored in the direction perpendicular to the direction of loading across the entire width of the shear plane. After scoring was completed, the shear plane was cleaned using compressed air. The depth of roughening was then measured and verified at several random locations using a digital caliper as shown in Figure 3.13.

Figure 3.12 Roughening Tool

Figure 3.13 Example of Roughened Surface and Measuring of Roughness

3.4.4. Concrete Curing. The specimens along with cylinders were covered with plastic immediately after casting the concrete. After a 24-hour period, the specimens and cylinders were de-molded and placed inside the moist-cure room located in the Concrete Materials Laboratory in the Butler-Carlton Hall at Missouri S&T. This room is maintained at 70 degrees Fahrenheit and 100 percent humidity. The specimens and cylinders were kept in the moist-cure room until the day before testing. The night before testing, the specimens and cylinders were removed from the moist-cure room and allowed to dry off in order to be tested the next day. Casting and test dates are summarized in Table 3.11.

Table 3.11 Specimen Casting and Testing Dates

Specimen Series	Casting Date	Test Date	Age at Test Date (days)	Number of Tests
N-MO	1/23/2015	2/20/2015	28	4
S-SH-MO	1/28/2015	2/25/2015	28	4
A-SH-MO	2/6/2015	3/6/2015	28	4
S-SL-CJ	1/30/2015	2/27/2015	28	4
A-SL-CJ	4/27/2015	5/25/2015	28	4
S-CL-CJ	4/8/2015	5/6/2015	28	4
A-CL-CJ	3/16/2015	4/13/2015	28	4

3.5. TEST SETUP

This research expands on previous research conducted by Shaw (Shaw, 2013). Therefore, this research utilizes a similar test setup as used by Shaw. Two trial specimens were constructed to confirm the test setup used previously and to test the data acquisition system. This section describes the test setup including the support conditions, loading protocol, pre-cracking procedure (where applicable), and flange confinement. Data acquisition and instrumentation used to collect electronic data are discussed in this section as well.

3.5.1. Support Conditions. After thorough evaluation of previous research conducted, it was determined to follow the final support conditions used by Shaw (Shaw, 2013). This was done for two reasons: it was proven to work for the testing at Missouri S&T, and it was already available for this research. It was determined to not use the roller system used previously by Hofbeck (1969) due to minimal lateral translation of the specimen during testing observed by Shaw (2013). The support conditions for testing of specimens are shown in Figure 3.14. A hemispherical bearing head was used on top of the specimen to transfer the load from the crosshead of the Tinius Olsen universal testing machine to the specimen. The specimen was supported on the bottom by the steel platen of the Tinius Olson. Neoprene pads were placed between the specimen flanges and the steel plates used on the top and bottom to help distribute the load evenly.

Figure 3.14 Typical Support Conditions for Testing

3.5.2. Loading Protocol. As mentioned in the previous section, a Tinius Olsen Load Frame with 200-kip capacity was used to apply the load to the test specimens. The load frame is located in the Missouri S&T Jones Structure Materials Testing Laboratory in Butler-Carlton Hall. For this study, all specimens were tested under displacement controlled loading at a rate of 0.015 in. per minute. The specimens were tested until one of the following conditions occurred: a target slip of 0.3 in. was reached, or 60 percent of the ultimate strength was reached (after the ultimate strength was reached).

3.5.3. Pre-cracking of Monolithic Specimens. During the review of previously conducted research involving pre-cracking of monolithic specimens, it was discovered that different researchers used different methods to accomplish this task. The Mattock and Hawkins' (1972) approach was modified and used in this study. Prior to pre-cracking, the shear plane was painted white on both sides of the specimen. A crack was produced along the shear plane by applying a line load to both sides of the specimen using an in-house developed splitting tool shown in Figure 3.15. The specimen was placed on its side, and the pre-cracking tool edge was placed into the chamfers used to create the shear plane as shown in Figure 3.16. Loading was gradually increased until a significant drop in load occurred. At this point, the load was paused, and the specimen was examined visually for hairline cracks.

Figure 3.15 Pre-cracking Tool

Figure 3.16 Pre-cracking Setup

3.5.4. Flange Prestressing/Confinement Systems. Based on the research conducted by Shaw (2013) it was determined that primary and secondary confinement of the flanges would be used for all specimens tested in this study. The primary prestressing system is described in Section 3.5.4.1, and the secondary system is summarized in Section 3.5.4.2. It should be noted that no premature flange failures were observed in any of the tests included in this thesis.

3.5.4.1 Primary flange prestressing/confinement system. To avoid premature flange failure, the primary prestressing system was used as shown in Figure 3.17. All four all-thread rods with nuts were tightened to 50 lb-ft. This corresponds to approximately 325 psi of compression to each flange. The effect of prestressing was monitored using the strain gages mounted on the reinforcing bars crossing the shear plane. No effect outside of the noise levels of strain gages was seen during the primary prestressing.

3.5.4.2 Secondary flange prestressing/confinement system. The secondary system consisted of four 0.5 in. plates. On the back of the specimen they were held in place with two structural steel angles. On the front of the specimen the plates were pushed against the flange using four bolts per plate as seen in Figure 3.17. This confinement was intended to provide passive support in the event of flange failure out of plane.

Secondary Confinement System

Primary Confinement System

Dilation DC-LVDTs

Slip DC-LVDTs

Strain Gage Data Acquisition
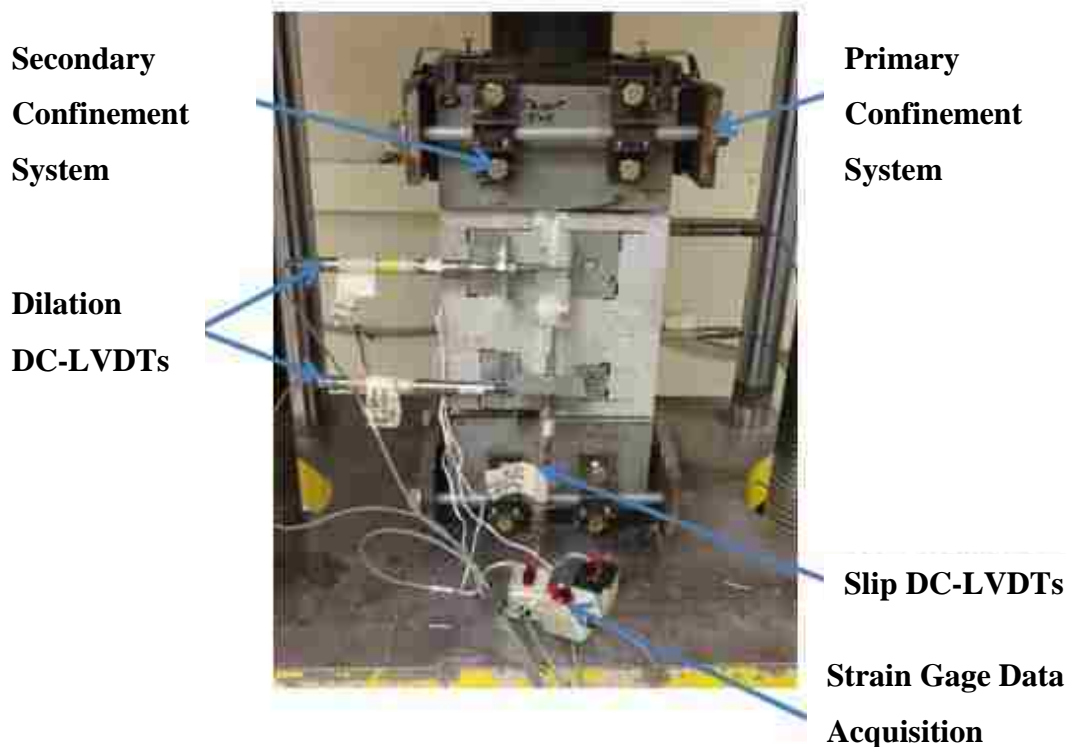
Figure 3.17 Primary and Secondary Flange Confinement Systems

3.5.5. Instrumentation and Data Acquisition. Eleven data channels were used to monitor each test. Six data channels were displacements measured with direct current-linear variable differential transducers (DC-LVDTs). Three channels recorded strains measured using uniaxial strain gages. The last two data channels were used to measure the load and global displacement (stroke) of the testing machine. Both of these measurements were acquired from the on board load cell and transducer on the bottom platen of the Tinius Olsen load frame. The specimen instrumentation is shown in Figure 3.17 (except for the load and global displacement). All channels were observed in real time throughout the test to ensure proper functioning of each data channel.

3.5.5.1 Direct current – LVDTs. Two DC-LVDTs were used to measure slip along the shear interface, and four DC-LVDTs were used to measure dilation of the shear interface. Three DC-LVDTs were mounted on the front face of the specimen, and an identical configuration was used on the back face of each specimen. The DC-LVDTs used to measure the dilation (horizontal separation) had ±1.0 in. stroke, while the DC-

LVDTs measuring slip had ±0.5 in. stroke. These were sufficient to measure the displacements experienced by each specimen. The DC-LVDTs were mounted to the aluminum brackets that were mounted on specimens using a hot-glue gun with a slow setting glue readily available at the local hardware store. This method was recommended by HILTI Test Lab staff from Tulsa, Oklahoma.

      3.5.5.2 Strain gages. Two sets of strain gages were mounted on the reinforcing steel used in this study. The first set of strain gages used were uniaxial electronic resistance strain gages (CEA-06-125UN-120) manufactured by Vishay Micro-measurements. The second set was type EA-06-250BG-120/LE by Vishay Micro-measurements ordered at a later date.

      Three strain gages per specimen were attached to the exterior face of the reinforcing bars crossing the shear plane. The strain gages were positioned so that they would be at the location of shear plane crack as shown in Figure 3.18. During the bar preparation (i.e. removing the lugs), special care was taken to not reduce the bar cross-sectional area. The manufacturer's instructions were followed to attach the strain gages. After the strain gage was attached, a protective covering – butyl rubber patch (Vishay Barrier E) was placed over the strain gage as shown in Figure 3.19. When the reinforcement cage was placed in the form, it was checked to ensure that strain gages were crossing the shear plane. All strain gages were checked for operation before the placement of concrete.

      During testing, it was observed that a large amount of noise was present in the strain gage readings. It took the research team several testing sessions to determine that the power supply on the strain gage data acquisition system was malfunctioning. However, this noise was later removed in the strain data.
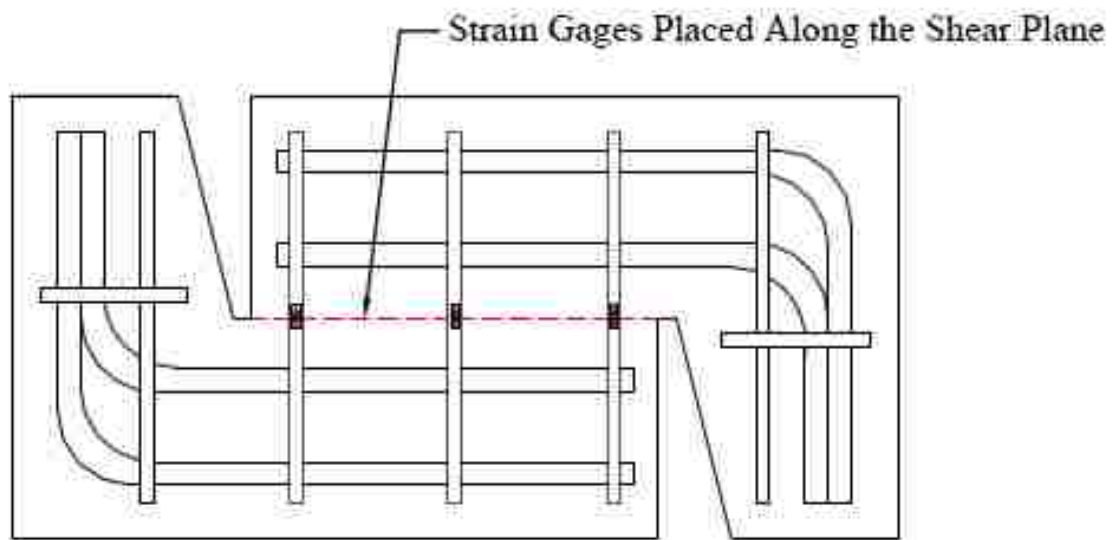
Figure 3.18 Location of Strain Gages

Figure 3.19 Strain Gages Attached to Shear Reinforcement

3.6. TEST RESULTS

This section presents the results of the experimental program outlined previously. Data presented in following sections include the shear force-slip relation, shear force-dilation relation, slip-dilation, stress-strain, slip-strain, and dilation-strain relation for each set of specimens. The values from the two DC-LVDTs measuring slip are averaged for the two faces of the specimen. The values from the DC-LVDTs measuring dilation are averaged also. The strain values, for which noise was an issue, were manually corrected. The strain values were then averaged for all properly functioning strain gages.

3.6.1. Normalweight Concrete Specimens. This section presents the results of the normalweight concrete specimens. Specimens presented in this section include series N-MO-U and N-MO-P. These specimens were tested on 2/20/2015. All specimens failed in shear along the shear plane. Horizontal hairline flexural cracks were observed on the side edges of the specimens as shown in Figure 3.20. These cracks were typical for all normalweight concrete specimens. The hairline cracks were observed to have no influence on the instrumentation and did not appear to affect the data being recorded. A significant amount of noise was observed in the strain readings during the testing. This can be seen in the figures that follow. The strain gage noise in specimen N-MO-P-1 exceeded values that the strain gage can read according to the manufacturer. For this reason the strain gage readings associated with specimen N-MO-P-1 were deemed unusable and are not displayed in the figures below. Figure 3.21 shows the applied shear force versus slip relations for all normalweight concrete specimens. Figure 3.22 presents the shear force versus interface dilation relations. Figure 3.23 displays slip versus dilation. Figure 3.24 shows the applied shear force versus shear reinforcement strain. Figure 3.25 shows the slip versus strain relations. And lastly, Figure 3.26 shows the dilation versus strain relations.

Figure 3.20 Location and Example of Hairline Flexural Cracks

Figure 3.21 Applied Shear Force vs. Slip for Normalweight Concrete Monolithic
Interface Specimens

Figure 3.22 Applied Shear Force vs. Dilation for Normalweight Concrete Monolithic Interface Specimens

Figure 3.23 Slip vs. Dilation for Normalweight Concrete Monolithic Interface Specimens

Figure 3.24 Applied Shear Force vs. Shear Reinforcement Strain for Normalweight
Concrete Monolithic Interface Specimens

Figure 3.25 Slip vs. Shear Reinforcement Strain for Normalweight Concrete Monolithic
Interface Specimens

Figure 3.26 Dilation vs. Shear Reinforcement Strain for Normalweight Concrete
Monolithic Interface Specimens

3.6.2. Sand-lightweight Concrete Specimens. This section presents the results
of the sand-lightweight concrete specimens with a monolithic or cold joint interface.
Specimens presented in this section include series S-SH-MO-U, S-SH-MO-P, S-SL-CJ-
R, S-SL-CJ-S, S-CL-CJ-R, and S-CL-CJ-S. The testing of expanded shale aggregate
sand-lightweight concrete specimens was conducted on 2/25/15. The testing of expanded
slate aggregate sand-lightweight concrete specimens was conducted on 2/27/15. The
testing of expanded clay aggregate sand-lightweight concrete was conducted on 5/6/15.

3.6.2.1 Shale aggregate sand-lightweight concrete specimens. All shale
aggregate concrete specimens had a monolithic interface. Specimens presented in this
section include series S-SH-MO-U and S-SH-MO-P. Hairline flexural cracking was
observed in the same location as for the normalweight concrete specimens (Section
3.6.1). A typical crack is shown in Figure 3.27. All specimens failed in shear along the
shear plane. Figure 3.28 shows the applied shear force versus slip relations for the shale
sand-lightweight concrete specimens. Figure 3.29 presents the shear force versus
interface dilation relations. Figure 3.30 displays the slip versus dilation relations. Figure
3.31 shows the applied shear force versus shear reinforcement strain. Figure 3.32 shows

the slip versus interface steel strain relations. And finally, Figure 3.33 shows dilation versus interface steel strain.

Figure 3.27 Typical Hairline Flexural Flange Crack Observed In Shale Aggregate Concrete Specimens
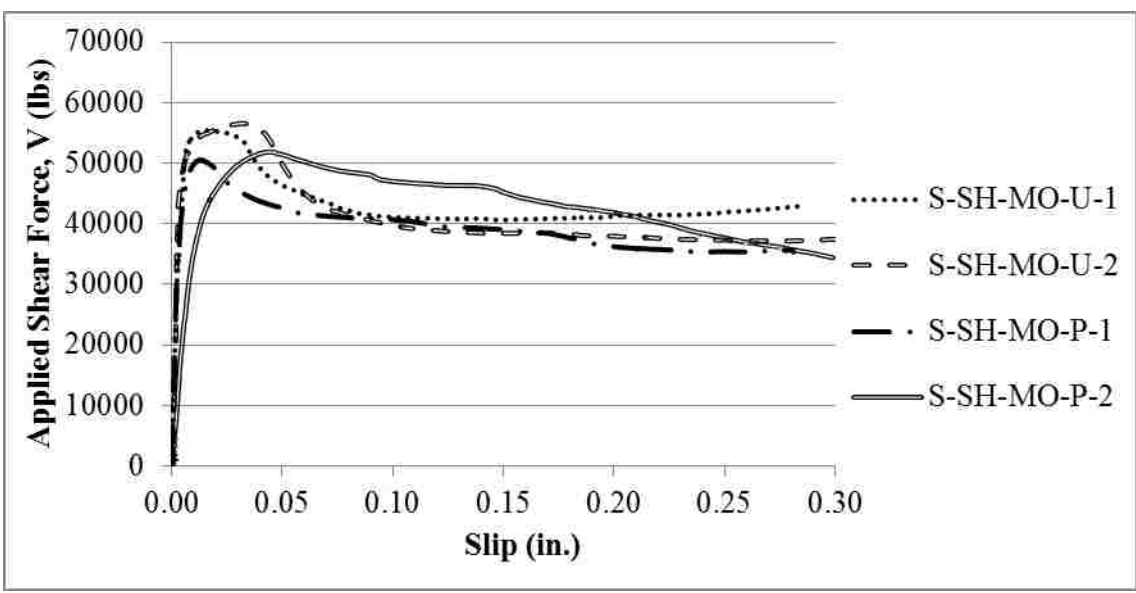
Figure 3.28 Applied Shear Force vs. Slip for Shale Sand-Lightweight Concrete Monolithic Interface Specimens

Figure 3.29 Applied Shear Force vs. Dilation for Shale Sand-Lightweight Concrete Monolithic Interface Specimens

Figure 3.30 Slip vs. Dilation for Shale Sand-Lightweight Concrete Monolithic Interface Specimens

Figure 3.31 Applied Shear Force vs. Shear Reinforcement Strain for Shale Sand-Lightweight Concrete Monolithic Interface Specimens

Figure 3.32 Slip vs. Shear Reinforcement Strain for Shale Sand-Lightweight Concrete Monolithic Interface Specimens

Figure 3.33 Dilation vs. Shear Reinforcement Strain for Shale Sand-Lightweight
Concrete Monolithic Interface Specimens

3.6.2.2 Slate aggregate sand-lightweight concrete specimens. All slate
aggregate sand-lightweight concrete specimens had a cold joint interface. Specimens
presented in this section include series S-SL-CJ-R and S-SL-CJ-S. All specimens failed
in shear along the shear plane. During the testing of specimens S-SL-CJ-S-1 and S-SL-
CJ-S-2, concrete cover spalling near the shear plane crack was observed late in the test
(after the peak load was achieved). This spalling is shown in Figure 3.34. Hairline
flexural flange cracking experienced by the sand-lightweight shale aggregate concrete
specimens (Section 3.6.2.1) and normalweight concrete specimens (Section 3.6.1) was
also experienced by all four slate aggregate sand-lightweight concrete specimens. During
the testing of the slate aggregate sand-lightweight concrete specimens a large amount of
noise was observed in the measured strain data. Figure 3.35 shows the applied shear force
versus slip relations for the slate sand-lightweight concrete specimens. Figure 3.36 shows
the shear force versus interface dilation relations. Figure 3.37 shows the slip versus
dilation relations. Figure 3.38 shows the applied shear force versus strain in shear plane
reinforcement. Figure 3.39 shows slip versus strain in the shear plane reinforcement. It
must be noticed, that the scale for the slip was changed for this graph in order to reduce

the noise displayed. Figure 3.40 shows dilations versus strain in the shear plane reinforcement. The scale for Figure 3.40 was also adjusted in order to reduce the strain noise shown.

Figure 3.34 Concrete Cover Spalling Experienced by Specimen S-SL-CJ-S-1 (left), Specimen S-SL-CJ-S-2 (right)
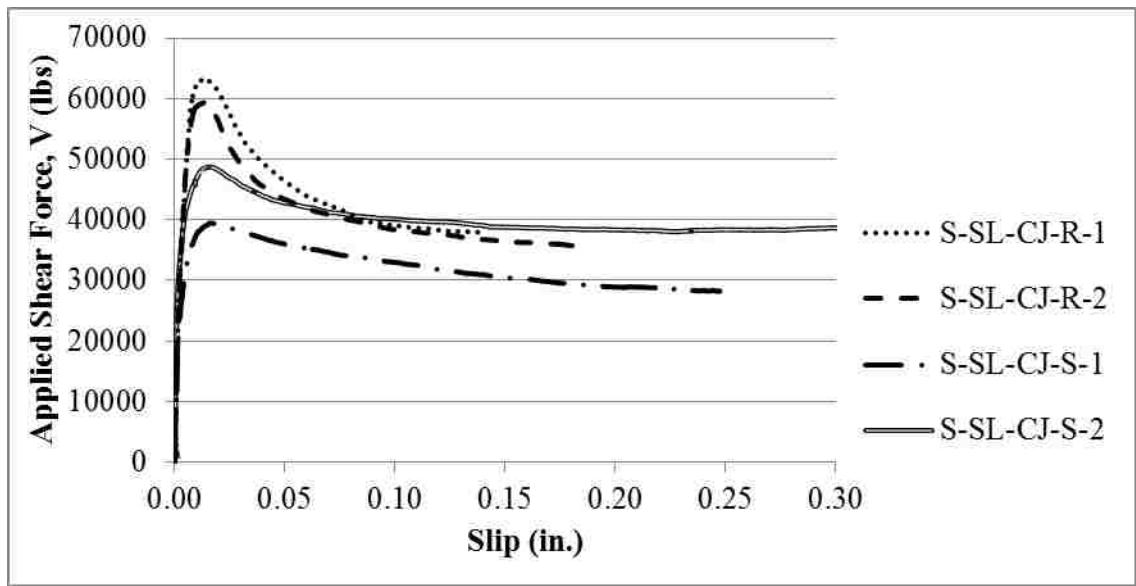
Figure 3.35 Applied Shear Force vs. Slip for Slate Sand-Lightweight Concrete Cold Joint Interface Specimens
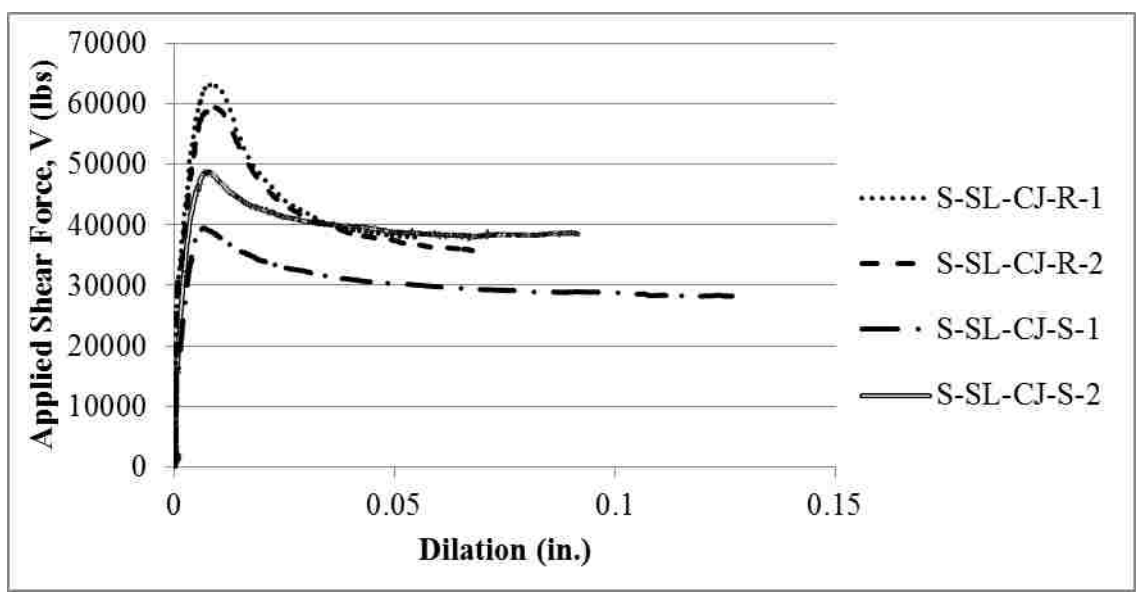
Figure 3.36 Applied Shear Force vs. Dilation for Shale Sand-Lightweight Concrete Cold Joint Interface Specimens

Figure 3.37 Slip vs. Dilation for Shale Sand-Lightweight Concrete Cold Joint Interface Specimens

Figure 3.38 Applied Shear Force vs. Shear Reinforcement Strain for Slate Sand-Lightweight Concrete Cold Joint Interface Specimens

Figure 3.39 Slip vs. Shear Reinforcement Strain for Slate Sand-Lightweight Concrete Cold Joint Interface Specimens
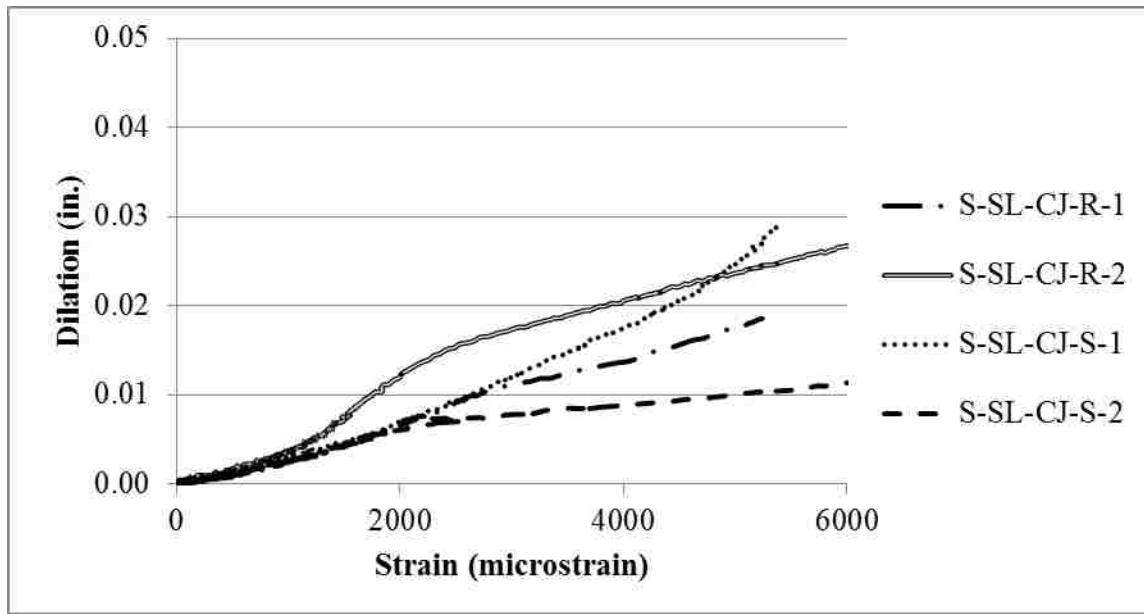
Figure 3.40 Dilation vs. Shear Reinforcement Strain for Slate Sand-Lightweight Concrete Cold Joint Interface Specimens

3.6.2.3 Clay aggregate sand-lightweight concrete specimens. All clay aggregate sand-lightweight concrete specimens presented in this section had a cold joint interface and include series S-CL-CJ-R and S-CL-CJ-S. All specimens failed in shear along the shear plane. During testing of specimen S-CL-CJ-R-1 the steel bracket holding the front vertical and the front bottom horizontal DC-LVDT fell off because of excess moisture interfering with the glue as shown in Figure 3.41. Therefore measurements by these devices were disregarded. Figure 3.42 shows the applied shear versus slip relations for the clay sand-lightweight concrete specimens. Figure 3.43 shows the shear force versus interface dilation relations. Figure 3.44 shows the slip versus dilation relations. Figure 3.45 shows the applied shear force versus strain in shear plane reinforcement. Figure 3.46 shows slip versus strain in shear plane reinforcement. Figure 3.47 shows the dilation versus strain in shear plane reinforcement relations. It must be mentioned that the strain readings for the series S-CL-CJ experienced large strain data noise.

Figure 3.41 Detached DC-LVDTs on specimen S-CL-CJ-R-1
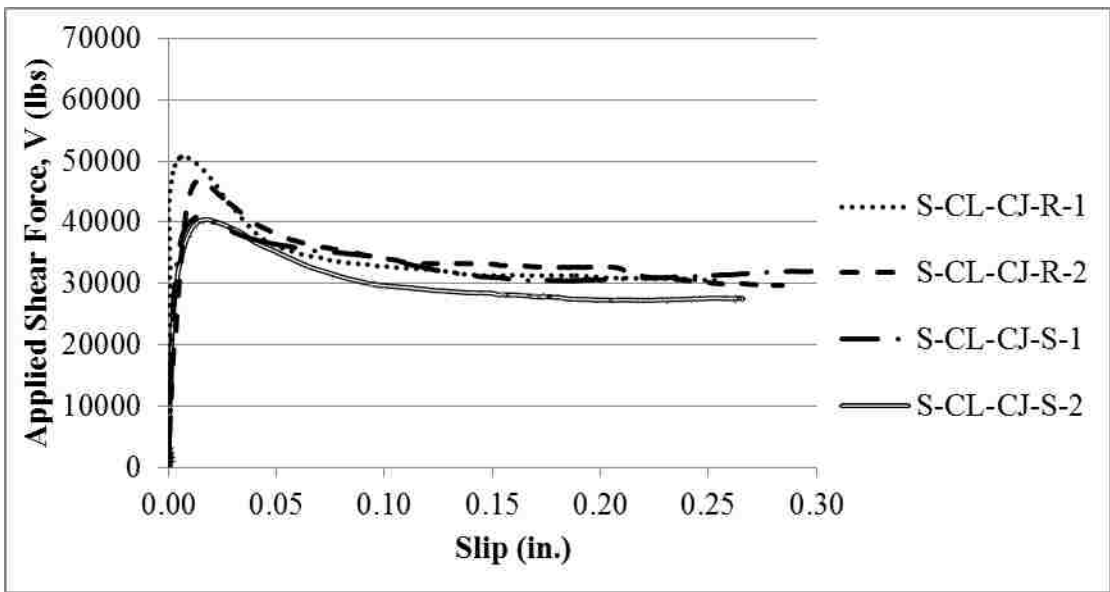
Figure 3.42 Applied Shear Force vs. Slip for Clay Sand-Lightweight Concrete Cold Joint Interface Specimens
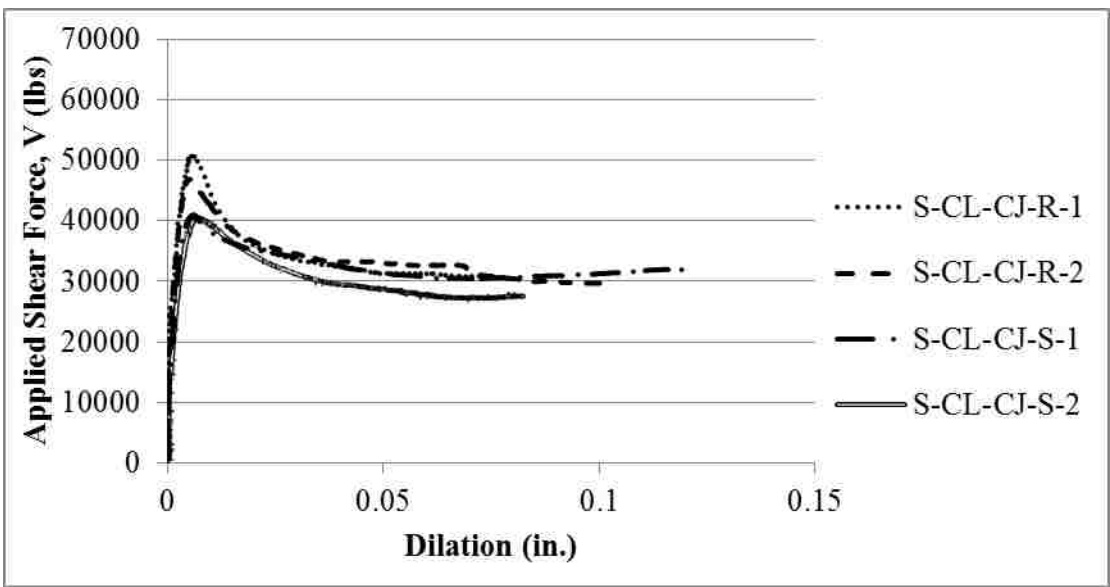
Figure 3.43 Applied Shear Force vs. Dilation for Clay Sand-Lightweight Concrete Cold Joint Interface Specimens
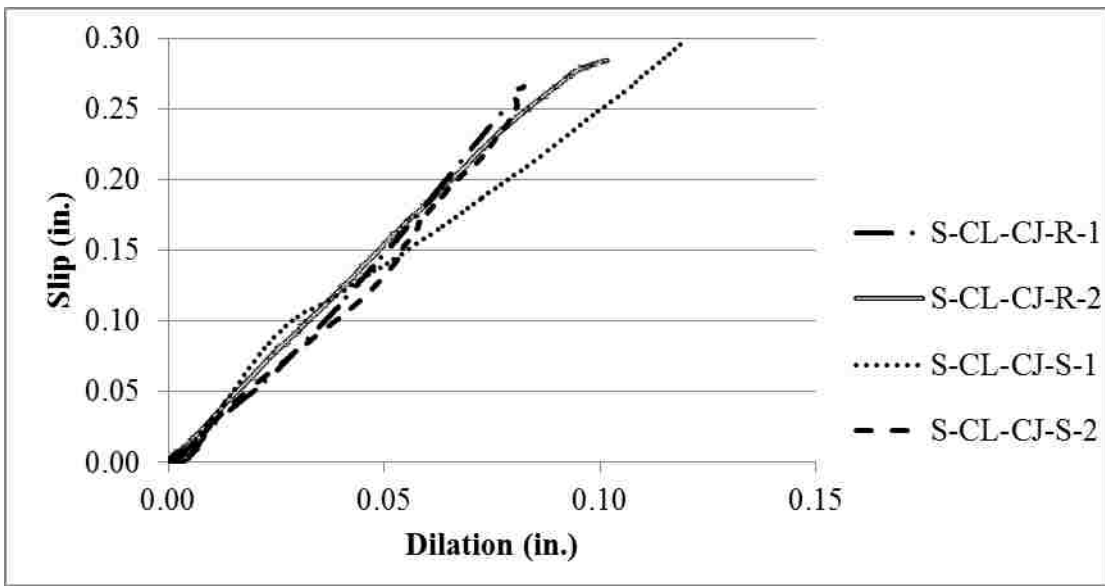
Figure 3.44 Slip vs. Dilation for Clay Sand-Lightweight Concrete Cold Joint Interface Specimens
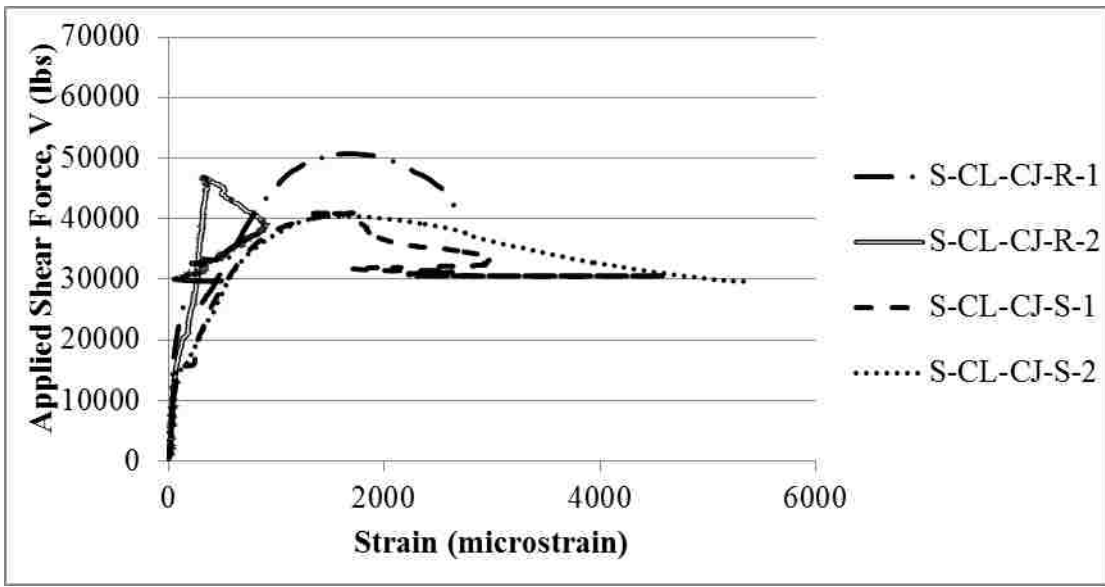
Figure 3.45 Applied Shear Force vs. Shear Reinforcement Strain for Clay Sand-Lightweight Concrete Cold Joint Interface Specimens
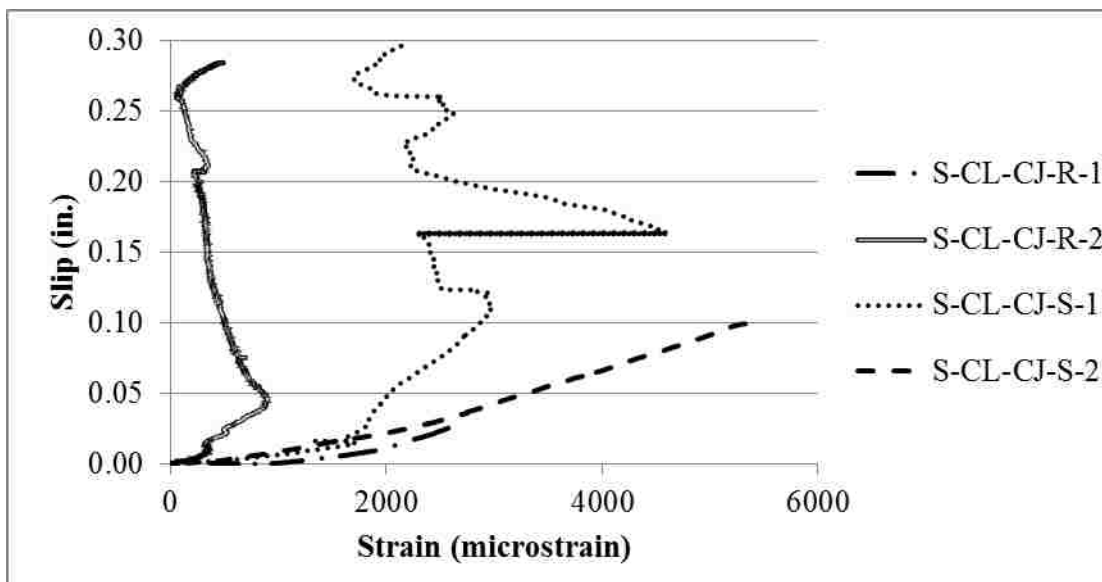
Figure 3.46 Slip vs. Shear Reinforcement Strain for Clay Sand-Lightweight Concrete
Cold Joint Interface Specimens
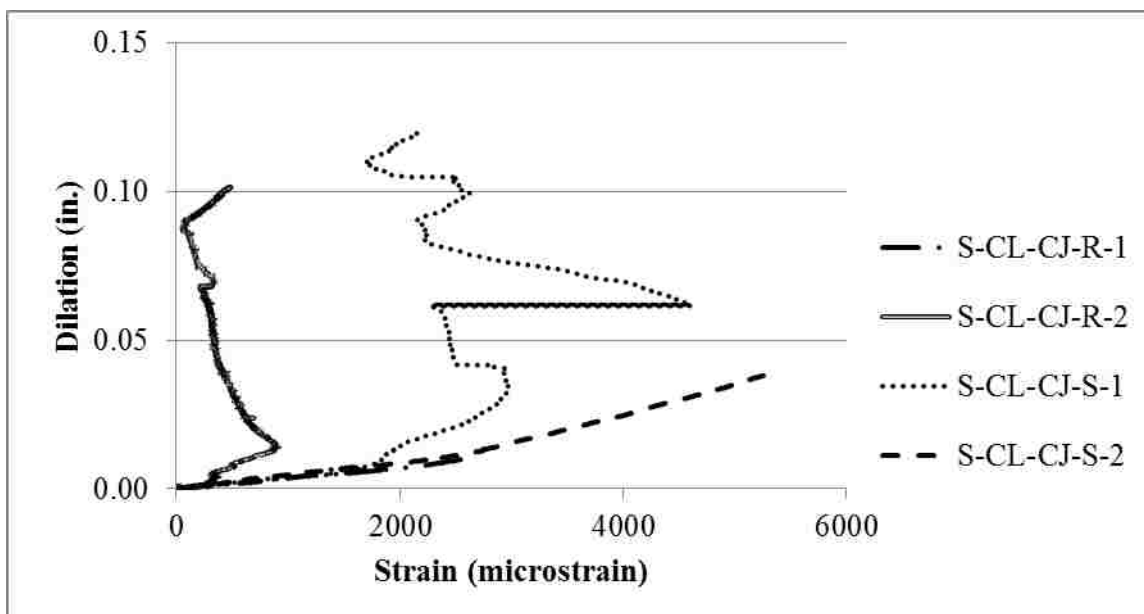
Figure 3.47 Dilation vs. Shear Reinforcement Strain for Clay Sand-Lightweight Concrete
Cold Joint Interface Specimens

3.6.3. All-lightweight Concrete Specimens. This section presents the results of the all-lightweight concrete specimens with a monolithic or cold joint interface. Specimens presented in the following section include series A-SH-MO-U, A-SH-MO-P, A-SL-CJ-R, A-SL-CJ-S, A-CL-CJ-R, and A-CL-CJ-S. Shale aggregate all-lightweight concrete specimens were tested on 3/6/2015. Slate aggregate all-lightweight concrete specimens were tested on 5/25/2015. Clay aggregate all-lightweight concrete specimens were tested on 4/13/2015.

3.6.3.1 Shale aggregate all-lightweight concrete specimens. All shale all-lightweight specimens were cast monolithically as described in Section 3.4.2.1. All specimens failed in shear along the shear plane. DC-LVDTs measuring back face bottom dilation and back face slip of specimen A-SH-MO-P-2 detached during testing due to concrete cover spalling shown in Figure 3.48. During the testing of specimen A-SH-MO-P-1, strain readings exceeding the range of the strain gages were observed. For this reason, the strain data for specimen A-SH-MO-P-1 is not displayed in figures below. The behavior of the shale aggregate all-lightweight concrete specimens is shown in Figure 3.49 through Figure 3.54. Figure 3.49 shows the relations between applied shear force and slip. Figure 3.50 shows the applied shear versus dilation relations. Figure 3.51 shows the slip versus dilation relations. Figure 3.52 shows applied shear force versus strain relations. Figure 3.53 shows slip versus strain relations. Lastly, Figure 3.54 shows the dilation versus strain relations.

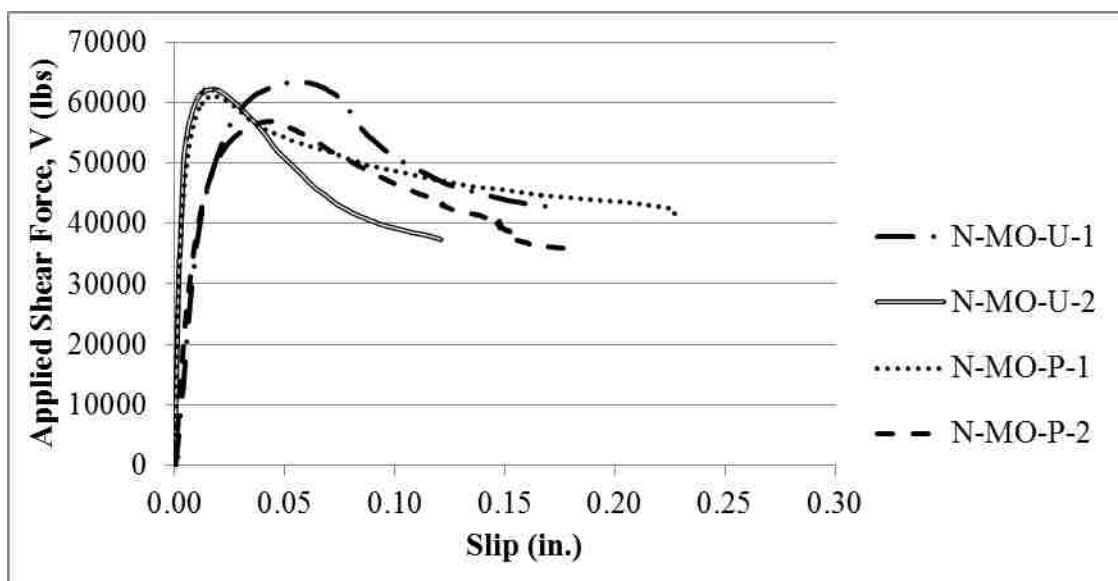Figure 3.48 Concrete Spalling on Specimen A-SH-MO-P-2
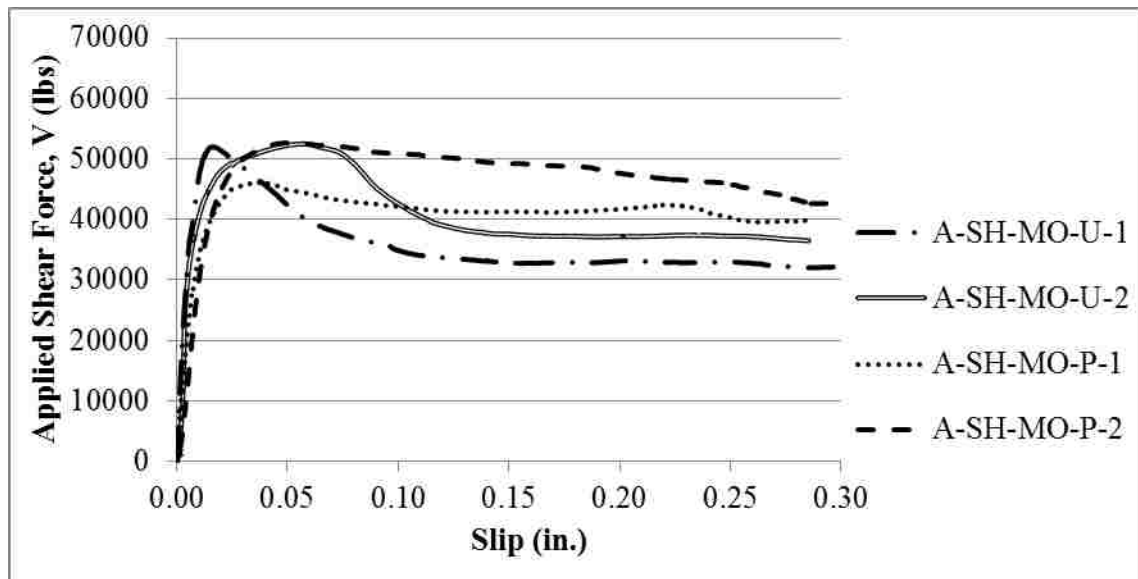
Figure 3.49 Applied Shear Force vs. Slip for Shale All-Lightweight Concrete Monolithic
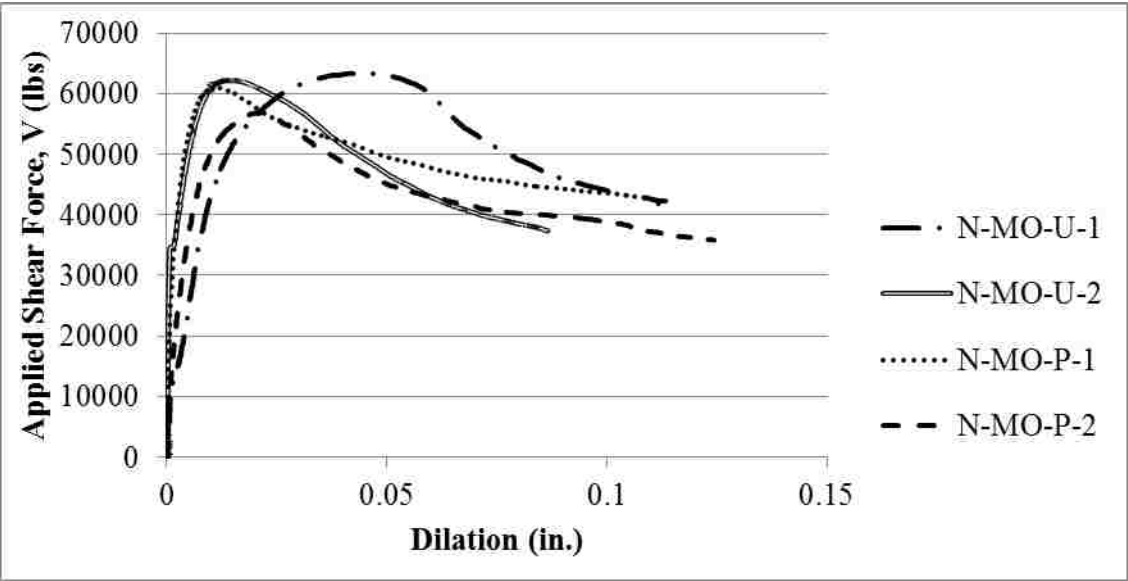Interface Specimens
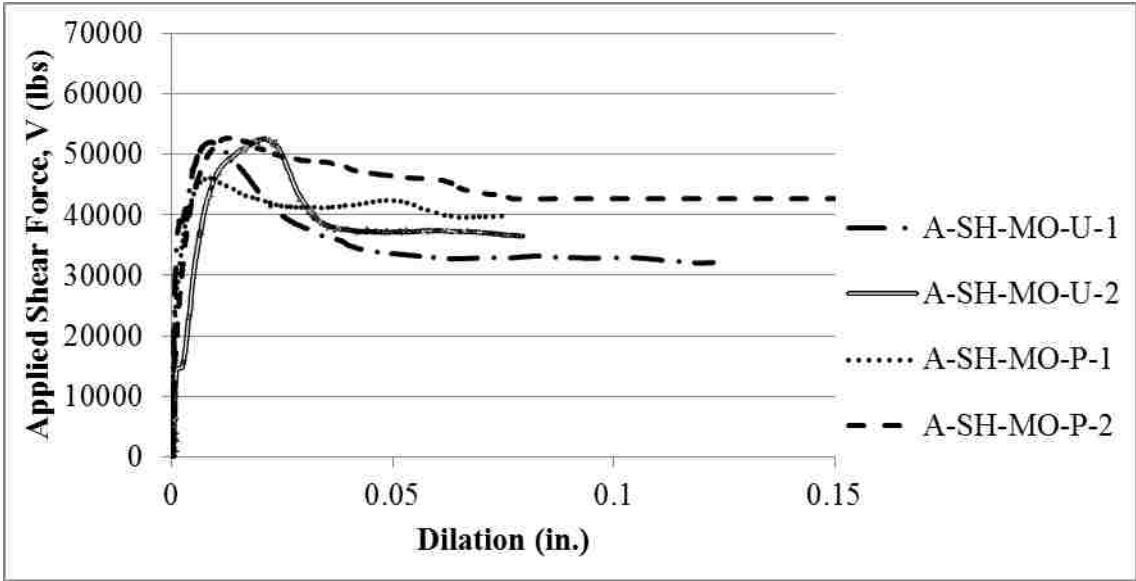
Figure 3.50 Applied Shear Force vs. Dilation for Shale All-Lightweight Concrete Monolithic Interface Specimens
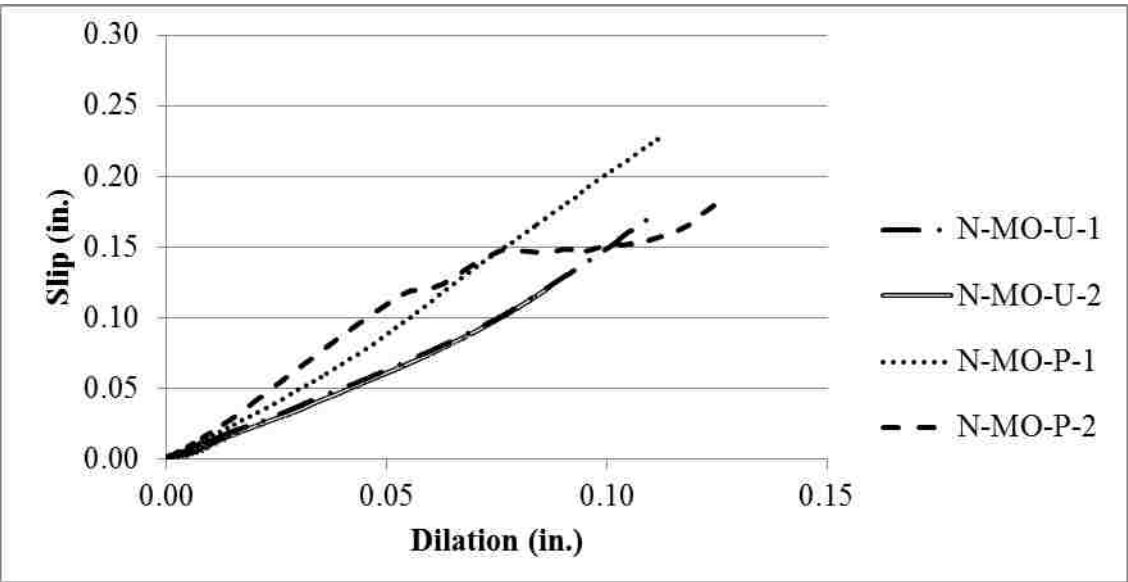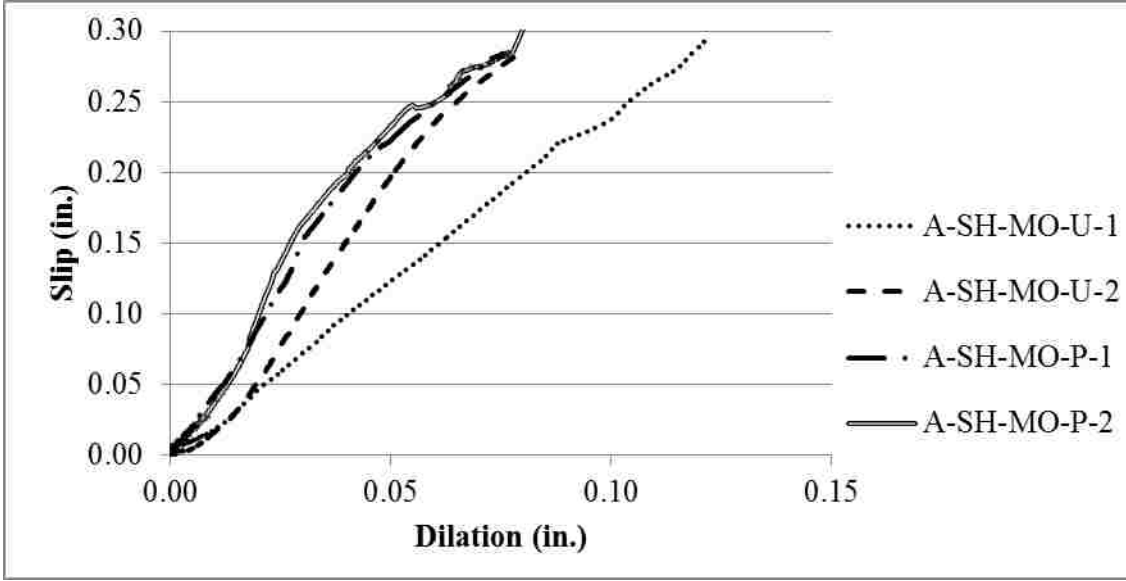

Figure 3.51 Slip vs. Dilation for Shale All-Lightweight Concrete Monolithic Interface Specimens
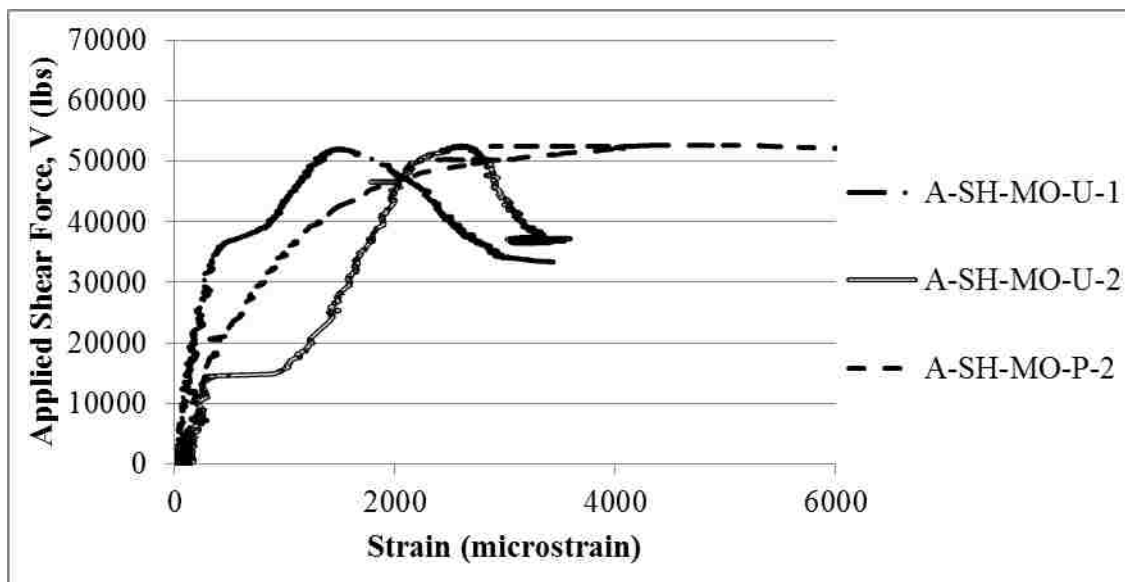
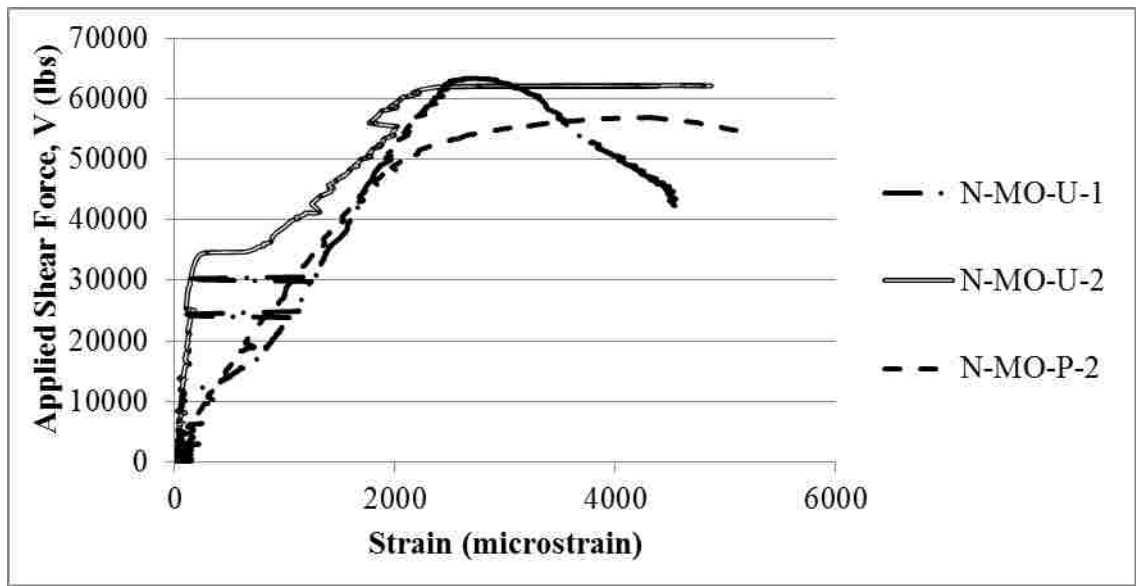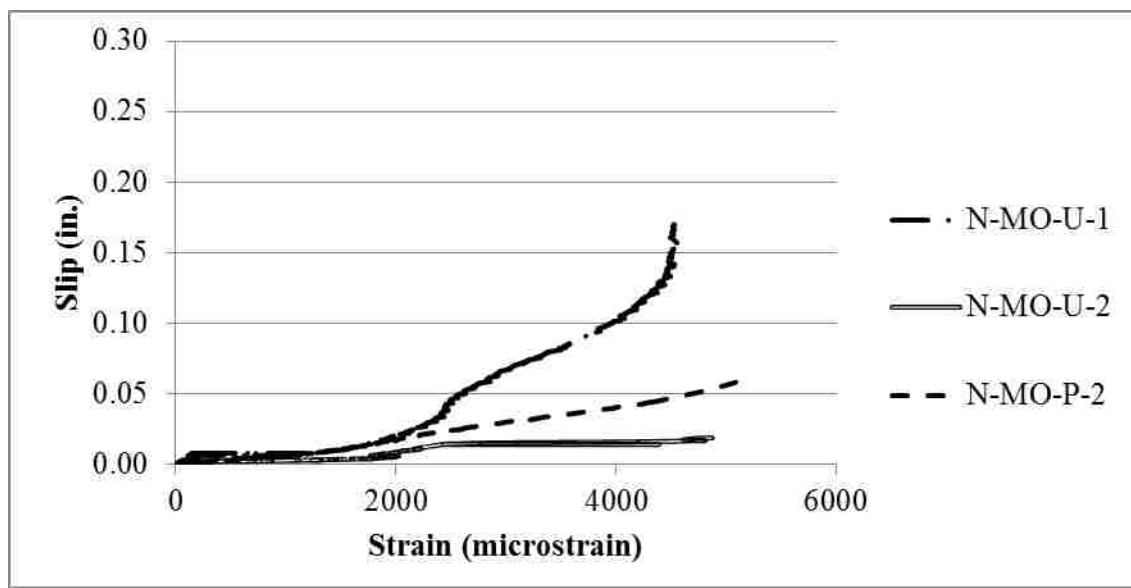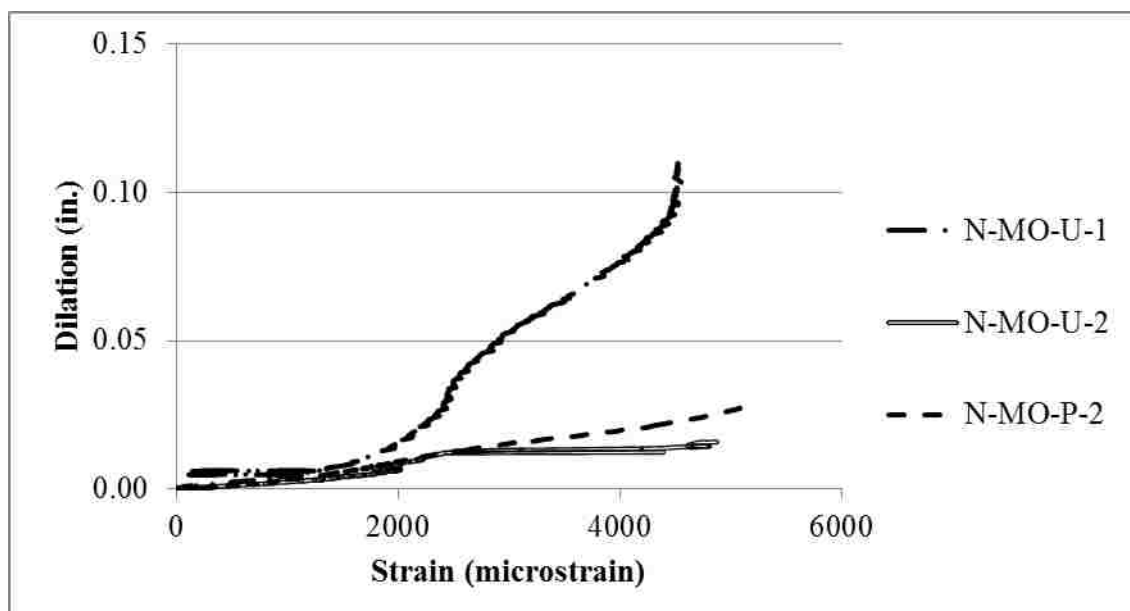Figure 3.52 Applied Shear Force vs. Shear Reinforcement Strain for Shale All-Lightweight Concrete Specimens
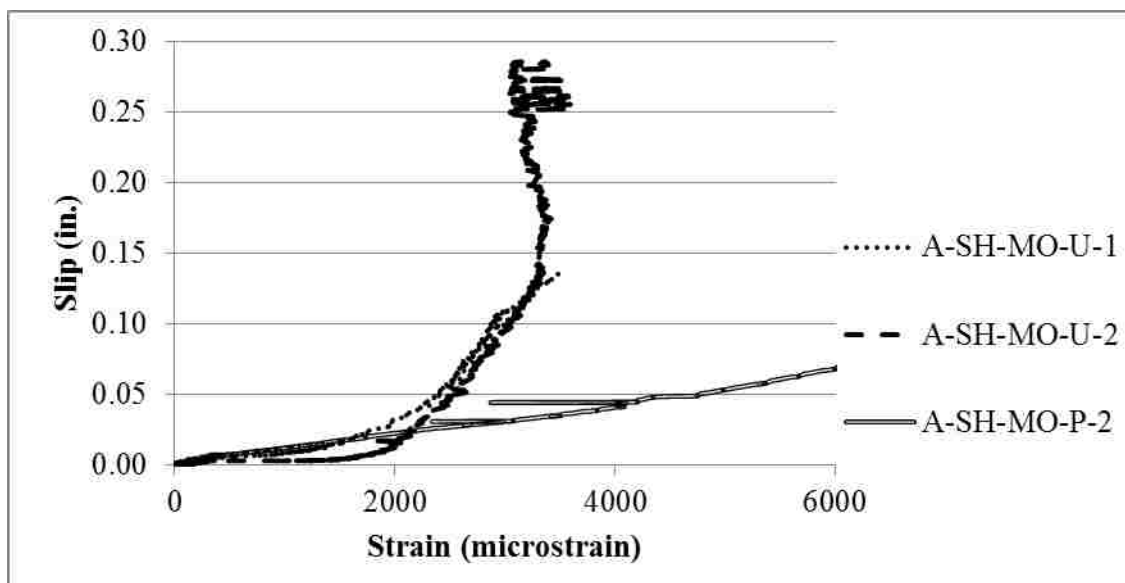
Figure 3.53 Slip vs. Shear Reinforcement Strain for Shale All-Lightweight Concrete Monolithic Interface Specimens
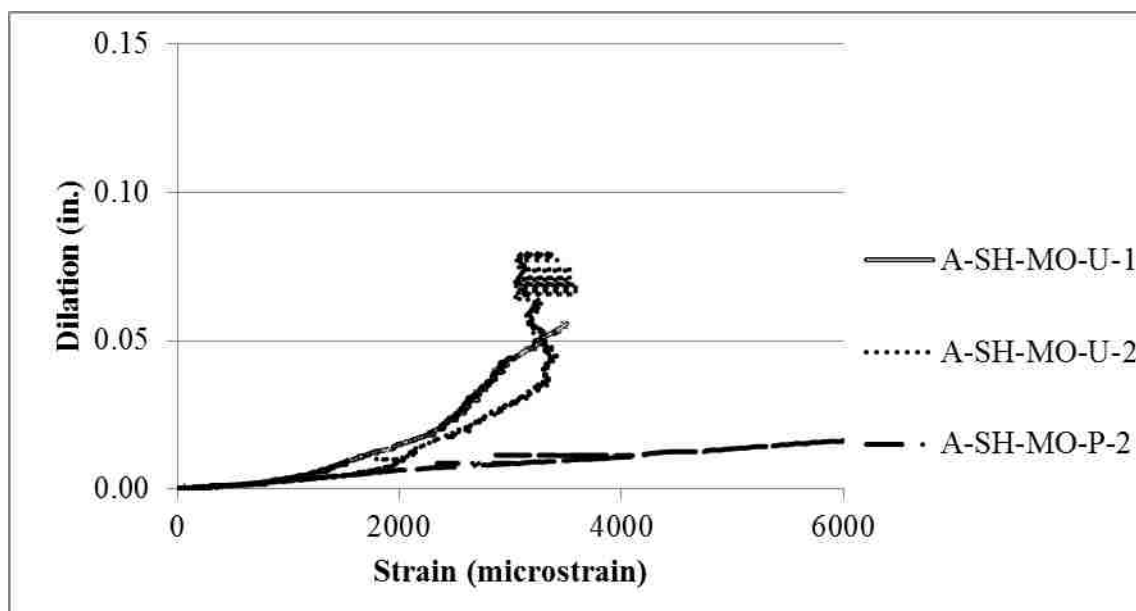
Figure 3.54 Dilation vs. Shear Reinforcement Strain for Shale All-Lightweight Concrete
Monolithic Interface Specimens

3.6.3.2 Slate aggregate all-lightweight concrete specimens. All slate aggregate
all-lightweight concrete specimens had a cold joint interface. Specimens presented in this
section include series A-SL-CJ-R and A-SL-CJ-S. All specimens failed in shear along the
shear plane. The behavior of slate aggregate all-lightweight concrete specimens is shown
in Figure 3.55 through Figure 3.60. Figure 3.55 shows the relations between applied
shear force and slip. Figure 3.56 shows the applied shear versus dilation relations. Figure
3.57 shows the slip versus dilation relations. Figure 3.58 shows the applied shear force
versus strain relations. Figure 3.59 shows the slip versus strain relations. Figure 3.60
shows the dilation versus shear plane reinforcement strain relations.
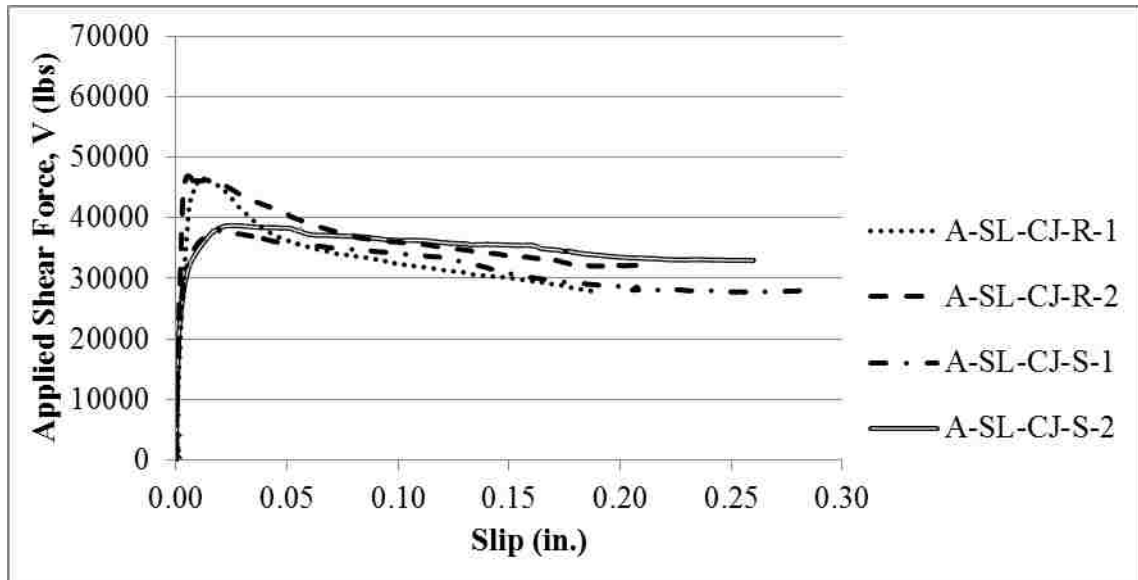
Figure 3.55 Applied Shear Force vs. Slip for Slate All-Lightweight Concrete Cold Joint Interface Specimens
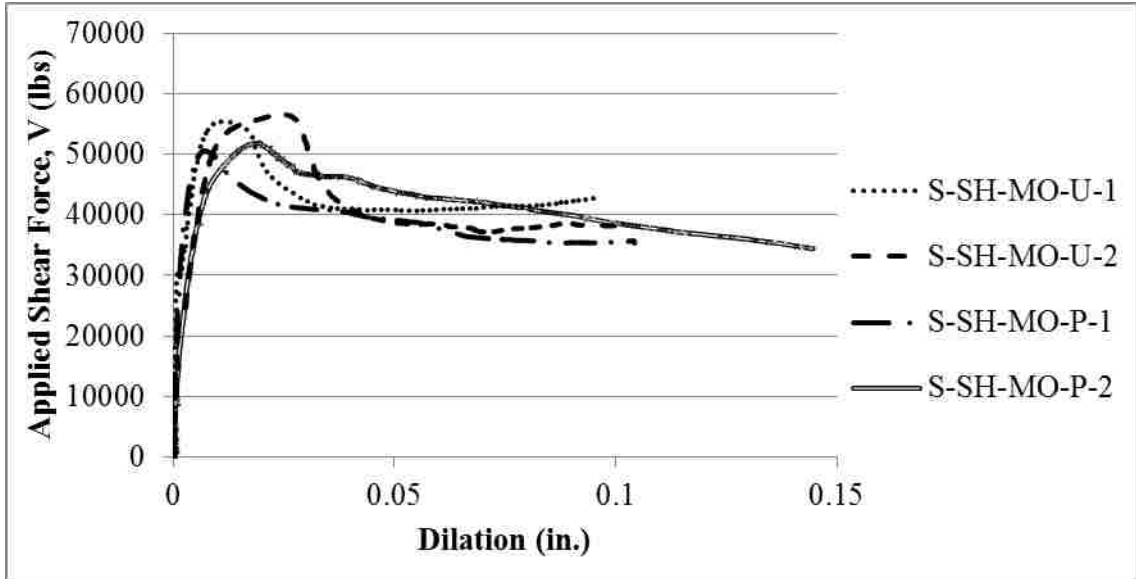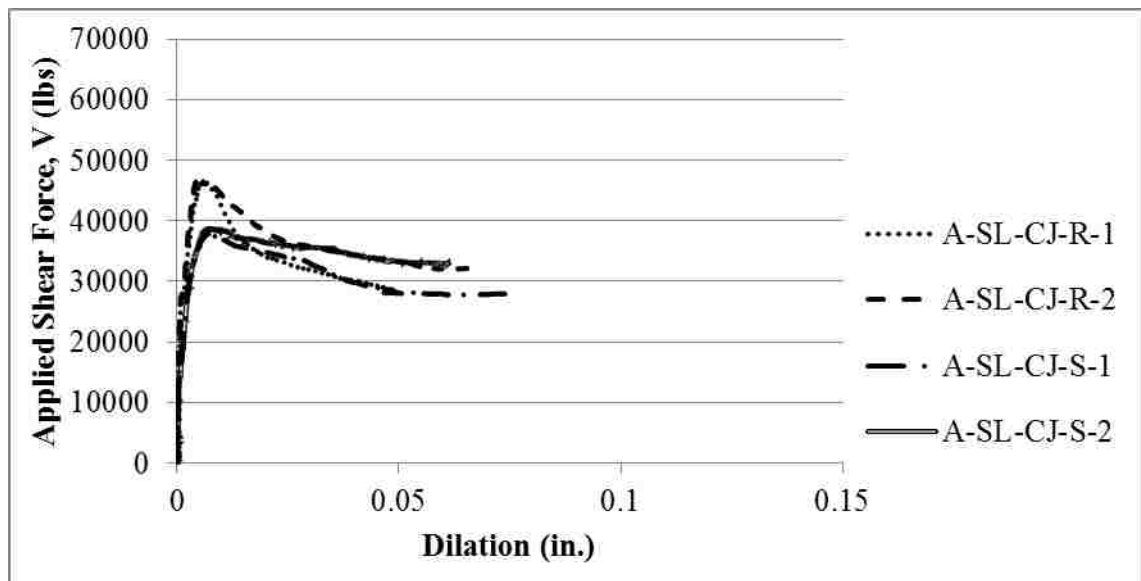

Figure 3.56 Applied Shear Force vs. Dilation for Slate All-Lightweight Concrete Cold Joint Interface Specimens
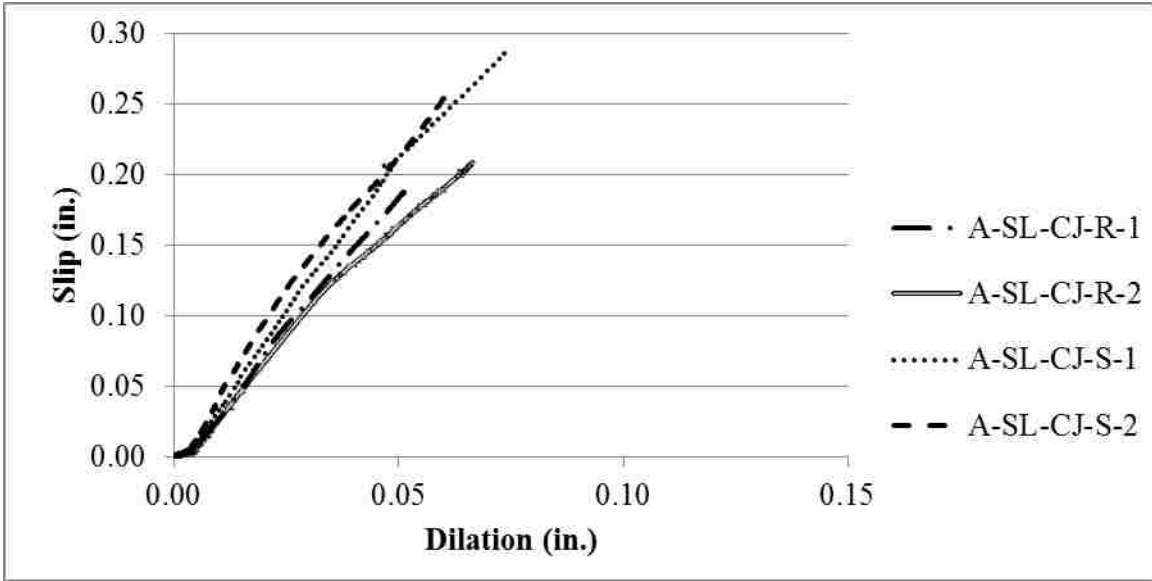
Figure 3.57 Slip vs. Dilation for Slate All-Lightweight Concrete Cold Joint Interface Specimens
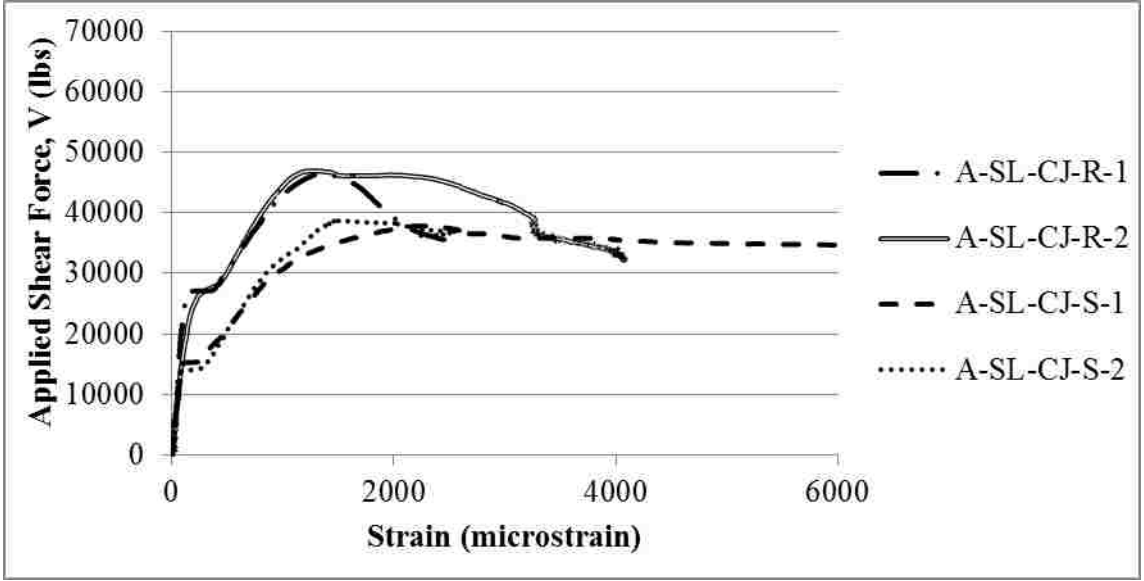
Figure 3.58 Applied Shear Force vs. Shear Reinforcement Strain for Slate All-Lightweight Concrete Cold Joint Interface Specimens
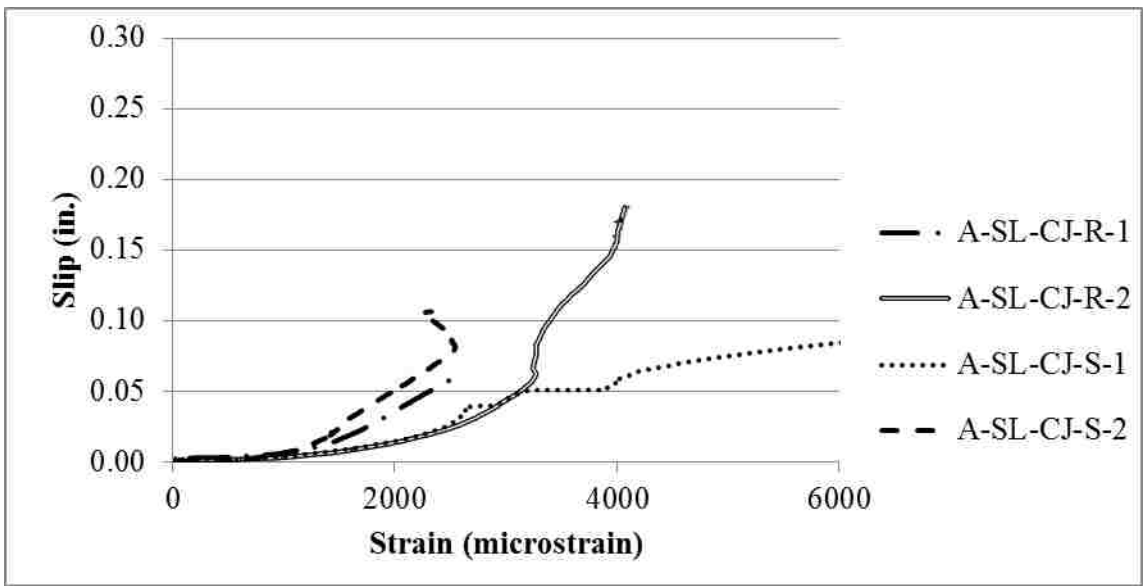
Figure 3.59 Slip vs. Shear Reinforcement Strain for Slate All-Lightweight Concrete Cold Joint Interface Specimens
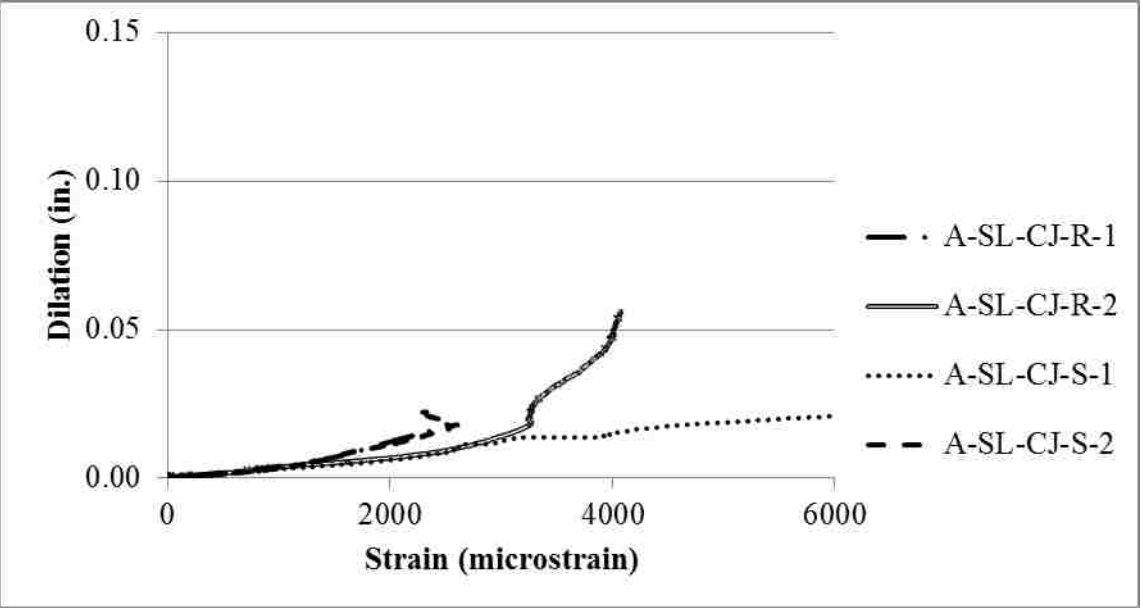
Figure 3.60 Dilation vs. Shear Reinforcement Strain for Slate All-Lightweight Concrete Cold Joint Interface Specimens

3.6.3.3 Clay aggregate all-lightweight concrete specimens. All clay all-lightweight concrete specimens had a cold joint interface. Specimens presented in this section include series A-CL-CJ-R and A-CL-CJ-S. All specimens failed in shear along the shear plane. Severe cracking of the concrete cover was observed during testing specimen A-CL-CJ-R-1 prior to reaching the ultimate force. The cracking is shown in Figure 3.61. The cracked concrete cover was physically removed after the test was completed and the result is shown in Figure 3.61. The behavior of the clay aggregate all-lightweight concrete specimens is shown in Figure 3.62 through Figure 3.67. Figure 3.62 shows the relations between applied shear force and slip. Figure 3.63 shows the applied shear versus dilation relations. Figure 3.64 shows the slip versus dilation relations. Figure 3.65 shows the applied shear force versus strain relations. Figure 3.66 shows the slip versus strain relations. Finally, Figure 3.67 shows the dilation versus strain relations.

Figure 3.61 Concrete Cracking on A-CL-CJ-R-1 (left), After the Removal of All Loose Concrete (right)
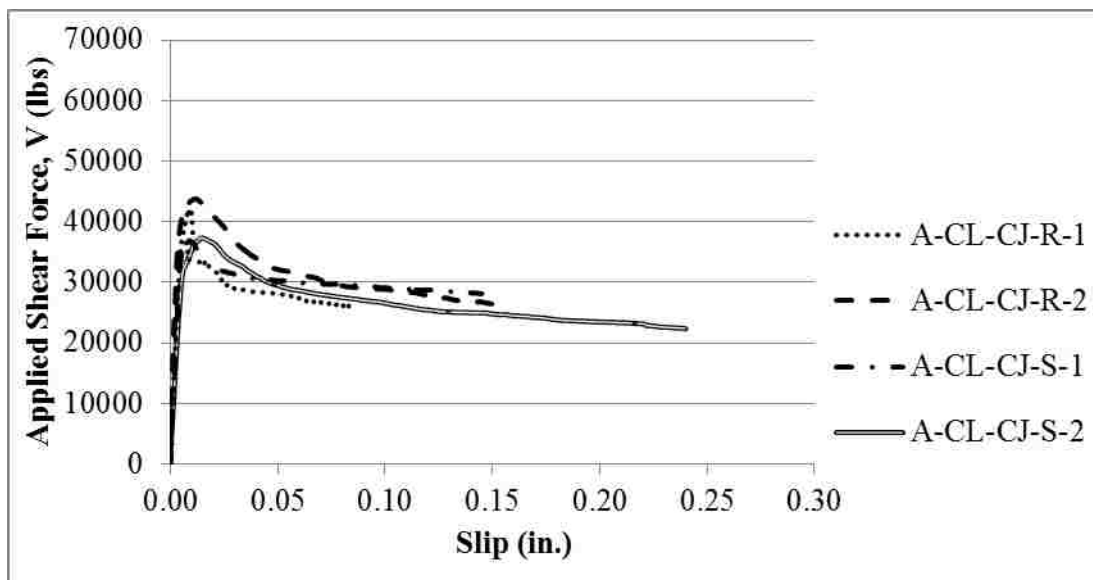
Figure 3.62 Applied Shear Force vs. Slip for Clay All-Lightweight Concrete Cold Joint Interface Specimens
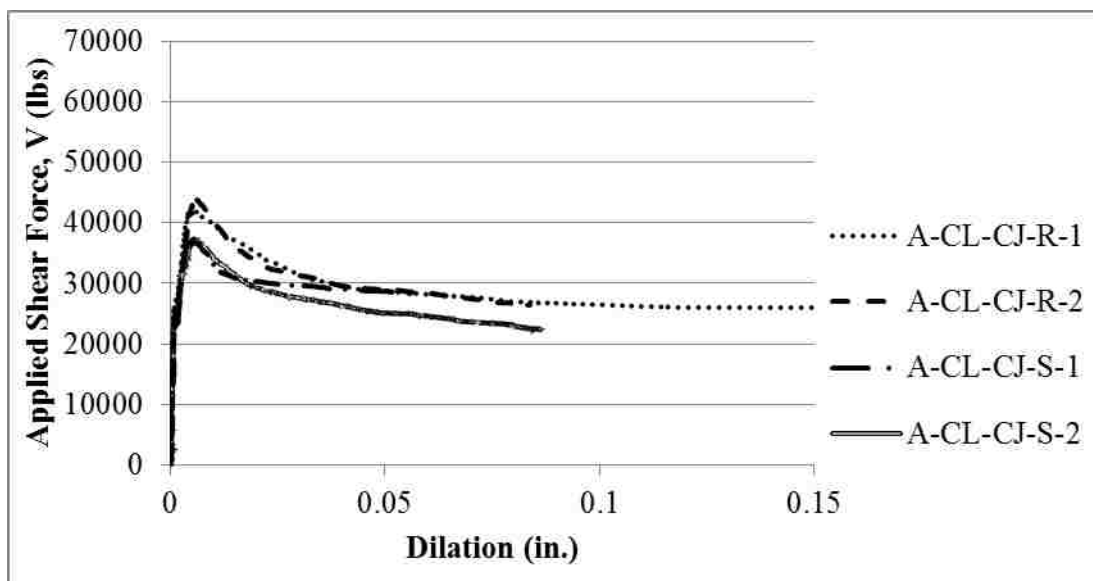
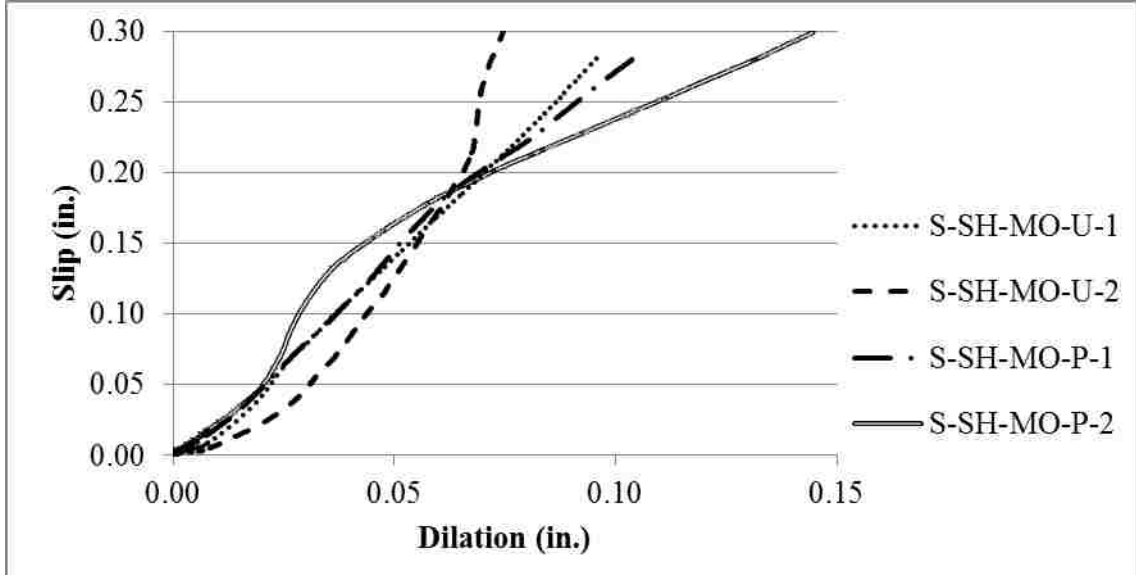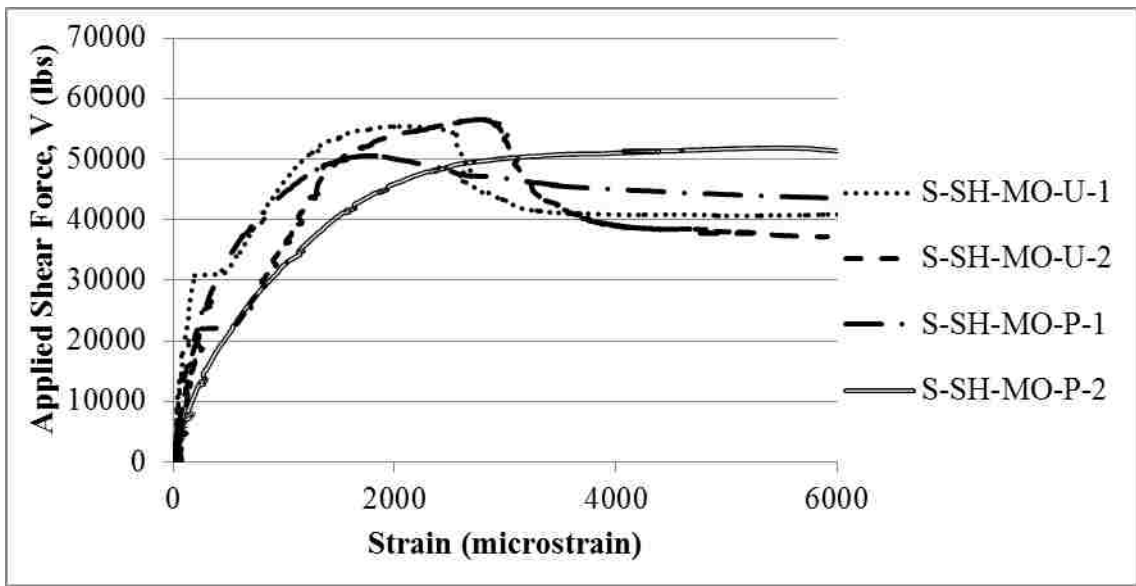Figure 3.63 Applied Shear Force vs. Dilation for Clay All-Lightweight Concrete Cold Joint Interface Specimens
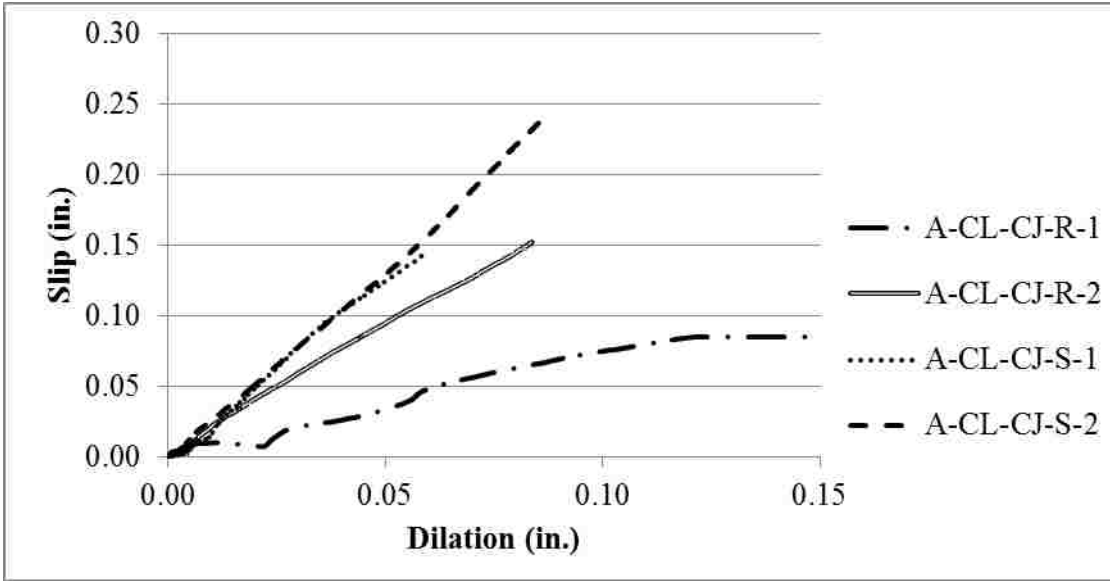
Figure 3.64 Slip vs. Dilation for Clay All-Lightweight Concrete Cold Joint Interface Specimens
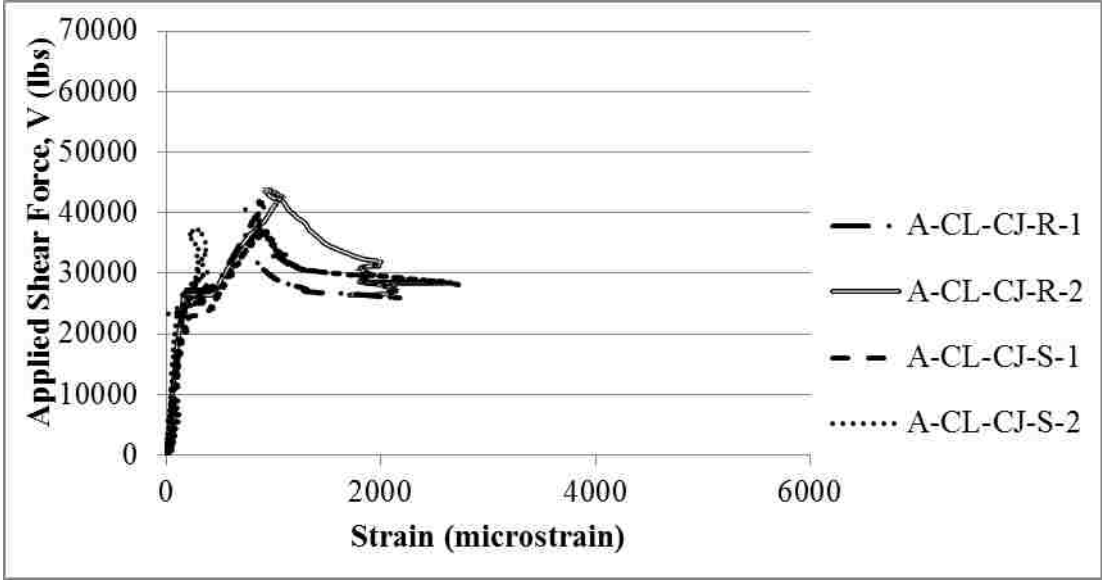
Figure 3.65 Applied Shear Force vs. Shear Reinforcement Strain for Clay All-Lightweight Concrete Cold Joint Interface Specimens
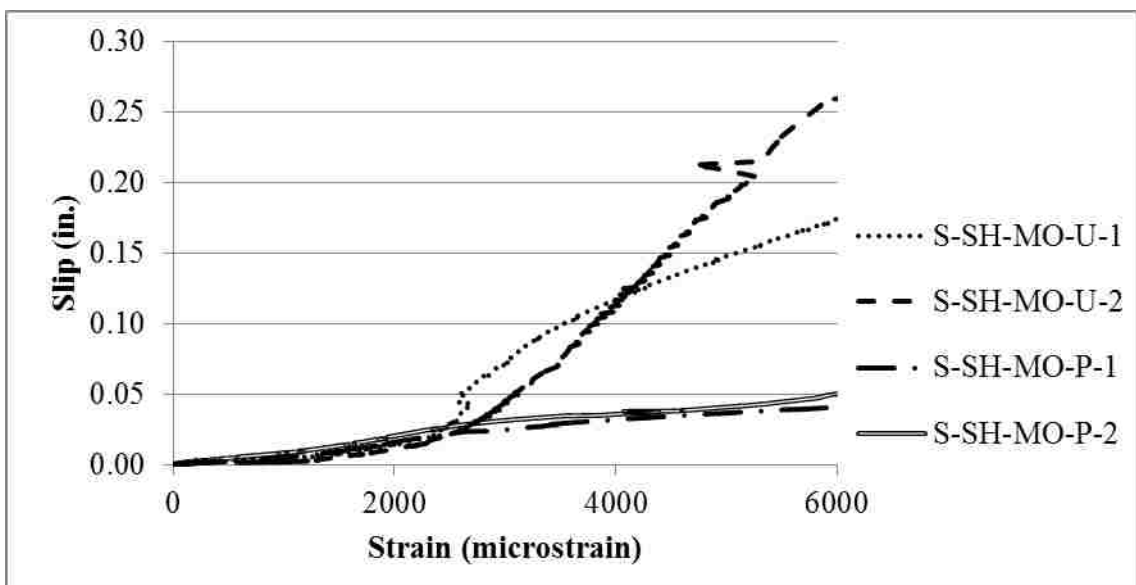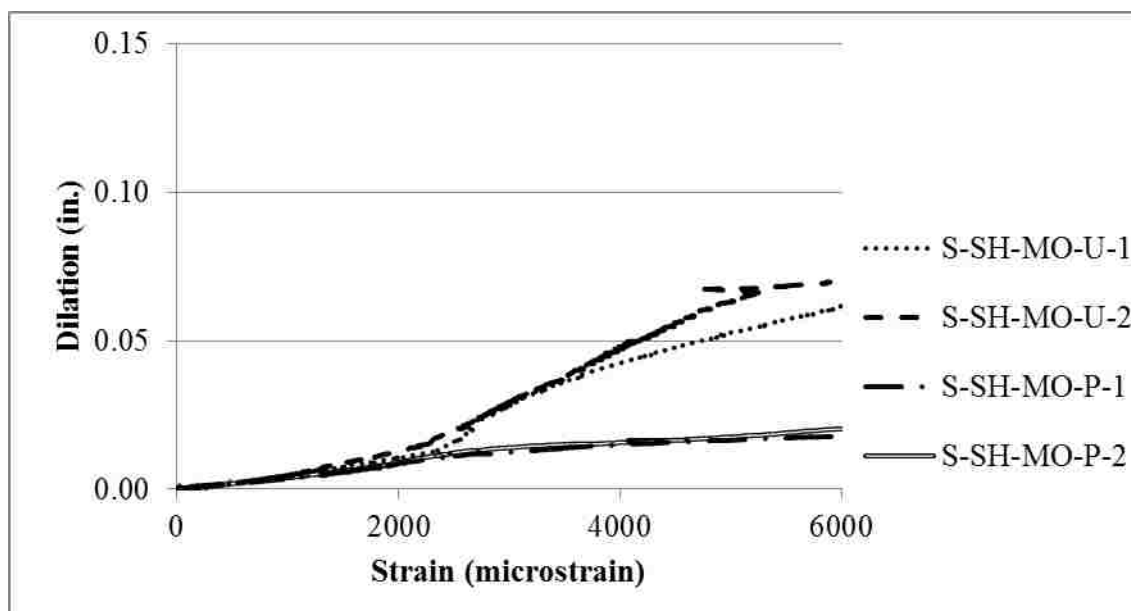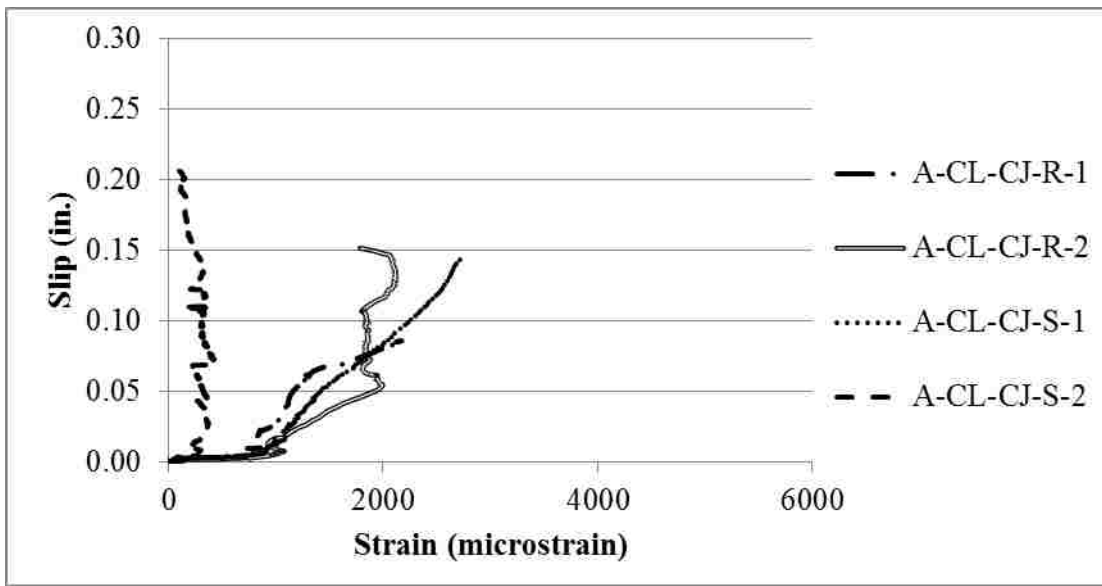
Figure 3.66 Slip vs. Shear Reinforcement Strain for Clay All-Lightweight Concrete Cold Joint Interface Specimens
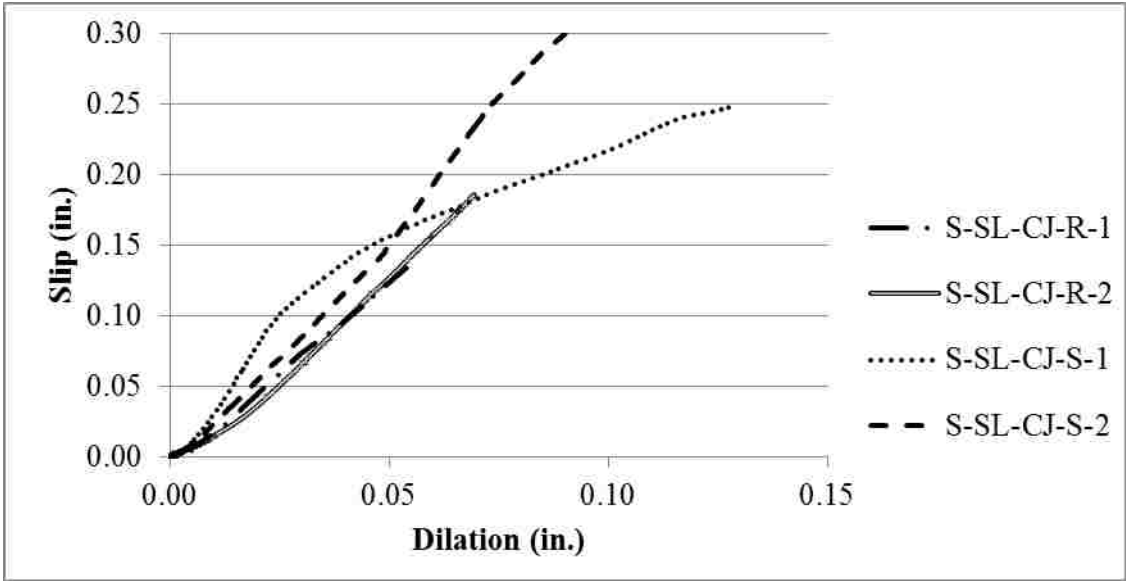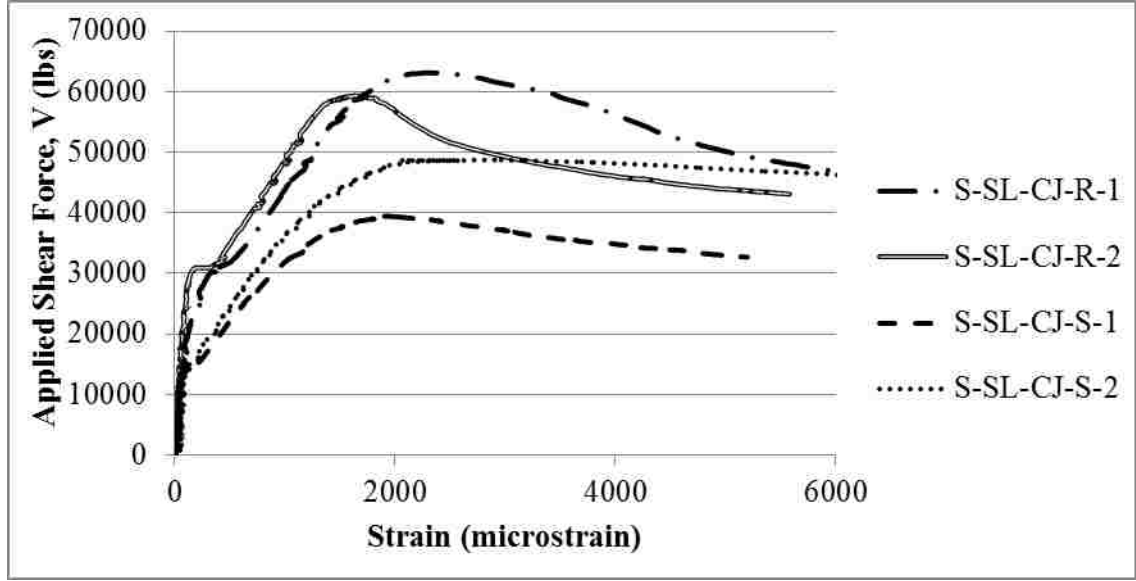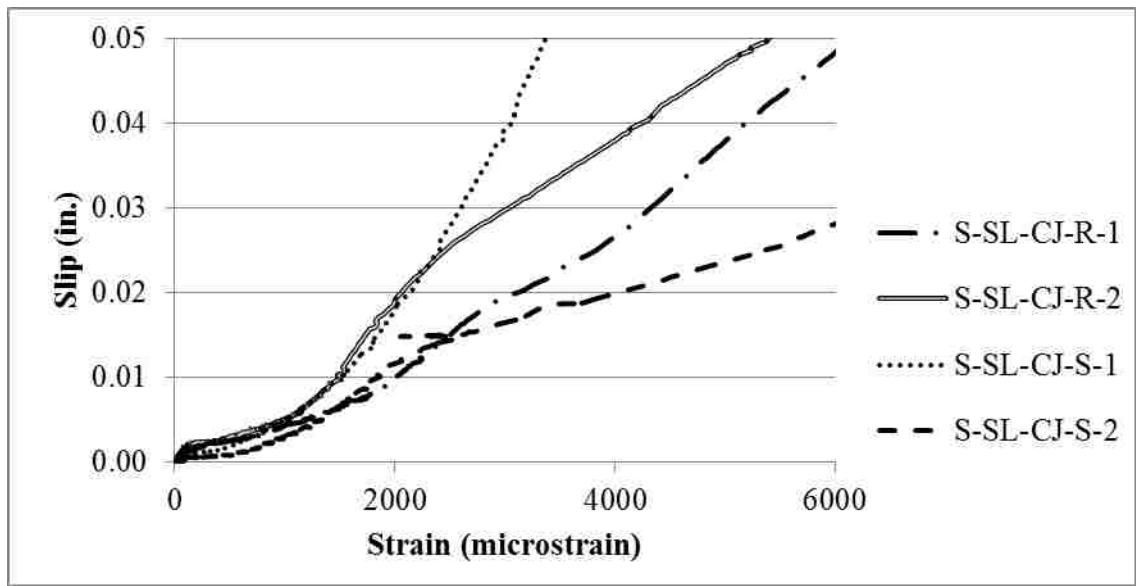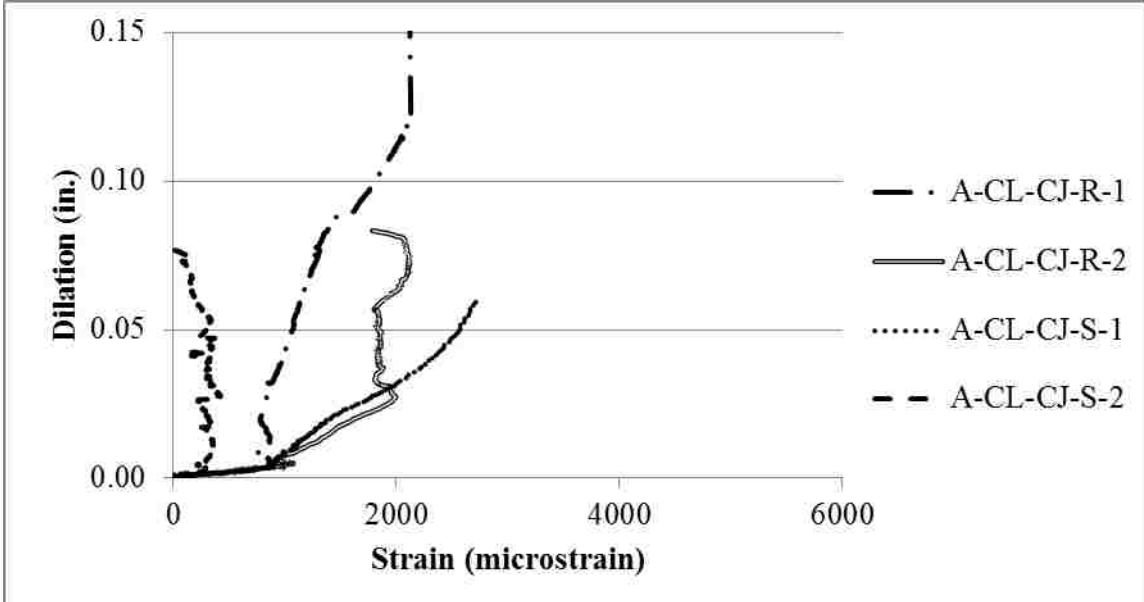

Figure 3.67 Dilation vs. Shear Reinforcement Strain for Clay All-Lightweight Concrete Cold Joint Interface Specimens

4. ANALYSIS AND DISCUSSION

4.1. INTRODUCTION

This section analyzes and discusses results of the experiments presented in Section 3.6. A comprehensive summary of the test results is presented in Table 4.1. These results are used to analyze the influence of the test variables. The measured values presented in Table 4.1 include the peak (ultimate) applied shear force V_u, peak applied shear stress v_u ($v_u = V_u/A_{cr}$), slip at V_u, dilation at V_u, residual force V_{ur}, and residual stress v_{ur} ($v_{ur} = V_{ur}/A_{cr}$). The residual force V_{ur} is defined as the load corresponding to a slip of 0.15 in. For the calculation of stresses v_u and v_{ur} the area used was the cross-sectional area of the shear plane equal to 49.5 in^2. Average values of stresses v_u and v_{ur}, for each series are shown as $v_{u,avg}$ and $v_{ur,avg}$, respectively. Finally, the average values for peak-to-residual shear stress ratio (v_u/v_{ur}) are also presented in Table 4.1 for each series.

The values listed in Table 4.1 as N/A are for specimens that reached 60% of their ultimate shear strength (post-peak) before reaching the slip of 0.15 that is used to define the residual shear strength, v_{ur}. However, these values can be estimated from the applied shear force vs. slip plots presented in Section 3.6. For N-MO-U-2 the residual shear strength is estimated to be 35,000 lbs or 700 psi. The residual shear strength of S-SL-CJ-R-1 can be extrapolated to be 37,000 lbs or 750 psi. The residual shear strength of specimens A-CL-CJ-R-1 and A-CL-CJ-S-1 is estimated to be 24,000 lbs or 480 psi and 28,000 lbs or 560 psi, respectively.

In the sections that follow, the results of the experiments are compared on the basis of general behavior, and the influence of the test variables is examined in terms of peak shear strength and residual shear strength. Results are also compared to previous studies summarized in Section 2.4. Finally, results are compared to previous and current editions of the ACI 318 code (2014) and the PCI Design Handbook (2004 and 2010).

Table 4.1 Summary of Testing Results

Specimen ID	f'_c at test day (psi)	V_u (lbs)	v_u[1] (psi)	$v_{u,\,avg}$ (psi)	Slip at V_u (in)	Dilation at V_u (in)	V_{ur}[2] (lbs)	v_{ur}[1] (psi)	$v_{ur,\,avg}$ (psi)	$(v_u/v_{ur})_{avg}$
N-MO-U-1		63410	1281	1269	0.019	0.014	40729	823	823	1.54
N-MO-U-2	4840	62203	1257		0.017	0.015	N/A	N/A		
N-MO-P-1		61071	1234	1192	0.017	0.011	45537	920	1011	1.18
N-MO-P-2		56973	1151		0.023	0.012	54598	1103		
S-SH-MO-U-1		55434	1120	1132	0.011	0.009	40773	824	801	1.41
S-SH-MO-U-2	4770	56588	1143		0.010	0.010	38501	778		
S-SH-MO-P-1		50593	1022	1035	0.013	0.007	39068	789	830	1.25
S-SH-MO-P-2		51884	1048		0.020	0.009	43098	871		
A-SH-MO-U-1		52032	1051	1056	0.016	0.009	32821	663	707	1.49
A-SH-MO-U-2	4700	52549	1062		0.013	0.009	37162	751		
A-SH-MO-P-1		46120	932	998	0.038	0.009	41332	835	906	1.10
A-SH-MO-P-2		52692	1064		0.026	0.007	48352	977		
S-SL-CJ-R-1		63167	1276	1238	0.013	0.008	N/A	N/A	735	1.68
S-SL-CJ-R-2	5570	59370	1199		0.013	0.009	36363	735		
S-SL-CJ-S-1		39487	798	891	0.017	0.007	30508	616	700	1.27
S-SL-CJ-S-2		48767	985		0.016	0.008	38771	783		
A-SL-CJ-R-1		46525	940	944	0.012	0.006	30148	609	645	1.46
A-SL-CJ-R-2	4380	46925	948		0.005	0.005	33741	682		
A-SL-CJ-S-1		37842	764	774	0.019	0.007	30810	622	671	1.15
A-SL-CJ-S-2		38751	783		0.024	0.007	35575	719		
S-CL-CJ-R-1		50785	1026	986	0.007	0.006	31310	633	651	1.51
S-CL-CJ-R-2	4640	46885	947		0.015	0.005	33178	670		
S-CL-CJ-S-1		41006	828	822	0.015	0.006	31025	627	600	1.37
S-CL-CJ-S-2		40436	817		0.018	0.007	28402	574		
A-CL-CJ-R-1		41858	846	865	0.009	0.006	N/A	N/A	534	1.62
A-CL-CJ-R-2	4460	43816	885		0.011	0.006	26451	534		
A-CL-CJ-S-1		36966	747	750	0.008	0.005	N/A	N/A	501	1.50
A-CL-CJ-S-2		37324	754		0.015	0.006	24795	501		

[1]Shear stresses v_u and v_{ur} are defined as the peak and residual applied shear force respectively, divided by the area of the shear plane

[2] Residual shear force V_{ur} is defined as the load at 0.15 in. of slip as described in Section 3.6

4.2. GENERAL BEHAVIOR

Specimen behavior will be described in terms of cracking stress, applied shear force versus slip relations, and applied shear force versus interface reinforcement strain relations.

4.2.1. Cracking. Typical shear-plane cracks are shown in Figure 4.1. Dilation of the shear-plane crack at the peak applied shear force was the most significant for normalweight concrete specimens, which is likely the result of the use of a larger maximum aggregate size (i.e. 3/4 in.). This larger aggregate creates greater dilation as described by the saw-tooth analogy by Birkeland and Birkeland (1966). This dilation ranges from 0.011 in. to 0.015 in. at the peak applied shear force. For sand-lightweight concrete and all-lightweight concrete the maximum aggregate size was 3/8 in. causing the shear crack separation at the peak applied shear force to range from 0.005 in. to 0.010 in. The crack separation difference between smooth and roughened interface specimens was insignificant. Flexural cracks in the flanges were described in Section 3.6 and are shown in Figures 3.20, 3.27, and 3.61. Spalling of concrete cover was described in Section 3.6 and is shown in Figures 3.34, 3.48, and 3.61. The cracking shown in these figures was most likely due to the slight eccentricities of reinforcement during construction that caused the concrete cover to be smaller than specified and/or concrete splitting.

Figure 4.1 Typical Shear Plane Crack Normalweight Concrete Monolithic Interface (left), Shale Sand-lightweight Concrete Monolithic Interface (right)

4.2.2. Applied Shear Force – Slip Relations. Applied shear force – slip relations for normalweight, sand-lightweight, and all-lightweight concrete monolithic and cold joint specimens are shown in Figures 3.21, 3.28, 3.35, 3.42, 3.49, 3.55, and 3.62 in Section 3.6. These figures illustrate initial linear elastic behavior, shear plane cracking represented by the peak value of the applied shear force V_u, followed by decrease in the applied shear force until a near-constant force is reached. The post-peak shear force V_{ur} is defined in this study as the shear force that corresponds to slip of 0.15 in. The behavior shown in the applied shear force – slip relations reflects the behavior observed previously by Shaw (2013).

From the figures mentioned above, it can be seen that the normalweight monolithic interface specimens exhibit roughly the same stiffness prior to the peak applied shear force. The maximum applied shear force is not significantly affected by pre-cracking as summarized in Table 4.2. For monolithic pre-cracked specimens, the slip is larger at the peak applied shear force compared to the uncracked specimens. After the peak shear force is achieved, the shear force of the normalweight uncracked specimens decreases more rapidly with increasing slip than the normalweight pre-cracked specimens. This behavior is shown in Figure 3.21 but can also be observed in Table 4.1 where v_u/v_{ur} ratio is larger for uncracked monolithic normalweight specimens than the pre-cracked monolithic mornalweight specimens.

The shale sand-lightweight concrete monolithic interface specimens show very similar initial stiffness. The maximum applied shear force is larger for the uncracked specimens than the pre-cracked specimens (see Figure 3.28). Quasi-brittle behavior is observed with uncracked specimens, i.e. after reaching the peak applied shear force, the shear force decreases rapidly with increasing slip (see v_u/v_{ur} ratio Table 4.1) .

The shale all-lightweight concrete monolithic interface specimens have nearly identical initial stiffness. The peak applied shear force is unaffected by pre-cracking of the specimens (see Figure 3.49). However, the uncracked specimens exhibit more quasi-brittle post-peak behavior compared to the pre-cracked specimens (Table 4.1).

The slate and clay sand-lightweight concrete cold joint interface specimens have very similar initial stiffness (Figures 3.35 and 3.42). The peak values correspond to a slip of about 0.015 in. A significantly higher peak applied shear force is achieved with the

roughened interface specimens compared to smooth interface specimens. This higher peak applied shear strength is accompanied with quasi-brittle post-peak behavior (Table 4.1). The post-peak shear strength is not affected by the shear plane surface preparation.

The slate and clay all-lightweight concrete cold joint interface specimens have nearly identical initial stiffness (Figures 3.55 and 3.62). The peak values correspond to a slip of 0.015 in. to 0.020 in. A higher peak applied shear force is observed in roughened interface specimens than the corresponding smooth interface specimens. This higher peak applied shear strength is accompanied with quasi-brittle post-peak behavior (Table 4.1). The post-peak shear strength is not affected by the shear plane surface preparation.

4.2.3. Applied Shear Force – Interface Reinforcement Strain Relations. The applied shear force – interface reinforcement strain relations are shown in Figures 3.24, 3.31, 3.38, 3.45, 3.52, 3.58, and 3.65 in Section 3.6. For monolithic specimens included in series N-MO, S-SH-MO, and A-SH-MO, the formation of the shear crack can be observed for the uncracked specimens by examining these relations in detail. The pre-cracked specimens are not included in this section because the crack was initiated prior to testing. When the shear crack forms, the shear reinforcement engages, which can be detected from the strain measurements as a sudden increase in strain. This cracking is associated with a "plateau" on the applied shear stress v ($v=V/A_{cr}$) versus interface reinforcement strain plot. A typical example of this behavior is shown in Figure 4.2. The stress associated with crack formation, v_{cr}, determined from the applied shear stress versus interface reinforcement strain plot is also shown. For the uncracked specimens the average cracking stress ranges between 300 psi to 700 psi.

For the cold joint interface specimens included in series S-SL-CJ, A-SL-CJ, S-CL-CJ, and A-CL-CJ, the interface cracking stress was determined in the same manner as for the monolithic specimens. A typical plot of the applied shear stress versus interface reinforcement strain for cold joint specimens is shown in Figure 4.3. This figure shows the typical behavior of all cold joint interface specimens, where roughened specimens achieve higher shear strength at the same strain level.

Values of v_{cr} associated with the interfacial crack formation for all specimens are summarized and compared in Figure 4.4 and Table 4.3 (The values for series N-MO-U and S-CL-CJ-R in Figure 4.4 and Table 4.3 are not the averaged values because cracking

was not detected by the strain readings in specimens N-MO-U-1 and S-CL-CJ-R-2). The values of v_{cr} in Table 4.3 are the average determined from each of the shear force – strain relations for all properly functioning gages of the corresponding specimens. Values are reported to the nearest 25 psi. It must be noted that the interfacial crack formation does not correspond to the ultimate shear strength of specimens as seen in Figures 4.2 and 4.3. The ultimate shear strength of specimens is roughly associated with the visual formation of the shear crack. Interfacial crack formation was not detected by the strain gages in specimens N-MO-U-1 and S-CL-CJ-R-2.

Table 4.2 Average Peak Applied Shear Stress Percent Difference between Uncracked and Pre-cracked Monolithic Specimens

Specimen ID	Average Peak Applied Shear Stress, $v_{u,avg}$ (psi)	% Difference
N-MO-U	1269	6.2
N-MO-P	1192	
S-SH-MO-U	1132	8.9
S-SH-MO-P	1035	
A-SH-MO-U	1056	5.7
A-SH-MO-P	998	
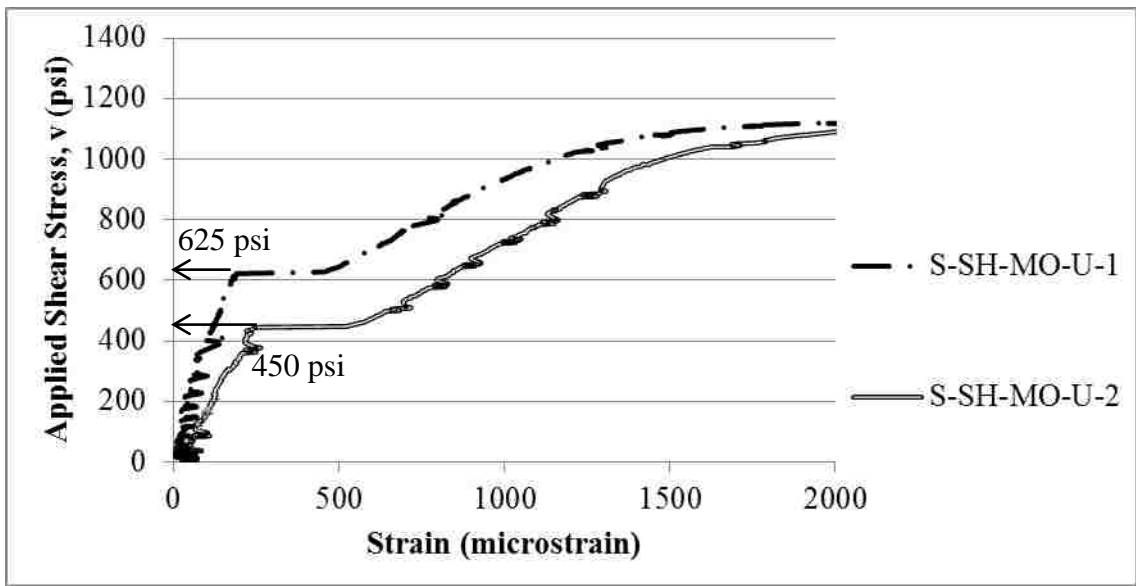
Figure 4.2 Typical Applied Shear Stress vs. Interface Reinforcement Strain Plot Showing Crack Formation in Monolithic Uncracked Specimens (Specimens in Series S-SH-MO Shown)
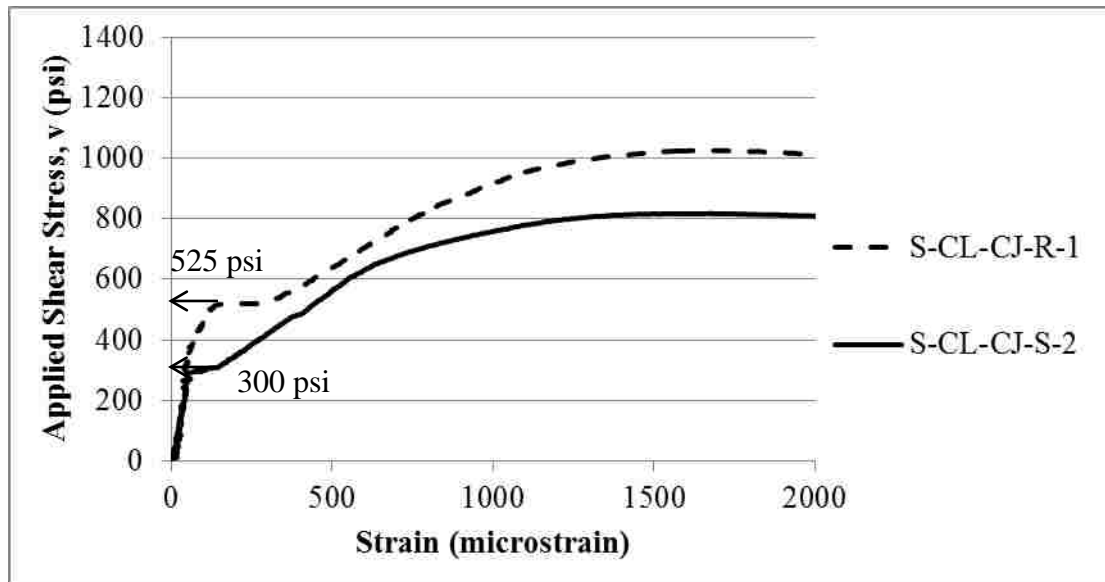
Figure 4.3 Typical Applied Shear Stress vs. Interface Reinforcement Strain Plot Showing Crack Formation in Cold Joint Specimens (Specimens in Series S-CL-CJ Shown)
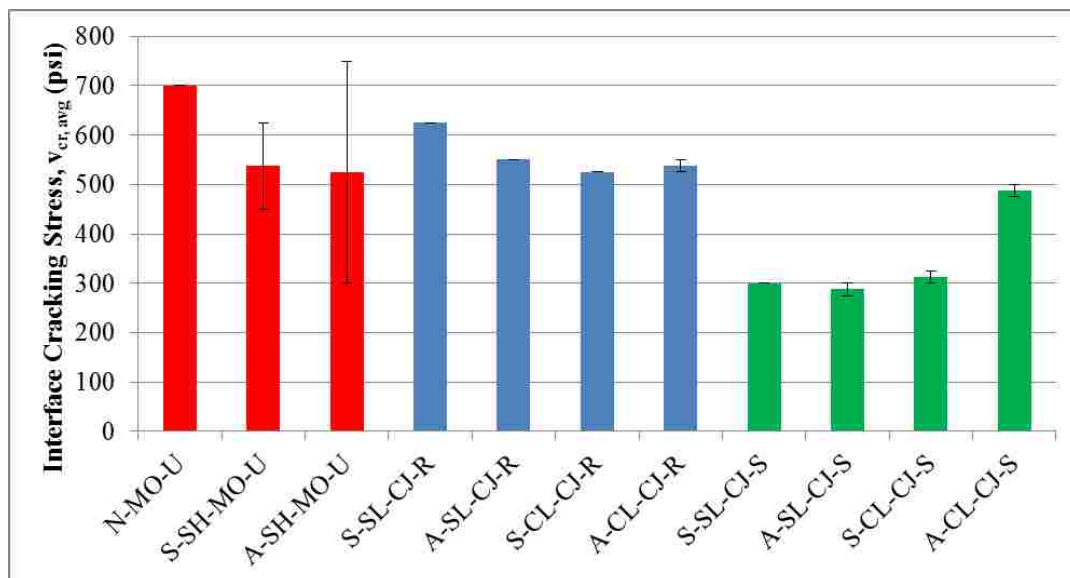
Figure 4.4 Average Value of Stress Associated with Interface Cracking $v_{cr, avg}$ Determined From Strain Measuruments

Table 4.3 Summary of Interface Cracking Stresses v_{cr} Determined From Strain Measuremnts

Specimen ID	Interface Condition	v_{cr} (psi)	$v_{cr,avg}$ (psi)	SD $v_{cr,avg}$ (psi)
N-MO-U-1	Uncracked	N/A[1]	700	0
N-MO-U-2	Uncracked	700		
S-SH-MO-U-1	Uncracked	625	538	87.5
S-SH-MO-U-2	Uncracked	450		
A-SH-MO-U-1	Uncracked	750	525	225
A-SH-MO-U-2	Uncracked	300		
S-SL-CJ-R-1	Rough	625	625	0
S-SL-CJ-R-2	Rough	625		
S-SL-CJ-S-1	Smooth	300	300	0
S-SL-CJ-S-2	Smooth	300		
A-SL-CJ-R-1	Rough	550	550	0
A-SL-CJ-R-2	Rough	550		
A-SL-CJ-S-1	Smooth	300	288	12.5
A-SL-CJ-S-2	Smooth	275		
S-CL-CJ-R-1	Rough	525	525	0
S-CL-CJ-R-2	Rough	N/A[1]		
S-CL-CJ-S-1	Smooth	325	313	12.5
S-CL-CJ-S-2	Smooth	300		
A-CL-CJ-R-1	Rough	550	538	12.5
A-CL-CJ-R-2	Rough	525		
A-CL-CJ-S-1	Smooth	475	488	12.5
A-CL-CJ-S-2	Smooth	500		

[1] Cracking was not detected from strain measurements

4.3. INFLUENCE OF TEST VARIABLES

This section analyzes the experimental results presented in Section 3.6 to determine the influence of the test variables. The studied test variables include concrete unit weight, aggregate type, and shear interface preparation.

4.3.1. Effect of Concrete Unit Weight. In this study, normalweight, sand-lightweight, and all-lightweight concrete types were used. The unit weight (measured on fresh concrete) ranged from 88 lb/ft3 for all-lightweight concrete to 148 lb/ft3 for normalweight concrete. For more detailed discussion of the concrete mixtures see Section 3.3.2. In this section, the effect of concrete unit weight on the shear transfer strength is analyzed. Monolithic interface specimens and cold joint interface specimens are compared separately.

Figures 4.5 through 4.8 show the comparison of the shear strength, v_u, and residual shear strength, v_{ur}, to concrete unit weight for the monolithic specimens. Figure 4.5 shows the relation of the peak (ultimate) shear stress v_u versus concrete unit weight. Trendlines are also plotted on this graph for the uncracked and pre-cracked specimens, maintaining the distinction between the different interface conditions. The trends show that for monolithic concrete specimens, the peak shear stress increases with increasing unit weight. This is true for both uncracked and pre-cracked specimens. The slopes of the trendlines are close suggesting that the increase in peak shear stress with increasing concrete unit weight is independent of a pre-existing crack. Figure 4.6 shows the normalized plot of the ultimate shear strength versus unit weight of concrete. Due to the different compressive strengths of concrete on test date, the plot was normalized with respect to the compressive strength of concrete. This plot shows behavior similar to that of Figure 4.5.

Figure 4.7 plots the residual shear strength versus concrete unit weight. Increasing residual shear stress with increasing unit weight is observed in Figure 4.7. The residual shear strength values have slightly greater deviation between the two specimens of each series compared to the peak shear stress values from Figure 4.5. The slopes of the trendlines suggest increasing residual shear strength with increasing concrete unit weight. Figure 4.8 plots the normalized residual shear strength versus concrete unit weight. Normalization is performed with respect to the concrete compressive strength. The trendlines suggest increasing residual shear strength with increasing concrete unit weight.

Figures 4.9 through 4.12 show the comparison of the shear strength v_u and residual shear strength v_{ur} to concrete unit weight for the cold joint specimens in this study. Figure 4.9 plots the peak shear stress versus concrete unit weight for the cold joint

specimens, along with trendlines, maintaining the distinction between roughened and smooth interface specimens. The trendlines show that the peak shear strength increases with increasing unit weight. The increasing trend is more significant for the roughened interface concrete specimens. Figure 4.10 shows the same plot but with the shear strength normalized with respect to the concrete compressive strength on test day. This plot suggests that normalized shear strength is not affected by concrete unit weight for the smooth interface concrete specimens. However, the trend of increasing shear strength with increasing concrete unit weight remains the same for roughened interface concrete specimens. Figure 4.11 plots the residual shear strength versus unit weight of concrete. The trendlines suggest increasing residual shear strength with increasing concrete unit weight. However, Figure 4.12 shows that this increase in shear strength is not significant when the shear strength is normalized with respect to concrete compressive strength. It should be noted, however, that the normalweight concrete specimens had a larger maximum aggregate size (3/4 in.) than the sand-lightweight and all-lightweight concrete specimens (3/8 in.) as discussed in Section 4.2.1.
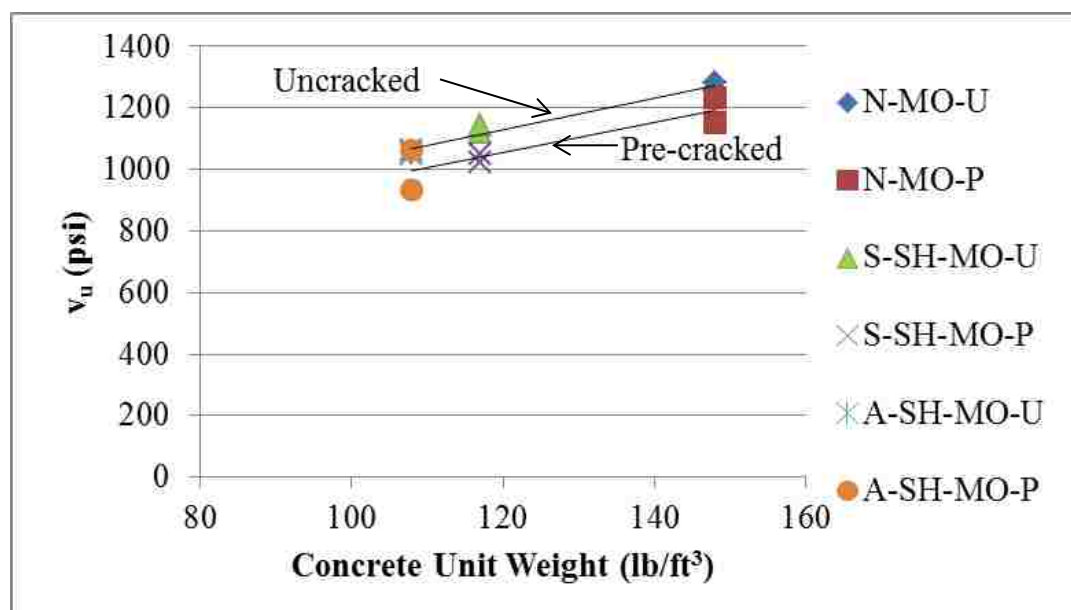
Figure 4.5 Shear Strength v_u vs. Concrete Unit Weight for Monolithic Interface Specimens
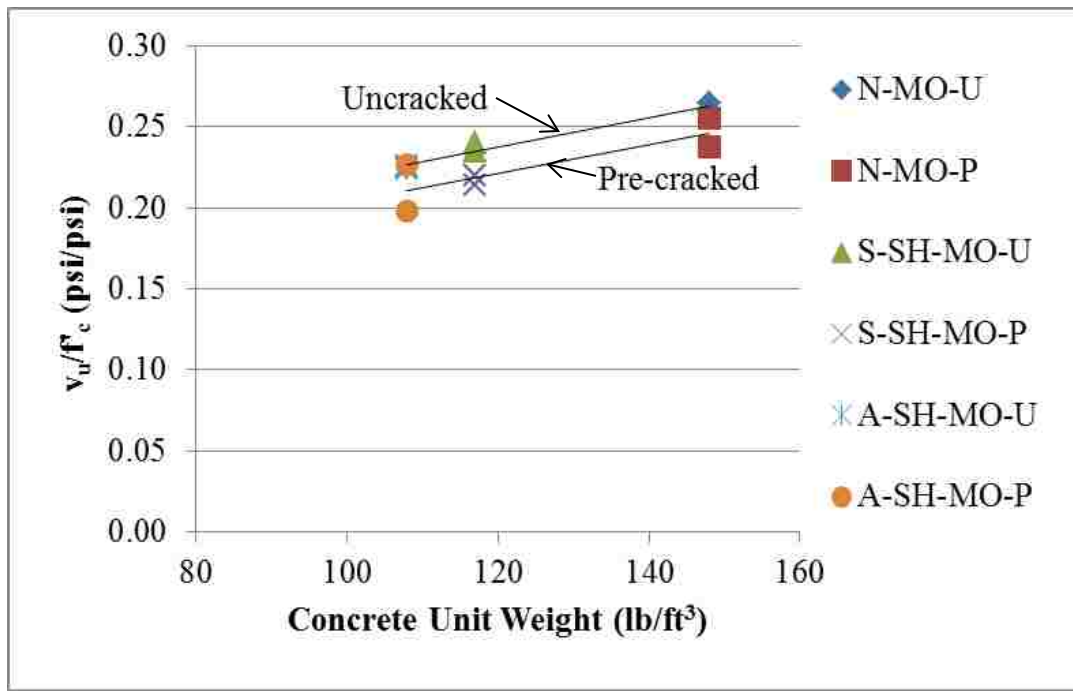
Figure 4.6 Normalized Shear Strength v_u vs. Concrete Unit Weight for Monolithic Interface Specimens
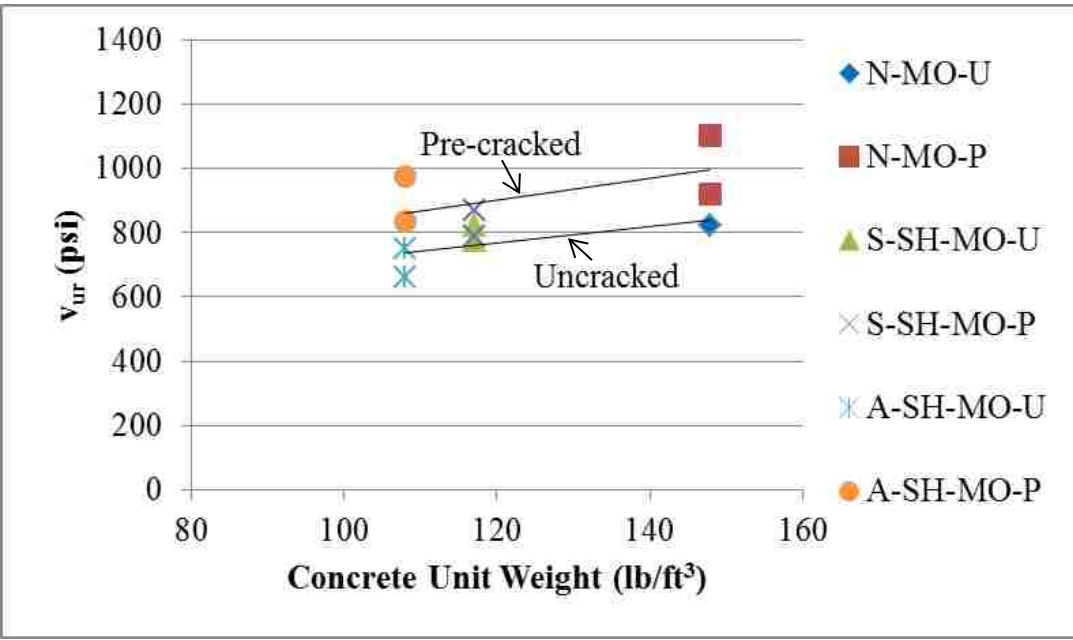
Figure 4.7 Residual Shear Strength v_{ur} vs. Concrete Unit Weight for Monolithic Interface Specimens
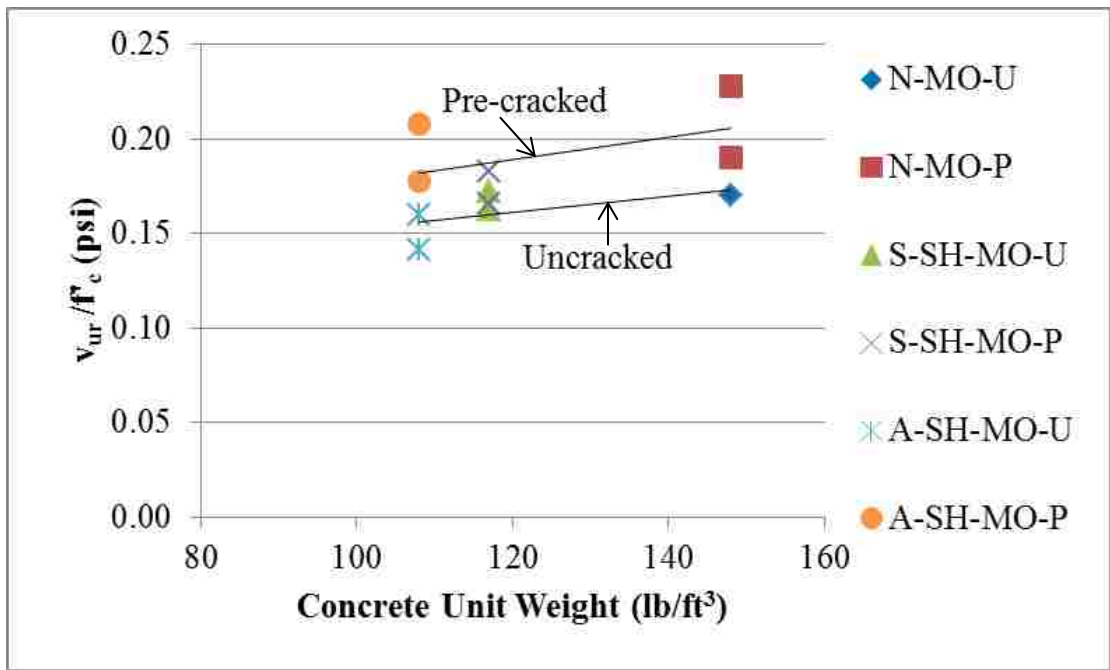
Figure 4.8 Normalized Residual Shear Strength v_{ur} vs. Concrete Unit Weight for Monolithic Interface Specimens
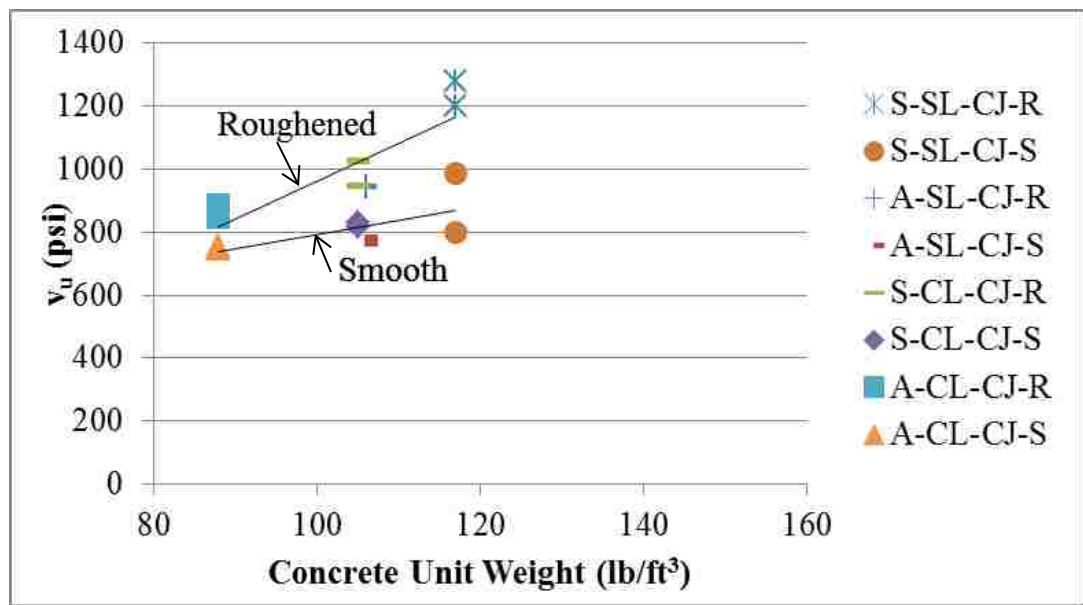
Figure 4.9 Shear Strength v_u vs. Concrete Unit Weight for Cold Joint Specimens
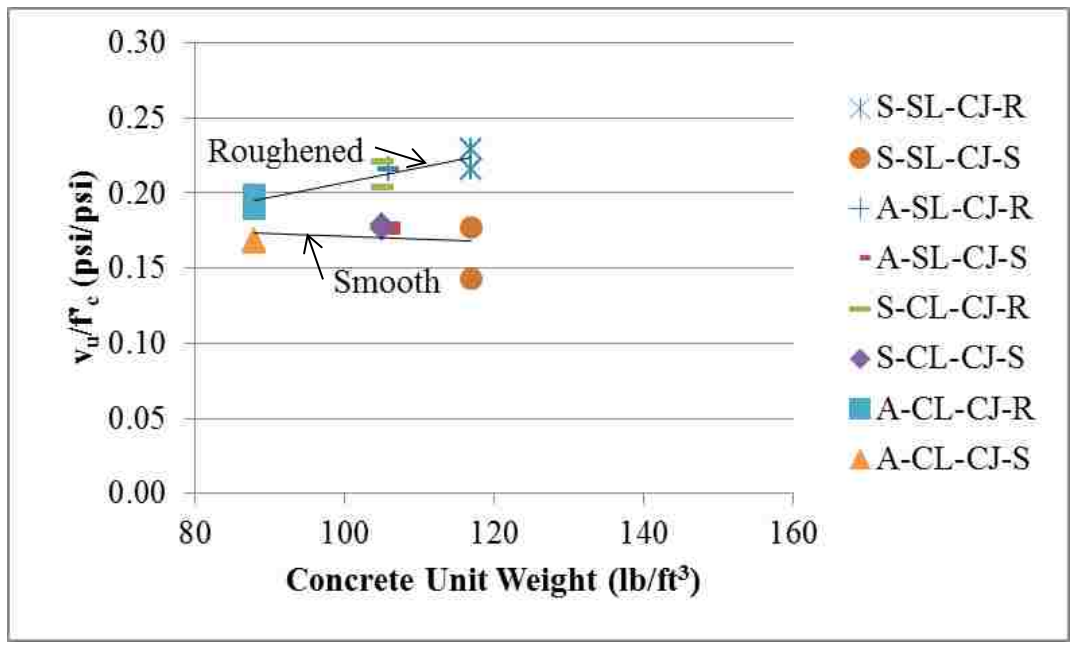
Figure 4.10 Normalized Shear Strength v_u vs. Concrete Unit Weight for Cold Joint Specimens
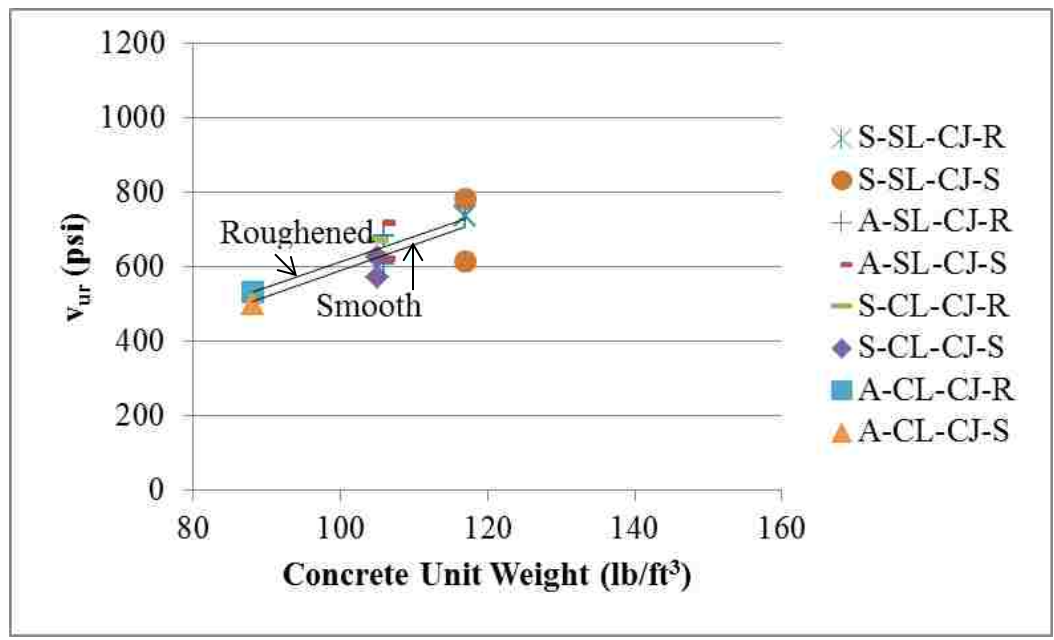
Figure 4.11 Residual Shear Strength v_{ur} vs. Concrete Unit Weight for Cold Joint Specimens
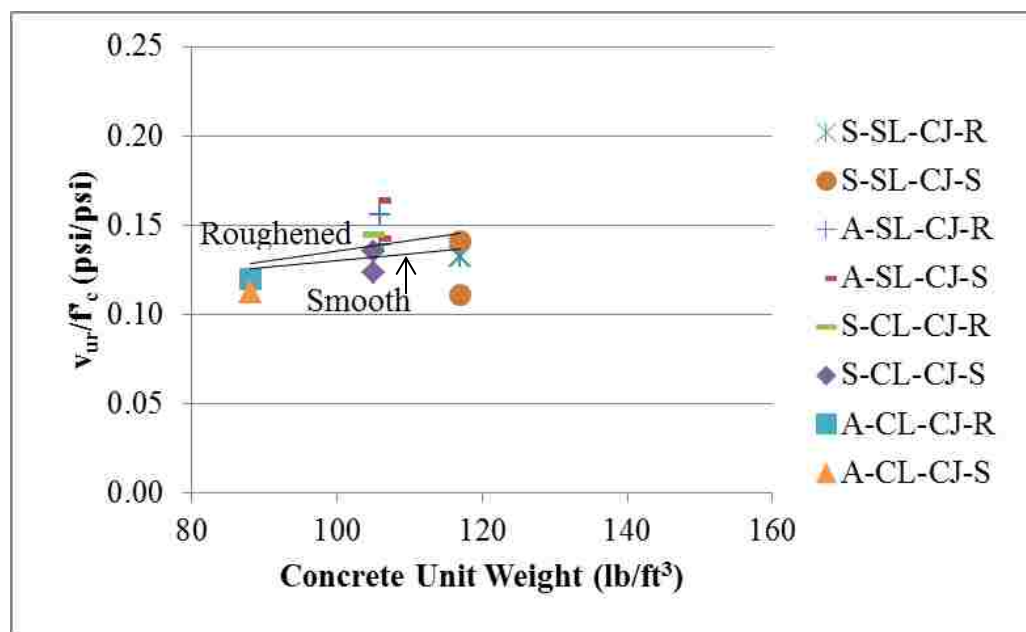
Figure 4.12 Normalized Residual Shear Strength v_{ur} vs. Concrete Unit Weight for Cold Joint Specimens

4.3.2. Effect of Lightweight Aggregate Type. Three types of lightweight aggregate (expanded shale, expanded slate, and expanded clay) were included in this study. For more detailed discussion of lightweight aggregates used in this study see Section 3.3.1. This section examines the effect of lightweight aggregate type on the shear transfer strength. Monolithic specimens are compared first. Cold joint specimens are analyzed later in this section.

Figures 4.13 and 4.14 show the applied shear force versus slip relations for all uncracked and pre-cracked monolithic specimens, respectively. Specimens with normalweight concrete have the highest shear strength followed by shale sand-lightweight concrete specimens. The weakest specimens in terms of shear strength are the all-lightweight shale specimens. The percent difference in the peak shear load V_u between uncracked and pre-cracked specimens for concrete with the same aggregate type is summarized in Table 4.2. While the average peak applied shear stress of the uncracked specimens is consistently larger than that of the pre-cracked specimens, the percent difference for all monolithic specimens is below 9% suggesting that pre-cracking of the specimens has little effect on shear strength of the specimens regardless of the aggregate

type. Figure 4.15 suggests that specimens with normalweight aggregate have higher shear strength compared to shale sand-lightweight and all-lightweight concrete specimens. It also suggests that shear transfer strength is more dependent on concrete unit weight than aggregate type.

Figure 4.16 plots the relations between applied shear force and slip for the sand-lightweight concrete specimens in this study. The slate aggregate specimens achieved a higher peak applied shear force compared to the clay aggregate specimens for both a roughened and smooth interface. Figure 4.17 plots the relations between applied shear force and slip for the all-lightweight concrete specimens. The all-lightweight slate specimens achieved a higher peak applied shear force compared to the clay all-lightweight concrete specimens. The same findings can be seen in Figure 4.18 that plots the applied shear force for all cold joint specimens. The comparisons can be made for all pre-cracked and uncracked specimens. Specimens with slate aggregate achieved a higher shear transfer strength compared to specimens with clay aggregate for sand-lightweight and all-lightweight concrete, as well as for roughened and smooth interface preparation. This may be explained on basis of density of the aggregate. Expanded clay aggregate is less dense than expanded slate aggregate as described in Section 3.3.1.2. This suggests more air voids in clay aggregate. These air voids cause the aggregate to be lighter but also weaker in direct shear.
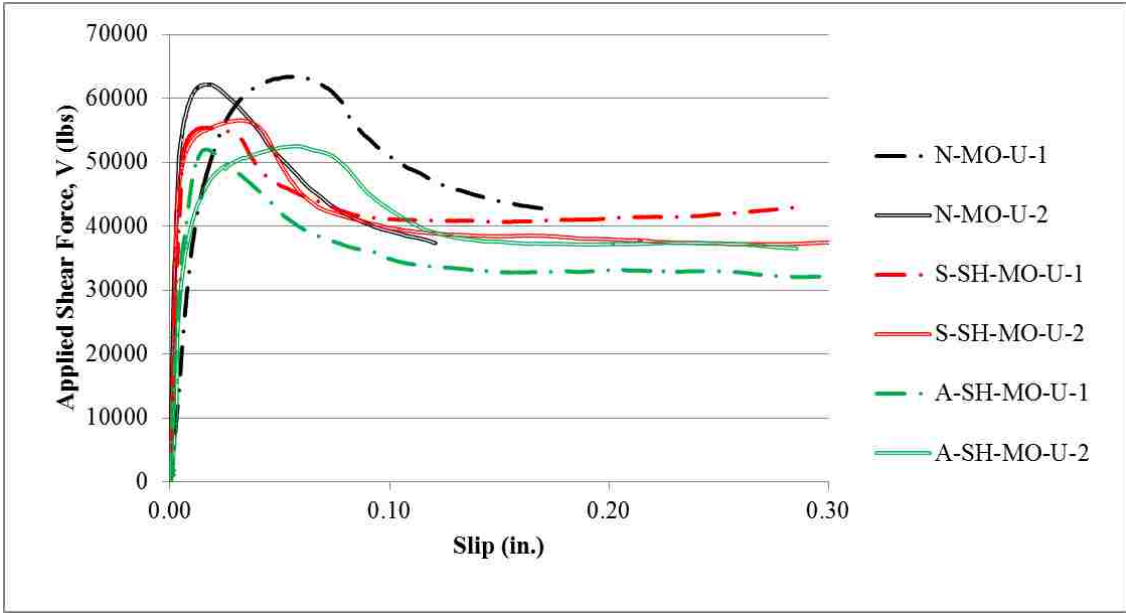
Figure 4.13 Applied Shear Force vs. Slip for Monolithic Uncracked Specimens
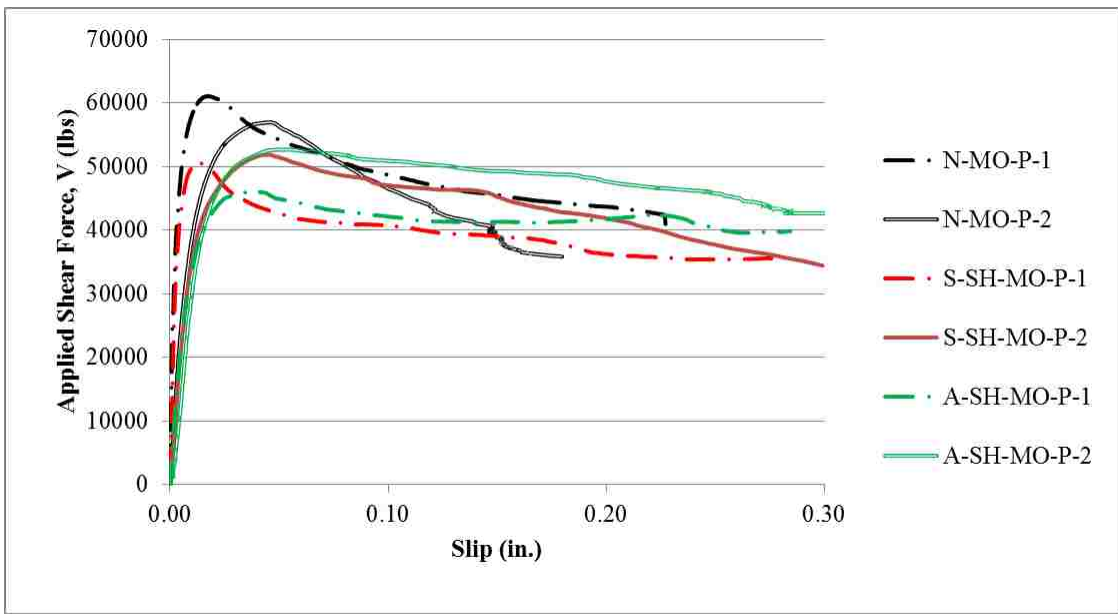
Figure 4.14 Applied Shear Force vs. Slip for Monolithic Pre-cracked Specimens
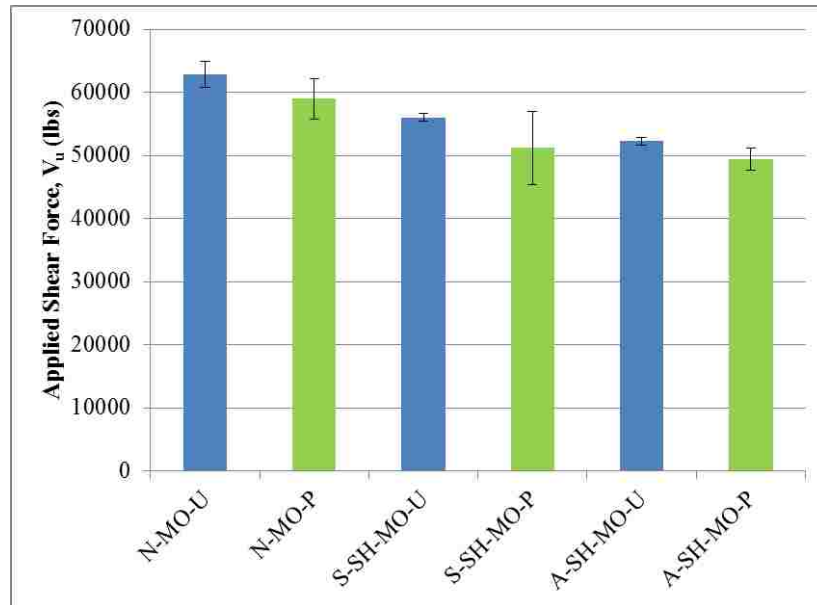
Figure 4.15 Comparison of Uncracked and Pre-cracked Monolithic Specimens in Terms of Average Peak Applied Shear Force
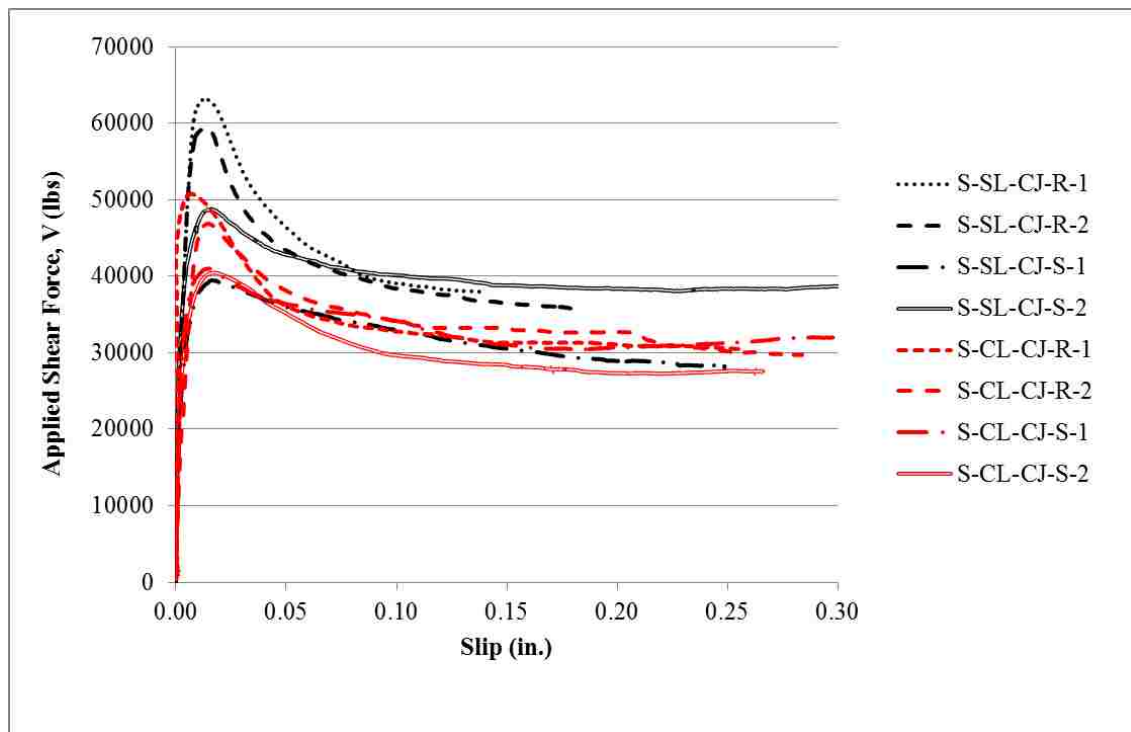
Figure 4.16 Applied Shear Force vs. Slip of Sand-lightweight Concrete Specimens
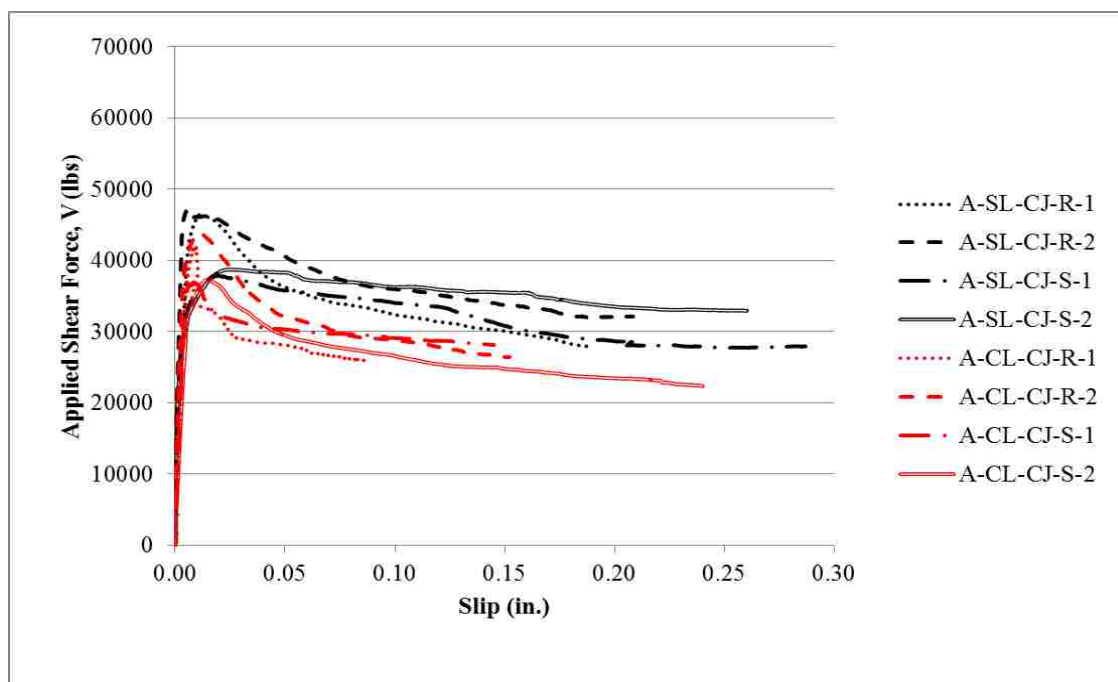
Figure 4.17 Applied Shear Force vs. Slip of All-lightweight Concrete Specimens
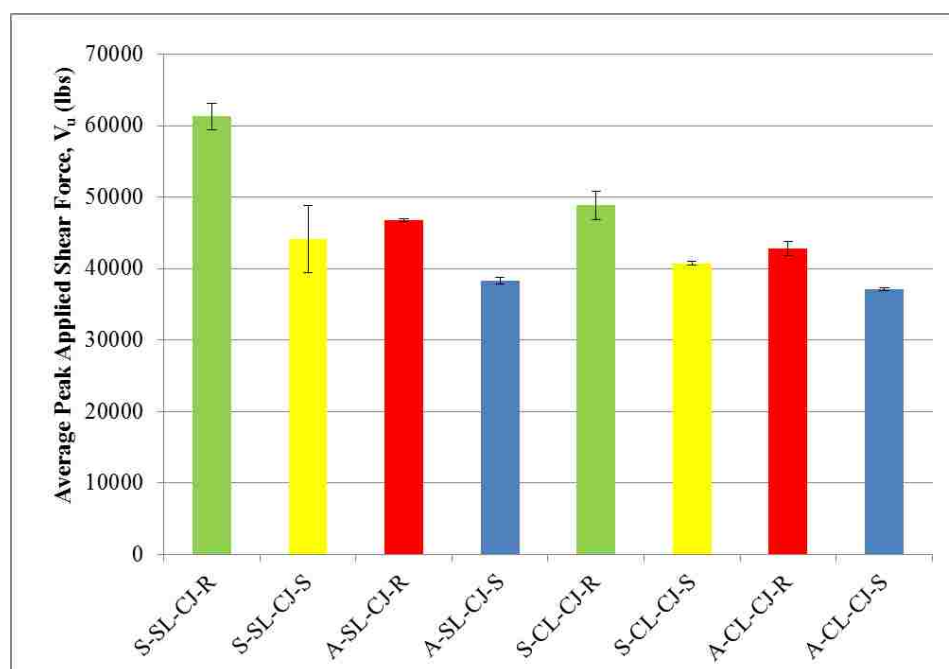
Figure 4.18 Comparison of Cold Joint Specimens with Slate and Clay Aggregate in Terms of Average Peak Applied Shear Force

4.3.3. Effect of Shear Interface Preparation. Specimens evaluating this variable include monolithic and non-monolithic (cold joint) interfaces. This section first examines the specimens with cold joint interfaces only, but then those results are compared to the monolithic cases. The cold joint interfaces were either troweled smooth or roughened to average amplitude of 1/4 in. To isolate the interface condition as the only parameter, specimens constructed using the same lightweight aggregate and having the same unit weight are compared in this section. In the graphs presented in this section, the horizontal scale for the slip is limited to 0.15 in. to compare the residual shear force V_{ur}. This is the only difference between Figures 4.19 through 4.22 and the figures presented in Section 3.6.

Figures 4.19 through 4.22 show the comparison between applied shear force and slip for the cold joint interface specimens studied in this project. The measured concrete compressive strength for each series is the same, leaving the interface preparation as the only variable. In all cases, specimens with roughened interface achieved a higher peak shear force than the specimens with smooth interface. This phenomenon can be explained on basis of aggregate interlock. The specimens with smooth interface have to rely solely on cohesion and dowel action before cracking along the shear plane and reaching their peak applied shear force. For the smooth specimens there is no contribution from interlocking of one roughened interface with the other. Once the initial crack has been formed, the smoothness of the interface allows for easier relative motion of the planes. The percent increase ranges from 14.2% to 32.5% in peak shear stress between corresponding smooth and roughened interface specimens is summarized in Table 4.4. From the cracking stress values v_{cr} in Table 4.3 it can also be seen that the cracking stress is lower for smooth interface specimens than corresponding roughened interface specimens. It should also be noted that the smooth specimens have smaller interface surface area compared to the roughened interface specimens, where the 1/4 in. grooves used to roughen the surface add to the surface area. This increase in area increases the area over which cohesion is acting, and therefore increases the cracking stress.

From Figures 4.19 through 4.22 it can also be observed that the residual shear force for the sand-lightweight and all-lightweight concrete specimens is roughly the same regardless of the interface preparation. Therefore the interface preparation does not

appear to influence the residual shear force for specimens with a cold joint interface. For the all-lightweight smooth interface concrete specimens, Figures 4.21 and 4.22 show that the peak shear force is similar to the residual shear force. However, in cases of sand-lightweight concrete, with both smooth and roughened interface as well as all-lightweight roughened interface specimens, quasi-brittle post peak behavior (where the peak shear force is significantly larger than the residual shear force) can be observed in Figures 4.19 to 4.22.

Table 4.5 shows that the average peak-to-residual stress ratios $(v_u/v_{ur})_{avg}$ for uncracked monolithic specimens and roughened interface cold joint specimens are similar. The uncracked monolithic specimens ratios are between 1.41 and 1.54, while the cold joint roughened specimens ratios range from 1.51 to 1.68. This means that the quasi-brittle post peak behavior observed in roughened interface specimens is similar to that of uncracked specimens.
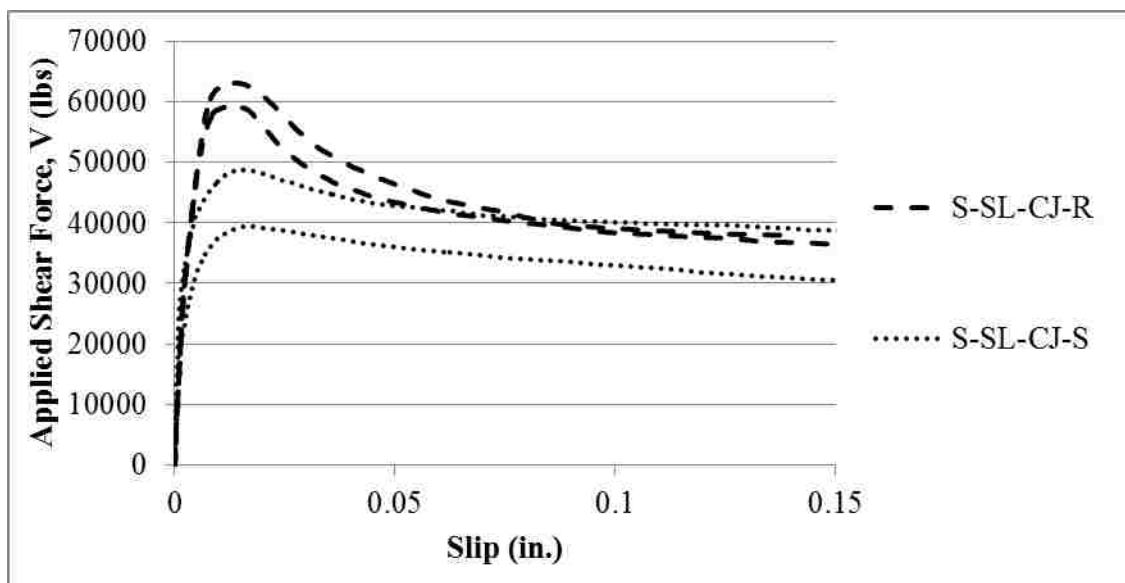
Figure 4.19 Applied Shear Force vs. Slip for Sand-lightweight Slate Concrete Specimens with a Cold Joint Interface
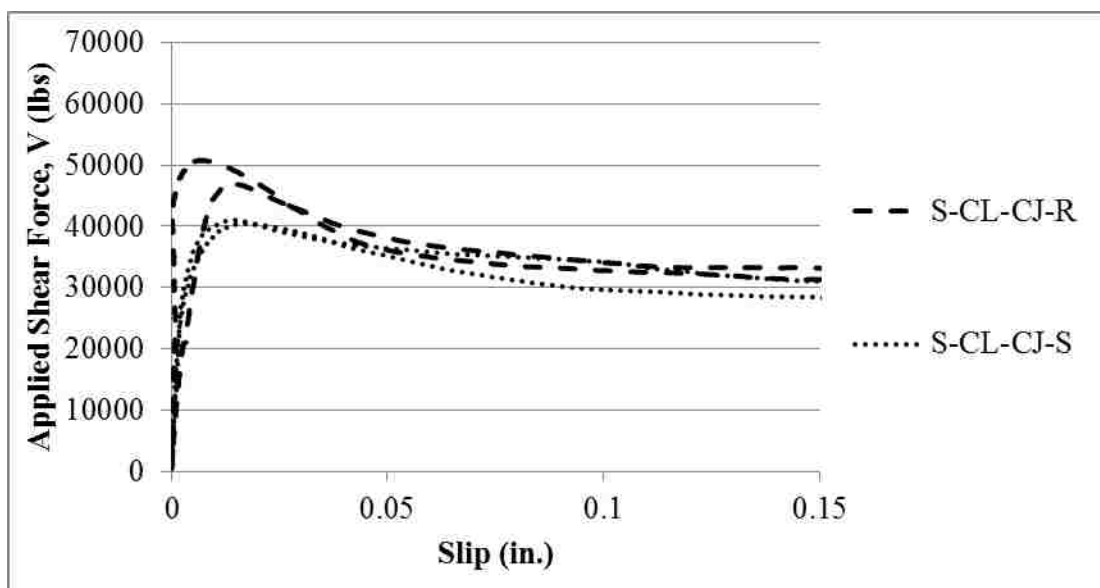
Figure 4.20 Applied Shear Force vs. Slip for Sand-lightweight Clay Concrete Specimens with a Cold Joint Interface
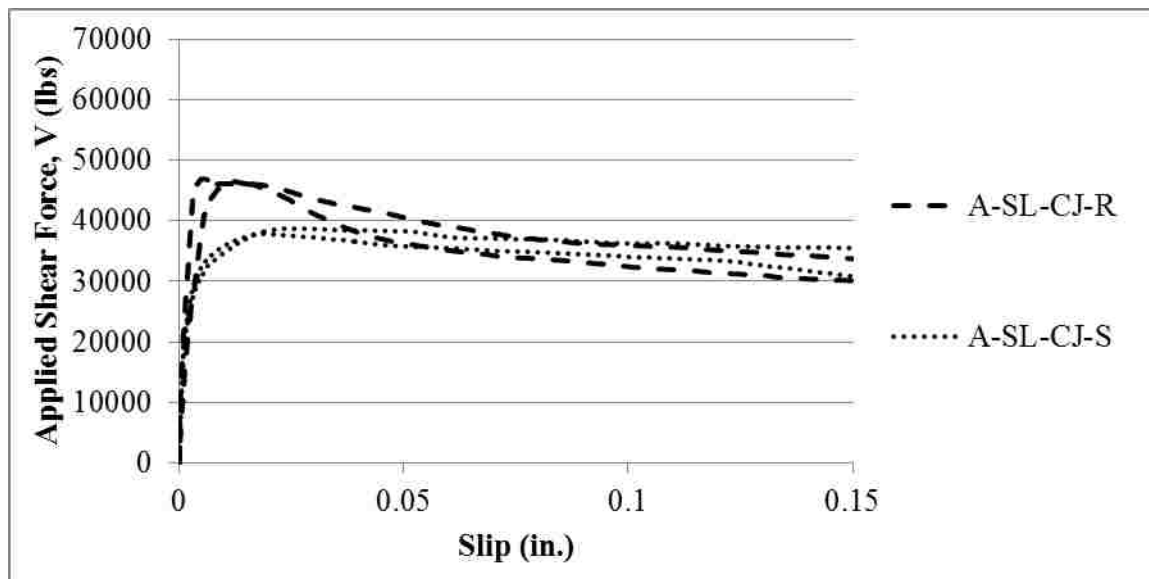
Figure 4.21 Applied Shear Force vs. Slip for All-lightweight Slate Concrete Specimens with a Cold Joint Interface
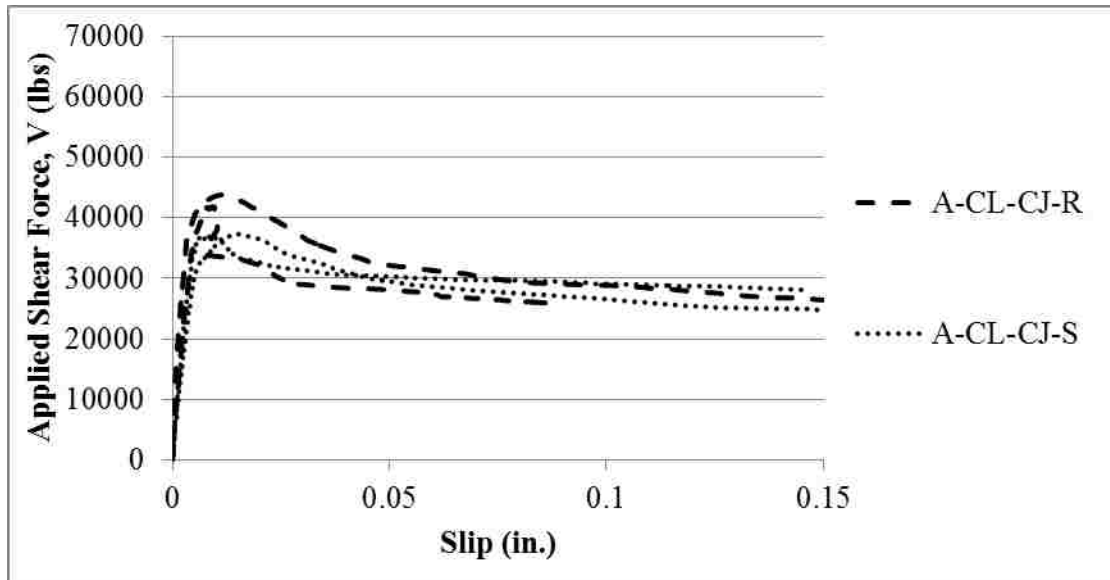
Figure 4.22 Applied Shear Force vs. Slip for All-lightweight Clay Concrete Specimens with a Cold Joint Interface

Table 4.4 Effect of Cold Joint Interface Preparation on the Peak Shear Stress

Specimen Series	Average Peak Shear Stress $v_{u,avg}$ (psi)		
	Interface Preparation		% Increase
	Smooth	Roughened	
S-SL-CJ	891	1238	32.5
A-SL-CJ	774	944	19.8
S-CL-CJ	822	986	18.1
A-CL-CJ	750	865	14.2

Table 4.5 Effect of Interface Preparation on Average Peak-to-Residual Stress Ratio

Specimen ID	Interface Condition	$(v_u/v_{ur})_{avg}$
N-MO-U-1	Uncracked	1.54
N-MO-U-2	Uncracked	
S-SH-MO-U-1	Uncracked	1.41
S-SH-MO-U-2	Uncracked	
A-SH-MO-U-1	Uncracked	1.49
A-SH-MO-U-2	Uncracked	
S-SL-CJ-R-1	Roughened	1.68
S-SL-CJ-R-2	Roughened	
A-SL-CJ-R-1	Roughened	1.46
A-SL-CJ-R-2	Roughened	
S-CL-CJ-R-1	Roughened	1.51
S-CL-CJ-R-2	Roughened	
A-CL-CJ-R-1	Roughened	1.62
A-CL-CJ-R-2	Roughened	

4.4. COMPARISON TO PREVIOUS STUDIES

In the ACI 318 code (2014) and PCI Design Handbook (2010) shear-friction design provisions, discussed in Section 2.3, the shear-friction coefficient μ is determined as the product of a term that accounts for interface preparation (ranging from 0.6 to 1.4) and a term that accounts for the presence of lightweight aggregates, λ (ranging from 0.75 to 1.0). In this section, the influence of lightweight aggregates and interface condition on the shear strength is examined using the results from this study supplemented with selected previous works. The objectives are to examine the trends using a larger database of results, and to facilitate the analysis of the shear-friction design provisions that will be discussed in Section 4.5.

To study the effect of lightweight aggregates, the shear strength of specimens with different unit weights are supplemented and compared with data from the literature for sand-lightweight and all-lightweight concrete (Hofbeck et al. 1969, Mattock et al. 1976, and Shaw 2013). A summary of the data used in this section is presented in Appendix A. To be comparable to this study, only specimens with the same reinforcement ratio (ρ≈0.013) were selected for comparison. It must be noted that the

shear plane of the specimens studied by Hofbeck et al. (1969) and Mattock et al. (1976) was 50 in^2 compared to 49.5 in^2 used by Shaw (2013) and that used for this study, while the number and size of reinforcing bars crossing the shear plane were the same. This slight change in shear plane area only influences the reinforcement ratio slightly.

Specimens tested by Mattock et al. were cast monolithically and were either uncracked or pre-cracked on the day of testing. These will be compared with the monolithic uncracked and pre-cracked specimens tested in this study. Specimens tested by Shaw were cast with a cold joint at the shear plane. Those specimens will be compared to the cold joint specimens in this study. One of the goals of this study is to determine the validity of the lightweight modification factor λ. To be able to analyze this factor, the shear strength was normalized with respect to the concrete compressive strength. Figures 4.23 through 4.26 show plots of the test results versus unit weight. Figure 4.23 graphs normalized shear strength (in terms of stress) versus unit weight of concrete for roughened interface cold joint specimens including the Shaw (2013) specimens. From the trendline it can be seen that as the unit weight of concrete increases, so does the normalized shear strength. Figure 4.24 plots normalized shear strength versus unit weight of concrete for smooth interface cold joint specimens. The trendline of the smooth interface condition plot contradicts the trendline for the roughened interface. The smooth interface trendline slope slightly decreases with increasing unit weight. In other words, the unit weight does not play a role in the shear strength for a cold joint smooth interface condition. This can be explained as the shear plane bond is provided solely by the cohesion of concrete cast against another smooth concrete and the dowel action of the reinforcement crossing the shear plane. Therefore, for the smooth interface cold joint specimens the concrete unit weight should be irrelevant. It should also be noted that the normalized shear strengths of smooth interface specimens in Figure 4.24 are on average lower than the normalized shear strengths of the roughened specimens in Figure 4.23.

Figure 4.25 plots the normalized shear strength versus unit weight of concrete for uncracked monolithic specimens including the Mattock et al. (1976) and the Hofbeck et al. (1969) specimens. This plot shows a slight increase in the normalized shear strength as the unit weight increases. Figure 4.26 shows the normalized shear strength versus the unit weight of concrete for normalweight, sand-lightweight, and all-lightweight monolithic

pre-cracked specimens. It must be noted that the scatter of the normalized shear strength is larger for pre-cracked specimens of the same type than for other interface conditions. This could be the result of the pre-cracking procedure being slightly different among the researchers or the fact that there is no uniform definition of a pre-cracked specimen. The large scatter of data shown in Figure 4.26 may be attributed in part to the pre-cracking techniques used by the different researchers. When a line load is applied to the shear plane, the force is not exactly applied in an infinitesimally narrow region. This means that a component of the applied force pushes the shear planes apart, which may cause variability in data. Figure 4.31 is an illustration of this mechanism. However, the overall trend of this plot shows an increase in shear strength with increasing unit weight of concrete.

To study the effect of interface preparation, the studies mentioned above plus data by Kahn and Mitchell (2002) are examined next. Again, only the specimens with a reinforcement ratio $\rho \approx 0.013$ were selected for the comparison. It must be noted that Kahn and Mitchel studied high strength normalweight concrete monolithic and cold joint specimens. Their cold joint specimens were not intentionally roughened, but a 1/4 in. as cast roughness amplitude is reported in all but two of the specimens. Figures 4.27 through 4.30 summarize the normalized shear strength for all above mentioned studies for different concrete types (normalweight, sand-lightweight, and all-lightweight). The variable in these figures is the interface surface condition (monolithic uncracked and pre-cracked, cold joint roughened and smooth). The specimens are grouped by the interface condition. Figure 4.27 shows the normalized shear strength for all the normalweight concrete specimens studied. In this figure, it is difficult to determine any trends in the shear strength for the uncracked, pre-cracked, roughened, or smooth interface specimens. The data that stand out are specimens studied by Kahn and Mitchell (2002). Due to the normalization of data with respect to the compressive strength of concrete, the normalized shear strength of these specimens is relatively low because of the relatively high compressive strength. Figure 4.28 plots the same relation but without the Kahn and Mitchell data. In this figure the effect of interface preparation is more pronounced. In this figure, the average normalized shear strength for monolithic uncracked specimens is 0.27,

monolithic pre-cracked is 0.25, cold joint roughened interface is 0.20, and cold joint smooth interface is 0.15.

Figure 4.29 plots the normalized shear strength for the sand-lightweight concrete specimens. The average normalized shear strength for monolithic uncracked specimens is 0.25, 0.21 for pre-cracked specimens, 0.23 for roughened interface specimens, and 0.17 for smooth interface specimens. Figure 4.30 shows the normalized shear strength for the all-lightweight concrete specimens. The average normalized shear strength for monolithic uncracked all-lightweight specimens is 0.24, monolithic pre-cracked 0.20, cold joint roughened 0.18, and cold joint smooth 0.15.

Finally, Table 4.6 summarizes and compares the average normalized shear strength (v_u/f'_c) for each type of concrete (normalweight, sand-lightweight, and all-lightweight) and each interface condition (monolithic uncracked, monolithic precracked, cold joint roughened, and cold joint smooth) considering all specimens included in this comparison. It can be seen from this table that, on average, as the unit weight of concrete decreases so does the average normalized shear strength. It is also observed that there is a correlation between interface preparation procedure and the average applied shear strength.
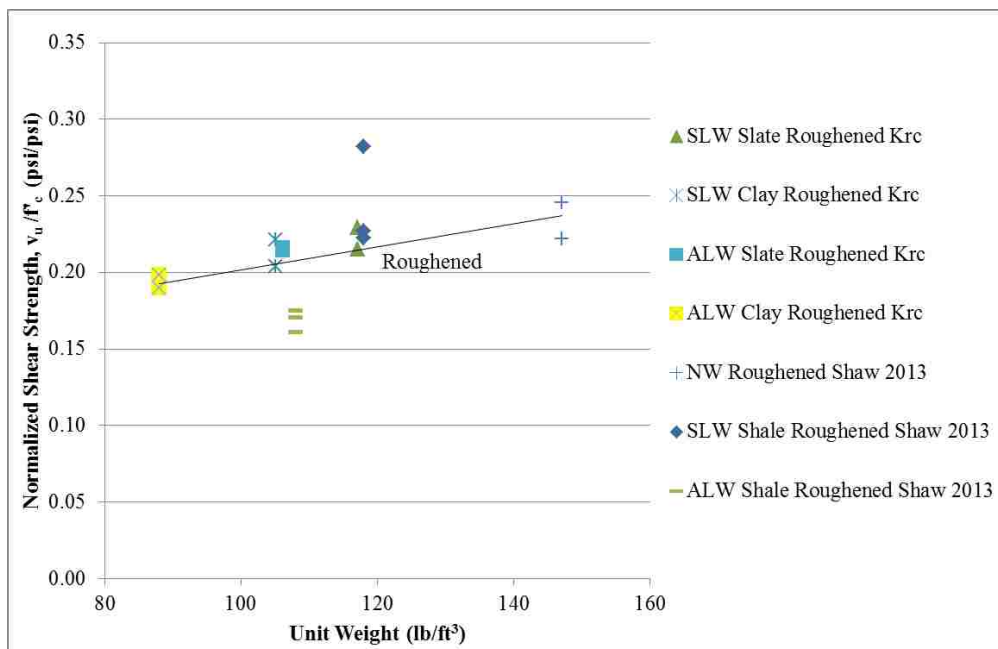
Figure 4.23 Normalized Shear Strength vs. Unit Weight of Concrete for Roughened Interface Cold Joint Specimens
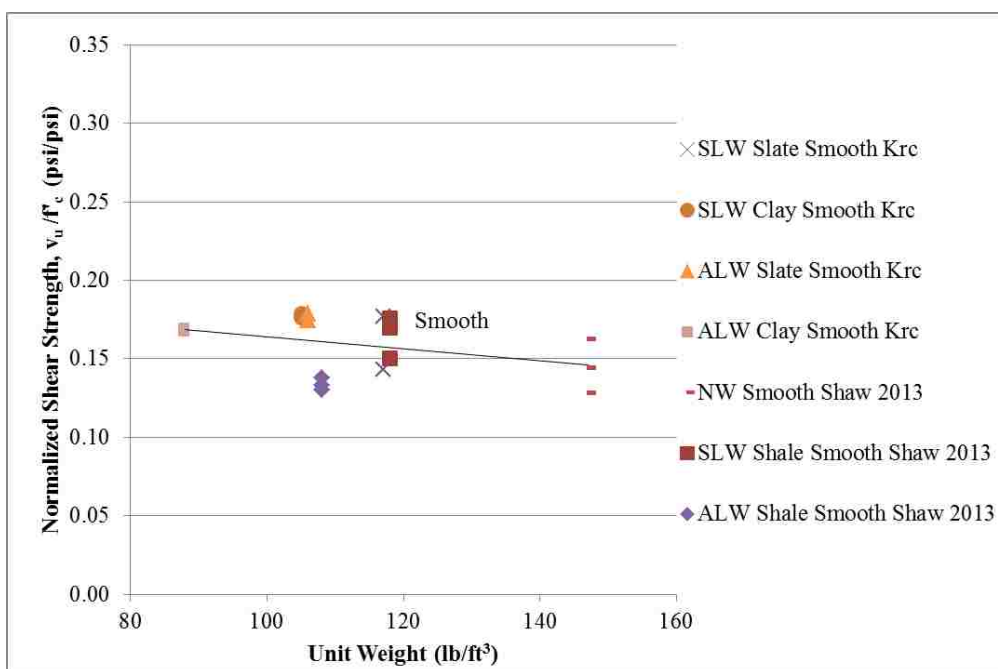
Figure 4.24 Normalized Shear Strength vs. Unit Weight of Concrete for Smooth Interface Cold Joint Specimens
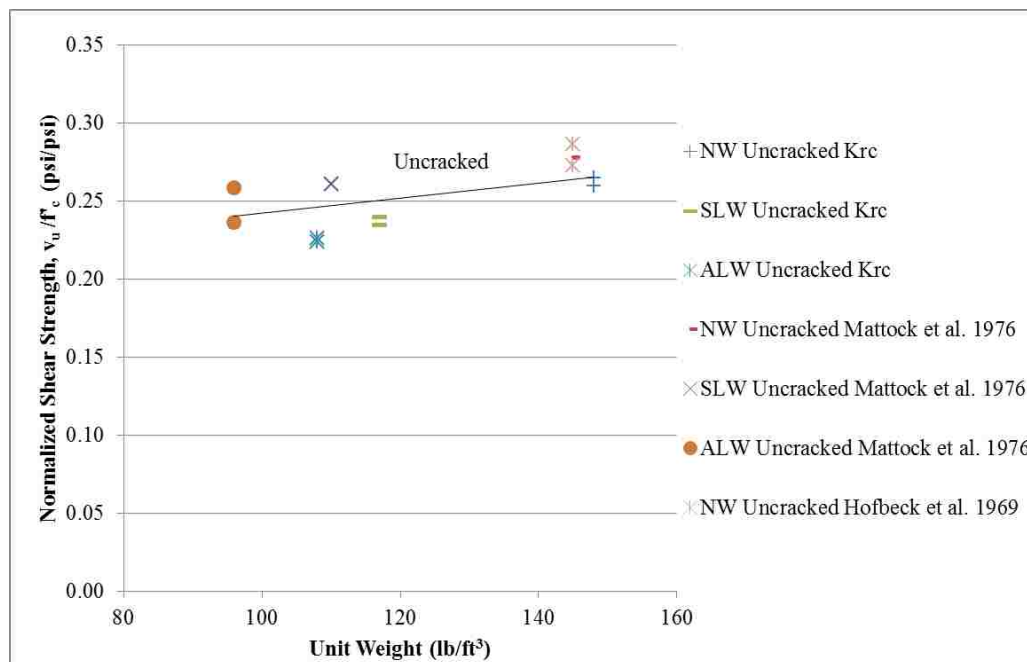
Figure 4.25 Normalized Shear Strength vs. Unit Weight of Concrete for Uncracked Monolithic Specimens
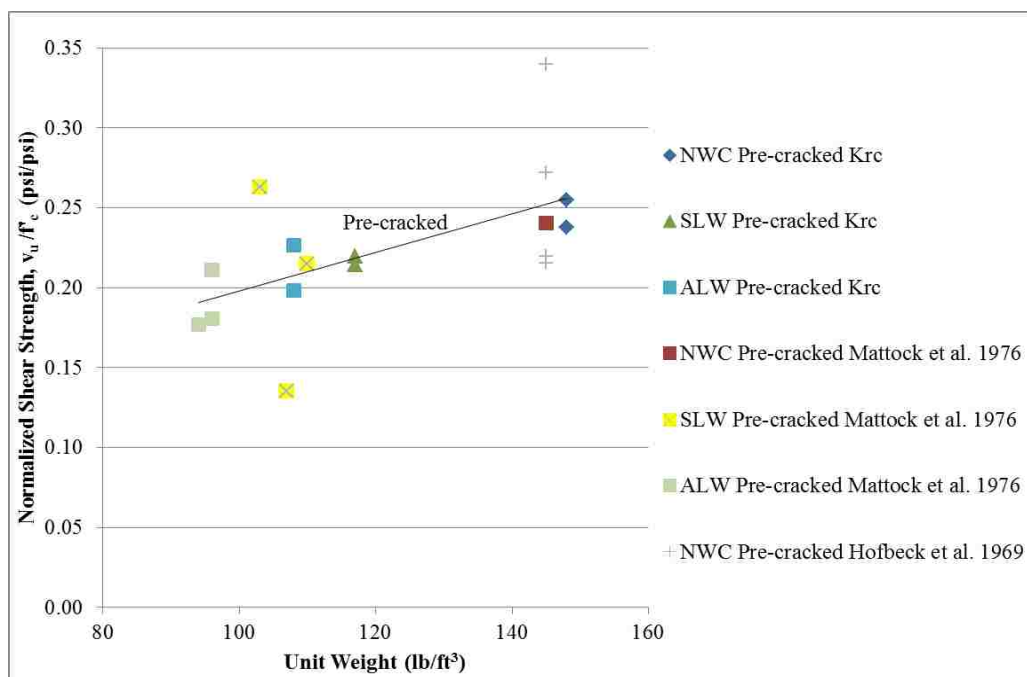
Figure 4.26 Normalized Shear Strength vs. Unit Weight of Concrete for Pre-cracked Monolithic Specimens

Figure 4.27 Normalized Shear Strength for Normalweight Specimens – Including High Strength Concrete
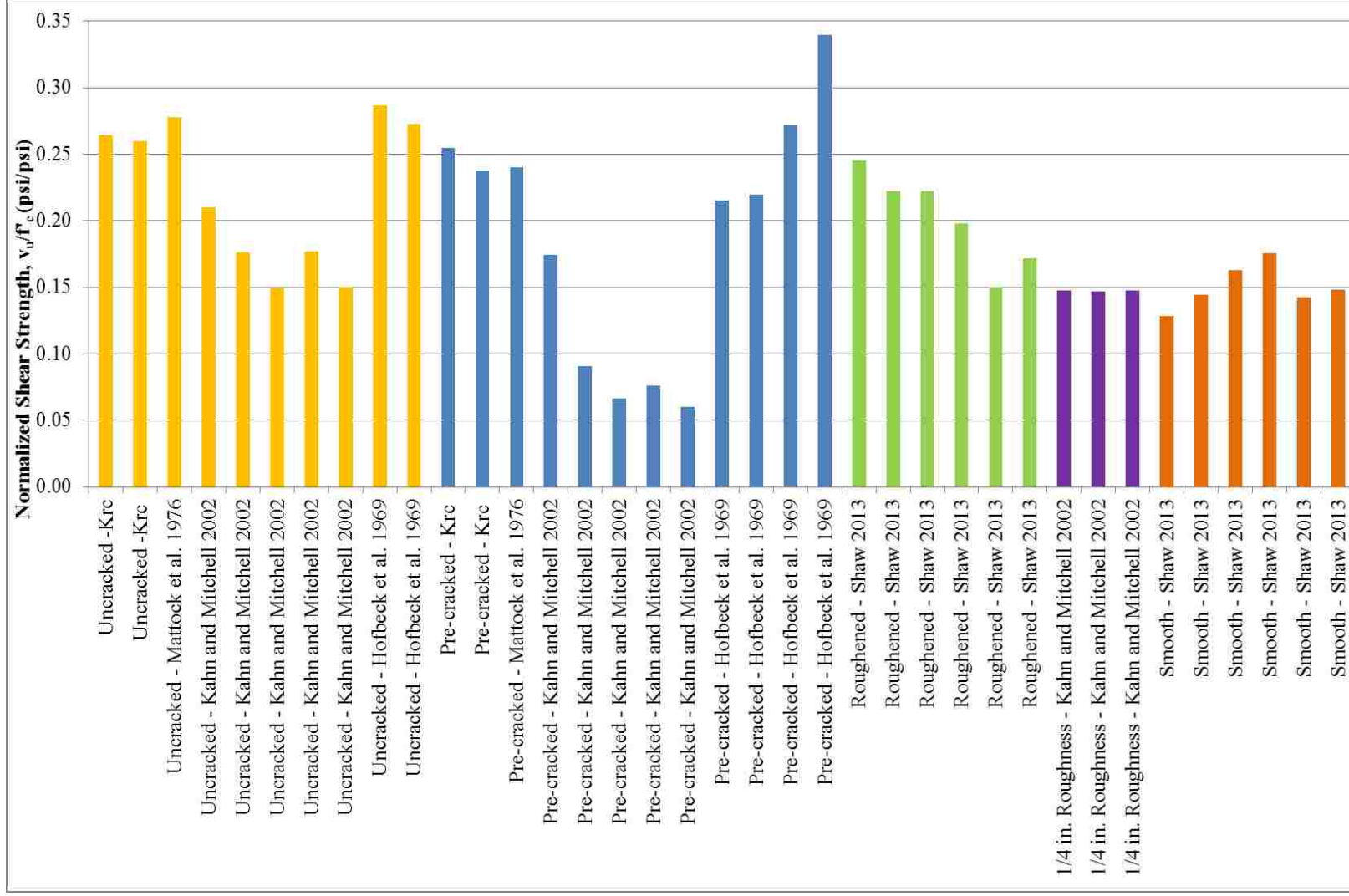
Figure 4.28 Normalized Shear Strength for Normalweight Specimens – Excluding High Strength Concrete
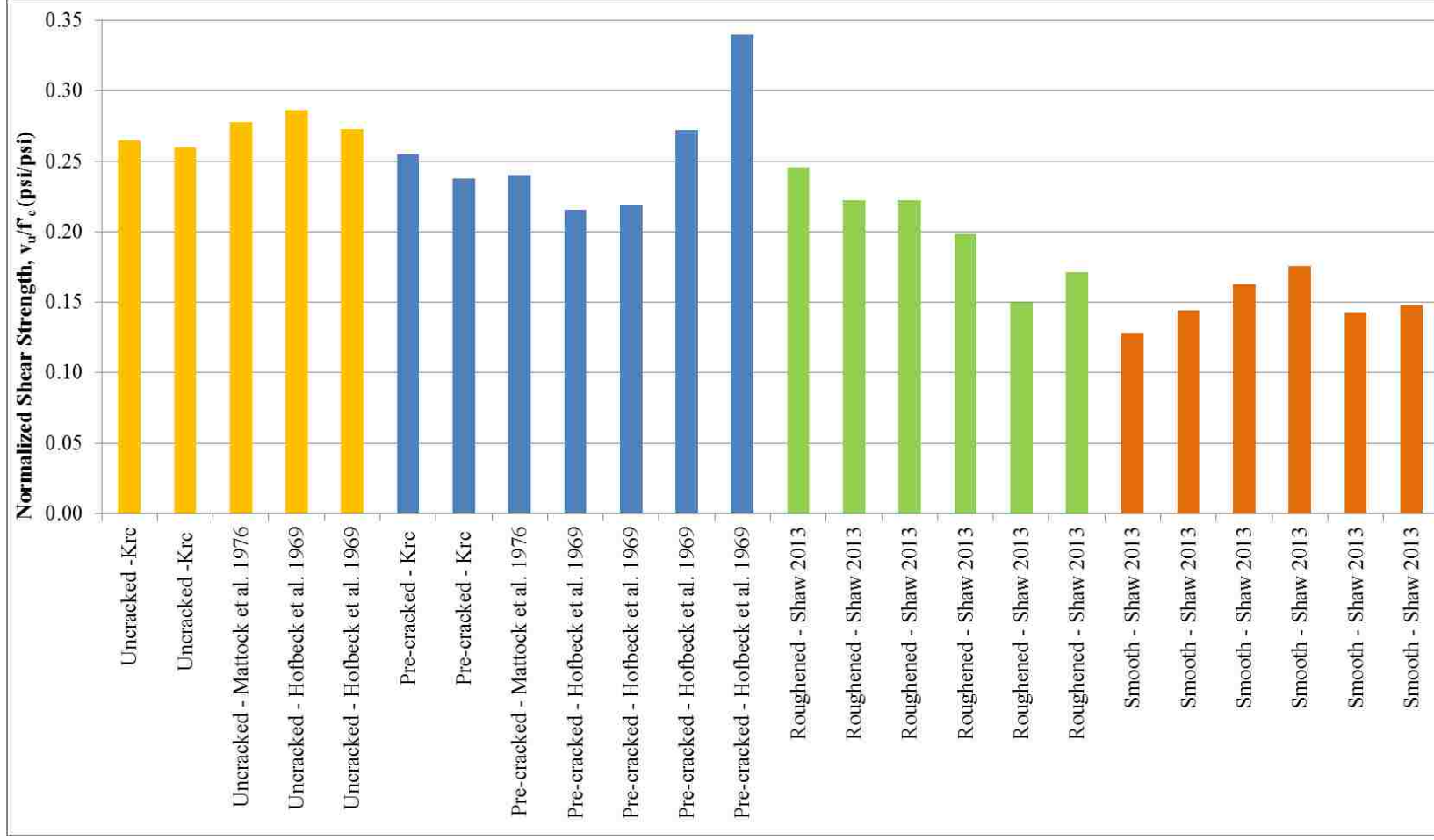
Figure 4.29 Normalized Shear Strength for Sand-lightweight Specimens
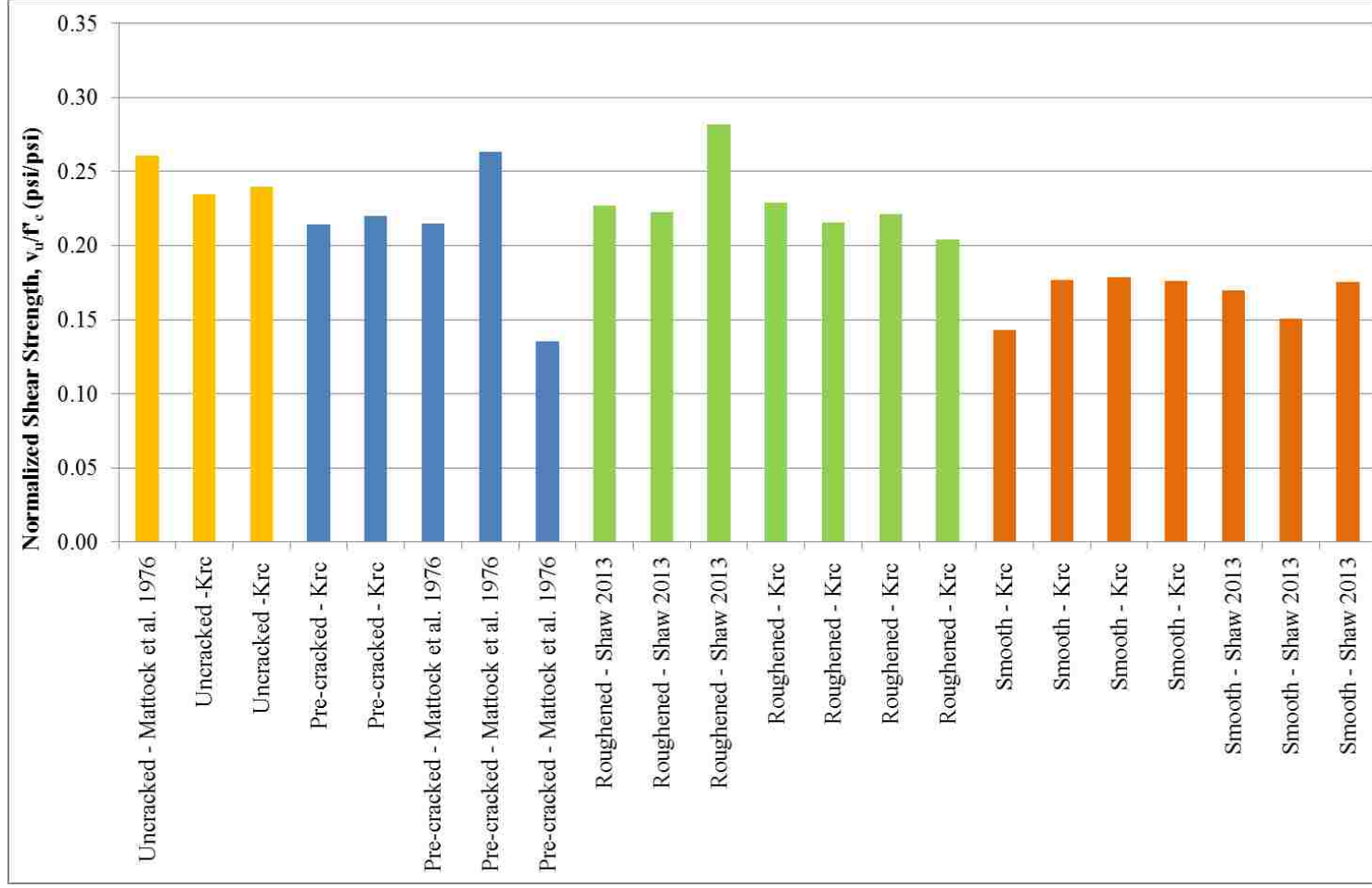
Figure 4.30 Normalized Shear Strength for All-lightweight Specimens
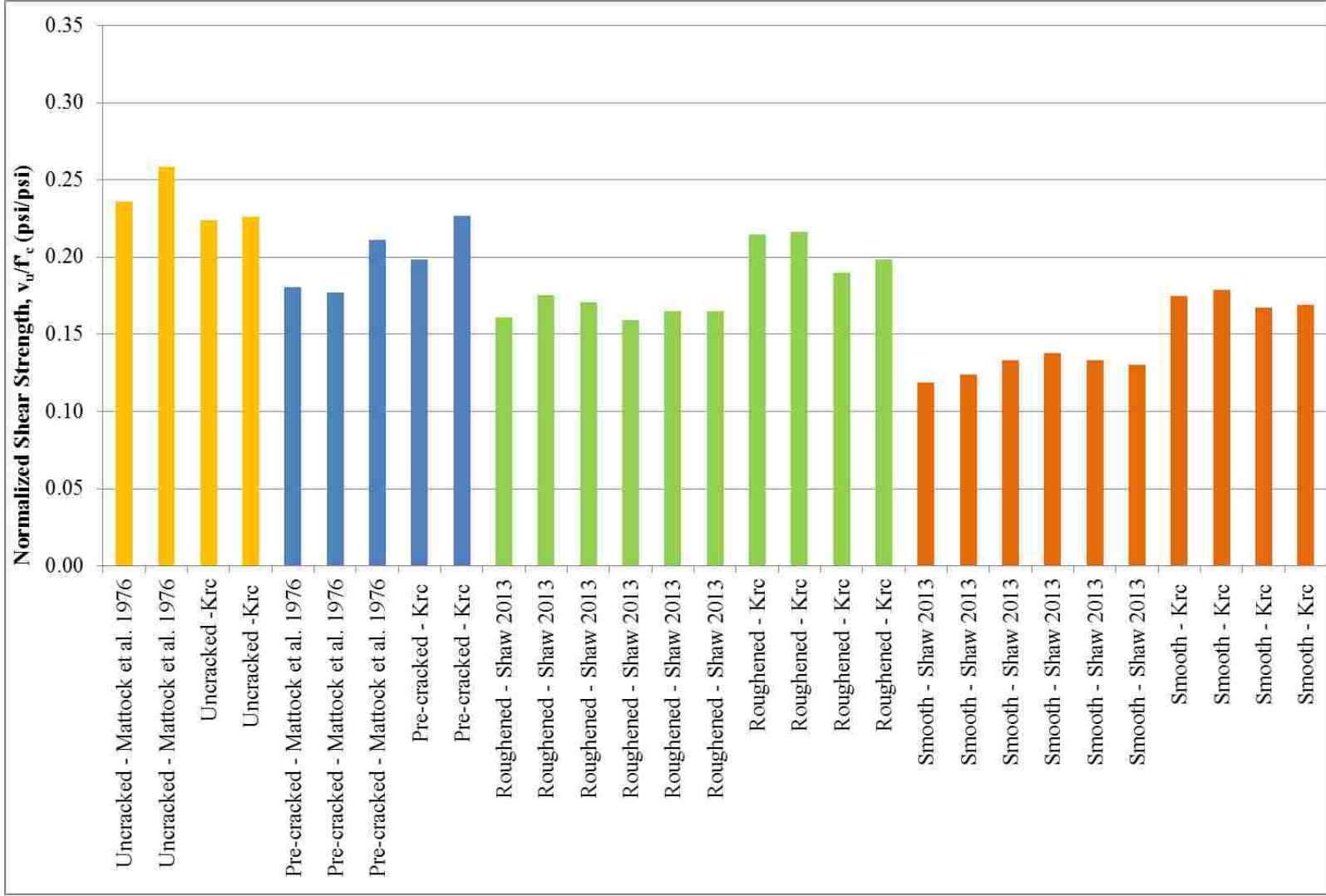
Table 4.6 Summary of Average Normalized Shear Strength (from Data in Appendix A)

Concrete Type	v_u/f'_c (psi/psi)			
	Monolithic		Cold Joint	
	Uncracked	Pre-cracked	Roughened	Smooth
Normalweight	0.27	0.25	0.20	0.15
Sand-lightweight	0.25	0.21	0.23	0.17
All-lightweight	0.24	0.20	0.18	0.15
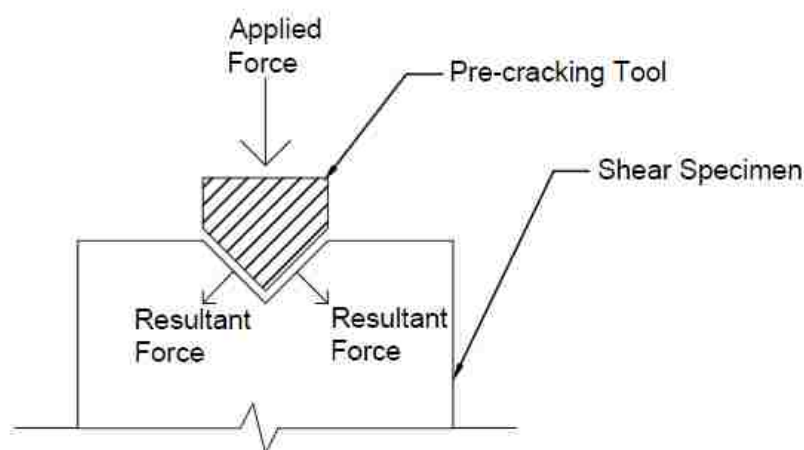
Figure 4.31 Mechanism of Applying a Line Load During Pre-cracking

4.5. COMPARISON TO PCI AND ACI DESIGN PROVISIONS

This section examines the shear-friction design provisions discussed in the PCI Design Handbook (2004, 2010) and the ACI 318 (2011, 2014) code in Section 2.3. These provisions are evaluated with respect to the results presented in this research and also the results presented in Section 4.4. This way the provisions are evaluated using a larger database of data than just this thesis. Section 4.5.1 presents the equations and limits used in shear-friction design in accordance with the PCI Design Handbook and ACI 318 code. Section 4.5.2 compares the shear strength determined from the test data to the nominal shear strength V_n computed using the PCI Design Handbook and the ACI 318 code using

the coefficient of friction approach as described in Section 4.5.2. In Section 4.5.3, results are compared on basis of the effective coefficient of friction μ_e as allowed by the PCI Design Handbook.

4.5.1. Shear-friction Design Provisions. This section presents the shear-friction design equations and limits set forth by the PCI Design Handbook 6th and 7th Editions (2004 and 2011) and the ACI 318-11 (2011) and the ACI 318-14 (2014) codes. These equations from the shear-friction provisions will be compared to the results of the test data. Table 4.7 presents the limitations required by the above mentioned documents. Table 4.8 summarizes the recommended shear-friction coefficients, and Table 4.9 offers the lightweight concrete modification factors and friction coefficients. Detailed discussion of the design provisions is provided in Section 2.3.

Table 4.7 Maximum Applied Shear Force Using Shear-friction Design Provisions

Case	PCI 6th Edition Max $V_u = \varphi V_n$	PCI 7th Edition Max V_u/φ	ACI 318-11 & ACI 318-14 Max V_n	
			Normalweight Concrete	Other
1	$0.30\lambda^2 f_c A_{cr} \leq 1000\lambda^2 A_{cr}$	$0.30\lambda f_c A_{cr} \leq 1000\lambda A_{cr}$	$0.2f_c A_c < (480+0.08f_c)A_c$ $< 1600A_c$	$0.2f_c A_c < 800A_c$
2	$0.25\lambda^2 f_c A_{cr} \leq 1000\lambda^2 A_{cr}$	$0.25\lambda f_c A_{cr} \leq 1000\lambda A_{cr}$		
3	$0.20\lambda^2 f_c A_{cr} \leq 800\lambda^2 A_{cr}$	$0.20\lambda f_c A_{cr} \leq 800\lambda A_{cr}$	$0.2f_c A_c < 800A_c$	
4	$0.30\lambda^2 f_c A_{cr} \leq 800\lambda^2 A_{cr}$	$0.20\lambda f_c A_{cr} \leq 800\lambda A_{cr}$		

Table 4.8 Summary of Recommended Shear-friction Coefficients

Case	Crack interface condition	PCI 6th Edition		PCI 7th Edition		ACI 318-11 & ACI 318-14
		μ	Max μ_e	μ	Max μ_e	μ
1	Concrete to concrete, monolithic	1.4λ	3.4	1.4λ	3.4	1.4λ
2	Concrete to concrete, cold joint – roughened	1.0λ	2.9	1.0λ	2.9	1.0λ
3	Concrete to concrete, cold joint – not intentionally roughened	0.6λ	2.2	0.6λ	N/A	0.6λ
4	Concrete to steel	0.7λ	2.4	0.7λ	N/A	0.7λ

Table 4.9 Summary of Lightweight Modification Factors and Coefficients of Friction for Cold Joint Interface Condition Used by the PCI Design Handbook and ACI 318 Code

Factors	Normalweight		Sand-lightweight		All-lightweight	
	Smooth	Roughened	Smooth	Roughened	Smooth	Roughened
λ	1.00	1.00	0.85	0.85	0.75	0.75
μ	0.60	1.00	0.51	0.85	0.45	0.75

4.5.1.1 PCI Design Handbook 6th Edition (2004). Equations 4.1 (PCI Eq. 4.3.6.1) and 4.2 (PCI Eq. 4.3.6.2) are presented in the PCI Design Handbook 6th Edition. These equations were previously discussed in Section 2.3.2.

$$A_{vf} = \frac{V_u}{\emptyset f_y \mu_e} \tag{4.1}$$

$$\mu_e = \frac{1000\lambda A_{cr}\mu}{V_u} \tag{4.2}$$

These equations apply to all four interface conditions as described in Table 4.8. Substituting Equation 4.2 into Equation 4.1 and realizing that $V_n=V_u/\phi$ and $V_n=v_nA_{cr}$, Equation 4.1 can be rearranged to obtain Equation 4.3:

$$v_n = 31.62\sqrt{\frac{\rho f_y \lambda \mu}{\phi}} \tag{4.3}$$

Using similar substitutions, Equation 4.1 can be rewritten as Equation 4.4:

$$\mu_e = \frac{v_n}{\rho f_y} \tag{4.4}$$

The maximum values of μ_e and $V_u=\phi V_n$ are presented in Tables 4.7 and 4.8. The maximum value for f_y is set to be 60 ksi per the PCI Design Handbook 6th Edition. Variables λ and μ for each case are presented in Table 4.9.

4.5.1.2 PCI Design Handbook 7th Edition (2011). Two approaches are permissible in the PCI Design Handbook 7th Edition to determine the shear reinforcement required to cross the shear plane. These approaches were discussed in Section 2.3.3. The first approach, Equation 4.8, which is also in the 6th Edition of the PCI Design Handbook, uses the effective coefficient of friction μ_e where permissible. The second approach allows for the use of coefficient of friction μ. Equation 4.5 (PCI Eq. 5-32a) presents the second approach and can be used for all four cases described in Table 4.8.

$$A_{vf} = \frac{V_u}{\emptyset f_y \mu} \tag{4.5}$$

Equation 4.5 can be rearranged to obtain Equations 4.6 and 4.7 using the same substitution described in Section 4.5.1.1.

$$\mu = \frac{v_n}{\rho f_y} \tag{4.6}$$

$$v_n = \rho f_y \mu \tag{4.7}$$

The first approach allowed by the PCI Design Handbook 7th Edition implements the use of the effective coefficient of friction. The required area of shear-friction reinforcement is determined according to Equation 4.8 (PCI Eq. 5.32b). The coefficient of friction is determined using Equation 4.9 (PCI Eq. 5-33).

$$A_{vf} = \frac{V_u}{\emptyset f_y \mu_e} \tag{4.8}$$

$$\mu_e = \frac{\phi 1000 \lambda A_{cr} \mu}{V_u} \tag{4.9}$$

It must be noted that Equations 4.8 and 4.9 are only applicable for Cases 1 and 2 from Table 4.8, namely concrete to concrete – cast monolithically and concrete to hardened concrete – roughened surface. The only difference between Equations 4.9 and 4.2 is the inclusion of the strength reduction factor ϕ in Equation 4.9. Equations 4.8 and 4.9 can be rearranged into Equations 4.10 and 4.11.

$$v_n = 31.62 \sqrt{\rho f_y \lambda \mu} \tag{4.10}$$

$$\mu_e = \frac{v_n}{\rho f_y} \tag{4.11}$$

The maximum values for V_u/ϕ, μ, and μ_e are presented in Tables 4.7 and 4.8. The maximum value for f_y is set to be 60 ksi per the PCI Design Handbook 7th Edition. Parameters λ and μ for each case are calculated in Table 4.9.

4.5.1.3 ACI 318-11 & ACI 318-14. Both ACI 318-11 (ACI Eq. 11-25) and ACI 318-14 (ACI Eq. 22.9.3.1) use Equation 4.12 to calculate the nominal shear strength.

$$V_n = A_{vf} f_y \mu \tag{4.12}$$

Utilizing the relationship $V_n = v_n A_{cr}$, Equation 4.13 is derived:

$$v_n = \rho f_y \mu \tag{4.13}$$

Equation 4.13 can be rearranged into Equation 4.14:

$$\mu = \frac{v_n}{\rho f_y} \tag{4.14}$$

The maximum values for V_n are shown in Table 4.7. The coefficient of friction μ is applicable to all four cases of Table 4.8.

4.5.2. Shear Strength. This section compares values for shear strength v_n predicted by the current PCI Design Handbook (7th Edition) and the ACI 318-14 code to the shear strength of the test specimens v_u. The predicted values are computed using the effective coefficient of friction μ_e from the PCI Design Handbook 7th Edition for a monolithic interface and a cold joint intentionally roughened interface (Eq. 4.10). However, to verify if removing the effective coefficient of friction approach from the 7th Edition of the PCI Design Handbook for cold joint smooth interface specimens was justified (refer to Section 2.3.3), the limit ($\mu e = 2.2$) from the PCI Design Handbook 6th Edition is used for this case. The predicted vn values by the ACI 318-14 are the same as the values predicted by the PCI Design Handbook 7th Edition for all four cases from Table 4.8 using the coefficient of friction approach (Eq. 4.7 and 4.13). The maximum values for the predicted vn values are based on Table 4.7. Using the coefficient of friction approach μ (PCI Design Handbook 7th Edition and ACI 318-14), the predicted value of vn is computed using Equations 4.7 and 4.13. The values of μ are presented in Table 4.9.

Using the effective coefficient of friction μe approach, the predicted values are computed using Equation 4.10.

Cold joint roughened and smooth interface values predicted are compared to the experimental data from tests reported in this thesis as well as the data from Shaw (2013). Cold joint interface specimens are presented in Figures 4.32 through 4.37. Figure 4.32 compares the of shear strength of the normalweight smooth interface specimens to the predicted values by Equations 4.10 and 4.13. It can be seen that the for 8000 psi concrete specimens by Shaw, the predictions are conservative (for the purpose of this research any experimental value greater than the predicted value for that experiment is considered conservative). However, for concrete with compressive strength of 5000 psi the PCI Design Handbook 7th Edition prediction is not always conservative (This is only true for one normalweight concrete specimens with a smooth interface condition.). It can be seen from Figures 4.33, 4.34, 4.36, and 4.37 that both the PCI Design Handbook and the ACI 318 code predictions are conservative regardless of aggregate type, interface preparation, or the unit weight of concrete, with the one exception noted previously.

Monolithic interface uncracked and pre-cracked values are compared to the experimental data from this thesis, as well as the monolithic interface data from Hofbeck et al. (1969) and Mattock et al. (1976). The data from these publications was previously presented in Section 4.4. It must be noted that the PCI Design Handbook and the ACI 318 code do not account for the effect of pre-cracking, therefore pre-cracked monolithic specimens were compared to the same predicted values as the uncracked monolithic specimens. However, they are presented separately in Figures 4.38 through 4.45. Figures 4.38 through 4.40 show monolithic uncracked specimens for normalweight, sand-lightweight, and all-lightweight concrete specimens, respectively. It can be seen that the values for all uncracked specimens are predicted conservatively by the PCI Design Handbook and ACI 318 code. Figures 4.41 through 4.43 show monolithic pre-cracked specimens for normalweight, sand-lightweight, and all-lightweight concrete specimens, respectively. Some of the pre-cracked specimen experimental data were uncoservatively predicted by the PCI Design Handbook and ACI 318 code in Figures 4.41 through 4.43. This implies that once the crack has been formed in a precast monolithic element, the PCI Design Handbook and ACI Code approach to calculating shear strength may not be

conservative if the lightweight modification factor λ is not included in the design equations.

Figure 4.44 compares the of shear strength v_u of the monolithic uncracked specimens with Equations 4.10 and 4.13 (with λ=1.0). It should be noted that the unit weight of concrete is not constant throughout the data plotted in Figure 4.44. It was chosen to use PCI Design Handbook 7th Edition and ACI 318-14 predictions for normalweight concrete (λ=1.0) in order to examine whether the lightweight modification factor is needed in the design equations for monolithic uncracked specimens. It can be seen in Figure 4.44 that the values of v_n are predicted conservatively without taking into account the lower mechanical properties of lightweight aggregate concrete. However, similar plots of monolithic pre-cracked and cold joint roughened and smooth interface are not conservative.
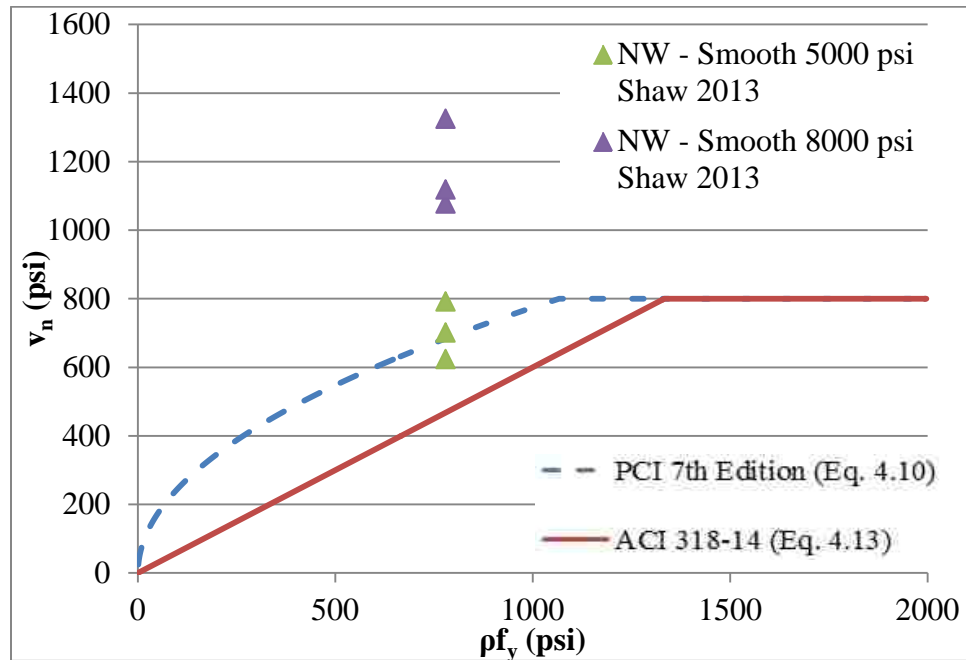
Figure 4.32 Comparison of Shear Strength v_u with Equations 4.10 and 4.13 for Normalweight Concrete Specimens with Smooth Interface (λ=1.0, μ=0.60)
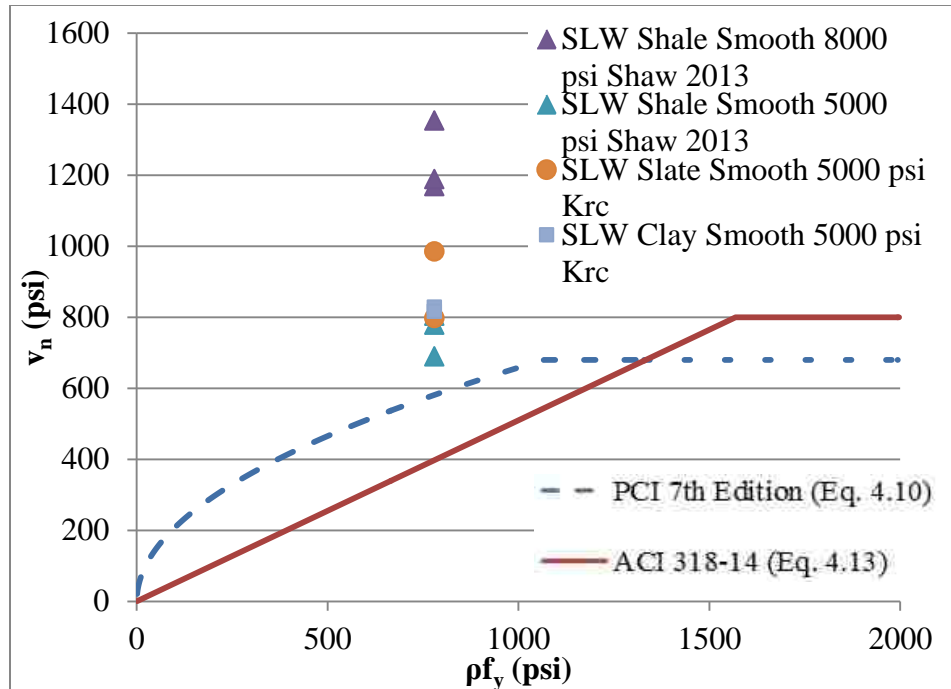
Figure 4.33 Comparison of Shear Strength v_u with Equations 4.10 and 4.13 for Sand-lightweight Concrete Specimens with Smooth Interface (λ=0.85, μ=0.51)
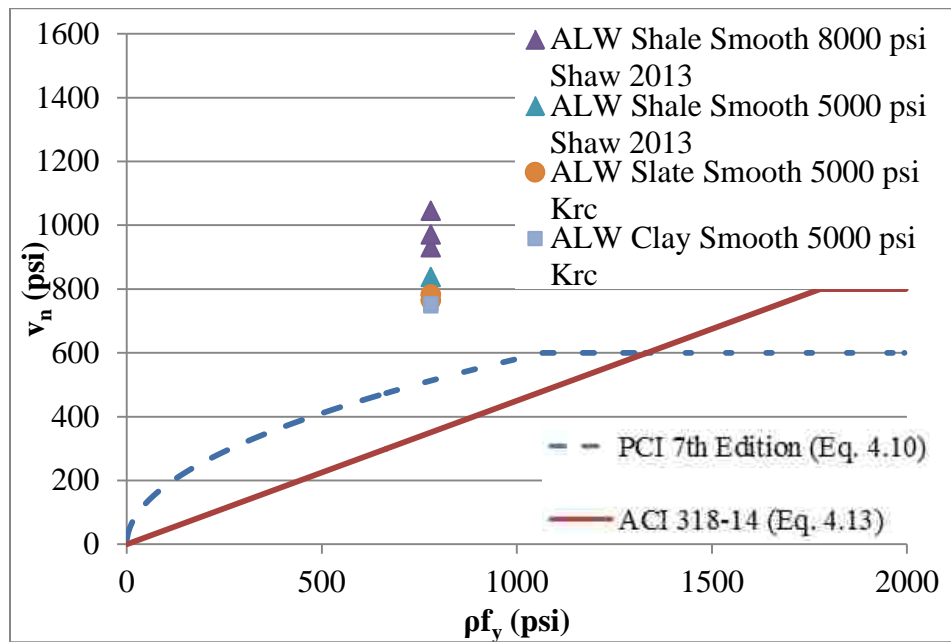
Figure 4.34 Comparison of Shear Strength v_u with Equations 4.10 and 4.13 for All-lightweight Concrete Specimens with Smooth Interface (λ=0.75, μ=0.45)
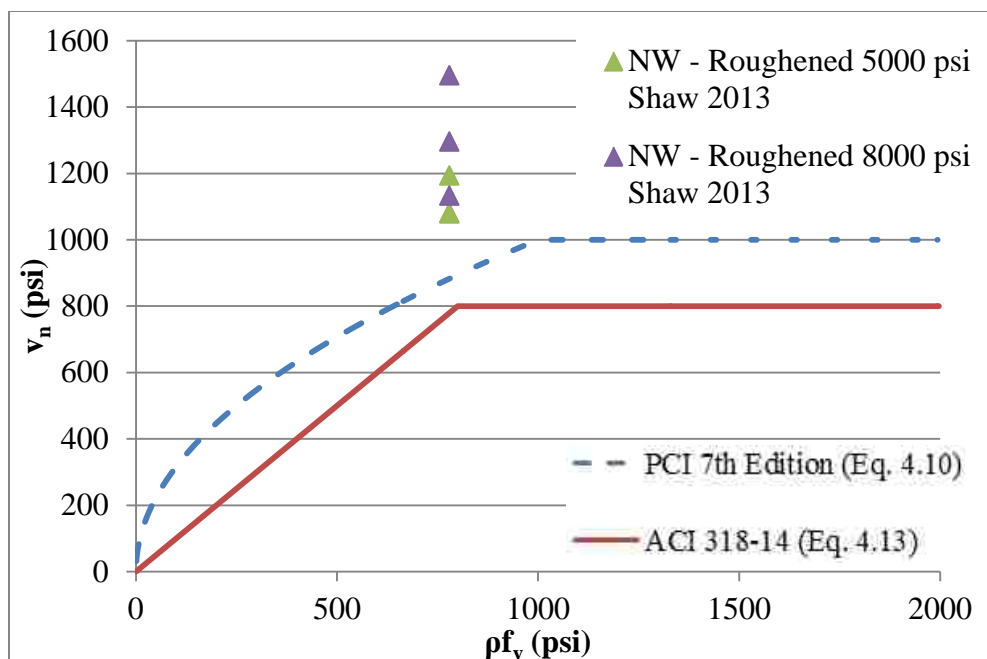
Figure 4.35 Comparison of Shear Strength v_u with Equations 4.10 and 4.13 for Normalweight Concrete Specimens with Roughened Interface (λ=1.0, μ=1.0)
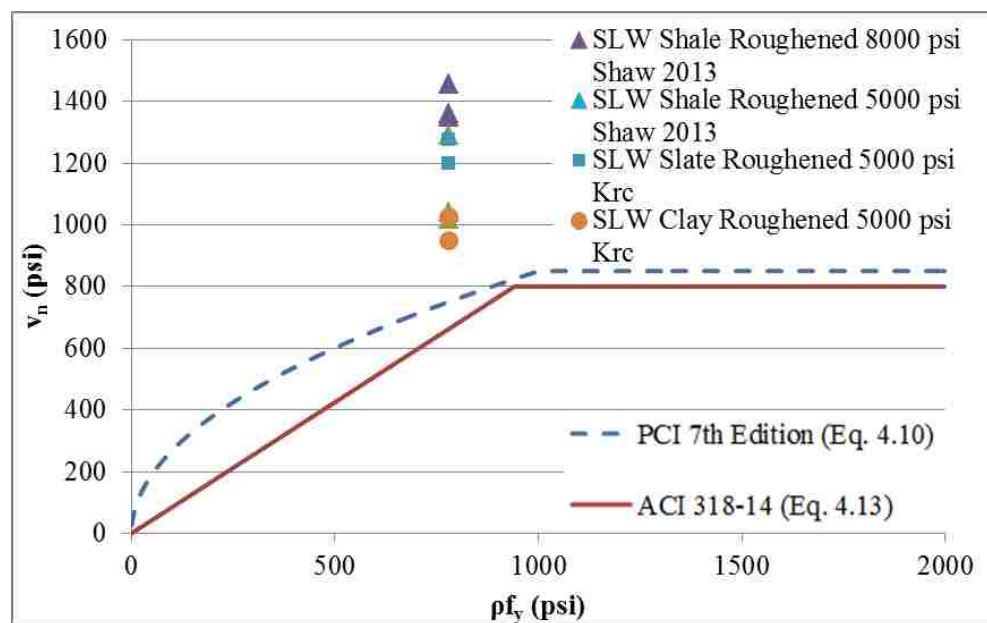
Figure 4.36 Comparison of Shear Strength v_u with Equations 4.10 and 4.13 for Sand-lightweight Concrete Specimens with Roughened Interface (λ=0.85, μ=0.85)
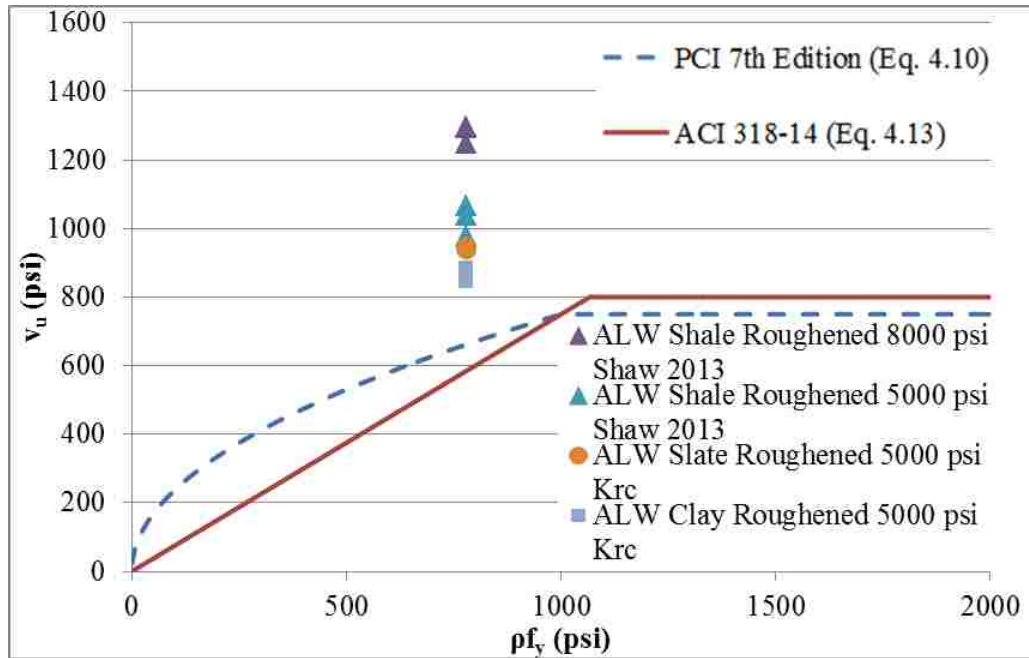
Figure 4.37 Comparison of Shear Strength v_u with Equations 4.10 and 4.13 for All-lightweight Concrete Specimens with Roughened Interface (λ=0.75, μ=0.75)
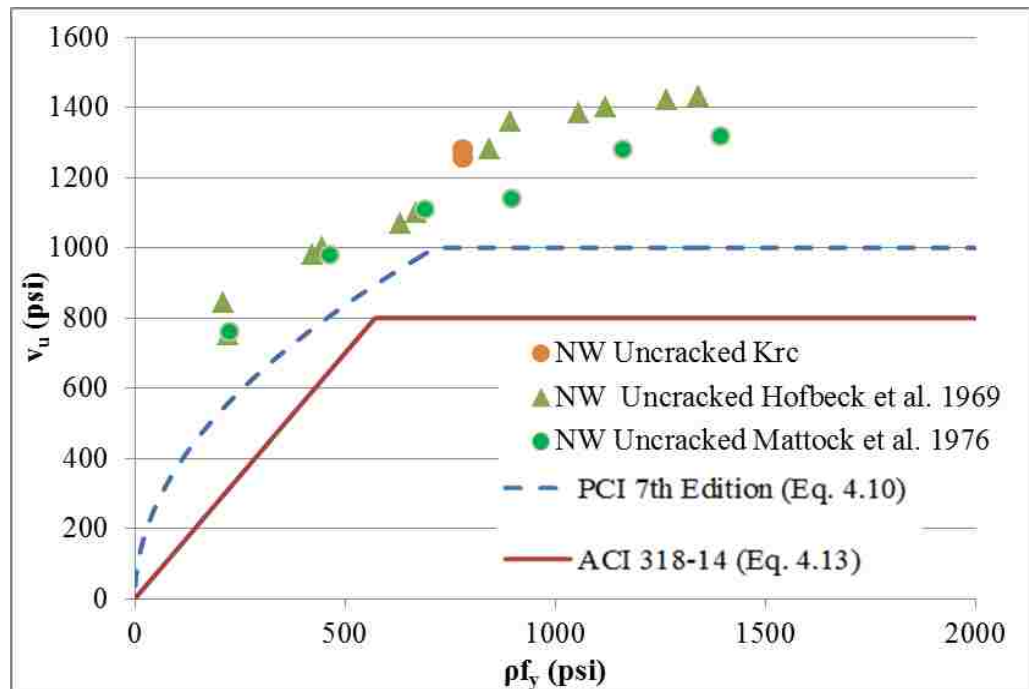
Figure 4.38 Comparison of Shear Strength v_u with Equations 4.10 and 4.13 for Normalweight Concrete Specimens with Monolithic Uncracked Interface (λ=1.0, μ=1.4)
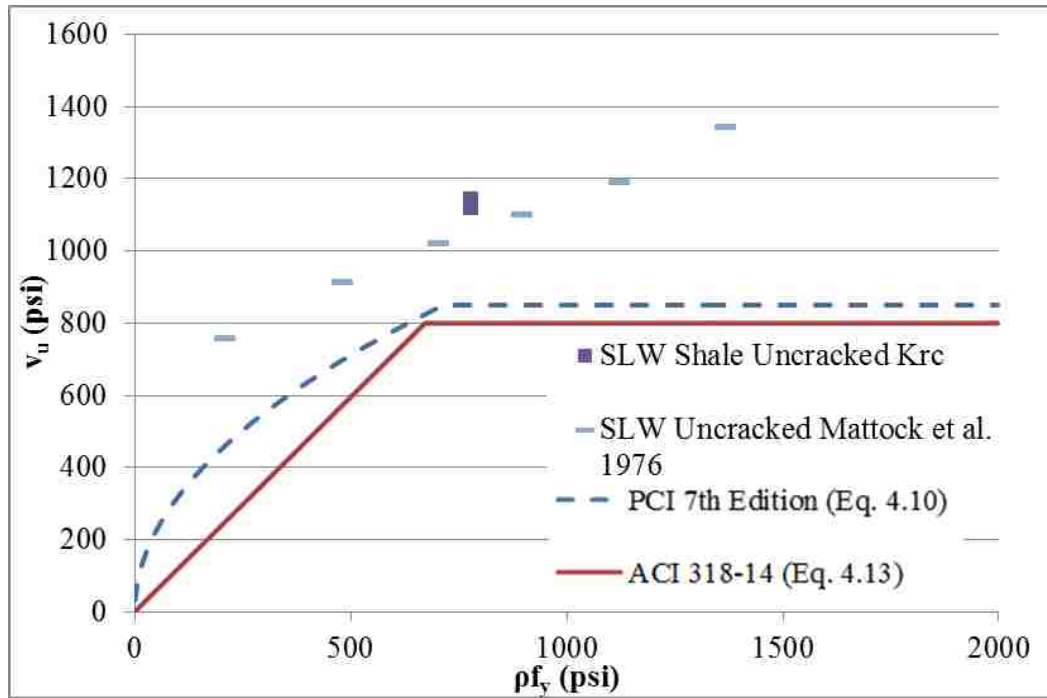
Figure 4.39 Comparison of Shear Strength v_u with Equations 4.10 and 4.13 for Sand-lightweight Concrete Specimens with Monolithic Uncracked Interface (λ=0.85, μ=1.19)
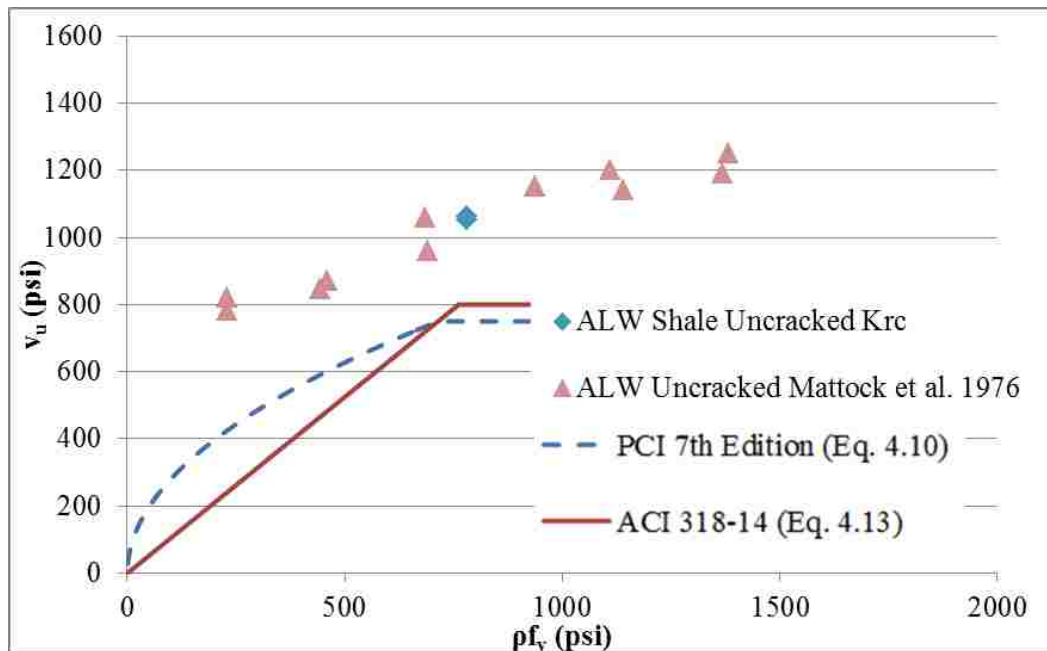
Figure 4.40 Comparison of Shear Strength v_u with Equations 4.10 and 4.13 for All-lightweight Concrete Specimens with Monolithic Uncracked Interface (λ=0.75, μ=1.05)
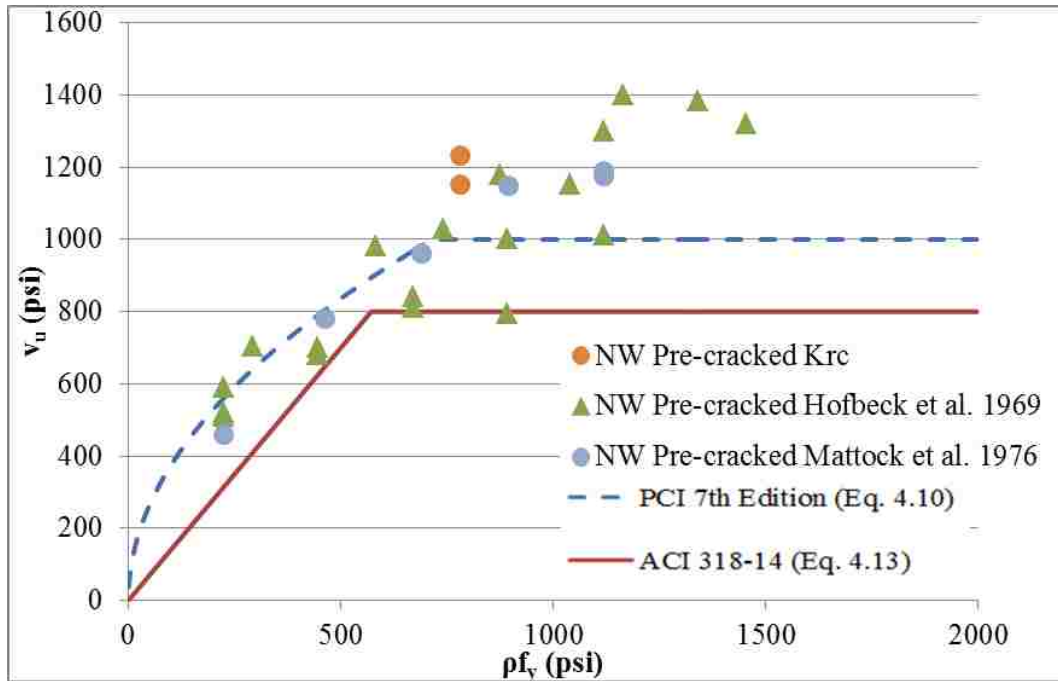
Figure 4.41 Comparison of Shear Strength v_u with Equations 4.10 and 4.13 for Normalweight Concrete Specimens with Monolithic Pre-cracked Interface (λ=1.0, μ=1.4)
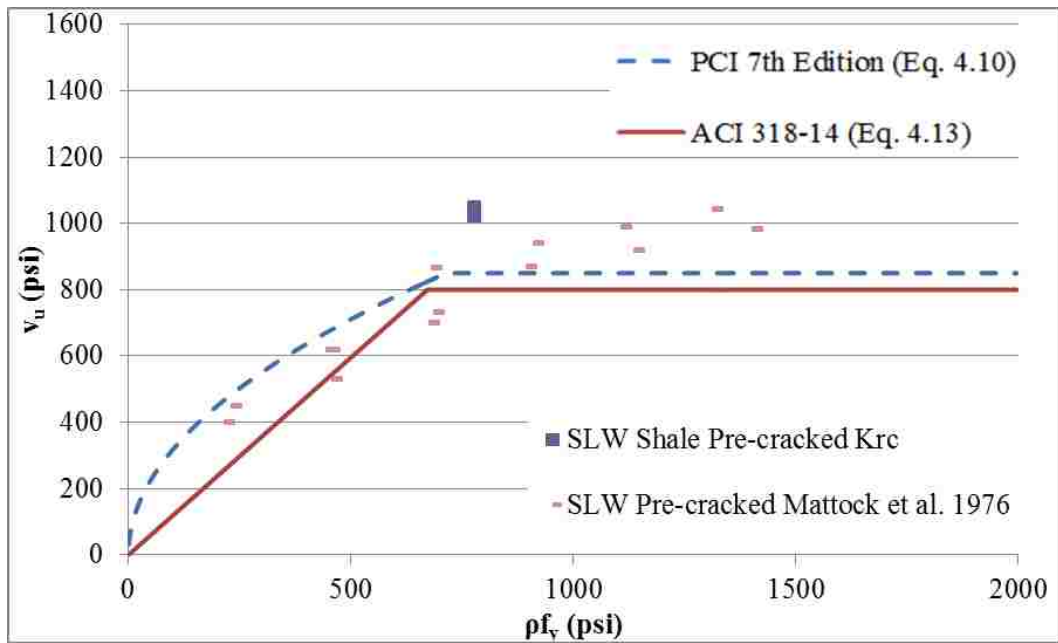
Figure 4.42 Comparison of Shear Strength v_u with Equations 4.10 and 4.13 for Sand-lightweight Concrete Specimens with Monolithic Pre-cracked Interface (λ=0.85, μ=1.19)
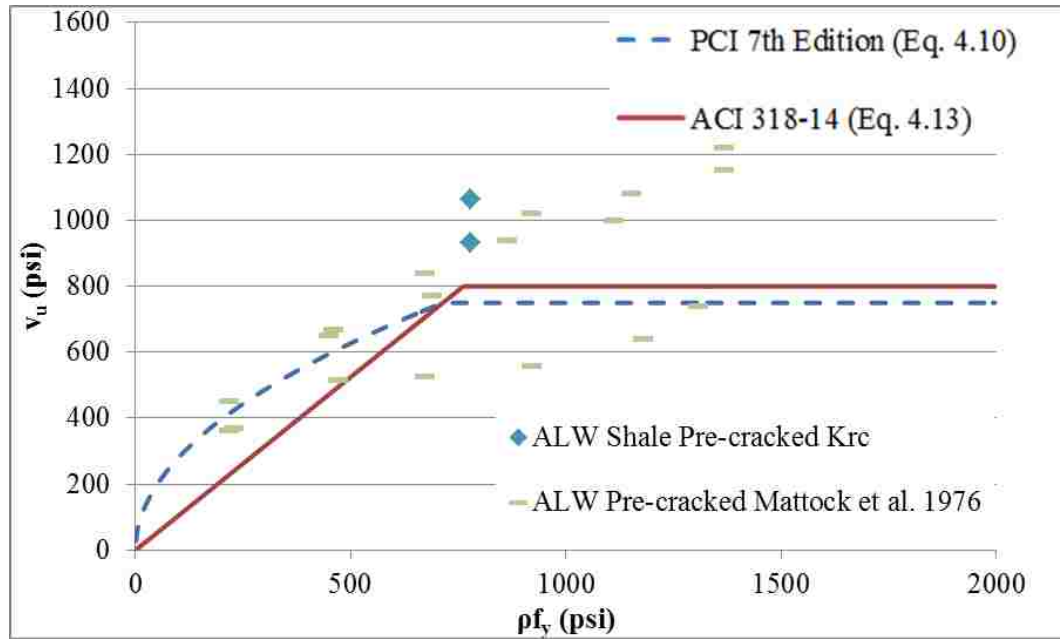
Figure 4.43 Comparison of Shear Strength v_u with Equations 4.10 and 4.13 for All-lightweight Concrete Specimens with Monolithic Pre-cracked Interface (λ=0.75, μ=1.05)
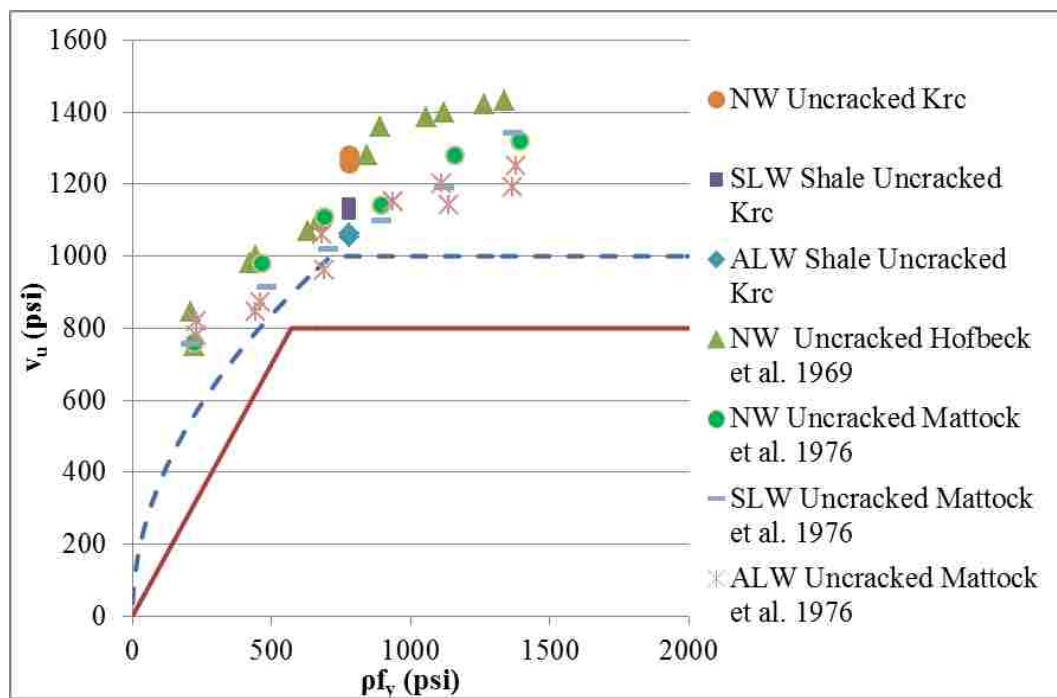
Figure 4.44 Comparison of Shear Strength v_u with Equations 4.10 and 4.13 for Monolithic Uncracked Concrete Specimens (with λ=1.0, μ=1.4)

4.5.3. Effective Coefficient of Friction, μ_e. Results from the experiments described in Section 3.6 of this thesis are compared in this section to the predicted values of the effective coefficient of friction μ_e. The effective coefficient of friction is predicted using Equation 4.9 as proposed by the PCI Design Handbook (2010). However, as described in Sections 2.3.3 and 4.5.1.2, this equation is not applicable to Case 3 (concrete placed against hardened concrete not intentionally roughened). For this reason, the maximum value for μ_e for Case 3 was taken from the PCI Design Handbook 6th Edition (μ_e=2.2). The maximum value for V_u/ϕ is also taken into account as presented in Table 4.7. In this section, it is examined if the equation for μ_e is conservative for the cold joint specimens studied in this thesis. Data analyzed in this section includes results from the Shaw (2013) study as well. Results from the monolithic specimens from this study along with data from Hofbeck (1969) and Mattock (1976) are compared to the predictions according to the Handbook (2010).

It must be made clear that the values of μ_e presented for each test specimen are calculated using Equation 4.11 with $v_u= \phi v_n$ where ϕ=1.0. The shear interface reinforcement yield point f_y is taken as the actual reported yield point (i.e., not limited to 60,000 psi). Lastly, only specimens with reinforcement ratios identical to the specimens in this thesis (i.e., $\rho \approx 0.013$) were taken from previous studies.

Figures 4.45 and 4.46 compare the measured values of μ_e to the predicted values for roughened interface sand-lightweight and all-lightweight concrete, respectively. Both figures show conservative (to the right and above the predicted values) correlation between the actual test results and predicted values. All values are predicted conservatively regardless of the concrete compressive strength or the lightweight aggregate type. With increasing concrete compressive strength it is observed that the level of conservatism also increases. Even though the values are conservative for all lightweight aggregate types, it should be recognized that the least conservative value is for the clay aggregate specimens in both sand-lightweight and all-lightweight concrete specimens.

Figures 4.47 and 4.48 compare the measured values μ_e to the predicted values for smooth interface sand-lightweight and all-lightweight concrete, respectively. With

increasing concrete compressive strength, an increasing level of conservatism is observed. The values are conservative for all lightweight aggregate types.

Figures 4.49 through 4.51 for monolithic concrete specimens show conservative correlation between the test results and the predicted values of μ_e for all uncracked specimens. This, however, is not true for some normalweight, sand-lightweight, and all-lightweight monolithic pre-cracked specimens in Figures 4.49 through 4.51. This is in agreement with the statement in Section 4.4 that the pre-cracking procedure introduces a new variable depending on pre-cracking procedure. For uncracked specimens, the test values of μ_e calculated from the results were conservative regardless of concrete type.
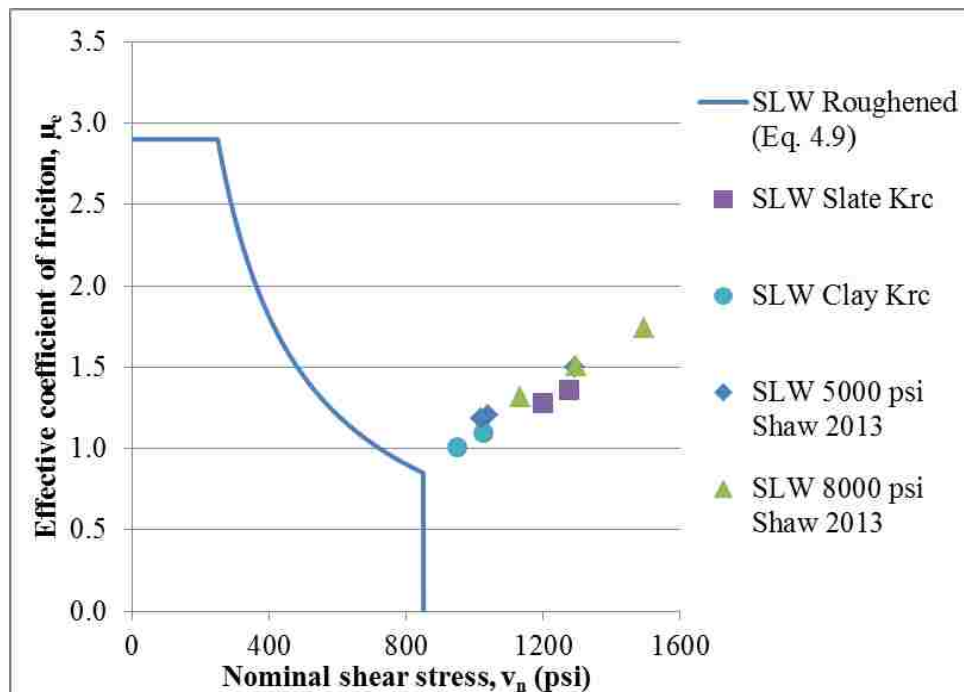
Figure 4.45 Analysis of the Effective Coefficient of Friction for Sand-lightweight Concrete with Roughened Interface
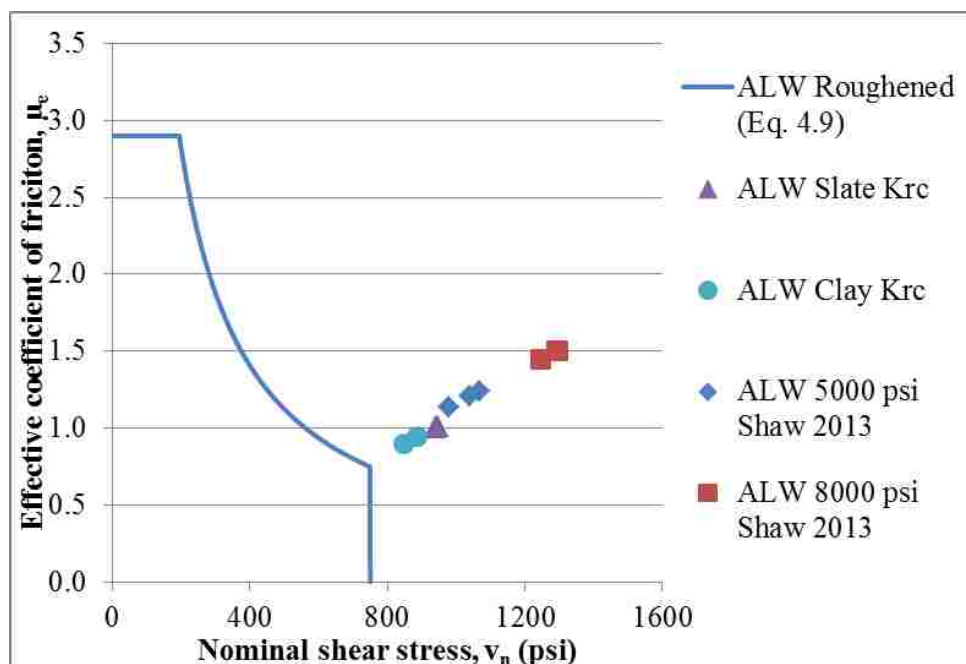
Figure 4.46 Analysis of the Effective Coefficient of Friction for All-lightweight Concrete with Roughened Interface
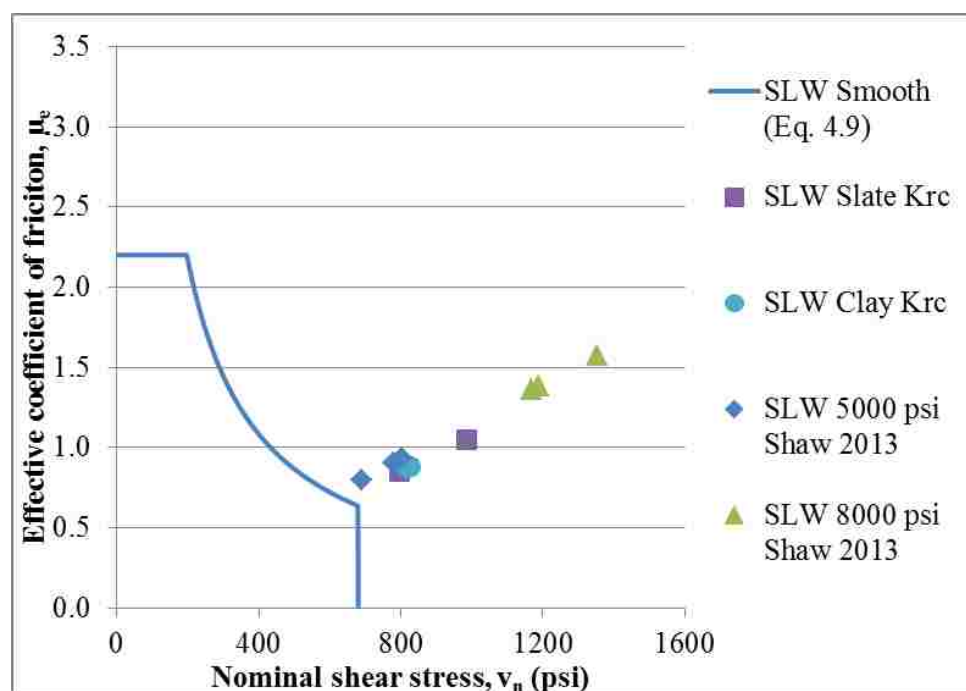
Figure 4.47 Analysis of the Effective Coefficient of Friction for Sand-lightweight Concrete with Smooth Interface
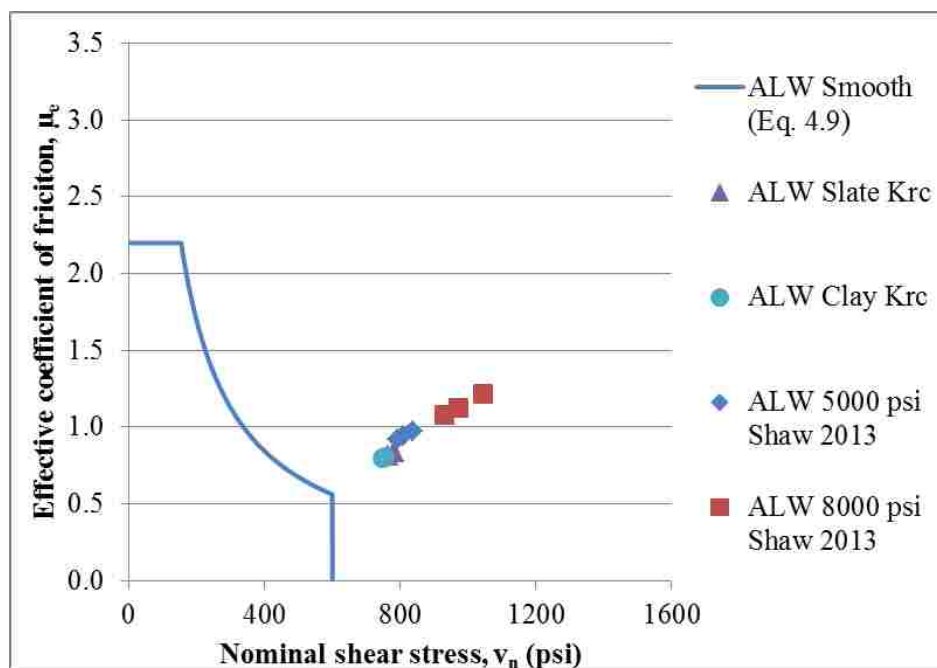
Figure 4.48 Analysis of the Effective Coefficient of Friction for All-lightweight Concrete Smooth Interface
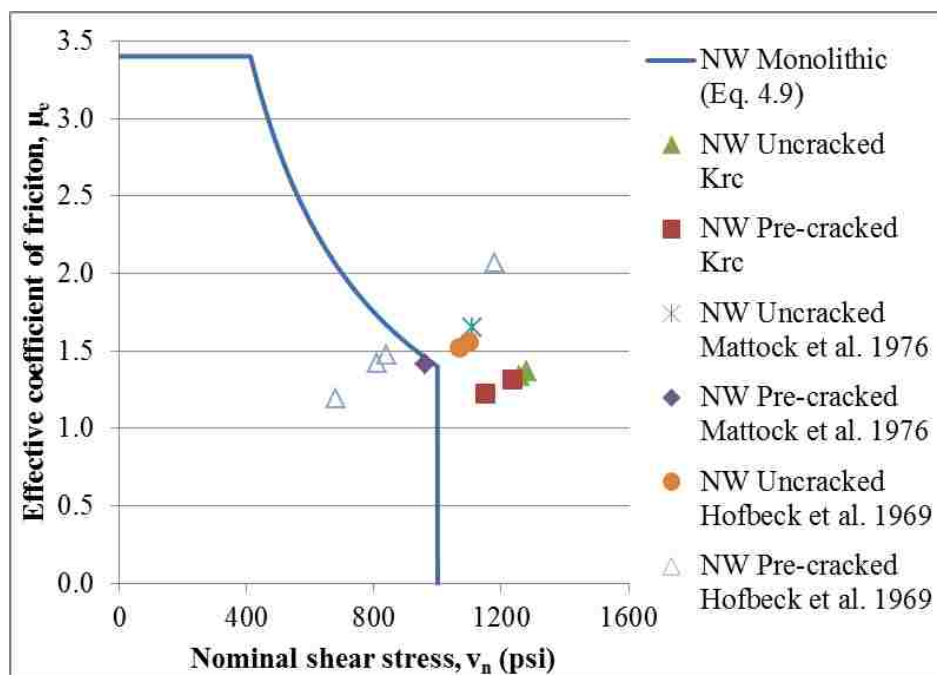
Figure 4.49 Analysis of the Effective Coefficient of Friction for Normalweight Concrete with Monolithic Interface
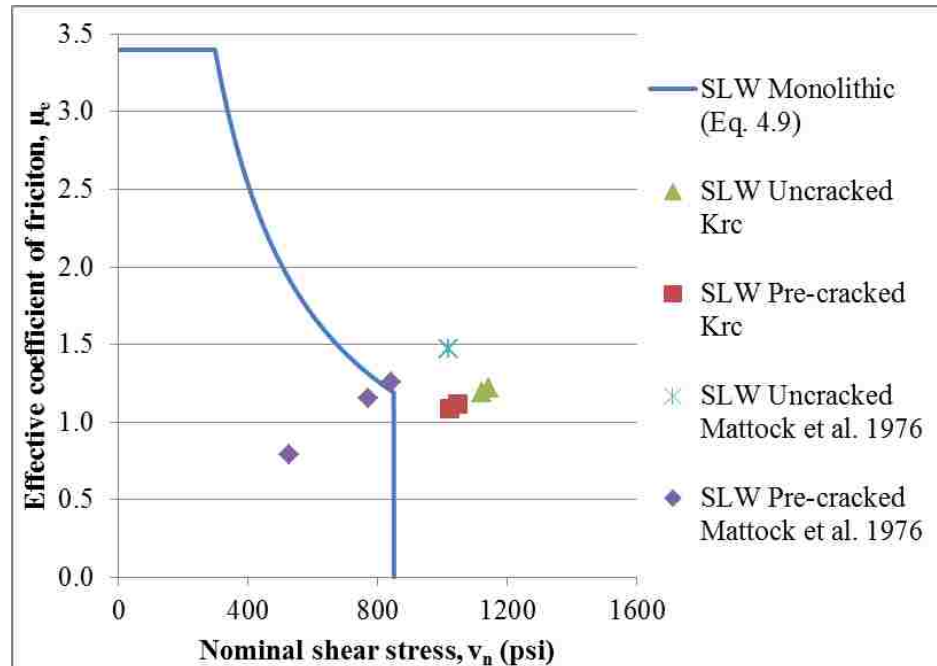
Figure 4.50 Analysis of the Effective Coefficient of Friction for Sand-lightweight Concrete with Monolithic Interface
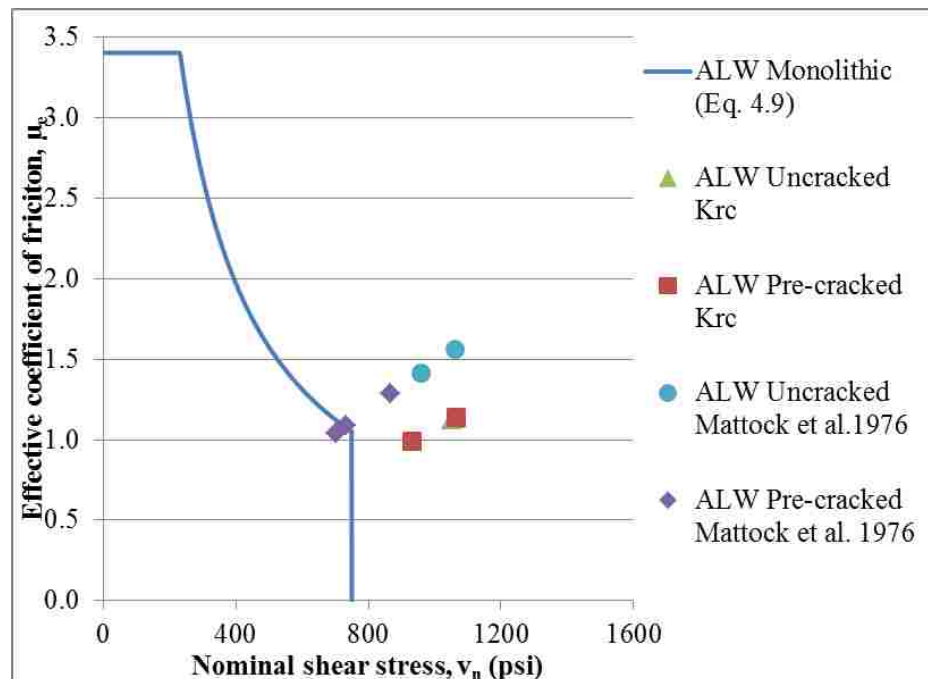
Figure 4.51 Analysis of the Effective Coefficient of Friction for All-lightweight Concrete with Monolithic Interface

As shown in Figures 4.45 through 4.49, the results for cold joint interface concrete specimens were conservative compared to the predicted values. This prompted the following question. In the calculation of μ_e using Equation 4.9, the modification factor for use of lightweight aggregate λ is included explicitly. This equation is also a function of shear-friction coefficient μ that also includes the lightweight aggregate modification factor. As a result, Equation 4.9 includes the term λ twice (i.e., λ^2) causing the predicted values to be extremely conservative. This level of conservatism may not be necessary in predicting of the effective coefficient of friction μ_e. Figures 4.52 and 4.53 plot the effective coefficient of friction for roughened and smooth cold joint interface specimens, respectively, without considering the lower mechanical properties of lightweight aggregate concrete. Values of v_u are averaged for the specimens of the same concrete type and interface condition. In Figure 4.52 all concrete types are combined (normalweight, sand-lightweight, and all-lightweight) and are compared to the value of μ_e computed for the normalweight roughened interface condition (λ=1.0 and μ=1.0). It is observed that most of the values are still predicted conservatively. The only unconservative test results are the all-lightweight slate and the all-lightweight clay. Figure 4.53 plots the same relation for all smooth interface cold joint specimens. The prediction in this figure is for normalweight smooth interface condition (λ=1.0 and μ=0.6). It is observed that nearly all test results are predicted conservatively. The only unconservative test result is the 5000 psi normalweight concrete specimen with a smooth interface tested by Shaw (2013). By examining at the results from Figures 4.52 and 4.53, the use of λ^2 term in Equation 4.9 can be questioned. Further discussion and proposed revisions are included in Section 4.5.4.
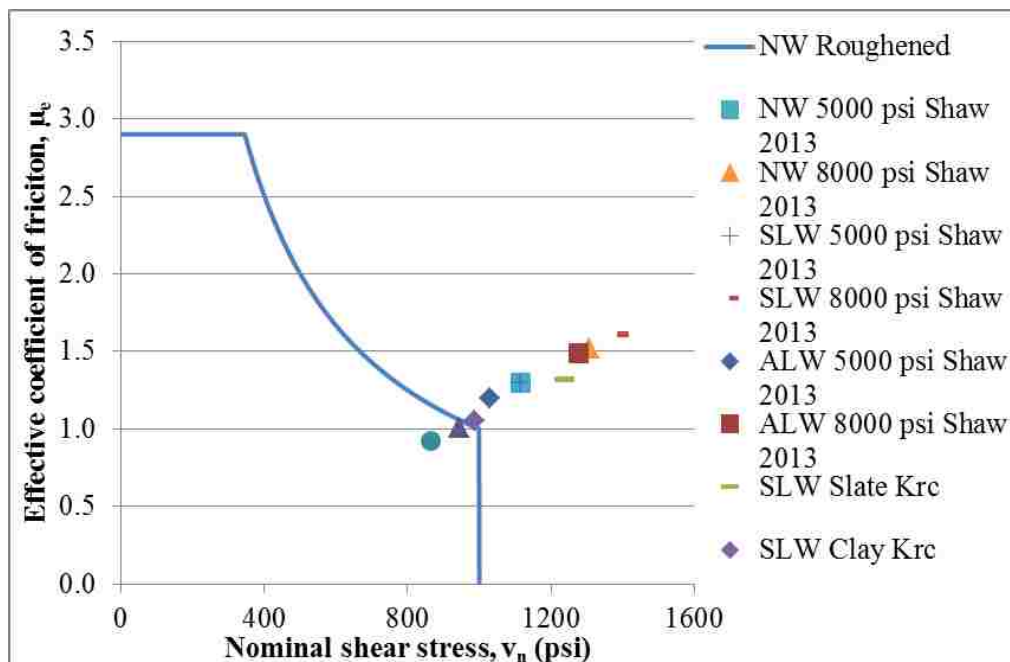
Figure 4.52 Analysis of the Effective Coefficient of Friction for All Roughened Interface Specimens (μ=1.0) with λ=1.0 for all Concrete Types
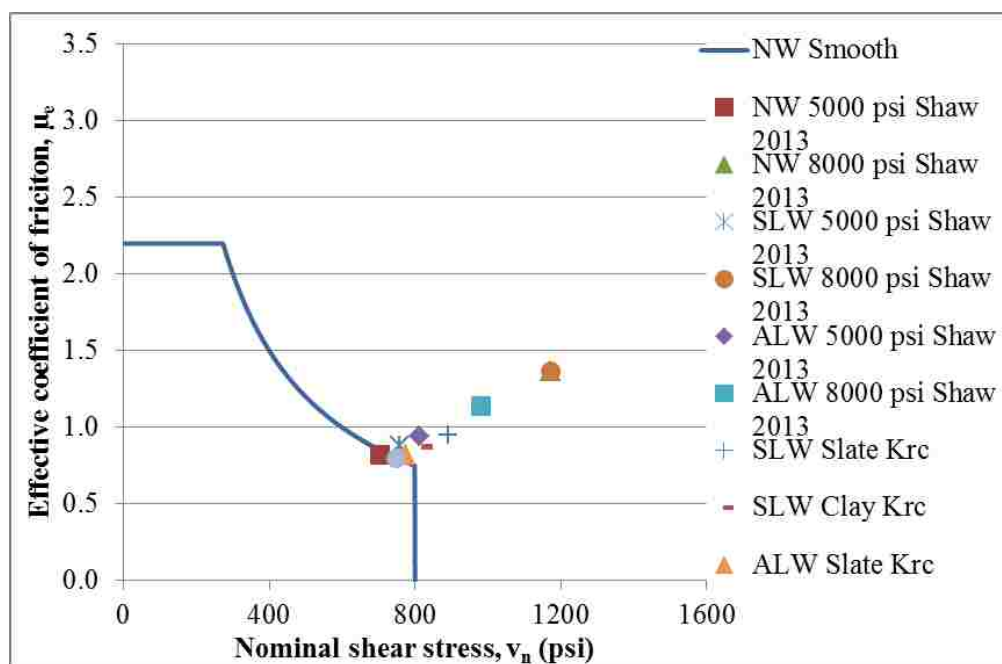
Figure 4.53 Analysis of the Effective Coefficient of Friction for All Smooth Interface Specimens (μ=0.6) with λ=1.0 for all Concrete Types

4.5.4. Proposed Revisions to Effective Coefficient of Friction. As pointed out by Tanner (2008), there is confusion regarding why the lightweight modification factor λ is accounted for twice (resulting in the factor λ^2) in calculating of the effective coefficient of friction μ_e in the PCI Design Handbook 7th Edition (Eq. 4.9). One term is explicitly included in Equation 4.9 and the other comes from the shear-friction coefficient μ (Table 4.8). It was shown in Figures 4.45 through 4.48 that including both λ terms results in conservative prediction for the shear strength in all types of lightweight concrete. This section proposes removing the explicit λ term from Equation 4.9. The use of lightweight concrete aggregate is accounted for only in the shear-friction coefficient μ. This proposed equation is shown in Equation 4.15.

$$\mu_e = \frac{\phi 1000 A_{cr}\mu}{V_u} \tag{4.15}$$

where A_{cr} is the area of the crack interface, V_u is the applied shear force, and μ is the shear-friction coefficient as defined in Table 4.8. The limits used for the upper bounds are consistent with the limits of the PCI Design Handbook 7th Edition presented in Table 4.7. It must be noted that the Equation 4.15 does not change the values that would be predicted for normalweight concrete specimens because λ=1.0. Therefore the normalweight concrete figures will not be included in the following discussion. Figures 4.54 through 4.59 re-plotted the Figures 4.45 through 4.51 with the exception of Figure 4.49 (normalweight concrete). However, Figures 4.54 through 4.59 also include the proposed Equation 4.15, including the proposed limits for monolithic, roughened, and smooth interface conditions. Figure 4.54 demonstrates that Equation 4.15 conservatively predicts the shear strength for roughened interface cold joint sand-lightweight specimens of all concrete strengths. Figure 4.55 shows that Equation 4.15 also conservatively predicts shear strengths for roughened interface cold joint all-lightweight specimens. Figure 4.56 demonstrates that the Equation 4.15 conservatively predicts the shear strength for smooth interface cold joint sand-lightweight specimens of all concrete strengths. Figure 4.57 shows that Equation 4.15 also conservatively predicts shear strengths for smooth interface cold joint all-lightweight specimens. Figures 4.58 and 4.59

demonstrate that the Equation 4.15 is not conservative for all tests on to sand-lightweight and all-lightweight concrete specimens with a monolithic interface. It must be noticed, that the unconservative value for the pre-cracked sand-lightweight specimen in Figures 4.58 and the unconservative values for the pre-cracked all-lightweight specimen in Figure 4.59 are unconservative for Equation 4.9 as well.

These results demonstrate that the shear-friction coefficient µ alone is enough to account for the reduced mechanical properties of lightweight aggregate concretes in effective coefficient of friction calculations, and the additional λ term may not be needed.
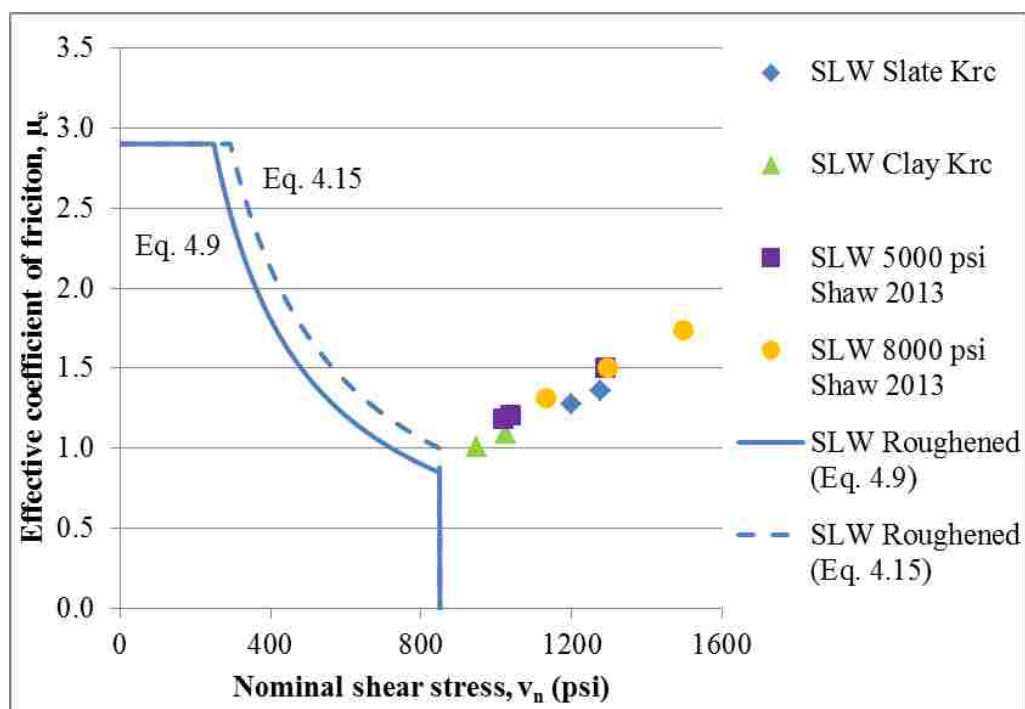
Figure 4.54 Analysis of the Proposed Effective Coefficient of Friction for Sand-lightweight Concrete with Roughened Interface
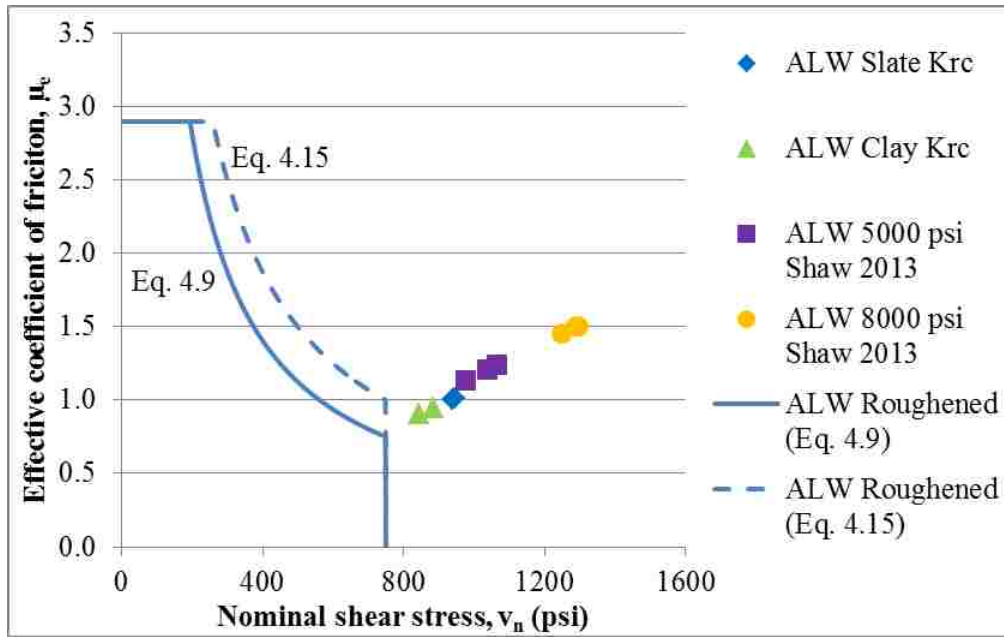
Figure 4.55 Analysis of the Proposed Effective Coefficient of Friction for All-lightweight Concrete with Roughened Interface
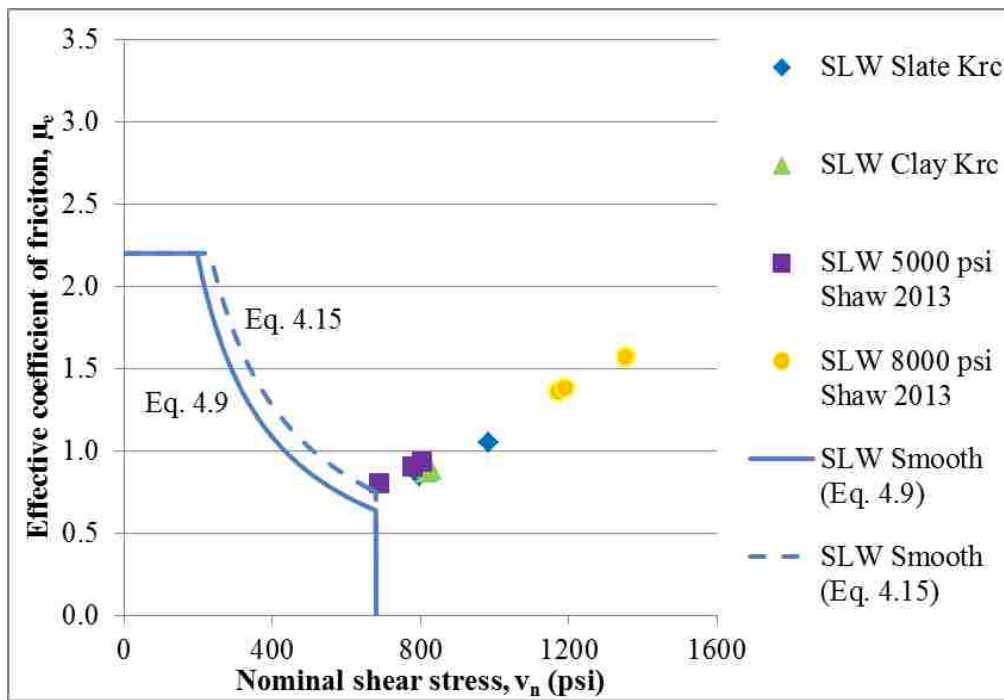
Figure 4.56 Analysis of the Proposed Effective Coefficient of Friction for Sand-lightweight Concrete with Smooth Interface
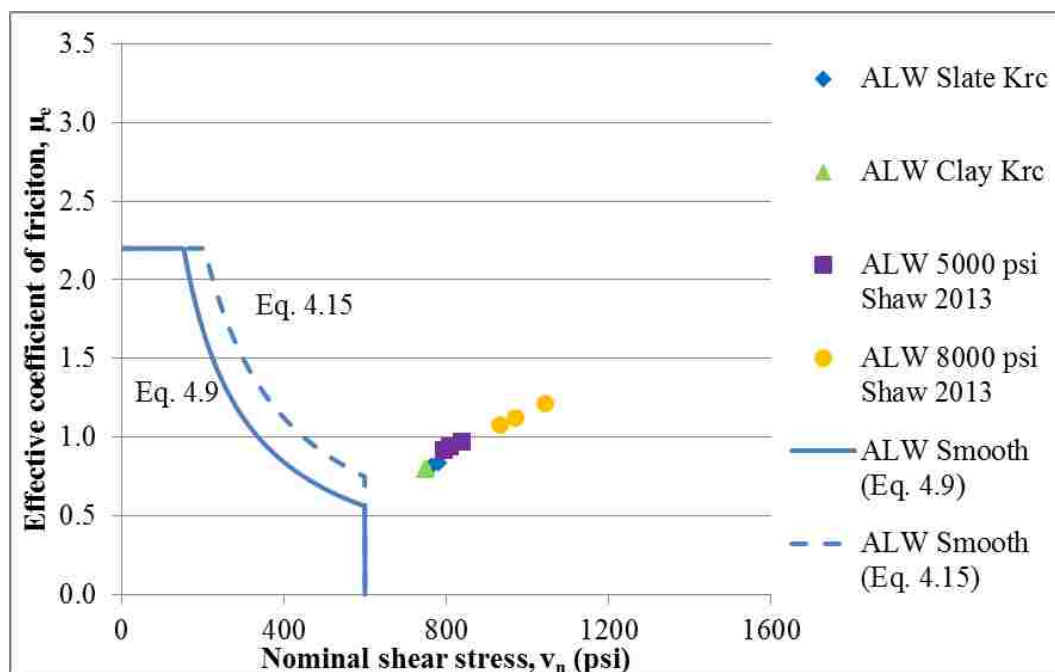
Figure 4.57 Analysis of the Proposed Effective Coefficient of Friction for All-lightweight Concrete with Smooth Interface
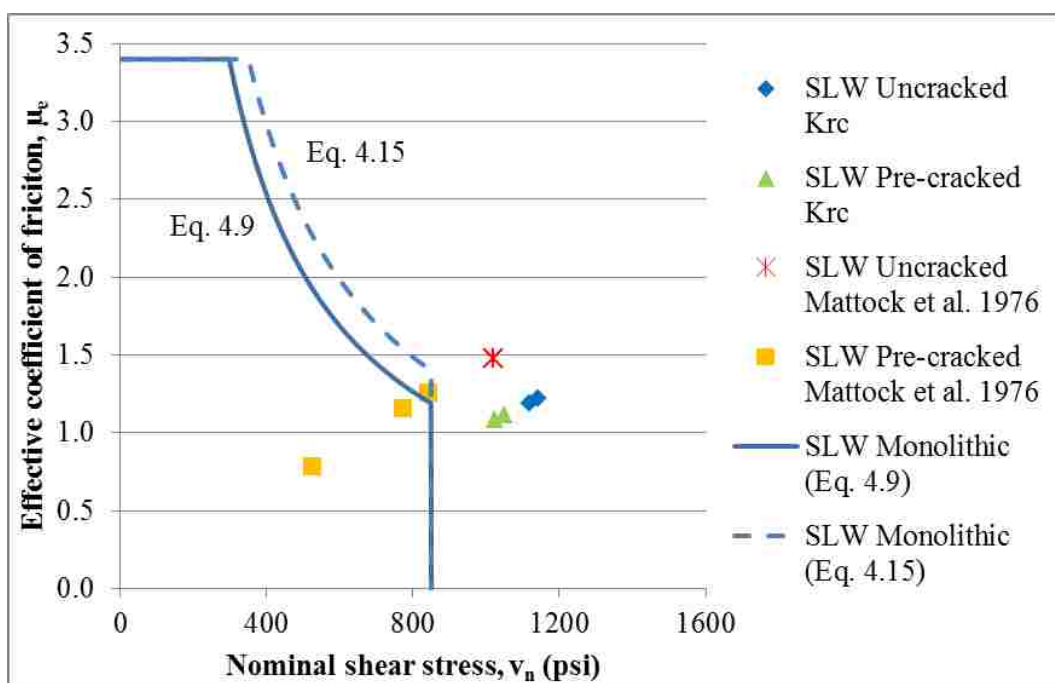
Figure 4.58 Analysis of the Proposed Effective Coefficient of Friction for Sand-lightweight Concrete with Monolithic Interface
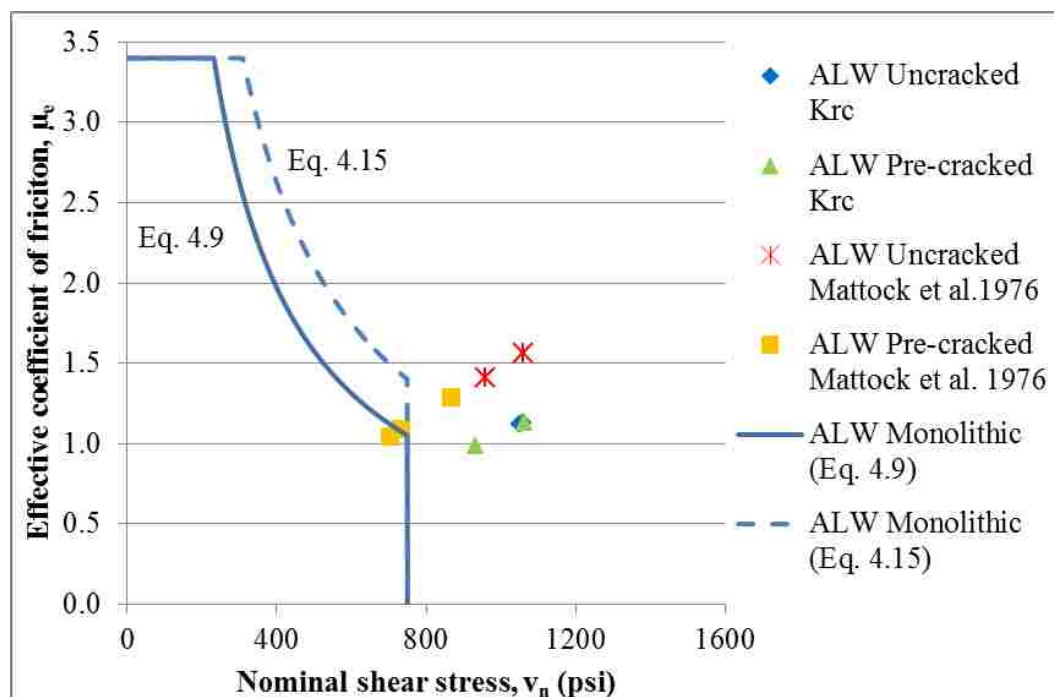
Figure 4.59 Analysis of the Proposed Effective Coefficient of Friction for All-lightweight Concrete with Monolithic Interface

5. SUMMARY, CONCLUSIONS, AND RECOMMENDATIONS

5.1. SUMMARY

This study examined the influence of concrete unit weight and lightweight aggregate type on the direct shear transfer across a concrete surface with different interface conditions, including monolithic and cold joints. Cold joint interfaces are common in precast and prestressed concrete elements such as corbels, composite sections, or connections of shear walls to foundations. In these cases, the shear-friction design provisions are used to design for the interface shear. The shear-friction design provisions in the PCI Design Handbook and the ACI 318 code are mainly empirical and based on experimental data. Limited data exists with respect to lightweight aggregate concretes. However, increasing use of lightweight concrete motivated this research to determine the validity and conservatism of the current shear-friction design provisions for sand-lightweight and all-lightweight concretes.

This thesis evaluated the results of 28 push-off type normalweight and lightweight concrete specimens. The specimens were cast either monolithically (12 total) or non-monolithically (16 total). Each specimen's target concrete compressive strength was 5000 psi. The unit weight of concretes used ranged between 88 pcf to 148 pcf. The specimens had the shear plane area of 49.5 in^2 that was crossed with three closed No. 3 deformed steel reinforcing bars with total steel cross sectional area of 0.66 in^2 resulting in a reinforcement ratio of 0.013. For the non-monolithic (cold joint) specimens, the shear plane was either troweled smooth or roughened to an average amplitude of 0.25 in. Lightweight aggregates used to make the lightweight concretes were expanded shale, expanded slate, and expanded clay. Data presented for each series included applied shear force – slip, applied shear force – dilation, applied shear force – strain, slip – strain, slip – dilation, and dilation – strain relations. Results were compared with the results of previous researchers. The new results were then combined with the results of previous researchers and compared to current design provisions of PCI Design Handbook and ACI 318 code.

5.2. CONCLUSIONS

Based on the results of this study alone, the following conclusions are made:

1. The shear strength of monolithic interface specimens increased with increasing unit weight for both uncracked and pre-cracked specimens.

2. The shear strength of cold joint specimens with an intentionally roughened interface increased as the unit weight of concrete increased. The shear strength of cold joint specimens with smooth interface appeared to be independent of concrete type (unit weight of concrete).

3. The shear strength of roughened interface cold joint specimens was higher than the shear strength of smooth interface cold joint specimens regardless of lightweight aggregate type.

4. The sand-lightweight concrete specimens achieved a higher shear strength than the all-lightweight concrete specimens with the same lightweight aggregate type for roughened and smooth cold joint interfaces as well as uncracked and pre-cracked monolithic interfaces.

5. A pre-existing crack reduced the shear strength of normalweight, sand-lightweight, and all-lightweight concrete specimens relative to the corresponding uncracked specimens. The percent difference between uncracked and pre-cracked specimens ranged from 5.7 to 8.9%. However, the average residual shear strength was higher in the pre-cracked specimens.

6. The shear strength appeared to be influenced by aggregate type for roughened cold joint interface specimens. The shear strength of concretes made with expanded slate aggregate was larger than the shear strength of concrete made with expanded clay aggregate for roughened interface cold joint specimens. The shear strength of specimens with smooth interface appeared to be independent of the aggregate type.

7. The shear strength was predicted conservatively by the PCI Design Handbook 6th Edition coefficient of friction approach, the 7th Edition effective coefficient of friction approach, and the ACI 318-14 code which is identical to PCI design Handbook 7th Edition coefficient of friction approach for all cold joint interface

specimens studied in this program regardless of aggregate type, concrete type, or surface condition.

8. The effective coefficient of friction μ_e used by the PCI Design Handbook was found to be conservative for sand-lightweight and all-lightweight cold joint specimens regardless of lightweight aggregate type or interface condition.

Based on the results of this study and the studies conducted by previous researchers, the following conclusions are made:

1. The value of the effective coefficient of friction μ_e used in the PCI Design Handbook 7th Edition was found to be conservative for all of the lightweight (i.e., sand-lightweight and all-lightweight) concrete cold joint specimens included in this study regardless of the surface condition or aggregate type.

2. The sand-lightweight concrete aggregate with highest shear transfer strength was found to be the expanded shale, followed by the expanded slate, and finally the expanded clay. This was true for both roughened and smooth interface conditions.

3. The all-lightweight concrete aggregate with the highest shear transfer strength was found to be the expanded slate, followed by the expanded clay, followed by the expanded shale. This was true for both roughened and smooth interface conditions.

4. The shear strength was predicted conservatively by both the PCI Design Handbook 7th Edition using both approaches (i.e., μ and μ_e) and the ACI 318-14 code for all sand-lightweight and all-lightweight concrete non-monolithic specimens presented in this study regardless of aggregate type or interface condition.

5. The shear strength of monolithic uncracked concrete specimens can be conservatively predicted using the lightweight concrete modification factor $\lambda=1.0$ (normalweight concrete case) for normalweight and sand-lightweight concrete using the PCI Design Handbook 7th Edition using the μ and μ_e approaches. It can also be predicted conservatively (using the same $\lambda=1.0$) by the ACI 318-14 code for all concrete types (unit weights).

6. The use of the lightweight concrete modification factor λ in the calculation of the effective coefficient of friction was deemed very conservative for all of the normalweight and sand-lightweight concrete roughened interface cold joint specimens as demonstrated in Figure 4.47. This, however, was not true for all all-lightweight concrete specimens.

7. The use of the lightweight concrete modification factor λ in the calculation of the effective coefficient of friction was found very conservative for all of the sand-lightweight and all-lightweight concrete smooth interface cold joint specimens.

5.3. RECOMMENDATIONS FOR DESIGN EQUATIONS

As discussed in Section 4.5.3, the effective coefficient of friction μ_e is computed conservatively using the PCI Design Handbook approach for sand-lightweight and all-lightweight non-monolithic concrete specimens regardless of the interface condition or lightweight aggregate type. That is, μ_e is predicted conservatively for Case 2 and Case 3 of PCI Design Handbook approach. However, the use of the effective coefficient of friction μ_e is not permitted for concrete placed against concrete that is not intentionally roughened (Case 3) in the PCI Design Handbook 7th Edition. It was shown by these tests that using the approach of the PCI Design Handbook 7th Edition with the limits for μ_e from the PCI Design Handbook 6th Edition (Case 3) the values are predicted conservatively. Therefore it is recommended that the PCI Design Handbook 7th Edition approach be permitted to be used in Cases 1 through 3 with the limits for μ_e from PCI Design Handbook 6th Edition.

It was also shown in Section 4.5.3 that value of the effective coefficient of friction μ_e computed using the PCI Design Handbook 7th Edition was very conservative for normalweight and sand-lightweight concrete with roughened interface cold joint specimens. Likewise, it was also found very conservative for all concrete types with a smooth cold joint interface. The effect of the lightweight modification factor λ is exacerbated because it is squared in the calculation of the effective coefficient of friction μ_e in the PCI Design Handbook which led to very conservative results for the lightweight aggregate concretes. Results from this research show re-evaluation of this modification factor, λ for the purposes of calculating the effective coefficient of friction μ_e is

warranted. An equation for μ_e was proposed in Section 4.5.4 in which the term λ is not squared (see Equation 4.15). Equation 4.15 was shown to predict the shear transfer strengths conservatively for roughened and smooth interface cold joint specimens of all lightweight aggregate types, unit weights of concrete, and compressive strengths.

5.4. RECOMMENDATIONS FOR FUTURE WORK

The variables included in this study were lightweight aggregate type, unit weight of concrete, and shear interface condition (monolithic and cold joint). However, other parameters have been shown to influence the shear transfer strength. Following are recommendations for future work:

1. The lightweight aggregates used in this study (expanded shale, slate, clay) all had the same maximum nominal size (3/8 in.). Follow-up research is needed to investigate the influence of maximum aggregate size on shear-friction in cold joint specimens.

2. For the purposes of this research the compressive strength of each lightweight aggregate type concrete was nominally the same. Further investigation is needed to determine the effect of various compressive strengths for each lightweight aggregate type concrete.

3. The size of shear plane for the push-off type specimens has not changed much throughout the history of shear-friction investigation. It is recommended to examine the effect of the shear plane area (keeping the reinforcement ratio constant) on shear transfer capacity.

4. In this study, the casting of the two parts of cold joint specimens was performed with an eight-hour delay to eliminate differences in compressive strength of concretes. This, however, is not the case in the precast prestressed concrete industry. Further research is needed to investigate the influence of longer time period between the casting of the two sections on the shear transfer strength.

5. During the process of this research, it was found that there is no uniform procedure used in pre-cracking monolithic specimens. This may be one of the causes for the relatively large amount of scatter in the data for specimens with a monolithic pre-cracked interface. It would be beneficial for the consistency of

data to determine the most efficient and uniform way to pre-crack the push off type specimens.

APPENDIX A

DATABASES

Table A.1 Summary of Results from Tests Conducted for This Thesis

Specimen ID	f'c at test day (psi)	Concrete unit weight (lb/ft³)	Vu (lbs)	vu¹ (psi)	vu/f'c (psi/psi)	vu,avg (psi)	Std. Dev. vu,avg (psi)	vu/f'c (psi/psi)	Slip at Vu (in)	Dilation at Vu (in)	Vur² (lbs)	vur¹ (psi)	vur/f'c (psi/psi)	vur,avg (psi)	Std. Dev. vur,avg (psi)	vur/f'c avg (psi/psi)	(vu/vur)avg
N-MO-U-1	4840	148	63410	1281	0.265	1269	12	0.26	0.019	0.014	40729	823	0.17	823	N/A	0.17	1.54
N-MO-U-2		148	62203	1257	0.260				0.017	0.015	N/A	N/A	N/A				
N-MO-P-1		148	61071	1234	0.255	1192	41	0.25	0.017	0.011	45537	920	0.19	1011	92	0.21	1.18
N-MO-P-2		148	56973	1151	0.238				0.023	0.012	54598	1103	0.23				
S-SH-MO-U-1	4770	117	55434	1120	0.235	1132	12	0.24	0.011	0.009	40773	824	0.17	801	23	0.17	1.41
S-SH-MO-U-2		117	56588	1143	0.240				0.010	0.010	38501	778	0.16				
S-SH-MO-P-1		117	50593	1022	0.214	1035	13	0.22	0.013	0.007	39068	789	0.17	830	41	0.17	1.25
S-SH-MO-P-2		117	51884	1048	0.220				0.020	0.009	43098	871	0.18				
A-SH-MO-U-1	4700	108	52032	1051	0.224	1056	5	0.22	0.016	0.009	32821	663	0.14	707	44	0.15	1.49
A-SH-MO-U-2		108	52549	1062	0.226				0.013	0.009	37162	751	0.16				
A-SH-MO-P-1		108	46120	932	0.198	998	66	0.21	0.038	0.009	41332	835	0.18	906	71	0.19	1.10
A-SH-MO-P-2		108	52692	1064	0.226				0.026	0.007	48352	977	0.21				
S-SL-CJ-R-1	5570	117	63167	1276	0.229	1238	38	0.22	0.013	0.008	N/A	N/A	N/A	735	N/A	0.13	1.68
S-SL-CJ-R-2		117	59370	1199	0.215				0.013	0.009	36363	735	0.13				
S-SL-CJ-S-1		117	39487	798	0.143	891	94	0.16	0.017	0.007	30508	616	0.11	700	83	0.13	1.27
S-SL-CJ-S-2		117	48767	985	0.177				0.016	0.008	38771	783	0.14				
A-SL-CJ-R-1	4380	106	46525	940	0.215	944	4	0.22	0.012	0.006	30148	609	0.14	645	36	0.15	1.46
A-SL-CJ-R-2		106	46925	948	0.216				0.005	0.005	33741	682	0.16				
A-SL-CJ-S-1		106	37842	764	0.175	774	9	0.18	0.019	0.007	30810	622	0.14	671	48	0.15	1.15
A-SL-CJ-S-2		106	38751	783	0.179				0.024	0.007	35575	719	0.16				
S-CL-CJ-R-1	4640	105	50785	1026	0.221	986	39	0.21	0.007	0.006	31310	633	0.14	651	19	0.14	1.51
S-CL-CJ-R-2		105	46885	947	0.204				0.015	0.005	33178	670	0.14				
S-CL-CJ-S-1		105	41006	828	0.179	822	6	0.18	0.015	0.006	31025	627	0.14	600	26	0.13	1.37
S-CL-CJ-S-2		105	40436	817	0.176				0.018	0.007	28402	574	0.12				
A-CL-CJ-R-1	4460	88	41858	846	0.190	865	20	0.19	0.009	0.006	N/A	N/A	N/A	534	N/A	0.12	1.62
A-CL-CJ-R-2		88	43816	885	0.198				0.011	0.006	26451	534	0.12				
A-CL-CJ-S-1		88	36966	747	0.167	750	4	0.17	0.008	0.005	N/A	N/A	N/A	501	N/A	0.11	1.50
A-CL-CJ-S-2		88	37324	754	0.169				0.015	0.006	24795	501	0.11				

Table A.2 Summary of Previous Research Used for Analysis

Table A.3 Database of Monolithic Uncracked Push-off Type Specimens without External Axial Force

Researcher(s)	Specimen ID	Concrete Type	f'_c (psi)	A_{cr} (in^2)	ρ	$f_{y, actual}$ (psi)	$f_{y,specified}$ (psi)	V_u (lbs)	v_u (psi)
Hofbeck, Ibrahim, and Mattock, 1969	1.1A	NWC	3920	50	0.004	50700	40000	37500	750
	1.1B	NWC	4340	50	0.004	48000	40000	42200	844
	1.2A	NWC	3840	50	0.009	50700	40000	50000	1000
	1.2B	NWC	4180	50	0.009	48000	40000	49000	980
	1.3A	NWC	3840	50	0.013	50700	40000	55000	1100
	1.3B	NWC	3920	50	0.013	48000	40000	53500	1070
	1.4A	NWC	4510	50	0.018	50700	40000	68000	1360
	1.4B	NWC	3855	50	0.018	48000	40000	64000	1280
	1.5A	NWC	4510	50	0.022	50700	40000	70000	1400
	1.5B	NWC	4065	50	0.022	48000	40000	69200	1384
	1.6A	NWC	4310	50	0.026	50700	40000	71600	1432
	1.6B	NWC	4050	50	0.026	48000	40000	71000	1420
Mattock, Li, and Wang, 1976	A1	SLW	3740	50	0.004	47700	40000	37900	758
	A2	SLW	4095	50	0.009	53600	40000	45700	914
	A3	SLW	3910	50	0.013	53200	40000	51000	1020
	A4	SLW	4100	50	0.018	50900	40000	55000	1100
	A5	SLW	3960	50	0.022	50900	40000	59500	1190
	A6	SLW	4250	50	0.026	51800	40000	67200	1344
	E1	ALW	4150	50	0.004	52300	40000	39000	780
	E2	ALW	4030	50	0.009	52300	40000	43600	872
	E3	ALW	4065	50	0.013	52300	40000	48000	960
	E4	ALW	4040	50	0.018	53200	40000	57500	1150
	E5	ALW	4115	50	0.022	50500	40000	60000	1200
	E6	ALW	4050	50	0.026	52300	40000	62500	1250
	G1	ALW	4145	50	0.004	52300	40000	41000	820
	G2	ALW	3880	50	0.009	50500	40000	42300	846
	G3	ALW	4100	50	0.013	51800	40000	53000	1060
	G4	ALW	4420	50	0.018	53200	40000	57500	1150
	G5	ALW	4005	50	0.022	51800	40000	57000	1140
	G6	ALW	4005	50	0.026	51800	40000	59500	1190
	M1	NWC	4180	50	0.004	50900	40000	38000	760
	M2	NWC	3900	50	0.009	52700	40000	49000	980
	M3	NWC	3995	50	0.013	52300	40000	55500	1110
	M4	NWC	4150	50	0.018	50900	40000	57000	1140
	M5	NWC	3935	50	0.022	52700	40000	64000	1280
	M6	NWC	4120	50	0.026	52700	40000	66000	1320
Mattock, Johal, and Chow, 1975	F1U	NWC	4035	84	0.016	52200	40000	114996	1369
	F4U	NWC	4175	84	0.016	53200	40000	96012	1143
	F6U	NWC	4245	84	0.016	51000	40000	89544	1066
	E1U	NWC	4060	84	0.010	52700	40000	91476	1089
	E4U	NWC	3860	84	0.010	49100	40000	79464	946
	E6U	NWC	4120	84	0.010	50800	40000	50988	607

Researcher(s)	Specimen ID	Concrete Type	f'c (psi)	Acr (in²)	ρ	fy, actual (psi)	fy,specified (psi)	Vu (lbs)	vu (psi)
Kahn and Mitchell, 2002	SF-4-1-U	NWC	6805	60	0.004	69500	60000	57900	965
	SF4-2-U	NWC	6805	60	0.007	69500	60000	80100	1335
	SF-4-3-U	NWC	6805	60	0.011	69500	60000	85860	1431
	SF-7-1-U	NWC	11734	60	0.004	83000	60000	87540	1459
	SF-7-2-U	NWC	12410	60	0.007	83000	60000	118140	1969
	SF-7-3-U	NWC	13103	60	0.011	83000	60000	138420	2307
	SF-7-4-U	NWC	12471	60	0.015	83000	60000	149100	2485
	SF-10-1-U-a	NWC	12053	60	0.004	83000	60000	100080	1668
	SF-10-1-U-b	NWC	14326	60	0.004	83000	60000	91860	1531
	SF-10-2-U-a	NWC	14767	60	0.007	83000	60000	130680	2178
	SF-10-2-U-b	NWC	14804	60	0.007	83000	60000	124080	2068
	SF-10-3-U-a	NWC	16170	60	0.011	83000	60000	144840	2414
	SF-10-3-U-b	NWC	13934	60	0.011	83000	60000	147900	2465
	SF-10-4-U-a	NWC	15468	60	0.015	83000	60000	156060	2601
	SF-10-4-U-b	NWC	16476	60	0.015	83000	60000	160020	2667
	SF-14-1-U	NWC	17957	60	0.004	83000	60000	94980	1583
	SF-14-2-U	NWC	17362	60	0.007	83000	60000	108480	1808
	SF-14-3-U	NWC	16255	60	0.011	83000	60000	146220	2437
	SF-14-4-U	NWC	16059	60	0.015	83000	60000	156000	2600
Harries, Zeno, and Shahrooz, 2012	615-3A	NWC	4220	160	0.004	67300	60000	112500	700
	615-3B	NWC	4220	160	0.004	67300	60000	96500	590
	615-4A	NWC	4220	160	0.007	61500	60000	114500	690
	615-4B	NWC	4220	160	0.007	61500	60000	129000	790
	1035-3A	NWC	4220	160	0.004	130000	100000	90000	570
	1035-3B	NWC	4220	160	0.004	126000	100000	105000	650
	1035-4A	NWC	4220	160	0.007	140000	100000	135700	840
	1035-4B	NWC	4220	160	0.008	131300	100000	113500	710
Krc, 2015	N-MO-U-1	NWC	4840	49.5	0.013	72200	60000	63410	1281
	N-MO-U-2	NWC	4840	49.5	0.013	72200	60000	62203	1257
	S-SH-MO-U-1	SLW	4770	49.5	0.013	72200	60000	55434	1120
	S-SH-MO-U-2	SLW	4770	49.5	0.013	72200	60000	56588	1143
	A-SH-MO-U-1	ALW	4700	49.5	0.013	72200	60000	52032	1051
	A-SH-MO-U-2	ALW	4700	49.5	0.013	72200	60000	52549	1062

Table A.4 Database of Monolithic Pre-cracked Push-off Type Specimens without External Axial Force

Researcher(s)	Specimen ID	Concrete Type	f'_c (psi)	A_{cr} (in^2)	ρ	$f_{y, actual}$ (psi)	$f_{y,specified}$ (psi)	V_u (lbs)	v_u (psi)
Hofbeck, Ibrahim, and Mattock, 1969	2.1	NWC	3100	50	0.004	50700	40000	29500	590
	2.2	NWC	3100	50	0.009	50700	40000	34000	680
	2.3	NWC	3900	50	0.013	50700	40000	42000	840
	2.4	NWC	3900	50	0.018	50700	40000	50000	1000
	2.5	NWC	4180	50	0.022	50700	40000	65000	1300
	2.6	NWC	4180	50	0.026	50700	40000	69250	1385
	3.3	NWC	3100	50	0.004	50700	40000	34000	680
	3.4	NWC	4040	50	0.008	47200	40000	51400	1028
	3.5	NWC	4040	50	0.012	42400	40000	57600	1152
	4.1	NWC	4070	50	0.004	66100	40000	35200	704
	4.2	NWC	4070	50	0.009	66100	40000	49000	980
	4.3	NWC	4340	50	0.013	66100	40000	59000	1180
	4.4	NWC	4340	50	0.018	66100	40000	70000	1400
	4.5	NWC	4390	50	0.022	66100	40000	66000	1320
	5.1	NWC	2450	50	0.004	50700	40000	25500	510
	5.2	NWC	2620	50	0.009	50700	40000	35000	700
	5.3	NWC	2385	50	0.013	50700	40000	40500	810
	5.4	NWC	2580	50	0.018	50700	40000	39750	795
	5.5	NWC	2620	50	0.022	50700	40000	50500	1010
Mattock, Li, and Wang, 1976	B1	SLW	3740	50	0.004	49600	40000	22500	450
	B2	SLW	3360	50	0.009	50900	40000	32600	652
	B3	SLW	3910	50	0.013	50900	40000	42000	840
	B4	SLW	4100	50	0.018	49100	40000	47000	940
	B5	SLW	3960	50	0.022	50500	40000	50000	1000
	B6	SLW	4250	50	0.026	51800	40000	57700	1154
	C1	SLW	2330	50	0.004	49600	40000	18200	364
	C2	SLW	2330	50	0.009	53600	40000	25700	514
	C3	SLW	2000	50	0.013	50900	40000	26300	526
	C4	SLW	2050	50	0.018	52300	40000	28000	560
	C5	SLW	2330	50	0.022	53600	40000	32000	640
	C6	SLW	2330	50	0.026	49600	40000	37000	740
	D1	SLW	5995	50	0.004	51800	40000	18500	370
	D2	SLW	5995	50	0.009	52300	40000	33400	668
	D3	SLW	5710	50	0.013	52300	40000	38600	772
	D4	SLW	5710	50	0.018	52300	40000	51100	1022
	D5	SLW	5600	50	0.022	52300	40000	54100	1082
	D6	SLW	5600	50	0.026	51800	40000	61000	1220
	F1	ALW	4150	50	0.004	53200	40000	22500	450
	F2	ALW	4030	50	0.009	52300	40000	26500	530
	F2A	ALW	3970	50	0.009	50900	40000	31000	620
	F3	ALW	4065	50	0.013	52300	40000	36700	734
	F3A	ALW	3970	50	0.013	51400	40000	35100	702
	F4	ALW	4040	50	0.018	50900	40000	43500	870
	F5	ALW	4115	50	0.022	51800	40000	46000	920
	F6	ALW	4050	50	0.026	53200	40000	49100	982
	H1	ALW	4145	50	0.004	49800	40000	20000	400
	H2	ALW	3880	50	0.009	51800	40000	31000	620
	H3	ALW	4100	50	0.013	51800	40000	43300	866
	H4	ALW	4420	50	0.018	51800	40000	47000	940
	H5	ALW	3950	50	0.022	50500	40000	49500	990
	H6	ALW	4080	50	0.026	49800	40000	52100	1042
	N1	NWC	4180	50	0.004	50900	40000	23000	460
	N2	NWC	3900	50	0.009	52700	40000	39000	780
	N3	NWC	3995	50	0.013	52300	40000	48000	960
	N4	NWC	4150	50	0.018	50900	40000	57500	1150
	N5	NWC	3935	50	0.022	50900	40000	58750	1175
	N6	NWC	4120	50	0.026	50900	40000	59500	1190

Researcher(s)	Specimen ID	Concrete Type	f'_c (psi)	A_{cr} (in^2)	ρ	$f_{y, actual}$ (psi)	$f_{y, specified}$ (psi)	V_u (lbs)	v_u (psi)
Mattock, Johal, and Chow, 1975	E1C	NWC	3855	84	0.010	51800	40000	74004	881
	E2C	NWC	4220	84	0.010	52100	40000	78036	929
	E3C	NWC	3960	84	0.010	52700	40000	59976	714
	E4C	NWC	3820	84	0.010	50500	40000	56532	673
	E5C	NWC	4020	84	0.010	52300	40000	44268	527
	E6C	NWC	3985	84	0.010	50900	40000	30996	369
	F1C	NWC	4220	84	0.016	50100	40000	82992	988
	F4C	NWC	3890	84	0.016	51300	40000	70476	839
	F6C	NWC	4150	84	0.016	51700	40000	67536	804
Kahn and Mitchell, 2002	SF-4-1-C	NWC	6805	60	0.004	69500	60000	35000	583
	SF-4-2-C	NWC	6805	60	0.007	69500	60000	55690	928
	SF-4-3-C	NWC	6805	60	0.011	69500	60000	71130	1186
	SF-7-1-C	NWC	11734	60	0.004	83000	60000	41680	695
	SF-7-2-C	NWC	12410	60	0.007	83000	60000	51730	862
	SF-7-3-C	NWC	13103	60	0.011	83000	60000	71510	1192
	SF-7-4-C	NWC	12471	60	0.015	83000	60000	62730	1046
	SF-10-1-C-a	NWC	12053	60	0.004	83000	60000	25780	430
	SF-10-1-C-b	NWC	14326	60	0.004	83000	60000	29970	500
	SF-10-2-C-a	NWC	14676	60	0.007	83000	60000	50780	846
	SF-10-2-C-b	NWC	14804	60	0.007	83000	60000	48110	802
	SF-10-3-C-a	NWC	16170	60	0.011	83000	60000	64650	1078
	SF-10-3-C-b	NWC	13924	60	0.011	83000	60000	63360	1056
	SF-10-4-C-a	NWC	15468	60	0.015	83000	60000	74160	1236
	SF-10-4-C-b	NWC	16476	60	0.015	83000	60000	76280	1271
	SF-14-1-C	NWC	16015	60	0.004	83000	60000	24880	415
	SF-14-2-C	NWC	15496	60	0.007	83000	60000	40180	670
	SF-14-3-C	NWC	15392	60	0.011	83000	60000	55500	925
	SF-14-4-C	NWC	15982	60	0.015	83000	60000	73270	1221
Krc, 2015	N-MO-P-1	NWC	4840	49.5	0.013	72200	60000	1233758	1234
	N-MO-P-2	NWC	4840	49.5	0.013	72200	60000	1150970	1151
	S-SH-MO-P-1	SLW	4770	49.5	0.013	72200	60000	1022081	1022
	S-SH-MO-P-2	SLW	4770	49.5	0.013	72200	60000	1048162	1048
	A-SH-MO-P-1	ALW	4700	49.5	0.013	72200	60000	931717	932
	A-SH-MO-P-2	ALW	4700	49.5	0.013	72200	60000	1064485	1064

Table A.5 Database of Cold Joint Roughened Push-off Type Specimens without External Axial Force

Researcher(s)	Specimen ID	Concrete Type	f'_c (psi)	A_{cr} (in^2)	ρ	$f_{y, actual}$ (psi)	$f_{y,specified}$ (psi)	V_u (lbs)	v_u (psi)
Mattock, 1976	B1	NWC	6085	50	0.004	51270	40000	24350	487
	B2	NWC	6085	50	0.009	50550	40000	35000	700
	B3	NWC	6140	50	0.013	51270	40000	52700	1054
	B4	NWC	6363	50	0.018	53820	40000	63800	1276
	B5	NWC	5968	50	0.025	49250	40000	78500	1570
	B6	NWC	5968	50	0.032	49250	40000	85000	1700
	D1	NWC	5008	50	0.004	51270	40000	29500	590
	D2	NWC	5008	50	0.009	51270	40000	46000	920
	D3	NWC	4425	50	0.013	56000	40000	50500	1010
	D4	NWC	4425	50	0.018	56000	40000	50100	1002
	D4A	NWC	4290	50	0.018	54000	40000	49700	994
	D5	NWC	4578	50	0.025	47742	40000	60500	1210
	D5A	NWC	4540	50	0.025	48831	40000	62500	1250
	D6	NWC	4578	50	0.032	48500	40000	73500	1470
Kahn and Mitchell, 2002	SF-7-1-CJ	NWC	11734	60	0.004	83000	60000	54000	900
	SF-7-2-CJ	NWC	11734	60	0.007	83000	60000	82100	1368
	SF-7-3-CJ	NWC	12471	60	0.011	83000	60000	110300	1838
	SF-7-4-CJ	NWC	12471	60	0.015	83000	60000	132680	2211
	SF-10-1-CJ	NWC	14326	60	0.004	83000	60000	31730	529
	SF-10-2-CJ	NWC	12053	60	0.007	83000	60000	49290	822
	SF-10-3-CJ	NWC	12953	60	0.011	83000	60000	113910	1899
	SF-10-4-CJ	NWC	12953	60	0.015	83000	60000	126040	2101
	SF-14-1-CJ	NWC	14756	60	0.004	83000	60000	90910	1515
	SF-14-2-CJ	NWC	14756	60	0.007	83000	60000	99190	1653
	SF-14-3-CJ	NWC	15218	60	0.011	83000	60000	134710	2245
	SF-14-4-CJ	NWC	15218	60	0.015	69500	60000	153120	2552
Harries, Zeno, and Shahrooz 2012	615-3A	NWC	4220	160	0.004	67300	60000	112500	700
	615-3B	NWC	4220	160	0.004	67300	60000	96500	590
	615-4A	NWC	4220	160	0.007	61500	60000	114500	690
	615-4B	NWC	4220	160	0.007	61500	60000	129000	790
	1035-3A	NWC	4220	160	0.004	130000	100000	90000	570
	1035-3B	NWC	4220	160	0.004	126000	100000	105000	650
	1035-4A	NWC	4220	160	0.007	140000	100000	135700	840
	1035-4B	NWC	4220	160	0.008	131300	100000	113500	710
Shaw, 2013	N-5-R-4	NWC	4860	49.5	0.013	66200	60000	59060	1193
	N-5-R-5	NWC	4860	49.5	0.013	66200	60000	53420	1079
	N-5-R-6	NWC	4860	49.5	0.013	66200	60000	53440	1080
	S-5-R-1	SLW	4580	49.5	0.013	66200	60000	51431	1039
	S-5-R-2	SLW	4580	49.5	0.013	66200	60000	50396	1018
	S-5-R-3	SLW	4580	49.5	0.013	66200	60000	63904	1291
	A-5-R-1	ALW	6080	49.5	0.013	66200	60000	48439	979
	A-5-R-2	ALW	6080	49.5	0.013	66200	60000	52797	1067
	A-5-R-3	ALW	6080	49.5	0.013	66200	60000	51408	1039
	N-8-R-1	NWC	7550	49.5	0.013	66200	60000	74039	1496
	N-8-R-2	NWC	7550	49.5	0.013	66200	60000	56092	1133
	N-8-R-3	NWC	7550	49.5	0.013	66200	60000	64138	1296
	S-8-R-1	SLW	7200	49.5	0.013	66200	60000	72044	1455
	S-8-R-2	SLW	7200	49.5	0.013	66200	60000	67380	1361
	S-8-R-3	SLW	7200	49.5	0.013	66200	60000	66724	1348
	A-8-R-1	ALW	7843	49.5	0.013	66200	60000	61774	1248
	A-8-R-2	ALW	7843	49.5	0.013	66200	60000	63937	1292
	A-8-R-3	ALW	7843	49.5	0.013	66200	60000	64126	1295

Researcher(s)	Specimen ID	Concrete Type	f'_c (psi)	A_{cr} (in^2)	ρ	$f_{y, actual}$ (psi)	$f_{y,specified}$ (psi)	V_u (lbs)	v_u (psi)
	S-SL-CJ-09-R-1	SLW	5380	49.5	0.009	72200	60000	49342	997
	S-SL-CJ-09-R-2	SLW	5380	49.5	0.009	72200	60000	50478	1020
	S-SL-CJ-13-R-1	SLW	5570	49.5	0.013	72200	60000	63167	1276
	S-SL-CJ-13-R-2	SLW	5570	49.5	0.013	72200	60000	59370	1199
	S-SL-CJ-17-R-1	SLW	4950	49.5	0.017	72200	60000	62384	1260
	S-SL-CJ-17-R-2	SLW	4950	49.5	0.017	72200	60000	65152	1316
	S-SL-CJ-22-R-1	SLW	5000	49.5	0.022	72200	60000	64455	1302
	S-SL-CJ-22-R-2	SLW	5000	49.5	0.022	72200	60000	57589	1163
	A-SL-CJ-13-R-1	ALW	4380	49.5	0.013	72200	60000	46500	939
Krc, 2015 and Wermager, 2015	A-SL-CJ-13-R-2	ALW	4380	49.5	0.013	72200	60000	46900	947
	S-CL-CJ-9-R-1	SLW	4770	49.5	0.009	72200	60000	37100	749
	S-CL-CJ-9-R-2	SLW	4770	49.5	0.009	72200	60000	42900	867
	S-CL-CJ-13-R-1	SLW	4640	49.5	0.013	72200	60000	50800	1026
	S-CL-CJ-13-R-2	SLW	4640	49.5	0.013	72200	60000	46900	947
	S-CL-CJ-17-R-1	SLW	4550	49.5	0.017	72200	60000	51200	1034
	S-CL-CJ-17-R-2	SLW	4550	49.5	0.017	72200	60000	56700	1145
	S-CL-CJ-22-R-1	SLW	4790	49.5	0.022	72200	60000	56700	1145
	S-CL-CJ-22-R-2	SLW	4790	49.5	0.022	72200	60000	53200	1075
	A-CL-CJ-13-R-1	ALW	4460	49.5	0.013	72200	60000	41800	844
	A-CL-CJ-13-R-2	ALW	4460	49.5	0.013	72200	60000	43800	885

Table A.6 Database of Cold Joint Smooth Push-off Type Specimens without External Axial Force

Researcher(s)	Specimen ID	Concrete Type	f'_c (psi)	A_{cr} (in²)	ρ	$f_{y, actual}$ (psi)	$f_{y,specified}$ (psi)	V_u (lbs)	v_u (psi)
Mattock, 1976	C1	NWC	5870	50	0.004	50910	40000	10500	210
	C2	NWC	5870	50	0.009	50910	40000	18000	360
	C3	NWC	5980	50	0.013	50550	40000	21400	428
	C4	NWC	5980	50	0.018	51640	40000	30000	600
	C5	NWC	6165	50	0.022	52730	40000	39000	780
	C6	NWC	6165	50	0.032	45250	40000	44100	882
	G1	NWC	5870	50	0.004	50910	40000	8000	160
	G2	NWC	5870	50	0.009	50910	40000	13200	264
	G3	NWC	5980	50	0.013	50550	40000	19200	384
	G4	NWC	5980	50	0.018	51640	40000	25000	500
	G5	NWC	6165	50	0.022	52730	40000	29300	586
	G6	NWC	6165	50	0.032	45250	40000	38900	778
	H1	NWC	5820	50	0.004	55450	40000	9400	188
	H2	NWC	6080	50	0.009	55450	40000	16100	322
	H3	NWC	6080	50	0.013	55450	40000	23000	460
	H4	NWC	6075	50	0.018	53640	40000	25500	510
	H5	NWC	6180	50	0.025	46653	40000	32700	654
	H6	NWC	5900	50	0.032	46800	40000	38000	760
Shaw, 2013	N-5-S-4	NWC	4860	49.5	0.013	66200	60000	30850	623
	N-5-S-5	NWC	4860	49.5	0.013	66200	60000	34678	701
	N-5-S-6	NWC	4860	49.5	0.013	66200	60000	39154	791
	S-5-S-1	SLW	4580	49.5	0.013	66200	60000	38532	778
	S-5-S-2	SLW	4580	49.5	0.013	66200	60000	34112	689
	S-5-S-3	SLW	4580	49.5	0.013	66200	60000	39796	804
	A-5-S-1	ALW	6080	49.5	0.013	66200	60000	41471	838
	A-5-S-2	ALW	6080	49.5	0.013	66200	60000	40079	810
	A-5-S-3	ALW	6080	49.5	0.013	66200	60000	39247	793
	N-8-S-1	NWC	7550	49.5	0.013	66200	60000	65557	1324
	N-8-S-2	NWC	7550	49.5	0.013	66200	60000	53304	1077
	N-8-S-3	NWC	7550	49.5	0.013	66200	60000	55327	1118
	S-8-S-1	SLW	7200	49.5	0.013	66200	60000	67025	1354
	S-8-S-2	SLW	7200	49.5	0.013	66200	60000	57876	1169
	S-8-S-3	SLW	7200	49.5	0.013	66200	60000	58863	1189
	A-8-S-1	ALW	7843	49.5	0.013	66200	60000	46089	931
	A-8-S-2	ALW	7843	49.5	0.013	66200	60000	48036	970
	A-8-S-3	ALW	7843	49.5	0.013	66200	60000	51741	1045
Krc, 2015 and Wermager, 2015	S-SL-CJ-09-S-1	SLW	5380	49.5	0.009	72200	60000	26946	544
	S-SL-CJ-09-S-2	SLW	5380	49.5	0.009	72200	60000	32592	658
	S-SL-CJ-13-S-1	SLW	5570	49.5	0.013	72200	60000	39487	798
	S-SL-CJ-13-S-2	SLW	5570	49.5	0.013	72200	60000	48767	985
	S-SL-CJ-17-S-1	SLW	4950	49.5	0.017	72200	60000	49813	1006
	S-SL-CJ-17-S-2	SLW	4950	49.5	0.017	72200	60000	56533	1142
	S-SL-CJ-22-S-1	SLW	5000	49.5	0.022	72200	60000	49813	1006
	S-SL-CJ-22-S-2	SLW	5000	49.5	0.022	72200	60000	56533	1142
	A-SL-CJ-13-S-1	ALW	4380	49.5	0.013	72200	60000	37800	764
	A-SL-CJ-13-S-2	ALW	4380	49.5	0.013	72200	60000	38800	784
	S-CL-CJ-9-S-1	SLW	4770	49.5	0.009	72200	60000	31900	644
	S-CL-CJ-9-S-2	SLW	4770	49.5	0.009	72200	60000	37900	766
	S-CL-CJ-13-S-1	SLW	4640	49.5	0.013	72200	60000	41000	828
	S-CL-CJ-13-S-2	SLW	4640	49.5	0.013	72200	60000	40400	816
	S-CL-CJ-17-S-1	SLW	4550	49.5	0.017	72200	60000	43100	871
	S-CL-CJ-17-S-2	SLW	4550	49.5	0.017	72200	60000	48900	988
	S-CL-CJ-22-S-1	SLW	4790	49.5	0.022	72200	60000	52400	1059
	S-CL-CJ-22-S-2	SLW	4790	49.5	0.022	72200	60000	52600	1063
	A-CL-CJ-13-S-1	ALW	4460	49.5	0.013	72200	60000	36900	745
	A-CL-CJ-13-S-2	ALW	4460	49.5	0.013	72200	60000	37300	754

APPENDIX B

RESIDUAL SHEAR STRENGTH ANALYSIS

RESIDUAL SHEAR STRENGTH ANALYSIS

Even though studying the residual shear strength was not one of the objectives of this research work, it may be of interest to analyze how the ACI 318-14 code and the PCI Design Handbook 7th Edition design values compare to the residual shear strength of shear-friction specimens. This may be of particular interest for seismic design, where the structure is not designed solely on the basis of ultimate shear strength but also its ductility. Presented in Table B.1 is the summary of residual shear strengths in terms of stress for the specimens tested in this study. Included are also specimens from Shaw (2013). Shaw used the same definition of residual shear strength; that is the shear strength at a slip of 0.15 in. Values in the table shown as N/A were for the specimens that reached 60 percent of their post-peak strength prior to reaching 0.15 in. slip. It should be noted that for smooth interface cold joint specimens (Case 3), the values presented are calculated using the PCI Design Handbook 6th Edition approach. It can be seen in Table B.1 that ACI design values are conservative more often than the PCI design values. It can also be seen in the Shaw data that the 8000 psi concrete specimens design values are conservative more often than the 5000 psi concrete specimens. It can also be seen that the slate aggregate specimens residual shear strength are conservative more often than the clay aggregate specimens residual shear strength for both the ACI and PCI design values.

Table B.1 Analysis of Residual Shear Strength and its Comparison to PCI Design Handbook 7th Edition and ACI 318-14 Design Values

Researcher	Specimen ID	f'$_c$	V$_u$	v$_u$	v$_{ur}$	PCI 7th Edition - μ$_e$		ACI 318-14 Code	
						v$_{u,PCI}$	v$_{ur}$/v$_{u,PCI}$	v$_{u,ACI}$	v$_{ur}$/v$_{u,ACI}$
		psi	lbs	psi	psi	psi		psi	
Shaw, 2015	N-5-R-4	4860	59060	1193	797	883	0.90	780	1.02
	N-5-R-5	4860	53420	1079	811	883	0.92	780	1.04
	N-5-R-6	4860	53440	1080	775	883	0.88	780	0.99
	N-5-S-4	4860	30850	623	629	684	0.92	468	1.34
	N-5-S-5	4860	34678	701	660	684	0.97	468	1.41
	N-5-S-6	4860	39154	791	646	684	0.95	468	1.38
	S-5-R-1	4580	51431	1039	616	751	0.82	663	0.93
	S-5-R-2	4580	50396	1018	598	751	0.80	663	0.90
	S-5-R-3	4580	63904	1291	592	751	0.79	663	0.89
	S-5-S-1	4580	38532	778	671	581	1.15	398	1.69
	S-5-S-2	4580	34112	689	564	581	0.97	398	1.42
	S-5-S-3	4580	39796	804	596	581	1.03	398	1.50
	A-5-R-1	6080	48439	979	707	662	1.07	585	1.21
	A-5-R-2	6080	52797	1067	869	662	1.31	585	1.48
	A-5-R-3	6080	51408	1039	818	662	1.24	585	1.40
	A-5-S-1	6080	41471	838	778	513	1.52	351	2.22
	A-5-S-2	6080	40079	810	646	513	1.26	351	1.84
	A-5-S-3	6080	39247	793	747	513	1.46	351	2.13
	N-8-R-1	7550	74039	1496	960	883	1.09	780	1.23
	N-8-R-2	7550	56092	1133	789	883	0.89	780	1.01
	N-8-R-3	7550	64138	1296	869	883	0.98	780	1.11
	N-8-S-1	7550	65557	1324	1000	684	1.46	468	2.14
	N-8-S-2	7550	53304	1077	868	684	1.27	468	1.85
	N-8-S-3	7550	55327	1118	943	684	1.38	468	2.02
	S-8-R-1	7200	72044	1455	882	751	1.17	663	1.33
	S-8-R-2	7200	67380	1361	733	751	0.98	663	1.11
	S-8-R-3	7200	66724	1348	N/A	751	N/A	663	N/A
	S-8-S-1	7200	67025	1354	899	581	1.55	398	2.26
	S-8-S-2	7200	57876	1169	747	581	1.29	398	1.88
	S-8-S-3	7200	58863	1189	815	581	1.40	398	2.05
	A-8-R-1	7843	61774	1248	835	662	1.26	585	1.43
	A-8-R-2	7843	63937	1292	925	662	1.40	585	1.58
	A-8-R-3	7843	64126	1295	797	662	1.20	585	1.36
	A-8-S-1	7843	46089	931	763	513	1.49	351	2.18
	A-8-S-2	7843	48036	970	812	513	1.58	351	2.31
	A-8-S-3	7843	51741	1045	851	513	1.66	351	2.43

Researcher	Specimen ID	f'_c	V_u	v_u	v_{ur}	PCI 7th Edition - μ_e		ACI 318-14 Code	
						$v_{u,PCI}$	$v_{ur}/v_{u,PCI}$	$v_{u,ACI}$	$v_{ur}/v_{u,ACI}$
		psi	lbs	psi	psi	psi		psi	
Krc, 2015	N-MO-U-1	4840	63410	1281	823	1000	0.82	800	1.03
	N-MO-U-2	4840	62203	1257	N/A	1000	N/A	800	N/A
	N-MO-P-1	4840	61071	1234	920	1000	0.92	800	1.15
	N-MO-P-2	4840	56973	1151	1103	1000	1.10	800	1.38
	S-SH-MO-U-1	4770	55434	1120	824	850	0.97	800	1.03
	S-SH-MO-U-2	4770	56588	1143	778	850	0.92	800	0.97
	S-SH-MO-P-1	4770	50593	1022	789	850	0.93	800	0.99
	S-SH-MO-P-2	4770	51884	1048	871	850	1.02	800	1.09
	A-SH-MO-U-1	4700	52032	1051	663	750	0.88	800	0.83
	A-SH-MO-U-2	4700	52549	1062	751	750	1.00	800	0.94
	A-SH-MO-P-1	4700	46120	932	835	750	1.11	800	1.04
	A-SH-MO-P-2	4700	52692	1064	977	750	1.30	800	1.22
	S-SL-CJ-R-1	5570	63167	1276	N/A	760	N/A	680	N/A
	S-SL-CJ-R-2	5570	59370	1199	735	760	0.97	680	1.08
	S-SL-CJ-S-1	5570	39487	798	616	589	1.05	408	1.51
	S-SL-CJ-S-2	5570	48767	985	783	589	1.33	408	1.92
	A-SL-CJ-R-1	4380	46525	940	609	671	0.91	600	1.02
	A-SL-CJ-R-2	4380	46925	948	682	671	1.02	600	1.14
	A-SL-CJ-S-1	4380	37842	764	622	520	1.20	360	1.73
	A-SL-CJ-S-2	4380	38751	783	719	520	1.38	360	2.00
	S-CL-CJ-R-1	4640	50785	1026	633	760	0.83	680	0.93
	S-CL-CJ-R-2	4640	46885	947	670	760	0.88	680	0.99
	S-CL-CJ-S-1	4640	41006	828	627	589	1.06	408	1.54
	S-CL-CJ-S-2	4640	40436	817	574	589	0.97	408	1.41
	A-CL-CJ-R-1	4460	41858	846	N/A	671	N/A	600	N/A
	A-CL-CJ-R-2	4460	43816	885	534	671	0.80	600	0.89
	A-CL-CJ-S-1	4460	36966	747	N/A	520	N/A	360	N/A
	A-CL-CJ-S-2	4460	37324	754	501	520	0.96	360	1.39

REFERENCES

AASHTO (2010) "AASHTO LRFD Bridge Design Specifications," Third edition, American Association of State Highway and Transportation Officials (AASHTO), Washington, DC.

ACI Committee 318 (2011). "Building Code Requirements for Structural Concrete and Commentary (ACI 318-11)," Farmington Hills, MI: American Concrete Institute.

ACI Committee 318 (2014). "Building Code Requirements for Structural Concrete and Commentary (ACI 318-14)," Farmington Hills, MI: American Concrete Institute.

ASTM A370 (2012a)." Standard Test Methods and Definitions for Mechanical Testing of Steel Products" Annual book of ASTM standards, ASTM, West Conshohocken, Pennsylvania.

ASTM A615 (2012)." Standard Specification for Deformed and Plain Carbon-Steel Bars for Concrete Reinforcement" Annual book of ASTM standards, ASTM, West Conshohocken, Pennsylvania.

ASTM C29 (2009)." Standard Test Method for Bulk Density (Unit Weight) and Voids in Aggregate" Annual book of ASTM standards, ASTM, West Conshohocken, Pennsylvania.

ASTM C33 (2013). "Standard Specification for Concrete Aggregates" Annual book of ASTM standards, ASTM, West Conshohocken, Pennsylvania.

ASTM C39 (2015). "Standard Test Method for Compressive Strength of Cylindrical Concrete Specimens" Annual book of ASTM standards, ASTM, West Conshohocken, Pennsylvania.

ASTM C127 (2012). "Standard Test Method for Density, Relative Density (Specific Gravity), and Absorption of Coarse Aggregate." Annual book of ASTM standards, ASTM, West Conshohocken, Pennsylvania.

ASTM C128 (2012)."Standard Test Method for Density, Relative Density (Specific Gravity), and Absorption of Fine Aggregate." Annual book of ASTM standards, ASTM, West Conshohocken, Pennsylvania.

ASTM C136 (2006). "Standard Test Method for Sieve Analysis of Fine and Coarse Aggregates." Annual book of ASTM standards, ASTM, West Conshohocken, Pennsylvania.

ASTM C138 (2014). "Standard Test Method for Density (Unit Weight), Yield, and Air Content (Gravimetric) of Concrete." Annual book of ASTM standards, ASTM, West Conshohocken, Pennsylvania.

ASTM Cl43 (2015). "Standard Test Method for Slump of Hydraulic-Cement Concrete." Annual book of ASTM standards, ASTM, West Conshohocken, Pennsylvania.

ASTM Cl73 (2014). "Standard Test Method for Air Content of Freshly Mixed Concrete by the Volumetric Method." Annual book of ASTM standards, ASTM, West Conshohocken, Pennsylvania.

ASTM C192 (2012). "Standard Practice for Making and Curing Concrete Test Specimens in the Laboratory." Annual book of ASTM standards, ASTM, West Conshohocken, Pennsylvania.

ASTM C231 (2010). "Standard Test Method for Air Content of Freshly Mixed Concrete by the Pressure Method." Annual book of ASTM standards, ASTM, West Conshohocken, Pennsylvania.

ASTM C330 (2014). "Standard Specification for Lightweight Aggregates for Structural Concrete." Annual book of ASTM standards, ASTM, West Conshohocken, Pennsylvania.

ASTM C469 (2010). "Standard Test Method for Static Modulus of Elasticity and Poisson's Ratio of Concrete in Compression." Annual book of ASTM standards, ASTM, West Conshohocken, Pennsylvania.

ASTM C496 (2011). "Standard Test Method for Splitting Tensile Strength of Cylindrical Concrete Specimens." Annual book of ASTM standards, ASTM, West Conshohocken, Pennsylvania.

ASTM C1231 (2012). "Standard Practice for Use of Unbonded Caps in Determination of Compressive Strength of Concrete Cylinders." Annual book of ASTM standards, ASTM, West Conshohocken, Pennsylvania.

Birkeland, P.W. and H.W. Birkeland. (1966). "Connections in Precast Concrete Construction," ACI Journal, *Proceedings*, Vol. 63, No. 3, pp. 345-368.

Hanson, N.W. (1960). "Precast-Prestressed Concrete Bridges 2: Horizontal Shear Connections," *PCA – Journal of the Research and Development Division*, Vol. 2, No. 2, pp. 38-58.

Hofbeck, J. A. Ibrahim, I. O. and Mattock, A. H. (1969). "Shear Transfer in Reinforced Concrete," ACI Journal, *Proceedings,* V. 66, No. 2, pp. 119-128.

Hsu, T.T.C., Mau S.T., and Bin Chen. (1987). "Theory of Shear Transfer Strength of Reinforced Concrete," *ACI Structural Journal*, Vol. 84, No. 2, pp. 149-160.

Kahn, L.F. and A.D. Mitchell. (2002). "Shear-friction Tests with High-Strength Concrete", *ACI Structural Journal*, Vol. 99, No. 1, pp. 98-103.

Loov, R.E. and A.K. Patnaik. (1994). "Horizontal Shear Strength of Composite Beams with a Rough Interface," *PCI Journal*, Vol. 39, No. 1, pp. 48-58.

Mast, R.F. (1968). "Auxiliary Reinforcement in Concrete Connections", *ASCE Journal of the Structural Division Proceedings*, Vol. 94, No. ST6, pp. 1485-1504

Mattock, A. H., W. K. Li, and T. C. Wang. (1976). "Shear Transfer in Lightweight Reinforced Concrete." *PCI Journal*, Vol. 21, No. 1, pp. 20-39.

Mattock, A. (1974). *Effect of aggregate type on single direction shear transfer strength in monolithic concrete: Final report : Part 1*. Seattle, Wash.: Dept. of Civil Engineering, Univ. of Washington.

Mattock, A.H. (1976). "Shear Transfer Under Monotonic Loading Across and Interface Between Concretes Cast at Different Times", *University of Washington Department of Civil Engineering Report SM 76-3*.

Mattock, A.H. (2001). "Shear-friction and High-Strength Concrete", *ACI Structural Journal*, Vol. 98, No. 1, pp. 50-59.

Mattock, A. H., Johal, L, and Chow, C. H. (1975). "Shear transfer in reinforced concrete with moment or tension acting across the shear plane." *PCI Journal*, Vol. 20, No. 4, pp. 76-93.

Mattock, A.H. and N.M. Hawkins. (1972). "Shear Transfer in Reinforced Concrete – Recent Research," *PCI Journal*, Vol. 17, No. 2, pp. 55-75.

Precast/Prestressed Concrete Institute (2004). *PCI Design Handbook: Precast and Prestressed Concrete Institute*. 6th ed. Chicago: Precast/Prestressed Concrete Institute.

Precast/Prestressed Concrete Institute (2010). *PCI Design Handbook: Precast and Prestressed Concrete Institute*. 7th ed. Chicago: Precast/Prestressed Concrete Institute.

Raths, C. H. (1977). "Reader Comments: Design Proposals for Reinforced Concrete Corbels." *PCI Journal*, Vol. 21, No. 3, pp 93–98.

Scott, J. (2010) "Interface Shear Strength in Lightweight Concrete Bridge Girders." MS Thesis. Virginia Polytechnic Institute.

Shaw, D.M. (2013). *Direct Shear Transfer of Lightweight Aggregate Concretes with Non-monolithic Interface Conditions* Unpublished master's thesis, Missouri University of Science and Technology, Rolla, Missouri.

Shaikh, F. A. (1978). "Proposed Revisions to Shear-friction Provisions." *PCI Journal,* Vol. 23, No. 2, pp. 12-21.

Tanner, J. A. (2008). "Calculating Shear-friction Using Effective Coefficient of Friction." *PCI Journal*, Vol. 53, No. 3, pp. 114-20.

Wermager, S.L. (2015). *Shear-Friction of Sand-lightweight Clay and Slate Aggregate Concretes with Varied Reinforcement Ratio* Unpublished master's thesis, Missouri University of Science and Technology, Rolla, Missouri.

Wight, J., and MacGregor, J. (2012). *Reinforced concrete: Mechanics and design* (6th ed., pp. 858-869). Upper Saddle River, N.J.: PEARSON PRENTICE HALL**.**

VITA

Kristian Krc was born in Trnava, Slovakia in 1990. His passion for concrete and structural engineering was born during long hot summers of working in the construction industry.

In May 2012, he received his Bachelors of Science in Physics with pre-engineering emphasis from Ouachita Baptist University in Arkansas. He graduated suma cum laude with GPA of 4.0. He started his Masters of Science in Civil Engineering at the Missouri University of Science and Technology in August of 2013. In December of 2015 he completed this degree. He accepted a job with Walter P. Moore and Associates in Dallas, TX, and started his career in January 2016.